Follicular Regulatory T cell Migration and Differentiation



Ine Vanderleyden

Clare Hall

The Babraham Institute

University of Cambridge

This dissertation is submitted for the degree of Doctor of Philosophy

September 2018

SUMMARY

Follicular regulatory T cell migration and differentiation

Ine Vanderleyden

The germinal centre (GC) response is critical for generating highly effective humoral immune responses and immunological memory that forms the basis of successful immunisation. Control of the output of the GC response requires Follicular regulatory T (Tfr) cells, a subset of Foxp3^{+} Treg cells located within germinal centres. Tfr cells were first characterised in detail in 2011 and because of this relatively little is known about the exact role of Tfr cells within the GC, and the mechanism/s through which they exert their suppressive function. At the outset of this work, the major barrier to understanding Tfr cell biology was the lack of appropriate tools to study Tfr cells specifically, without affecting Tfh cells or other Treg cell subsets. This thesis set out to develop a strain of mice that specifically lacks Tfr cells. A unique feature of Tfr cells is their CXCR5-dependent localisation within the GC. Therefore, genetic strategies that exclude Treg cells from entering the GC are a rational approach to generating a mouse model that lacks Tfr cells. To this end, I generated a strain of mice that lacks CXCR5 on Foxp3^{+} Treg cells. These animals show a ~50% reduction in GC localised Tfr cells, and a GC response that is comparable to control animals. These data indicated that redundant mechanisms are involved in Treg cell homing to the GC. I identified CXCR4 as a chemokine receptor that is also highly expressed on Tfr cells, and hypothesised that it may also be involved in Tfr cell localisation to the GC. Surprisingly, simultaneous deletion of both CXCR4 and CXCR5 in Treg cells resulted in a less marked reduction in Tfr cells compared to deletion of CXCR5 alone, suggesting that CXCR4 might be involved in negative regulation of Treg homing to the GC. These data identify both CXCR4 and CXCR5 as key regulators of Tfr cell biology.

Bcl6 drives Tfr cell differentiation, but how this transcriptional repressor facilitates commitment to the Tfr cell subset is unknown. I hypothesised that *Bcl6* drives Tfr cell differentiation by repressing *Tbx21*, the transcriptional regulator involved in the differentiation of Th1-like Treg cells. I tested this hypothesis in *Bcl6*$^{fl/fl}$ *CD4*$^{cre/+}$ animals and unexpectedly found that loss of Bcl6 regulates Treg cell differentiation in the absence of immunisation or infection. I have demonstrated that thymic loss of Bcl6 results in an increase in activated effector Treg cells, which occurs very early in life. These data point to a novel

role for Bcl6 in preventing early thymic Treg activation, indicating that Bcl6 has a global role in Treg development and differentiation that is not simply limited to Tfr cells.

ACKNOWLEDGEMENTS

First and foremost, I am extremely grateful to my supervisor, Michelle Linterman, for providing me the opportunity to carry out research in her lab. Her door was always open for discussing academic, as well as pastoral issues. Her guidance, advice and unparalleled enthusiasm for science have driven my research projects, and made this thesis possible.

I wish to acknowledge the Cambridge Trust and the Babraham Institute for my funding, along with the Babraham graduate committee who have allowed me to participate in an international conference and summer schools.

I would like to extend a sincere thanks to all the members of the Linterman group, past and present. Someone who was instrumental to the first two years of my PhD is Wim, who was a patient mentor and taught me many techniques. I am grateful to Alice for proofreading my thesis. Special thanks to Silvia, for assisting me with experiments, and especially her patience while doing so. I would also like to thank Sigrid for the many hours of confocal imaging, you have really saved me a few times. Thanks to my office buddies Marisa and Alyssa for the great company and welcome distractions every now and again. Thanks should also go to Danika, Louise, Ed and Alex for all the valuable advice, scientific discussions and helping to put general PhD struggles in perspective. Thank you all for making this PhD a unique experience.

I wish to thank my parents for their unwavering support and advice throughout the years, as well as constructive criticism from time to time. My sister, Els, deserves special thanks for her relentless, albeit fruitless, attempts at teaching me the virtues of stoicism. A warm thank you to Nora for being a wonderful friend, and unquestionably a role model (most of the time). It is fair to say that without her as a great example in the first few years of university, I would never have embarked on a PhD in the first place. Thank you Kate for being such a lovely friend over the past 4 years, and the many walks and talks during the thesis writing, we did it in the end! Last but not least, a heartfelt thanks to Jimmy for making the last two years of my PhD so enjoyable with his exceptional optimism, positive outlook and, most importantly, exquisite cooking skills.

DECLARATION

This dissertation is the result of my own work and includes nothing which is the outcome of work done in collaboration except as declared in the Preface and specified in the text.

It is not substantially the same as any that I have submitted, or, is being concurrently submitted for a degree or diploma or other qualification at the University of Cambridge or any other University or similar institution except as declared in the Preface and specified in the text. I further state that no substantial part of my dissertation has already been submitted, or, is being concurrently submitted for any such degree, diploma or other qualification at the University of Cambridge or any other University or similar institution except as declared in the Preface and specified in the text

The research in this thesis was carried out under the supervision of Dr. Michelle Linterman in the Laboratory of Lymphocyte Signalling and Development at the Babraham Institute, Cambridge between October 2014 and October 2018.

It does not exceed the prescribed word limit of 60,000 words.

Ine Vanderleyden

TABLE OF ACKNOWLEDGEMENT OF ASSISTANCE RECEIVED DURING COURSE OF THESIS

1. Initial training in techniques and laboratory practice and subsequent mentoring: -Michelle Linterman: Mouse dissection techniques, flow cytometry, bone marrow chimaera -Wim Pierson: PCR, flow cytometry -Alice Denton: IF staining
2. Data obtained from a technical service provider (*e.g.* DNA sequencing, illustrations, simple bioinformatics information etc) -Genotyping: Transnetyx -BSU transgenics unit: Breeding and day-to-day maintenance of mice -BSU experimental unit: *i.p.* , *i.v.* and *s.c.* injections, irradations. -BSU import unit: infections -Flow cytometry facility: FACS sorting -Babraham Bioinformatics: RNA seq data processing
3. Data produced jointly (e.g. where it was necessary or desirable to have two pairs of hands) -Silvia Innocentin: Help with dissections and processing of samples -Alyssa Silva-Cayetano: flow cytometry staining $Cxcr4^{fl/fl}Cxcr5^{fl/fl}Foxp3^{cre\text{-}ERT2}$ repeat two and Chemotaxis essay -Marisa Stebegg: Processing of samples $Cxcr4^{fl/fl}Cxcr5^{fl/fl}Foxp3^{cre\text{-}ERT2}$ repeat two -Danika Hill: acquiring samples on flow cytometer for $Cxcr4^{fl/fl}Cxcr5^{fl/fl}Foxp3^{cre\text{-}ERT2}$ repeat

two, tSNE Analysis

-Sigrid Fra-Bido: IF and Confocal imaging

- Simon Walker and Hannke Okkenhaug: help with confocal imaging and imaging analysis

-Amélie Bonaud and Marion Espéli, INSERM, France: Biomark essay

-Oliver Burton and Adrian Liston: 27-parameter FACSymphony Experiment

3. Data/materials provided by someone else (e.g. one-off analysis, bioinformatics analysis, where parallel data or technical provision in a very different area is needed to provide a connected account in the thesis)

- Christel Krueger: Bcl6 motif analysis

LIST OF PUBLICATIONS

- **Vanderleyden, I.** & Linterman, M.A. Identifying Follicular Regulatory T Cells by Confocal Microscopy. *Methods in molecular biology* **1623**, 87-93 (2017).
- Afzali, B., J. Gronholm, J. Vandrovcova, C. O'Brien, H. W. Sun, **Vanderleyden I.**, et al., BACH2 immunodeficiency illustrates an association between super-enhancers and haploinsufficiency. *Nature immunology* **18**, 813-823 (2017).
- **Vanderleyden, I**., Linterman, M.A. & Smith, K.G. Regulatory T cells and control of the germinal centre response. *Arthritis Research & Therapy* **16** (2014).

LIST OF TABLES

Table 1. List of mouse models used in this thesis. *36*

Table 2. List of anti-mouse antibodies used for flow cytometry. *43*

Table 3. Sequences of the CXCR5 primers (Sigma) used for PCR based genotyping assay. Primers were reconstituted to 100μM. *48*

Table 4. Reagents and concentrations used for PCR reactions. *49*

Table 5. Thermocycling conditions used in PCR reactions. *50*

Table 6. Expected outcome and corresponding band sizes for each PCR reaction. *51*

Table 7. Thermocycling conditions used for reverse transcription. *52*

Table 8. List of TaqMan probes used for Biomark essay (Applied Biosystems). *56*

LIST OF FIGURES

Figure 1.1 Overview of T cell development in the thymus. 7

Figure 1.2 Differentiation of $CD4^+$ Tconv cells and $Foxp3^+$ Treg cells. 14

Figure 1.3 Overview of the GC response and Tfr-mediated control of the GC response. 31

Figure 3.1 Deletion of CXCR5 on Treg cells in $Cxcr5^{fl/fl}Foxp3^{cre}$ mice. 64

Figure 3.2 $Cxcr5^{fl/fl}Foxp3^{cre}$ mice show normal numbers of GC B cells and Tfh cells. 66

Figure 3.3 $Cxcr5^{fl/fl}Foxp3^{cre}$ mice show normal plasma cell responses in the spleen after re-challenge. 69

Figure 3.4 $Cxcr5^{fl/fl}Foxp3^{cre}$ mice show normal GC B cell and memory B cell responses in the spleen after re-challenge. 72

Figure 3.5 $Cxcr5^{fl/fl}Foxp3^{cre}$ mice show normal plasma cell homing to the bone marrow. 73

Figure 3.6 $Cxcr5^{fl/fl}Foxp3^{cre}$ mice show non-specific deletion of CXCR5 in non-Treg cells. 76

Figure 3.7 $Foxp3^+$ Treg cells are still present in the GC of $Cxcr5^{fl/fl}Foxp3^{cre}$ mice. 79

Figure 3.8 $Cxcr5^{fl/fl}Cd4^{cre/+}$ mice lack CXCR5 on $Foxp3^+$ and $Foxp3^-$ cells. 81

Figure 3.9 $Cxcr5^{fl/fl}Cd4^{cre/+}$ mice show a normal GC response with regular numbers of Tfh and Tfr cells. 84

Figure 4.1 $Foxp3^{cre\text{-}ERT2}$ system principle. 88

Figure 4.2 $Cxcr5^{fl/fl}Foxp3^{cre\text{-}ERT2}$ mice show specific deletion of CXCR5 in $Foxp3^+$ Treg cells. 90

Figure 4.3 $Cxcr5^{fl/fl}Foxp3^{cre\text{-}ERT2}$ mice have a reduced proportion, but not absence, of Tfr cells. 93

Figure 4.4 Normal GC B cell responses and immunoglobulin production in $Cxcr5^{fl/fl}Foxp3^{cre\text{-}ERT2}$ mice. 95

Figure 4.5 $Cxcr5^{fl/fl}Foxp3^{cre\text{-}ERT2}$ mice show normal plasma cell and memory B cell responses. 96

Figure 4.6 Normal GC response after antigen re-challenge in $Cxcr5^{fl/fl}Foxp3^{creERT2}$ mice. 99

Figure 4.7 Normal plasma cell responses prior to, and after antigen re-challenge, and immunoglobulin production after re-challenge. 101

Figure 4.9 Gene expression analysis of Tfr cells compared to Tfh cells, Treg cells and naïve T cells. *106*

Figure 4.10 RNA–seq analysis of Tfr cells. *108*

Figure 5.1 Cxcr4$^{fl/fl}$Foxp3$^{cre-ERT2}$ mice show delayed deletion of CXCR4 in Treg cells. *115*

Figure 5.2 CXCR4 is reduced, but not completely deleted on Treg cells in Cxcr4$^{fl/fl}$Foxp3$^{cre-ERT2}$ mice. *117*

Figure 5.3 Tconv cells express normal levels of CXCR4 in Cxcr4$^{fl/fl}$Foxp3$^{cre-ERT2}$ mice. *118*

Figure 5.4 CXCR4 MFI on Tfr cells, Tfh cells and B cells. *120*

Figure 5.5 Normal numbers of Tfr cells in Cxcr4$^{fl/fl}$Foxp3$^{cre-ERT2}$ mice. *121*

Figure 5.6 Cxcr4$^{fl/fl}$Foxp3$^{cre-ERT2}$ mice show normal numbers of GC B cells and Tfh cells. *122*

Figure 5.7 Plasma cells and immunoglobulin production in Cxcr4$^{fl/fl}$Foxp3$^{cre-ERT2}$ mice. *126*

Figure 5.8 Validation of the Cxcr4$^{fl/fl}$Cxcr5$^{fl/fl}$Foxp3$^{cre-ERT2}$ mouse model. *129*

Figure 5.9 CXCR4 MFI on Tfr cells, Tfh cells and B cells. *131*

Figure 5.10 The GC response in Cxcr4$^{fl/fl}$Cxcr5$^{fl/fl}$Foxp3$^{cre-ERT2}$ mice. *133*

Figure 5.11 Confocal analysis of the GC in Cxcr4$^{fl/fl}$Cxcr5$^{fl/fl}$Foxp3$^{cre-ERT2}$ mice 14 days after immunisation with NP-KLH/Alum. *135*

Figure 5.12 Plasma cells and immunoglobulin production in Cxcr4$^{fl/fl}$Cxcr5$^{fl/fl}$Foxp3$^{cre-ERT2}$ mice. ... *139*

Figure 6.1 Bcl6 structure. *143*

Figure 6.2 Cell-intrinsic increase in Tbet expression on Treg cells in Bcl6$^{fl/fl}$Cd4$^{cre/+}$ mice after influenza infection. *148*

Figure 6.3 Cell-intrinsic increase in Tbet expression on Treg cells in Bcl6$^{fl/fl}$Cd4$^{cre/+}$ mice in the absence of immunisation or infection. *151*

Figure 6.4 Bcl6 expression in thymocytes. *153*

Figure 6.6 Bcl6$^{fl/fl}$Foxp3$^{cre-ERT2}$ mice do not show a Treg cell activation phenotype. *159*

Figure 6.7 Bcl6$^{fl/fl}$Cd4$^{cre/+}$ mice show a Tconv/Treg activation phenotype early during development in the thymus. *162*

Figure 6.8 $Bcl6^{fl/fl}Cd4^{cre/+}$ mice show a Treg activation phenotype early during development in the spleen. *165*

Figure 6.9 In-depth phenotyping of $Bcl6^{fl/fl}Cd4^{cre/+}$ mice by high-parameter flow cytometry. *167*

Figure 6.10 Identification of Treg cell sub-populations in the thymus by tSNE. *170*

Figure 6.11 Identification of Treg cell sub-populations in the spleen by tSNE. *172*

Figure 6.12 Identification of Tconv cell sub-populations in the thymus by tSNE. *175*

Figure 6.13 Identification of Tconv cell sub-populations in the spleen by tSNE. *177*

Figure 6.14 Identification of sub-populations of DP ($CD4^+CD8^+$) cells in the thymus by tSNE. *180*

Figure 6.15 Treg super-enhancers are enriched for Bcl6 motifs. *182*

LIST OF ABBREVIATIONS AND ACRONYMS

ACK	Ammonium-Chloride-Potassium
AIRE	Autoimmune Regulator
APC	Antigen Presenting Cell
ASCL-2	Achaete-Scute Family BHLH Transcription Factor 2
ATAC seq	Assay for Transposase-Accessible Chromatin using sequencing
Bcl6	B-Cell Lymphoma 6
BCR	B cell Receptor
Blimp1	PR domain zinc finger protein 1
BSA	Bovine Serum Albumin
CCR7	C-C chemokine receptor
CD	Cluster of differentiation
CFA	complete freund's adjuvant
ChIP seq	Chromatin Immunoprecipitation sequencing
CNS	Conserved Non-coding Sequence
CTLA-4	Cytotoxic T-Lymphocyte Associated Protein 4
CXCR4	C-X-C chemokine Receptor 4
DC	Dendritic Cell
DN	Double negative
DP	Double positive
DTR	Diphteria Toxin Receptor
DZ	Dark Zone
EBI2	Epstein-Barr virus-induced G-protein coupled receptor 2
EDTA	Ethylenediaminetetraacetic acid
ELISA	Enzyme linked immunosorbent assay
FBS	Foetal Bovine Serum
Foxp3	Forkhead box P
GATA3	GATA binding protein 3
GC	Germinal Centre
GFP	Green Fluorescent Protein
GITR	glucocorticoid-induced TNFR-related protein
Gy	Gray
HRP	Horseradish Peroxidase
i.n.	Intranasal
i.p.	Intraperitoneal

i.v.	Intravenous
ICOS	Inducible T-cell costimulator
IFN-γ	Interferon gamma
Ig	Immunoglobulin
IL	Interleukin
IPEX	immune dysregulation, polyendocrinopathy, enteropathy, X-linked
KLF-2	Krüppel-like Factor 2
KLH	Keyhole Limpet Hemocyanin
KLRG-1	Killer-cell Lectin Like Receptor G1
KO	Knock-Out
LN	Lymph node
LZ	Light Zone
MHC	Major Histocompatibility Complex
MOG	Myelin Oligodendrocyte protein
mTEC	medullary thymic epithelial cells
mTOR	mammalian target of rapamycin
NFAT2	transcription factor Nuclear factor of activated T-cells
NGS	Normal Goat Serum
NK cell	Natural Killer cell
NP	4-Hydroxy-3-nitrophenylacetyl
Nrp-1	Neuropilin 1
OCT	Optimum Cutting Temperature
PAMP	Pathogen Associated Molecular Patterns
PBS	Phosphate Buffered Saline
PD-1	Programmed cell Death Protein 1
PFA	Paraformaldehyde
PI3K	Phosphatidylinositide 3-kinase
PLP	periodate-lysine-paraformaldehyde
PRR	Pathogen Recognition Receptor
PTEN	Phosphatase and tensin homolog
RAG	Recombination-Activating Gene
RFP	Red Fluorescent Protein
Rorγt	RAR-related orphan receptor gamma t
s.c.	Subcutaneous
S1PR(2)	Sphingosine-1-Phosphate Receptor (2)
SAP	Slam-Associated Protein
SE	Super-Enhancer
SHM	Somatic hyper-mutation

SP	Single Positive
SRBC	Sheep Red Blood Cells
STAT	Signal Transducer and Activator of Transcription
TBE	Tris/Borate/EDTA
Tbet	T-box transcription factor 21
TCF1	T Cell Factor 1
TCR	T cell Receptor
Tgfβ	Transforming growth factor beta
Th-Pok	Th inducing POZ-Kruppel Factor
TMB	3,3',5,5'-Tetramethylbenzidine
Treg cells	Regulatory T cells
TSA	Tissue Specific Antigen
tSNE	t-Distributed Stochastic Neighbor Embedding
WT	Wild-type
YFP	Yellow Fluorescent Protein

TABLE OF CONTENTS

Summary ..... **i**

Acknowledgements ..... **iii**

Declaration ..... **iv**

Table of acknowledgement of assistance received during course of thesis ..... **v**

List of Publications ..... **vii**

List of Tables ..... **viii**

List of Figures ..... **ix**

List of Abbreviations and Acronyms ..... **xii**

table of contents ..... **xv**

1 Introduction **1**

1.1 Innate and adaptive immunity at a glance 1

1.2 $CD4^+$ T cell development, activation and differentiation 3

1.2.1 $CD4^+$ T cell development 3

1.2.1.1 Notch signalling-dependent T cell development 4

1.2.1.2 TCR-dependent T cell development 4

1.2.1.2.1 Positive and negative selection 5

1.2.1.2.2 CD4/CD8 lineage commitment 5

1.2.1.2.3 Negative selection of autoreactive T cells 6

1.2.1.2.4 Thymic egress 6

1.2.2 Treg cell development 8

1.2.2.1 The transcription factor Foxp3 directs Treg cell identity 8

1.2.2.2 Thymic Treg differentiation 9

1.2.2.3 Peripheral Treg differentiation 10

1.2.3 $CD4^+$ T cell activation and differentiation 11

1.2.3.1 CD4 T cell differentiation 12

1.2.3.1.1 Conventional CD4 T cell differentiation 12

1.2.3.1.2 Treg differentiation 14

1.3 B Cell development, activation and differentiation 15

1.3.1 B cell development in the bone marrow 16

1.3.2 B cell activation: T-dependent vs T-independent 17

1.4 T-dependent B cell responses 18

1.4.1 B cell activation by protein antigens 18

1.4.2 The Extra-follicular antibody response 18

1.5 The GC response 19

1.5.1 Tfh cell differentiation 19

1.5.2 Tfh cell function 21

1.5.3 Control of the GC by $Foxp3^+$ Treg cells 21

1.6 Follicular regulatory T (Tfr) cells 22

1.6.1 Discovery 22

1.6.2 Origin 23

1.6.3 Differentiation and maintenance of Tfr cells 24

1.6.3.1 Negative regulators of Tfr cell differentiation 26

1.6.4 Tfr cell Function 27

1.6.5 Do Tfr cells function in an antigen-specific manner? 29

1.7 Conclusions and outstanding questions 32

2 Materials and Methods 33

2.1 Mice 33

2.1.2 Tamoxifen administration 36

2.2 Generation of bone-marrow chimeric mice 36

2.3 Immunisations and infections 37

2.3.1 NP-KLH immunisations 37

2.3.2 SRBC immunisations 37

2.3.3 Influenza A infections 37

2.4 Flow cytometry 38

2.4.1 Antibodies 38

2.4.2 Cell preparation 43

2.4.3 Staining procedure 44

2.4.3.1 Surface staining 44

2.4.3.2 Intra-cellular staining 44

2.4.4 Analysis 44

2.5 In-depth phenotyping of *Bcl6*$^{fl/fl}$*Cd4*$^{cre/+}$ mice by high-paramater flow cytometry 45

2.5.1 tSNE analysis 45

2.5.1.1 Spleen and thymus: Foxp3^{+}CD4^{+} cells 45

2.5.1.2 Spleen and thymus: All cells 46

2.5.1.3 Spleen: Foxp3^{-}CD4^{+} 46

2.5.1.4 Thymus: Foxp3^{-}CD4^{+} 46

2.6 Trans-well migration essay 47

2.7 PCR-based genotyping 47

2.8 Gene expression analysis by high-throughput RT-qPCR 51

2.9 RNA-Seq analysis 56

2.10 ELISA 57

2.10.1 NP-ELISA 57

2.11 Confocal imaging 57

2.11.1 Preparation of frozen tissue and cryo-sectioning 57

2.11.2 Immunofluorescence staining 58

2.11.3 Imaging and analysis 58

2.12 Bcl6 motif analysis 59

2.13 Statistical analysis 59

3 Validation of *Cxcr5$^{fl/fl}$Foxp3^{cre}* mice as a follicular regulatory T cell-deficient mouse model 60

3.1 Background 60

3.1.1 Treg homing to the GC 61

3.1.2 *In vivo* models to study Treg cells within the GC 61

3.2 Results 63

3.2.1 Deletion of CXCR5 on Treg cells in *Cxcr5$^{fl/fl}$Foxp3^{cre} mice* after SRBC immunisation 63

3.2.2 *Cxcr5$^{fl/fl}$Foxp3^{cre}* mice show normal numbers of GC B cells and Tfh cells 65

3.2.3 *Cxcr5$^{fl/fl}$Foxp3^{cre}* mice show normal plasma cell responses after re-challenge 67

3.2.4 *Cxcr5$^{fl/fl}$Foxp3^{cre}* mice show non-specific deletion of CXCR5 74

3.2.5 Treg cells are still present in the GC of *Cxcr5$^{fl/fl}$Foxp3cre* mice, albeit in reduced numbers 77

3.2.6 *Cxcr5$^{fl/fl}$Cd4$^{cre/+}$* mice show a normal GC response 80

3.3 Discussion 85

4 *Cxcr5$^{fl/fl}$Foxp3$^{cre-ERT2}$* mice show a reduction, but not a complete absence of follicular regulatory T cells 87

4.1 Background 87

4.2 Results 88

4.2.1 Specific deletion of CXCR5 in Foxp3^{+} Treg cells in *Cxcr5$^{fl/fl}$Foxp3$^{cre-ERT2}$* mice 88

4.2.2 *Cxcr5$^{fl/fl}$Foxp3$^{cre-ERT2}$* mice show a reduced proportion, but not complete absence of Tfr cells within the GC 91

4.2.3 *Cxcr5$^{fl/fl}$Foxp3$^{cre-ERT2}$* mice do not show a reduction in antigen-specific B cells 94

4.2.5 *Cxcr5$^{fl/fl}$Foxp3$^{cre-ERT2}$* mice show normal 'long-term' immune responses 97

4.2.6 Gene-expression profiling of Tfr cells 102

4.3 Discussion 109

5 Do CXCR4 and CXCR5 act redundantly in follicular regulatory T cells? 111

5.1 Background 111

5.2 Results 113

5.2.1 Validation of the *Cxcr4$^{fl/fl}$Foxp3$^{cre-ERT2}$* mouse model 113

5.2.2 *Cxcr4$^{fl/fl}$Foxp3$^{cre-ERT2}$* mice have normal GC responses 121

5.2.3 *Cxcr4$^{fl/fl}$Foxp3$^{cre-ERT2}$* mice show normal plasma cell numbers and antibody production 124

5.2.4 Validation of the *Cxcr4$^{fl/fl}$Cxcr5$^{fl/fl}$Foxp3$^{cre-ERT2}$* mouse model 127

5.2.5 The germinal centre response in *Cxcr4$^{fl/fl}$Cxcr5$^{fl/fl}$Foxp3$^{cre-ERT2}$* mice 132

5.2.6 *Cxcr4*$^{fl/fl}$*Cxcr5*$^{fl/fl}$*Foxp3*$^{cre\text{-}ERT2}$ mice show normal plasma cell numbers and antibody production 137

5.3 Discussion 140

6 The role of Bcl6 in regulatory T cell development 142

6.1 Introduction 142

6.1.1 Bcl6 directs gene expression of cells within the GC, and outside of the GC 142

6.1.2 Transcriptional mechanism of Bcl6 143

6.1.2.1 Bcl6 structure 143

6.1.3 The balanced expression of Tbet and Bcl6 drives Th1/Tfh differentiation 145

6.2 Results 146

6.2.1 *Bcl6*$^{fl/fl}$*Cd4*$^{cre/+}$ mice show a cell-intrinsic increase in Tbet expression in Treg cells in the absence of infection 146

6.2.2 Thymic Treg cells are highly activated in *Bcl6*$^{fl/fl}$*Cd4*$^{cre/+}$ mice 152

6.2.3 Does Bcl6 control the development or functional differentiation of Treg/Tconv cells? 157

6.2.4 In-depth phenotyping of *Bcl6*$^{fl/fl}$*Cd4*$^{cre/+}$ mice by high-parameter flow cytometry 166

6.2.5 GATA3 is highly up-regulated at the DP stage in thymus in *Bcl6*$^{fl/fl}$*Cd4*$^{cre/+}$mice 178

6.2.6 Potential role of Bcl6 in regulating Treg cell super-enhancer genes 181

6.3 Discussion 183

7 Discussion 185

7.1 Generating a Tfr-deficient mouse model 185

7.1.1 Potential redundant mechanisms for Treg cell access to the germinal centre 187

7.1.2 What is the function of Tfr cells within the GC? 188

7.1.3 Final remarks 189

7.2 The transcription factor Bcl6 shapes early thymic Treg development 190

7.2.1 Potential mechanisms for Bcl6 mediated control of thymic Treg cell development 190

7.2.2 Functional relevance 192

7.2.3 Final remarks 193

8 References 194

1 Introduction

1.1 Innate and adaptive immunity at a glance

The immune system is the host's defence mechanism against pathogens. In vertebrates, the immune system consists of two distinct but closely intertwined components: innate immunity and adaptive immunity. The innate immune system is the most ancient part of the immune system providing a fast and immediate first-line defence against pathogens (Hoffmann et al., 1999). Cells of the innate immune system include, but are not limited to, dendritic cells (DCs), macrophages and mast cells. Innate immune cells express germline-encoded pattern-recognition receptors (PRRs) that are triggered by recognition of evolutionary conserved molecular structures on pathogens referred to as Pathogen Associated Molecular Patterns (PAMPs), such as lipopolysacharides, glycolipids, lipoproteins and nucleic acids. Recognition of PAMPs by PRRs leads to inflammatory responses and innate host defence responses (Janeway, 1989, Janeway and Medzhitov, 2002, Medzhitov and Janeway, 2002). In addition, sensing of microbes by PRRs on antigen-presenting cells (APCs), in particular DCs, leads to activation of the adaptive immune system, linking innate and adaptive immunity (Janeway, 1989, Banchereau and Steinman, 1998).

The adaptive immune system is, in the context of evolution, a relatively novel system and only exists in vertebrates (Litman et al., 2010). After pathogen encounter, the effector mechanisms of the adaptive immune system take several days to be established. The adaptive immune response can mature without compromising host defence due to the innate system acting as the first line of protection (Medzhitov and Janeway, 2000). T and B lymphocytes are the key effector cells in adaptive immunity. T and B cells are characterised by the expression

of unique antigen-binding receptors on the cell surface that are able to distinguish discrete antigenic epitopes.

T and B cells develop from bone marrow-derived common lymphoid precursor cells. Whereas B cells complete their development in the bone marrow, T cell precursors migrate to the thymus and complete their maturation there. Early B and T cells undergo maturation and genetic rearrangement to give rise to immature lymphocytes each with different antigen receptors. The discovery of V(D)J recombination shed light on how such a diverse repertoire in lymphocyte receptors could be accomplished (Tonegawa, 1983). VDJ recombination is the process of genetic recombination of gene segments in lymphocytes and involves the random association between the Variable (V), Joining (J) and Diversity (D) segments. The Recombination Activation Genes, *RAG1* and *RAG2,* mediate this genetic re-shuffling by initiating double strand breaks and their subsequent joining (Schatz and Swanson, 2011). This process generates an immensely diverse receptor repertoire resulting in a pool of T and B cells with unique receptors that bind specific epitopes (antigenic determinant or small part of the antigen that is recognised). These receptors can be specific for anything, from bacterial antigens to synthetic chemicals, as well as self-antigens. The complex process of genetic recombination requires that the antigen receptors of these lymphocytes need to be tested throughout development to ensure that lymphocytes bearing antigen receptors that recognise self-antigens, or bind the antigen with too high affinity or too low affinity, are deleted (negative selection). Lymphocytes with intermediate affinity receptors receive survival signals (positive selection) and exit the bone-marrow or thymus to enter circulation (Nemazee, 2000).

B and T cell activation by antigen engagement in the periphery results in selection and subsequent clonal expansion of that particular lymphocyte. This ultimately leads to a repertoire of clones, bearing the same antigen-specific surface receptor. B cells mediate humoral immunity in the adaptive immune system and are able to bind free antigen through their B cell receptor (BCR), resulting in activation and differentiation into effector cells. B cells also differentiate into plasma cells that secrete antibodies in order to neutralise antigens, or mark them for destruction by innate cells such as macrophages. T cells facilitate cell-mediated immunity and, unlike B cells, require Major Histocompatibility Complex (MHC) engagement via their T cell Receptor (TCR) for their activation and differentiation into effector cells. After the pathogen or antigenic insult is cleared most lymphocytes die. However, a few remain as memory cells, thereby establishing long-lasting, antigen-specific,

immunological memory. This is a key aspect of adaptive immunity that protects the host against future infections and forms the basis of successful immunisation (Litman et al., 2010).

The generation of adaptive immune responses has been a huge leap forward in the evolution of the immune system. Nevertheless, adaptive and innate immunity act sequentially, with the innate immune system providing immediate pathogen clearance and adaptive immunity providing immunological memory. Therefore, these two branches of the immune system should not be regarded as independent, as communication between both is essential to mount a successful immune response (Janeway, 1989).

1.2 $CD4^+$ T cell development, activation and differentiation

T cell development is a multistage and multifactorial process: T cell progenitors originate in the bone marrow or fetal liver and migrate to the thymus where they integrate a variety of cues to enable a T cell fate. T cell development results in the generation of intraepithelial lymphocytes, γδT cells (expressing γ and δ T cell receptor chains), and αβ T cells (expressing α and β T cell receptor chains). The αβ T cell population includes $CD4^+$ conventional T cells (Tconv) and $CD4^+$ regulatory T cells (Treg), $CD8^+$ cytotoxic T cells and Natural Killer T cells. This thesis will focus on the development, differentiation and function of $CD4^+$ αβ T cells. After completing development in the thymus, mature $CD4^+$ αβ T cells migrate to the periphery where exposure to their cognate antigen results in their differentiation into specialised subsets. $CD4^+$ T cells are central players in the adaptive immune system for both cellular and humoral immune responses against a variety of pathogens.

The thymus is a unique microenvironment that supports T cell development and consists of several lobules that have two major areas; the cortex and the medulla. Immature thymocytes reside in the cortical areas, and more mature thymocytes can be found in the medulla (Figure 1.1).

1.2.1 $CD4^+$ T cell development

T cell development from thymic entry to the expression of a fully functional TCR can broadly be divided in a Notch-dependent stage and a TCR-dependent stage. I will discuss these two stages below.

1.2.1.1 Notch signalling-dependent T cell development

T cell progenitors homing to the thymus are not T-cell lineage committed, and do not express a TCR, or CD4 or CD8, characteristic for most T cells, and are referred to as double negative cells (DN). DN cells go through several progressive stages; DN1 (containing Early Thymic Progenitors), DN2a, DN2b, DN3a, DN3b and DN4, based on the expression of c-Kit, CD44 and CD25 (Rothenberg et al., 2010).

The earliest phase of T cell development is characterised by cell proliferation in response to cytokine signals, expansion of the precursor T cell population and the acquisition of typical T cell characteristics. T cells rapidly proliferate at this stage and retain their multi-potency (Yui and Rothenberg, 2014). Commitment to the T cell lineage is driven by the evolutionary-conserved Notch signalling pathway, and Notch-1 determines whether a lymphoid precursor commits to the T cell lineage or B cell lineage (Radtke et al., 1999). TCF-1 is an essential mediator of Notch signalling and induces T cell commitment and specification through induction of GATA-binding protein 3 (GATA3) and B-cell CLL/lymphoma 11b expression (Weber et al., 2011). T cells rapidly proliferate at this stage and retain their multi-potentiality (Yui and Rothenberg, 2014). Notch signalling remains crucial for T cell commitment throughout the entire DN1 to DN3 progression (Rothenberg et al., 2010).

The DN2 stage is marked by progressive T cell lineage commitment: while DN2a cells retain the potential to differentiate into DCs and NK cells, DN2b cells are committed to the T cell lineage (Rothenberg et al., 2010). TCR γ, δ and β gene rearrangement occurs during the DN2 stage. DN2a to DN2b transition marks commitment to the T cell lineage and from this point onwards all other developmental stages are closed off (Yui and Rothenberg, 2014). Successful β selection, *i.e*. the successful signalling through the rearranged pre-TCR composed of the rearranged β chain and a pre-α chain, eliminates the requirement of Notch signalling for T cell survival and proliferation, and allows the cells to pass a differentiation and proliferation checkpoint, the β-selection checkpoint, imposed at DN3a (Winandy et al., 1999, Barndt et al., 2000, Engel and Murre, 2004)(Figure 1.1).

1.2.1.2 TCR-dependent T cell development

Successful transition of the T cell precursor through the β-selection checkpoint (DN3a-DN3b), results in maturation into highly proliferative DN4 thymocytes. These DN4 cells start migrating in the direction of the thymic medulla and mature into $CD4^+CD8^+$ double positive (DP) thymocytes. Subsequent rearrangement of the TCR α locus, results in expression of a

fully mature TCRα chain that will associate with the TCR β chain. Once DP thymocytes express the αβ TCR, they are subjected to strict selection pressures and only those DP thymocytes with a functional TCR that either recognises peptides presented by MHCI or MHCII, will survive the selection process (Figure 1.1).

1.2.1.2.1 Positive and negative selection

Positive selection is the process by which $CD4^+CD8^+$ DP thymocytes that express a TCR able to recognise self-peptide:MHC complexes, can continue their maturation into $CD4^+$ SP or $CD8^+$ SP thymocytes. Positive selection ensures the survival of αβ T cells that can successfully interact with the host's MHC molecules. Positive interaction only takes place when the TCR binds the MHC-peptide complex with low to intermediate affinity (2-5% of DP cells). Over 90% of DP cells express a TCR that does not recognise peptide-MHC complexes, and these DP will undergo 'death by neglect" (Surh and Sprent, 1994). Alternatively, those thymocytes expressing a TCR that binds the peptide-MHC complex with high affinity, and are conducive for autoimmunity due to their auto-reactive nature, will undergo negative selection (Figure 1.1).

1.2.1.2.2 CD4/CD8 lineage commitment

How CD4/CD8 lineage commitment occurs after positive selection was a matter of intense debate for many years (Singer, 2002). It is now clear that regardless of the MHC specificity, TCR signalling after positive selection converts DP thymocytes into $CD4^+CD8^-$ intermediate thymocytes by default. These $CD4^+CD8^-$ intermediate thymocytes are characterised by *Cd8* gene repression and up-regulation of the transcription factor Thymocyte Selection- Associated High Mobility Box (TOX) regardless of TCR signalling in the context of MHCI or MHCII (Brugnera et al., 2000, Singer, 2002). TOX maintains CD4 transcription, giving rise to $CD4^+$CD8lo Thymocytes. In Class-II restricted thymocytes, TCR signalling continues and results in the up-regulation of GATA3 and Th inducing POZ-Kruppel Factor (Th-Pok), which drives CD4 lineage commitment (Hernandez-Hoyos et al., 2003, Sun et al., 2005). When thymocytes are Class-I restricted, TCR signalling will cease, resulting in the loss of GATA3 and Th-Pok expression, and up-regulation of the transcriptional regulator Runx3 and an increase in IL-7R signalling (Yu et al., 2003, Kohu et al., 2005, Liu et al., 2005). Runx3 silences Th-Pok expression and represses CD4-lineage potential, while initiating CD8 expression (Brugnera et al., 2000, Taniuchi et al., 2002, Setoguchi et al., 2008).

1.2.1.2.3 Negative selection of autoreactive T cells

Positive selection induces C-C chemokine receptor type 7 (CCR7)-dependent migration from the cortex to the medulla, where a second round of negative selection takes place and TCRs are tested for the recognition of self-antigen (Witt and Robey, 2004). Medullary thymic epithelial cells (mTECs) express the transcription factor autoimmune regulator (AIRE). AIRE induces the ectopic expression of tissue specific antigen (TSA), which are proteins usually expressed in peripheral tissues (Anderson et al., 2002, Derbinski et al., 2005, Sansom et al., 2014). mTECs present these TSAs via MHCII to the $CD4^+$ SP cells. $CD4^+$ SP cells that do not recognise these TSAs will survive and contribute to the mature CD4 T cell pool (Anderson and Su, 2016). $CD4^+$ SP thymocytes with a TCR that binds these TSAs will either undergo negative selection and die, or, alternatively, develop into $Foxp3^+$ Treg cells (Figure 1.1) (Jordan et al., 2001). In the absence of AIRE, this second round of negative selection is limited and this consequently results in the development of multi-organ autoimmune disease (Liston et al., 2003, Anderson et al., 2005, DeVoss et al., 2006).

1.2.1.2.4 Thymic egress

T cell development in the thymus ultimately results in the production $CD4^+$ Tconv cells and Treg cells that exit the thymus via the circulation in a Sphingosine 1-phosphate receptor 1 (S1PR1)-dependent manner, and migrate to the periphery (Figure 1.1) (Pappu et al., 2007). These newly developed $CD4^+$ T cells are referred to as recent thymic emigrants, which are immature and undergo final functional maturation into naïve $CD4^+$ T cells in peripheral lymphoid organs (Fink, 2013).

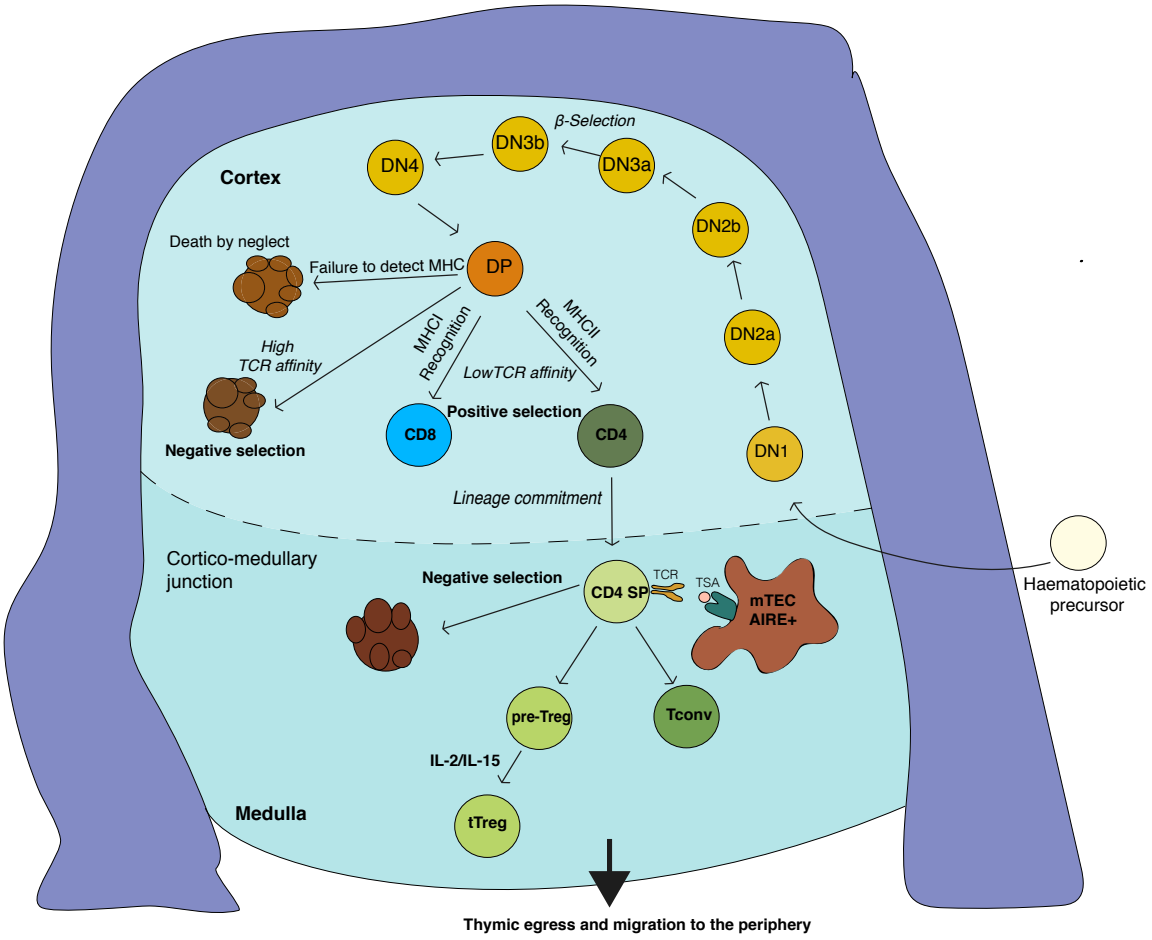


Figure 1.1 Overview of T cell development in the thymus.

T cells develop from haematopoietic precursors originating from the bone marrow or foetal liver. T cell precursors homing to the thymus lack a TCR and do not express CD4 or CD8; because of this they are called double-negative (DN) cells. DN cells can be further subdivided in at least 4 stages: DN1, DN2 (DN2a- DN2b), DN3 (DN3a-DN3b) and DN4. The DN2 stage is marked by rearrangement of the TCR β chain. The rearranged TCR β chain associates with a surrogate α chain to form the pre-TCR. Successful signalling through this pre-TCR results in cell proliferation and progression to the DN4 stage. DN4 cells subsequently migrate closer to the medulla and mature into $CD4^{+}CD8^{+}$ DP cells. Subsequent rearrangement of the TCR α-chain results in the formation of a complete αβ TCR. DP thymocytes that have a TCR that can engage MHCII with intermediate affinity will differentiate into a CD4-committed DP thymocyte and undergo positive selection, and will migrate to the medulla. Those DP thymocytes that fail to recognise MHC will undergo delayed apoptosis (death by neglect), whereas those that bind MHC with high-affinity will undergo negative selection. After CD4 commitment, CD4 SP T cells undergo a second round of selection in the medulla. Here CD4 SP T cells are tested for recognition of self-antigen. Medullary thymic epithelial cells (mTECs) present tissue specific antigens (TSA) on MHCII molecules. Failure of the CD4 T cells to engage their TCR with these TSA:MHCII results in survival of the CD4 T cell and egress from the thymus as a mature conventional CD4 Tconv cells. Those CD4 T cells that bind TSA:MHCII with high affinity will undergo negative selection, whereas TSA:MHCII with intermediate affinity will result in differentiation of the CD4 SP into a pre-Treg. After TCR signalling, IL-2/IL-15 signalling results in the upregulation of Foxp3 and differentiation into a thymic Treg (tTreg) cell

1.2.2 Treg cell development

Some of the self-reactive thymic $CD4^+$ T cells that do not undergo negative selection in the thymus and express Foxp3, become thymic Treg cells. These $Foxp3^+$ Treg cell are essential for maintaining immunological tolerance (Sakaguchi et al., 2008). Treg cells that develop in the thymus are referred to as thymic Treg (tTreg) cells (Hsieh et al., 2012, Abbas et al., 2013). In addition to tTreg cells, recent thymic emigrants can switch on Foxp3 expression, or non-Treg $CD4^+$ T cells can switch on Foxp3 expression in the periphery, and these are referred to as peripheral Treg (pTreg) cells (Paiva et al., 2013, Liston and Gray, 2014). pTreg are important in the establishment of tolerance against commensal bacteria, food and allergens and are enriched in specific organs exposed to these environmental cues, such as the gut (Hadis et al., 2011, Josefowicz et al., 2012). Finally, Treg cells can be generated *in vitro* in the presence of transforming growth factor β and other stimuli, are referred to as iTreg cells (Abbas et al., 2013). The mechanisms involved in development and differentiation of these three Treg subsets are different. This thesis will focus on the development of tTreg cells and I will briefly touch on pTreg cells.

1.2.2.1 The transcription factor Foxp3 directs Treg cell identity

The discovery of the X-chromosome encoded transcriptional regulator Foxp3 as the transcription factor essential for Treg cells allowed Treg cells to be considered as a separate cell lineage, and facilitated studying the ontogeny of these cells (Fontenot et al., 2003, Hori et al., 2003, Khattri et al., 2003). Mutations in the *Foxp3* gene that abrogate Treg cell development, result in severe multi-organ auto-inflammatory disease (Fontenot et al., 2003, Hori et al., 2003, Khattri et al., 2003). In humans, mutations in *FOXP3* lead to immune dysregulation, polyendocrinopathy, enteropathy, X-linked (IPEX) syndrome, which is characterised by severe systemic autoimmunity. Similarly, deficiency of Foxp3 in mice (first described as "scurfy" mice) leads to unrestrained T cell and humoral immune responses, in the absence of immunisation or infection (Fontenot et al., 2003, Hori et al., 2003, Chung et al., 2011). Furthermore, Foxp3 expression is sufficient to convert a CD4 Tconv cell into a suppressive Treg-like cell (Hori et al., 2003). Thus, the transcription factor Foxp3 delineates Treg cells and is necessary for Treg function.

The *Foxp3* promoter has limited transcriptional activity and expression of Foxp3 is reliant on the expression of three conserved non-coding regulatory sequences (CNS1-3) in the *Foxp3* locus (Mantel et al., 2006, Zheng et al., 2010). These cis-regulatory elements regulate the size,

maintenance and composition of the Treg population (Zheng et al., 2010). CNS1 controls peripheral, but not thymic, induction of Foxp3 by acting as a TGF-β sensor, important for pTreg cells (Zheng et al., 2010, Toker and Huehn, 2011) (see 1.2.2.3). CNS2 is important for Foxp3 expression in the progeny of dividing cells, and maintains Foxp3 expression in mature Treg cells (Zheng et al., 2010, Sakaguchi et al., 2013, Feng et al., 2014). CNS2 is enriched with CpG motifs, which are specifically demethylated during thymic Treg development (Floess et al., 2007). Whereas the CNS2 in Tconv is fully methylated, Treg cells acquire a specific DNA hypomethylation pattern. The CNS2 in Treg cells is therefore referred to as the Treg cell-specific demethylated region (TSDR) (Baron et al., 2007, Huehn et al., 2009). This epigenetic feature is essential for stable Treg cell specific gene expression patterns and Treg cell lineage commitment, and helps to maintain Foxp3 expression (Floess et al., 2007). Finally, CNS3 is a pioneer element for Treg cell development in the thymus (Zheng et al., 2010). CNS3 regulates *de novo Foxp3* expression and facilitates opening of the *Foxp3* locus in Treg cells precursors prior to selection, thereby increasing Foxp3 expression. The permissive H3K4me1 modification of histone H3, is enriched at the CNS3 from the DN1 stage, indicating that the CNS3 is in a poised state from a very early stage during T cell development (Feng et al., 2015). However, CNS3 is not required for Treg cell maintentance. CNS3-mediated epigenetic regulation of the Foxp3 promotor results in a more diverse TCR repertoire, essential for control of auto-reactive T cells escaping negative selection (Feng et al., 2015). Recently, a novel CNS, CNS0, was discovered that acts as a pioneering element essential for the initiation of Treg commitment. CNS0 is subsequently required for the activities of the other CNS elements that leads to Foxp3 expression (Kitagawa et al., 2017).

1.2.2.2 Thymic Treg differentiation

The first evidence showing that Treg cells develop in the thymus came from thymectomy experiments, where removal of the thymus on day 3, but not on day 7 after birth, results in spontaneous autoimmunity (Nishizuka and Sakakura, 1969). 30 years later, a subset of suppressive $CD25^{+}CD4^{+}$ T cells that mediate self-tolerance were discovered and named Regulatory T (Treg) cells (Asano et al., 1996). Transfer of these Treg cells into thymocetomised mice was able to prevent the spontaneous autoimmunity, demonstrating that thymic-derived Treg cells are essential for self-tolerance (Asano et al., 1996, Fontenot et al., 2005a). Furthermore, mature naïve Treg cells can be found in the periphery from day 4 after birth.

Self-reactivity drives the thymic Treg developmental pathway and Treg cell selection occurs when a TCR recognises self-antigen with higher affinity than that required for positive selection of Tconv cells (Maloy and Powrie, 2001, Moran et al., 2011). Furthermore, the $Foxp3^+$ Treg TCR repertoire overlaps to a large extent with that of auto-reactive T cells in Foxp3-deficient mice, rather than with that of naïve T cells (Hsieh et al., 2006, Pacholczyk et al., 2006).

Thymic Treg differentiation requires a two-step process involving TCR signalling to instruct thymocytes to become a pre-Treg, as well as signalling through the common γ chain cytokine receptor, which binds IL-2, IL-15 and IL-7 (Burchill et al., 2008, Lio and Hsieh, 2008, Vang et al., 2008). IL-2 signalling in particular is instrumental for Treg cell development. High-affinity TCR-MHCII interactions induce CD25 (the interleukin 2 receptor α chain (IL-2Rα)) expression on the pre-Treg, which together with CD122 (β chain) and the common γ chain make up the high-affinity heterotrimeric IL-2 receptor (Malek and Castro, 2010, Moran et al., 2011). IL-2 signalling activates the transcription factor signal transducer and activator of transcription (STAT) 5, which induces Foxp3 expression in developing $Foxp3^-CD25^+$ pre-Treg allowing them to differentiate into fully functional $Foxp3^+$ Treg cells (Furtado et al., 2002, Malek et al., 2002, Fontenot et al., 2005b, Burchill et al., 2007, Yao et al., 2007). Notably, despite their dependence on IL-2 signalling for growth and survival, Treg cells are incapable of autocrine production of IL-2 due to chromatin inaccessibility of the *Il2* locus in Treg cells (Su et al., 2004). In addition to TCR signalling, Treg cell development requires co-stimulatory signalling through CD28 to initiate the Treg differentiation program, and this is followed by CD27-CD70 interactions in the thymic medulla to prevent apoptosis (Tai et al., 2005, Coquet et al., 2013, Cowan et al., 2013).

To summarise, Treg development is dependent on a TCR-instructive step as well as appropriate TCR affinity, the appropriate cytokine environment, and co-stimulatory signals. Despite the fact that significant progress in understanding thymic Treg cell development has been made in the last decade, there are still many unanswered questions that need to be addressed. Which transcriptional mechanisms are involved in bifurcation between Tconv and Treg cells is one such question.

1.2.2.3 Peripheral Treg differentiation

The differential requirement for CNS1 in pTreg and tTreg suggests that these two types of Treg cells might have different origins. In peripheral tissues such as the gut, lungs and skin,

pTreg and tTreg often coexist. Despite reports suggesting neuropilin 1 (Nrp-1) and Helios as appropriate tTreg markers, there is no consensus in the literature as to whether these are genuine and exclusive markers for tTreg (Thornton et al., 2010, Weiss et al., 2012, Yadav et al., 2012).

Due to the current limitations in distinguishing between tTreg and pTreg in the periphery *in vivo*, the requirements for the generation of pTreg remain enigmatic. It is clear that TCR signalling and IL-2 are essential for both tTreg and pTreg (Yadav et al., 2013). Chronic exposure to low dose antigen supports the generation of pTreg *in vivo* (Apostolou and von Boehmer, 2004). $CD103^+$ DCs residing at gut-associated mucosal tissues, support the differentiation of pTreg cells from $Foxp3^-$ precursors through TGFβ and retinoic acid production (Benson et al., 2007, Coombes et al., 2007, Sun et al., 2007). Differentiation of peripheral Treg cells occurs in response to non-self antigens such as food antigens and commensal microbiota (Yadav et al., 2013). pTreg cells are therefore considered essential for immunologic tolerance at mucosal sites in direct contact with environmental antigens such as the gut and lungs (Josefowicz et al., 2012). In addition, the use of Incomplete Freud's Adjuvant (IFA) preferentially induces pTreg cells (Korn et al., 2008). Nevertheless, until the roles for tTreg and pTreg can be dissected *in vivo,* it is difficult to draw firm conclusions about the relative roles of Treg cells of different developmental origins.

1.2.3 $CD4^+$ T cell activation and differentiation

Naïve $CD4^+$ Tconv cells and Treg cells generated in the thymus, express CCR7 and CD62L, allowing them to circulate through secondary lymphoid organs where they can scan APCs. If a naïve $CD4^+$ T cell does not engage with any peptide-MHCII complexes, it exits the lymph node (LN) and joins the circulation. If a naïve T cell encounters an APC bearing its cognate antigen, it requires a minimum of two signals to be activated: peptide:MHCII molecules interacting with the TCR (signal 1) and positive co-stimulatory signalling, typically through CD28 expressed on the CD4 T cell and CD80/86 expressed on the APC (signal 2), which enhances TCR signalling (Ni and O'Neill, 1997). The culmination of TCR signalling and co-stimulation results in robust IL-2 production and secretion, an autocrine factor that stimulates the CD4 T cells to proliferate. IL-2 can also act as a paracrine factor, stimulating other cells in the vicinity such as Treg cells (Chinen et al., 2016). Similar to $CD4^+$ Tconv cells, $Foxp3^+$ Treg cells require TCR signalling as well as co-stimulatory signalling through CD28 to be

activated (Zhang et al., 2013a, Levine et al., 2014, Vahl et al., 2014). In addition, they require IL-2 for their survival (Chinen et al., 2016).

The requirement for co-stimulatory signals provided by an APC, in particular dendritic cells (DCs) during the early stage of the immune response, links the innate and adaptive immune system. DCs capture, process and present protein antigen to T cells via MHC molecules (Steinman and Idoyaga, 2010). Immature DCs reside in peripheral tissues where they scan the environment for pathogens. Pathogen recognition via PRR results in activation of the DC and migration to secondary lymphoid organs, where they complete their maturation process (Steinman and Witmer, 1978, Schnare et al., 2001). DC maturation induces the upregulation of MHCII complexes in the endocytic system and increases the display of peptide fragments (antigen) on MHCII complexes on the cell surface. DC maturation also results in the expression of the co-stimulatory molecules CD80 and CD86 on the cell surface, and potentiates the secretion of cytokines (Inaba et al., 2000). Thus, DCs that have not been activated by a pathogenic insult will not express significant amounts of co-stimulatory molecules on their surface, and will therefore not be able to activate naïve CD4 T cells. Furthermore, TCR interaction with peptide expressed on an immature DC, and consequently in the absence of co-stimulatory signals, results in T cell anergy, a state in which the $CD4^+$ Tconv cell is unable to respond to further stimuli. This requirement for co-stimulatory signals in the periphery decreases the probability that a self-reactive $CD4^+$ T cell that escaped negative selection in the thymus becomes activated.

In addition to TCR signalling and co-stimulation through CD28, it has become apparent that other signals such as cytokines and other co-stimulatory signals are required to complete T cell activation and drive CD4 T cell differentiation into distinct subsets, suited to the invading pathogen.

1.2.3.1 CD4 T cell differentiation

1.2.3.1.1 Conventional CD4 T cell differentiation

Functional differentiation of naïve T cells into distinct effector subsets requires the integration of a range of external cues such as local cytokines produced by APCs, as well as ligation of cell surface receptors (Walsh and Mills, 2013). This results in the up-regulation of subset-defining transcription factors that drive gene expression profiles that induce specific function, cytokine expression and migration patterns. $CD4^+$ T cell differentiation ultimately generates

effector cells tailored towards eliminating specific pathogens, including T helper (Th)1, Th2, Th17 and T follicular helper (Tfh) cells (Figure 1.2).

Th1 cells are important effector cells in viral infections and defence against other intracellular pathogens; the canonical Th1 cytokine produced is IFN-γ (Paul and Zhu, 2010). Th1 cell differentiation involves STAT1 activation in the presence of IL-12 and IFN-γ, which drives the expression of T-box transcription factor 21 (Tbet), the transcriptional regulator of the Th1 subset (Szabo et al., 2000). IL-12 promotes Th1 differentiation and IFN-γ production through STAT4 (Morinobu et al., 2002). Tbet drives up-regulation of CXC chemokine receptor (CXCR) 3, which promotes migration of Th1 cells to the sites of inflammation (Mullen et al., 2001, Afkarian et al., 2002).

Th2 cells are important in clearance of parasites and other extracellular pathogens through production of IL-4, IL-13 and IL-5 (Paul and Zhu, 2010). IL-4 supports Th2 differentiation through STAT6 and induction of GATA3, the transcriptional regulator of the Th2 subset (Ni and O'Neill, 1997, Litman et al., 2010, Wing et al., 2014).

Th17 cells play an important role in fungal infections, protection against extra-cellular bacteria, and immunity at mucosal surfaces. Th17 cells are characterised by the production of IL-17A, IL-17F and IL-22 (Harrington et al., 2005, Park et al., 2005, Korn et al., 2008). The cytokines IL-6, TGF-β, IL-21 as well as STAT3 have been implicated in driving Th17 differentiation by up-regulating retinoid-orphan receptor gamma (RORγt), the Th17 lineage specific transcription factor (Harrington et al., 2005, Park et al., 2005, Paul and Zhu, 2010, Green et al., 2011, Sage et al., 2014b). RORγt, in turn, drives IL-17 expression (Lee et al., 2015).

Tfh cells are located within the germinal centre (GC) and provide help to B cells to facilitate the production of long-lived plasma cells and memory B cells. IL-6, IL-21 and IL-27 have all been implicated in early Tfh cell differentiation, although none of these seem to be sufficient to initiate Tfh cell differentiation on their own (Vogelzang et al., 2008, Batten et al., 2010, Hiramatsu et al., 2010, Jandl et al., 2017). In addition to cytokines, Tfh cell differentiation requires co-stimulatory signalling though inducible co-stimulator (ICOS) (Choi et al., 2011). Together, these support Tfh cell differentiation by up-regulation of Bcl6, a transcriptional regulator that is required and sufficient for Tfh cell differentiation (Nurieva et al., 2009, Yu et al., 2009). I will elaborate more on the differentiation and function of these cells in section 1.5.

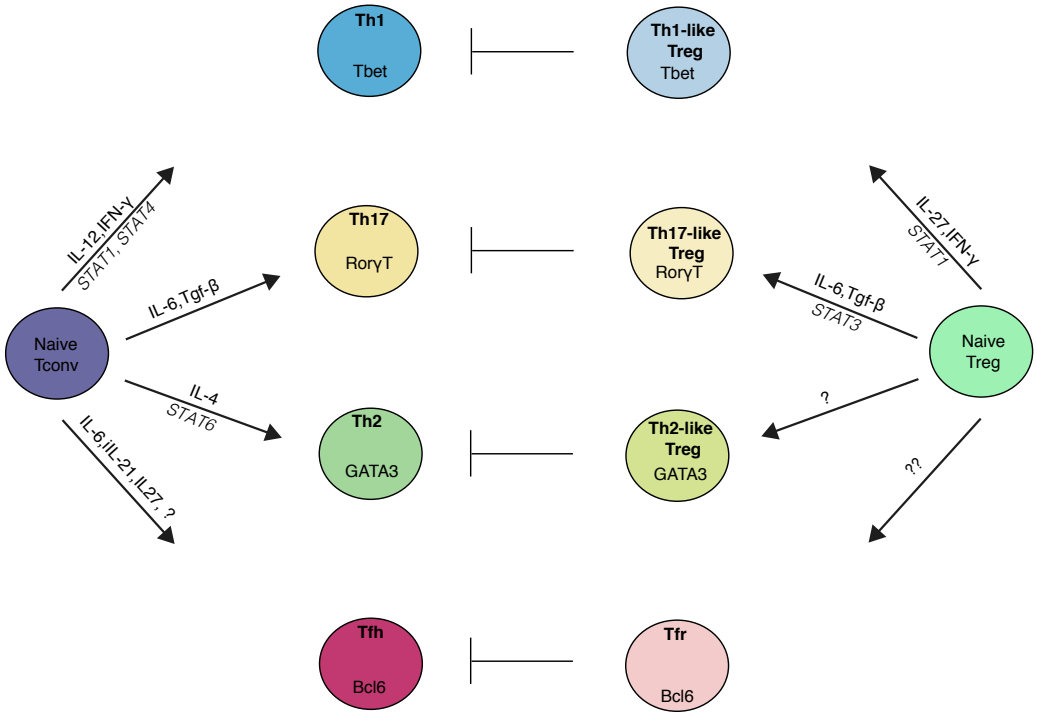


Figure 1.2 Differentiation of CD4$^+$ Tconv cells and Foxp3$^+$ Treg cells.

Differentiation of naïve CD4$^+$ T cells requires the integration of multiple environmental cues, such as polarising cytokines and co-stimulatory signals. These cues support the expression of key transcriptional regulators that drive differentiation. Tbet drives Th1 differentiation, GATA3 drives Th2 differentiation, Rorγt drives Th17 differentiation and Bcl6 drives Tfh differentiation. Under inflammatory conditions, Treg cells can co-opt these transcriptional programs and suppress the Th cell driven inflammatory responses. Adapted from Cretney *et al*, Trends in Immunology, 2013 (Cretney et al., 2013).

1.2.3.1.2 Treg differentiation

The majority of Treg cells reside in the circulation and secondary lymphoid organs. Naïve Treg cells recirculate through secondary lymphoid organs and differentiate into functionally and phenotypically diverse specialised subsets, similar to CD4$^+$ Tconv cells. Upon activation, Treg cells down-regulate CD62L and up-regulate CD44, ICOS, Glucocorticoid-induced TNFR-related protein (GITR), CD69, CD103 and CD38, marking 'effector" Treg cells (Cretney et al., 2013).

Foxp3$^+$ Treg cells can differentiate into several functional states in response to environmental cues, these Treg cell subsets are characterised by expression of specific transcription factors and chemokine receptors classically associated with different helper T (Th) cell subsets. It is

thought that by co-opting the Th differentiation profile they are able localise to the same place as their Tconv cell counterparts, and curtail these specific T helper-driven inflammatory responses (Figure 1.2).

During a Th1-skewed response, Foxp3$^+$ Treg cells up-regulate Tbet in a STAT1-dependent manner, the key transcription factor for Th1 differentiation (Koch et al., 2009, Koch et al., 2012). Tbet expression in Treg cells drives CXCR3 expression, as it does in Th1 cells, and enables these Th1-like Treg cells to migrate towards the site of inflammation where they can specifically regulate Th1 responses. The induction of these CXCR3$^+$Tbet$^+$ Treg cells occurs in an IFN-γ dependent manner, similar to Th1 cells (Koch et al., 2012). Th17 cell-mediated immune responses can be specifically controlled by Treg cells expressing Rorγt and STAT3 (Chaudhry et al., 2009, Yang et al., 2016). Thus, Treg cells are able to phenotypically and functionally diversify, facilitated by transcription factors classically associated with CD4$^+$ Tconv cells, and therefore control a wide-range of immune responses (Cretney et al., 2013). Notably, certain transcription factors associated with specific differentiation pathways play a broader role in Treg cell function. For example, deletion of GATA3, the transcription factor classically associated with Th2 differentiation, in Treg cells does not solely affect control of Th2 responses but results in a more general Treg cell defect with GATA3-deficient Treg cells acquiring the ability to produce Th17 cytokines (Wang et al., 2011). Moreover, GATA3 regulates Foxp3 expression through binding to the *Foxp3* CNS2 locus, and thus plays a role in Treg cell stability (Wang et al., 2011). Mice with a combined deletion of GATA3 and Tbet develop severe early onset autoimmune disease (Yu et al., 2015). These data indicate that these transcription factors do not only play a role during Treg differentiation but are also essential for Treg cell homeostasis.

Together, these findings show that during an immune response, Treg cells can be polarised by adopting similar transcriptional programs as CD4$^+$ Th subsets, allowing for specialised Treg suppression under distinct immunological conditions.

1.3 B Cell development, activation and differentiation

B cells are the central players in humoral immunity. Defects in B cell development or function lead to autoimmunity, malignancies such as acute lymphoblastic Lymphoma and Chronic Myeloid Leukemia, and immuno-deficiencies such as Systemic Lupus Erythematous (Vogler et al., 1978, LeBien and Tedder, 2008, Tobon et al., 2013). After birth, B cells

develop and mature in the bone marrow from haematopoietic precursors. Functional maturation of the B cells occurs in the periphery, in the LNs and the spleen.

1.3.1 B cell development in the bone marrow

In the bone marrow, B cell precursors progress through a number of stages involving initial commitment to the B cell lineage, the primary diversification of their Immunoglobulin (Ig) repertoire, and subsequent negative selection of auto-reactive B cells. The generation of a functional BCR, requires the productive rearrangement of the heavy (H) and, subsequently, light (L) chain Ig genes through RAG1/2-mediated V(D)J recombination. This genetic reshuffling event during B cell development generates a pool of B cells with a broad BCR repertoire, whilst minimising the generation of self-reactive receptors (Tonegawa, 1987).

Early B cell progenitors require IL-7 produced by stromal cells for survival, differentiation and maturation (Corfe and Paige, 2012). In addition, CXCL12 expression by stromal cells is important for CXCR4/CXCL12-mediated interaction of early B cell precursors with the bone marrow micro-environment (Tokoyoda et al., 2004). B cells develop from haematopoietic stem cells, which first give rise to common lymphoid progenitors. Common lymphoid progenitors acquire the expression of B220 and differentiate into pre-pro B cells. Pre-pro B cells start to rearrange the Igμ heavy H chain by recombining the D_H-J_H segment. In the early pro-B cell stage, rearrangement of the D_H-J_H segment is completed. This stage denotes B cell commitment and alternative developmental routes are closed off (Nutt et al., 1999). Next, recombination and joining of the upstream V_H gene segment to the rearranged DJ segment occurs, resulting in the expression of a complete Ig H chain (Cobaleda et al., 2007). The cells subsequently need to go through a pre-B cell checkpoint, where the Igμ H chain is selected for its ability to associate with a surrogate L chain, followed by signalling through this newly generated pre-BCR. If the heavy chain is unable to associate with a surrogate L chain, the cell will undergo apoptosis. Alternatively, signalling through the pre-BCR results in proliferation and successful progression through the first checkpoint. The generation of the pre-BCR marks the onset of the early pre-B-cell stage (Melchers, 2015).

Pre-B cells subsequently start to rearrange their L chain Ig (V_L and J_L) gene segments (Schlissel, 2003). Successful rearrangement of κ or λ L chain genes, results in association of the newly formed L chain with H chain and formation of functional IgM that is expressed on the cell surface. Successful signalling through IgM allows the cell to progress to the immature B cell stage (Herzog et al., 2009, Vettermann and Schlissel, 2010).

As the diversity in BCR specificity is generated by random genetic recombination events, there is a potential risk of generating self-reactive BCRs, which could contribute to the development of autoimmune responses if left uncensored. It is at the immature B cell stage that the newly generated BCR is tested for auto-reactivity. B cells expressing high-affinity, auto-reactive BCRs are negatively selected (Ubelhart and Jumaa, 2015). B cells that have an auto-reactive BCR that recognises membrane-bound antigen with high affinity undergo clonal deletion, a process of BCR-mediated apoptosis (Ubelhart and Jumaa, 2015). The mechanisms involved in generating central tolerance in the bone marrow microenvironment have not been fully characterised; a bone marrow equivalent of the AIRE-expressing mTEC that can facilitate deletion of auto-reactive B cells has not been identified so far. An alternative mechanism for the removal of auto-reactive B cells from the B-cell repertoire is light chain receptor editing, where a secondary Ig light (κ) is rearranged, which generates a new non-auto-reactive BCR (Ubelhart and Jumaa, 2015). Approximately 30% of immature B cells will undergo receptor editing (Pelanda and Torres, 2012). Despite central tolerance mechanisms being in place, not all auto-reactive B cells are deleted and some escape from the bone marrow into the periphery, thus necessitating additional rounds of selection in the periphery.

B cells expressing low-affinity auto-reactive BCRs can be positively selected and exit the bone-marrow and enter the pool of B1 type cells, which can be found in the peritoneal cavity and gut- and lung-associated lymphoid tissues (Pelanda and Torres, 2012). B cells that do not recognise auto-antigen are positively selected and enter the peripheral B2 cell pool (Pelanda and Torres, 2012). Immature B cells subsequently emerge from the bone marrow and migrate to the spleen. In the spleen, another round of negative selection ensues for those immature B cells that recognise auto-antigen (Pelanda and Torres, 2012). The immature B cells that are positively selected will further progress into fully mature marginal zone B cells in the spleen, or follicular B2 cells that recirculate though blood and lymphoid organs. These B2 cells are organised in B cell-rich follicles and can be triggered to differentiate if they encounter their cognate antigen. In the rest of this thesis I will be focusing on B2 cells and will from now on refer to them as ‘B cells’.

1.3.2 B cell activation: T-dependent vs T-independent

B cell activation occurs either in a Thymus-dependent (TD) or Thymus-independent manner (TI). T-independent B cell activation is typically triggered by polymerised or multivalent antigens such and bacterial polysaccharides that are able to crosslink the BCR (Mond et al.,

1995a). To become fully activated in a TI response, B cells also require a second signal to stimulate antibody production, either through TLR stimulation, or complement activation and CD21 stimulation (Mond et al., 1995a, Mond et al., 1995b, Vos et al., 2000). T-dependent B cell activation requires protein antigen to cross-link the BCR, as well as T cell 'help'. T cell help comprises co-stimulatory signalling through CD40 on the B cells and CD40L on the T cells. In this thesis, I will further focus only on T-dependent immune responses.

1.4 T-dependent B cell responses

1.4.1 B cell activation by protein antigens

Naïve mature B cells recirculate through secondary lymphoid tissues and enter the B cell follicle, which is located near sites of antigen entry: below the sub-capsular sinus in the LNs and underneath the marginal zone in the spleen (Batista and Harwood, 2009). In the follicle, naïve B cells scan for their specific antigen, which can be soluble, presented by sub-capsular sinus macrophages (Carrasco and Batista, 2007, Junt et al., 2007, Phan et al., 2007), DCs (Qi et al., 2006), or on the surface of follicular dendritic cells (FDCs) (Allen and Cyster, 2008). Ligation of the BCR by antigen triggers B cell activation. Then, B cells rapidly up-regulate CCR7, whose ligands, chemokine (C-C motif) ligand (CCL) 21 and CCL19, are expressed in the adjacent T cell zone. B cells use this gradient to migrate towards the T:B border, where they engage in cognate interactions with $CD4^+$ T helper cells (Okada et al., 2005, Kerfoot et al., 2011). B cells subsequently up-regulate the orphan G protein-coupled receptor Epstein-Barr virus-induced gene 2 (EBI2) allowing the B cell to migrate to the outer edges of the follicle where they begin to clonally expand (Gatto et al., 2009, Pereira et al., 2009). After division, B cells make a cell fate choice, they either take part in the extra-follicular antibody response, become memory B cells, or enter the B cell follicle to seed the GC (Chan et al., 2009).

1.4.2 The Extra-follicular antibody response

B cells that differentiate into extra-follicular plasma cells secrete class-switched or non-class-switched antibodies in the early phase of infection and undergo apoptosis *in situ* after a few days (Smith et al., 1996). This initial burst of antibody production is an important component of the early adaptive immune response against infectious organisms, and allows time for the GC to mature without compromising host defence during this time (MacLennan et al., 2003). The production of antibodies at this early time point also contributes to the formation of

immune complexes of antigen and antibodies, which are important for the selection of B cells within the GC (DeVoss et al., 2006).

1.5 The GC response

GCs are specialised microenvironments that form in B cell follicles within secondary lymphoid organs upon infection or immunisation with a T-dependent antigen. The effector products of the GC responses are long-lived high-affinity antibody secreting plasma cells and memory B cells (MacLennan, 1994). B cells that make the cell fate choice to enter the B cell follicle begin to rapidly divide which initiates the GC. After this initial clonal expansion, the GC divides into two distinct zones, the dark zone (DZ) and the light zone (LZ). In the DZ, B cell clones undergo somatic hyper-mutation (SHM), which introduces random point mutations in the V regions of their immunoglobulin (Ig) genes (Victora and Nussenzweig, 2012). This process is followed by affinity-based selection in the LZ that contains FDCs displaying immune complexes and Tfh cells. GC B cells compete with each other for help from Tfh cells by presenting antigen on MHCII (Smith et al., 2000, Phan et al., 2006). Those GC B cells that can engage Tfh cells will receive survival and differentiation cues to exit the GC as long-lived plasma cell, or memory cells, or to undergo further rounds of SHM.

1.5.1 Tfh cell differentiation

T cells arrive in the T zone of the LN from the circulation through high endothelial venules (Mackay et al., 1990). The chemokine receptor CCR7 enables migration of T cells towards its ligands CCL19 and CCL21 expressed by the fibroblastic reticular cells in the T zone (Ansel et al., 1999, Forster et al., 1999, Gunn et al., 1999, Haynes et al., 2007). Tfh cell differentiation is initiated by priming of the $CD4^+$ T cells by DCs via the engagement of the TCR by the MHCII peptide complex on DCs, in conjunction with co-stimulation between CD80/CD86 on the DC and CD28 on the T cell. During these T:DC interactions, the cytokines IL-6, IL-21, and IL-27, and the co-stimulatory molecule ICOS supports differentiation into Tfh-precursor (pre-Tfh) cells (Ballesteros-Tato and Randall, 2014). These signals are critical for induction of the transcription factor B cell lymphoma (Bcl)-6 (Choi et al., 2011), the transcription factor that is both necessary and sufficient for Tfh cell differentiation (Johnston et al., 2009, Nurieva et al., 2009, Yu et al., 2009). Bcl6 functions by actively repressing the master transcription factors of Th1 (Tbet), Th2 (GATA3), Th17 (RORγt) and Treg cells (Foxp3) as well as the transcription factor B-lymphocyte-induced maturation protein 1 (Blimp1) (Johnston et al.,

2009, Nurieva et al., 2009, Yu et al., 2009). Pre-Tfh cells also express the transcription factor Achaete-Scute Family BHLH Transcription Factor 2 (Ascl2), which regulates Tfh migration towards the GC by increasing CXCR5 expression and suppressing CCR7 and PSGL-1 expression (Haynes et al., 2007, Veerman et al., 2007, Poholek et al., 2010, Liu et al., 2014). The chemokine ligand for CXCR5, CXCL13 is expressed in the adjacent B cell follicle by FDCs creating a chemotactic pull to move Tfh cells towards the GC (Schaerli et al., 2000, Hardtke et al., 2005). Retention of Tfh cells in the GC requires sphingosine 1-phosphate receptor 2 (S1PR2), a $G_{12/13}$-coupled receptor that desensitises migration to other chemokines (Moriyama et al., 2014). Thus, the balanced expression of different chemokines and surface molecules allows the Tfh cells to localise within the GC.

During their differentiation, pre-Tfh cells also receive signals through ICOS via interactions with bystander B cells. This induces the phosphatidylinositide 3-kinase (PI3K) pathway and triggers actin waves and polarised pseudopod formation facilitating the migration of Tfh cells to the follicle (Rolf et al., 2010, Xu et al., 2013). In addition, PI3K signalling activates the mammalian target of rapamycin (mTOR), a serine/threonine kinase which is essential for Tfh cell differentiation and maintenance (Zeng et al., 2016). mTORC-1 regulates *de novo* Bcl6 synthesis and therefore constitutes a critical post-transcriptional control mechanism for Tfh cell formation (Yi et al., 2017).

After T cell priming, pre-Tfh cells also need to engage in cognate interactions with B cells in order to fully differentiate into GC Tfh cells, these stable interactions between pre-Tfh and B cells are mediated by ligation of the SLAM family of receptors, CD84 and Ly108, supported by the intracellular adaptor molecule SLAM-associated protein (SAP) (Cannons et al., 2010). In the absence of cognate B cells, Tfh cell differentiation can still take place and Tfh cells can enter the GC but these Tfh cells are not well maintained within the GC (Deenick et al., 2010, Kerfoot et al., 2011). Retention of Tfh cells within the GC is also a tightly regulated process. ICOS-dependent down-regulation of the transcriptional repressor (Krüppel-like Factor 2) Klf-2 is required for Tfh cell localisation in the GC and maintenance of their Tfh cell phenotype (Lee et al., 2015), as is down-regulation of EBI2 for Tfh cells to efficiently localise to the GC (Suan et al., 2015). The migration of Tfh cells to the GC and their maintenance within this microenvironment is critical for a productive GC response.

1.5.2 Tfh cell function

Fully differentiated Tfh cells are the mediators of positive selection in the GC and provide survival and differentiation signals to GC B cells through CD40L-CD40 interactions and secretion of cytokines, including IL-21 and IL-4 (Han et al., 1995, Bryant et al., 2007, Linterman et al., 2010, Yusuf et al., 2010, Zotos et al., 2010). This process of selection is iterative: B cells with somatically mutated BCRs collect antigen from the surface of FDCs, internalise it, and present peptide fragments to Tfh cells in the context of MHCII. B cells with the highest affinity BCRs are able to acquire more antigen from FDCs, and therefore present more peptide:MHCII to Tfh cells, thus out-competing lower affinity B cells for T cell help in the LZ (Shulman et al., 2013). Receipt of T cell help in the GC promotes the survival of GC B cells (Mayer et al., 2017). B cells that receive T cell help are able to re-enter the DZ and undergo further rounds of SHM and clonal expansion, which eventually results in the formation of high-affinity plasma cells and memory B cells that exit the GC (Victora et al., 2010, Gitlin et al., 2014).

Because the process of SHM is random, it can generate B cells with lower or higher affinity for antigen, and can even alter the specificity of the BCR to recognise self-antigens. Therefore, the selection of GC B cells by Tfh cells is essential for generating a potent B cell response that does not result in humoral autoimmunity. The dialogue between Tfh and GC B cells is not one directional, with B cells providing signals to Tfh cells that control their maintenance and function. PD-1 ligation on Tfh cells during interactions with B cells limits Tfh cell numbers and secretion of the cytokine IL-21, and CD80 expression on B cells supports Tfh survival via CD28 signalling (Good-Jacobson et al., 2010, Kawamoto et al., 2012). The bidirectional interaction of Tfh cells and GC B cells ultimately results in the positive selection of GC B cells, and their differentiation into antibody secreting plasma cells or memory B cells that can provide life-long humoral immunity.

1.5.3 Control of the GC by Foxp3$^+$ Treg cells

The size and specificity of the GC is influenced by a number of factors such as antibody feedback (Zhang et al., 2013b), Qa-1$^+$ CD8$^+$ regulatory T cells (Kim et al., 2010) and Foxp3$^+$ regulatory T cells (Chung et al., 2011, Linterman et al., 2011, Wollenberg et al., 2011). This thesis will focus on the latter cells and their role in controlling the GC response. Mice that lack Foxp3$^+$ Treg cells have unrestrained T cell and humoral immune responses, which

include spontaneous GC formation and Tfh cell expansion in the absence of immunisation or infection (Fontenot et al., 2003, Hori et al., 2003, Chung et al., 2011).

The control of humoral immunity by Treg cells appears to be due to specific functions or subsets of Treg cells. For example, mice in which Foxp3$^+$ cells lack IRF4 develop spontaneous GCs, but do not phenocopy Foxp3-deficient mice (Zheng et al., 2009). This suggests that IRF4 controls an aspect of Treg cell biology that is essential for moderating the GC itself, and that specific, cell-intrinsic molecular pathways mediate the suppression of the spontaneous GC response by Treg cells.

Cytotoxic T-Lymphocyte Associated Protein (CTLA)-4 signalling in Treg cells has also been implicated in control of GC responses. CTLA-4 is a co-inhibitory receptor that competes with CD28 for binding to CD80/86 on APCs (Walker and Sansom, 2011). CTLA-4 binds to CD80/86 with higher affinity and avidity compared with CD28, thereby outcompeting CD28 for binding. So, CTLA-4 signalling on Treg cells inhibits co-stimulation and therefore T cell activation (Qureshi et al., 2011, Walker and Sansom, 2011). CTLA-4 expressed by Treg cells modulates the GC response by limiting the expression of CD86 on B cells at the T:B border (Sage et al., 2014b, Wing et al., 2014). This limits differentiation of pre-Tfh cells due to reduced co-stimulatory signalling through CD28, which is continuously required during Tfh cell differentiation (Linterman et al., 2014). So, CTLA-4 signalling in Treg cells is able to impair the initiation of the GC response (Figure 1.3).

Foxp3$^+$ Treg cells can also support the GC response by limiting the availability of IL-2 during the early initiation phase of the GC response (Leon et al., 2014). IL-2 signalling negatively impacts on Tfh cell differentiation by up-regulating the transcription factor PR domain zinc finger protein 1 (Blimp-1) in a STAT5-dependent manner (Ballesteros-Tato et al., 2012, Johnston et al., 2012), suggesting that when Treg cells are not able to limit IL-2, primed T cells are skewed away from the Tfh lineage due to increased IL-2 signalling, thus impairing GC responses.

1.6 Follicular regulatory T (Tfr) cells

1.6.1 Discovery

In recent years it has become increasingly clear that like CD4$^+$ T helper cells, Treg cells are functionally and phenotypically diverse. Foxp3$^+$ Treg cells can differentiate into several functional states characterised by expression of specific transcription factors classically

associated with different helper T cell subsets. There is a subset of $Foxp3^+$ Treg cells that is found within the GC that phenotypically resemble Tfh cells and are thought to control the magnitude and output of the GC response (Chung et al., 2011, Linterman et al., 2011, Wollenberg et al., 2011). Lim *et al.* first identified $Foxp3^+$ cells within human tonsil GCs in 2004 (Lim et al., 2004). They also show that Treg cells, defined as $CD4^+CD25^+CD69^-$, can suppress T-dependent antibody production *in vitro*. However, this study has limitations as $CD4^+CD25^+CD69^-$ Treg cells express CCR7, and not CXCR5, making it unlikely that these $CD4^+CD25^+CD69^-$ Treg cells are all located within the GC. Interestingly, activation of $CD4^+CD25^+CD69^-$ Treg cells increased the expression of CXCR5, facilitating their migration towards CXCL13. This indicates that TCR activation is able to change the chemotactic profile of Treg cells to facilitate migration into the GC. In 2011, three independent groups used mouse models to demonstrate that $Foxp3^+CD4^+$ T cells are able to undergo functional differentiation into a specialised subset of Treg cells that migrate into the GC and control its size and output directly (Chung et al., 2011, Linterman et al., 2011, Wollenberg et al., 2011). These Treg cells located inside the GC are now referred to as follicular regulatory T (Tfr) cells. Tfr cells phenotypically resemble Tfh cells in many respects, as described in this literature overview. Tfr cells thus behave according to a model in which Treg cells co-opt aspects of specific T helper differentiation pathways, enabling them to migrate to sites where these T helper cells are functioning in immune responses. Once there, their suppressive effects help ensure that collateral damage is minimised during the fight against infection.

1.6.2 Origin

Tfr cells are a Treg subset that are localised within the GC, they phenotypically mirror Tfh cells in many aspects, including the expression of several Tfh cell markers; Bcl6, CXCR5, PD-1, ICOS, and SAP (Chung et al., 2011, Linterman et al., 2011). However, Tfr cells do not express the B cell helper molecules IL-21, IL-4 and CD40L (Linterman et al., 2011). Instead they also express a range of typical Treg markers such as GITR and CTLA-4 (Chung et al., 2011, Linterman et al., 2011). Gene expression profile analysis further showed that Tfr cells have a distinct transcriptional profile that is more similar to Treg cells than Tfh or other helper T cells (Linterman et al., 2011, Wing et al., 2017). Despite having phenotypic characteristics of both Tfh and Treg cells, Tfr cells are suppressive, clearly implicating these cells as a Treg cell subset (Wing et al., 2017).

Because Tfr cells have phenotypic characteristics of both Tfh and Treg cells, it was initially postulated that they could derive from Foxp3$^+$ Treg cells that enter the GC, or from Tfh cells that switch on Foxp3 within the GC. Adoptive transfer studies of both TCR-transgenic and polyclonal T cells showed that Tfr cells derive from Foxp3$^+$ cells (Chung et al., 2011, Linterman et al., 2011). In support of this, Tfr cells do not develop in mice depleted of Treg cells at the time of immunisation (Linterman et al., 2011). This may be largely because Tfh cells cannot be induced to express Foxp3$^+$ cells under Treg polarising conditions (Wollenberg et al., 2011). These data strongly indicated that Tfr cells derive from Foxp3$^+$ precursors rather than Tfh cells that turn on Foxp3 expression. A later study demonstrated that Tfr cells can form from CD4$^+$Foxp3$^+$ pTreg cells that have been induced to express Foxp3 at the time of immunisation when a pTreg-inducing adjuvant was used (Aloulou et al., 2016). Taken together, these data demonstrate that most Tfr cells derive from Foxp3$^+$ precursors. It is therefore likely that most Tfr cells derive from tTreg cells, but in conditions where pTreg cells are induced at the time of immunisation, these pTreg cells are also able to give rise to Tfr cells.

The key feature of Tfr cells is their location within the GC. Nevertheless, circulating counterparts of Tfr cells have been identified in the peripheral blood of humans and mice. Circulating Tfr cells correlate with humoral immune responses and are able to suppress T cell proliferation, but not B cell proliferation (Sage et al., 2014a, Fonseca et al., 2017). As opposed to GC Tfr cells, these 'circulating' Tfr cells do not require B cells, as B cell-deficient mice have normal numbers of blood Tfr cells but not GC Tfr cells (Sage et al., 2014a). In addition, circulating Tfr cells can form in B cell-deficient patients, indicating that they form prior to T:B interactions (Fonseca et al., 2017). Taken together, circulating Tfr cells indicate an on-going immune response and represent a precursor cell with a Tfr phenotype. In this work, I will focus on *bona fide* GC-resident Tfr cells, and not the peripheral circulating Tfr cell subset.

1.6.3 Differentiation and maintenance of Tfr cells

Tfr cell differentiation is a multi-step process, requiring several differentiation cues ultimately culminating in GC-resident Tfr cells. Akin to Tfh cell differentiation, Tfr cell differentiation depends on DC priming and subsequent SAP-dependent interactions with B cells for further development and expansion, as well as signaling through the co-stimulatory molecules CD28 and ICOS, which ultimately lead to the expression of Bcl6, the transcriptional repressor

required for Tfr cell differentiation (Sage et al., 2014a) (Qi et al., 2008, Linterman et al., 2011, Sage et al., 2013). Co-stimulation through ICOS and CD28 activates the PI3K-Akt-mTOR signalling pathway (Powell and Delgoffe, 2010). ICOS signalling promotes the interaction between the PI3K regulatory subunit p85alpha and intracellular osteopontin (OPN-i), resulting in nuclear translocation of OPN-i, and stabilisation of Bcl6, thereby promoting the Tfr cell fate (Leavenworth et al., 2015).

The PI3K pathway also activates mTOR signalling in Tfr cells, which has been implicated in Tfr cell differentiation and function (Xu et al., 2017). However, this paper defines Tfr cells as $CXCR5^{+}CD44^{+}$ cells, which probably includes non-Tfr cells. Therefore, further work is needed to clearly identify the contribution of mTOR signalling to Tfr cell biology.

Conventional Treg cells are highly dependent on IL-2 signalling for their development and maintenance; by contrast, Tfr cells express low levels of IL-2Ra (CD25), and IL-2 inhibits Tfr cell differentiation in a Blimp-1 dependent manner (Botta et al., 2017, Ritvo et al., 2017, Wing et al., 2017). Although Tfr cells derive from $CD25^{+}Foxp3^{+}$ precursors, they need to down-regulate CD25 in order to express Bcl6 and CXCR5 (Botta et al., 2017, Wing et al., 2017). Consistent with, and perhaps as a consequence of, loss of CD25 expression, Tfr cells express lower levels of Foxp3 compared with conventional Treg cells (Wing et al., 2017)(and our unpublished data). How Tfr cells are able to maintain Foxp3 expression in the absence of CD25 is unclear but may be due to expression of the lower affinity IL-2 receptors, IL-2Rβ (CD122) and IL-2Rγ, which maintain STAT5 signalling (Ritvo et al., 2017). Regardless of the exact molecular mechanism, IL-2 differentially regulates Tfr cells and conventional Treg cells, and Tfr cells are able to uniquely adapt to reduced IL-2 signalling whilst maintaining their Treg phenotype.

Like Tfh cells, Tfr cells absolutely require Bcl6 expression for their formation, suggesting that common developmental cues may be responsible for inducing their shared transcriptional regulator (Chung et al., 2011). Although *Bcl6*$^{-/-}$ mice are unable to form Tfr cells (Chung et al., 2011), it is not required for the initial up-regulation of CXCR5 (Vaeth et al., 2014). The transcription factor Nuclear factor of activated T-cells (NFAT)2 plays this role, and is required for up-regulation of CXCR5 (Vaeth et al., 2014). Interestingly, NFAT2 deficiency in T cells results in impaired CXCR5 expression in $Foxp3^{+}$ $CD4^{+}$ cells but not Tfh cells, suggesting that in Tfr cells, NFAT2 plays an analogous role to Ascl-2 in Tfh cells (Liu et al., 2014). This suggests that Bcl6 might be required for stabilising or maintaining Tfr cell development rather than initiating Tfr cell differentiation.

1.6.3.1 Negative regulators of Tfr cell differentiation

Tight control of Tfr cells is probably required to ensure appropriate, and avoid excessive, suppression of the GC. Therefore, several negative control mechanisms are in place. Roquin RNA-binding proteins inhibit the formation of Tfr cells by preventing differentiation of naïve Treg cells into Tfr cells (Essig et al., 2017). Roquin suppresses Tfr cell formation through Phosphatase and tensin homolog (PTEN)-dependent inhibition of PI3K, as well as inhibiting ICOS signalling (Essig et al., 2017). PTEN inhibits the PI3K pathway by de-phosporylating PIP3, whereas co-stimulatory signalling through ICOS is required for PI3K activation (Rolf et al., 2010). Furthermore, Roquin-deficient Treg cells lose CD25 in a PI3K-dependent manner, which is conducive for Tfr cell differentiation as IL-2 signalling needs to be dampened in order to establish the Tfr cell fate (Huynh et al., 2015). Thus, by controlling the PI3K signalling pathway at multiple levels, Roquin curtails Tfr cell differentiation.

IL-21 inhibits Tfr differentiation in a cell-intrinsic manner (Jandl et al., 2017). IL-21 can inhibit CD25 through Bcl6, thereby limiting Treg responsiveness to IL-2 (Jandl et al., 2017). An IL-21-dependent mechanism for limiting Tfr cells by inhibiting CD25 seems at odds with the fact that GC-resident Tfr cells do not express CD25. Indeed, this paper focuses on $CD25^+$ Tfr cells, and perhaps therefore "pre-Tfr" cells that have not yet down-regulated CD25 (Jandl et al., 2017). Therefore, these data suggest that IL-21 plays a role during the early stages of Tfr cell differentiation, when down-regulation of CD25 has not yet occurred. These findings also underline the importance of distinguishing between $CD25^+$ pre-Tfr and $CD25^-$ GC-Tfr cells when studying Tfr cell biology.

In addition to particular cues being required for their development, the size of the Tfr population is also controlled at a cell-intrinsic molecular level. In contrast to Tfh cells, a proportion of Tfr cells express Blimp-1, a transcription factor important for Treg function and for repressing Tfh development (Cretney et al., 2011). In the absence of Blimp-1, the Tfr population doubles in size, indicating that Blimp-1 is a negative regulator of Tfr cells (Linterman et al., 2011). Tfr cells also have high expression of the receptor PD-1, a co-inhibitory molecule that can dampen lymphocyte responsiveness to antigen (Linterman et al., 2011, Sage et al., 2013). Adoptive transfer experiments using cells from PD-1-deficient mice showed that PD-1 expression limits the size of the Tfr population (Sage et al., 2013). Together, these experiments demonstrate that Blimp-1 and PD-1 limit the size of the Tfr pool.

1.6.4 Tfr cell Function

It is tempting to speculate that the absence of Tfr cells might account for the spontaneous formation of GCs observed in Foxp3-deficient mice. Consideration of the kinetics of Tfr and Tfh cell formation argues against such a role for Tfr cells in controlling the initiation of the GC. Tfr cells are barely detectable in unimmunised mice and, after sheep red blood cell (SRBC) immunisation, Tfh cell numbers peak at day 7-11, prior to Tfr cells (day 11-17) (Vanderleyden et al., 2014). This demonstrates that Tfr cells are generated in response to immunisation, not prior to GC formation, and are therefore unlikely to suppress the formation of the GC. The kinetics of Tfr cell formation suggest that it is more plausible that Tfr cells control the function and output of an established GC, whereas extra-follicular Treg cells control the initiation of the GC.

In vitro Treg suppression assays showed that Tfr cells have a similar suppressive capacity compared to Treg cells (Linterman et al., 2011). However, their role *in vivo* has not been as easy to dissect. The three initial groups describing Tfr cells in mice used different experimental strategies to determine their function *in vivo,* leading to conflicting results. In a study by our laboratory, mixed bone marrow chimaeras (SAP-deficient mice and Foxp3-DTR mice) were used to examine the effect of a specific reduction in Tfr cells on the GC response. In this system, immunisation with a T-dependent antigen significantly increased the number of Tfh and GC B cells, indicating that Tfr cells can suppress features of the GC response *in vivo*. When the number of Tfr cells was reduced, a slight decrease in high-affinity antibodies was also observed. In addition, this reduction in Tfr cells resulted in fewer antigen-specific GC B cells, suggesting that Tfr cells can partly control the GC response by limiting development of non-antigen specific B cells (Linterman et al., 2011). In contrast, Chung *et al.* and Wollenberg *et al.,* transferred *Cxcr5*$^{-/-}$ or *Bcl6*$^{-/-}$ Treg cells, and wild type naïve CD4^{+} T cells, into T cell-deficient animals. They observed an increase in number of GC B cells as well as antibody titres after immunisation in mice that could not generate Tfr cells, although the number of Tfh cells was unaffected (Chung et al., 2011, Wollenberg et al., 2011). The discrepancies between these studies likely arise due to different experimental set-ups. An alternative explanation is that lack of CXCR5, SAP or Bcl6 in Treg cells might not affect the Tfr population alone, but may also have an impact on other aspects of Treg biology. While these studies show that Tfr cells limit the size of the GC response, new tools are required to fully understand the role that Tfr cells play in the GC.

To understand the specific role(s) of Tfr cells in controlling the GC, *Bcl6*$^{fl/fl}$*Foxp3*^{cre} mice were generated (Wu et al., 2016b). In these animals it is thought that deletion of Bcl6 in all Treg cells would result in the loss of Tfr cells specifically, without affecting any other Treg subsets, as the only described role for Bcl6 in Treg cells relates to Tfr differentiation (Wu et al., 2016a). The first report using these animals demonstrated that *Bcl6*$^{fl/fl}$*Foxp3*^{cre} mice did not exhibit changes in the number of Tfh cells and GC B cells after immunisation, but an increase in IgA titres and decreased affinity maturation. A second study using *Bcl6*$^{fl/fl}$*Foxp3*^{cre} mice showed that neither Tfh cells nor GC B cell numbers were altered in the absence of Tfr cells. However, there was a decrease in antigen-specific B cells, and an increase in plasma cells, indicating that Tfr cells may regulate the output of the GC response (Botta et al., 2017). Moreover, *Bcl6*$^{fl/fl}$*Foxp3*^{cre} mice showed increased anti-nuclear antibody (ANA) responses (Botta et al., 2017). This, combined with the observations that antigen-specific cells are diminished in Tfr-deficient chimeric mice, suggests that Tfr cells limit the outgrowth of auto-reactive clones from the GC (Linterman et al., 2011, Botta et al., 2017).

While it is clear that Tfr cells act to control the output of the GC response, the mechanism(s) by which they do this are not well defined. They could act directly on B cells or Tfh cells through cell-cell interaction, via cytokine production, or through a combination of these. Treg cells can directly inhibit B cell antibody production *in vitro* in a cell contact-dependent manner (Lim et al., 2005). Tfr cells cannot form in the absence of B cells or SAP, suggesting that Tfr cells or Tfr precursors interact with B cells *in vivo* (Linterman et al., 2011). Thus, Tfr cells may limit the GC response by interaction with GC B cells. However, Tfr cells are also able to suppress effector T cells directly *in vitro* (Lim et al., 2004), so Tfr cells may also act by suppressing the expansion or function of Tfh cells.

Within the GC, CTLA-4 on Tfr cells may be involved in direct suppression of GC B cells by regulating surface CD86 expression (Sage et al., 2014b, Wing et al., 2014). Thus, CTLA-4 is one candidate for direct Tfr-mediated suppression of the GC response. Besides the cell-contact dependent control mechanisms described above, Tfr cells also express the antagonist decoy receptor IL-1R2 which limits the IL-1-dependent activation of Tfh cells (Ritvo et al., 2017).

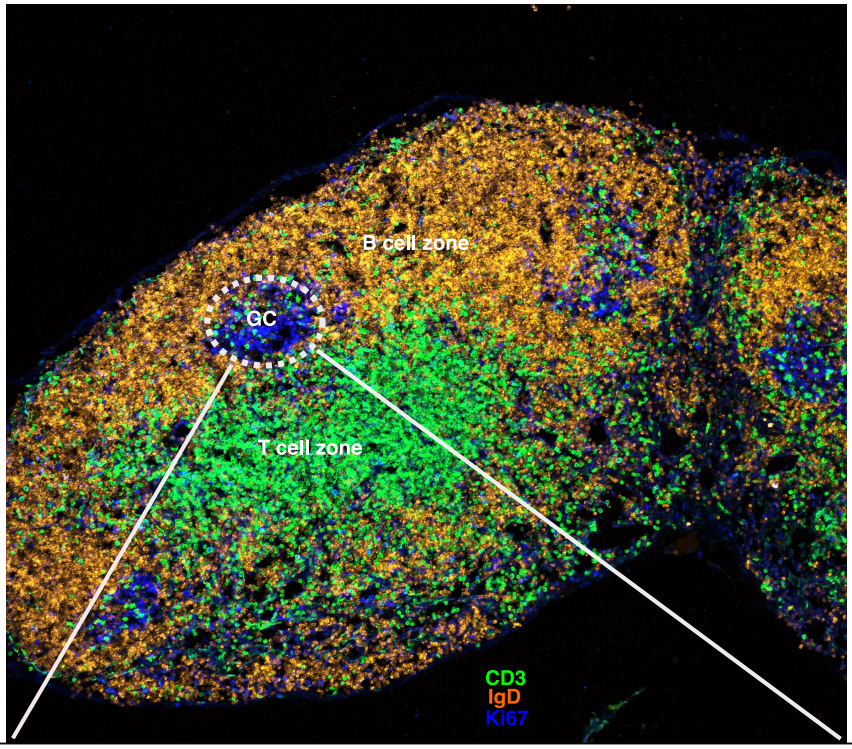
Tfr cells express IL-10, which has an established role in mediating Treg cell suppression (Saraiva and O'Garra, 2010). IL-10 signalling limits the size of the population of $CD4^{+}CXCR5^{+}$ T cells in secondary lymphoid organs (Cai et al., 2012), and seems to be involved in a positive feedback loop, enhancing its own production by Treg cells (Chaudhry

et al., 2011). This research suggests that Tfr cell-derived IL-10 regulates the GC response. Interestingly, this appears to be a GC-promoting role, as specific deletion of IL-10 in Tfr cells results in fewer GC B cells and plasma cells (Laidlaw et al., 2017). In addition, Treg-derived IL-10 induces a DZ phenotype in GC B cells through nuclear translocation of FOXO1. These findings indicate that IL-10 derived from Treg and Tfr cells supports the GC response (Laidlaw et al., 2017).

1.6.5 Do Tfr cells function in an antigen-specific manner?

Whether Tfr cells act in an antigen-specific manner remains contentious. Tfr cells are induced upon immunisation, indicative of being responsive to foreign antigen. Their origin from tTreg cells, which have a TCR repertoire skewed towards self-antigen, suggests that Tfr cells might be specific for self-antigen (Hsieh et al., 2006). Aloulou *et al*. used class II tetramers that detect $CD4^+$ T cells specific for Myelin Oligodendrocyte protein (MOG), a self-antigen in C57BL/6 mice, to identify self-antigen specific Tfr cells after MOG immunisation. However, MOG-specific Tfr cells could also be detected in *Nefm*$^{-/-}$*Mog*$^{-/-}$ mice, where MOG is a foreign antigen. This indicates that Tfr cells can be specific for the immunising antigen, both when it is a self-antigen and when it is a foreign antigen. TCR repertoire analysis revealed that the Tfr cell TCR repertoire more closely resembles that of Treg cells rather than that of Tfh cells (Maceiras et al., 2017).

The studies described here have limitations as they use highly manipulated mouse models and they study the specificity of a limited number of antigens. Further functional studies are required to characterise the TCR repertoire and to test whether Tfr cells preferentially bind self-antigens.


B cell zone
GC
T cell zone
CD3
IgD
Ki67

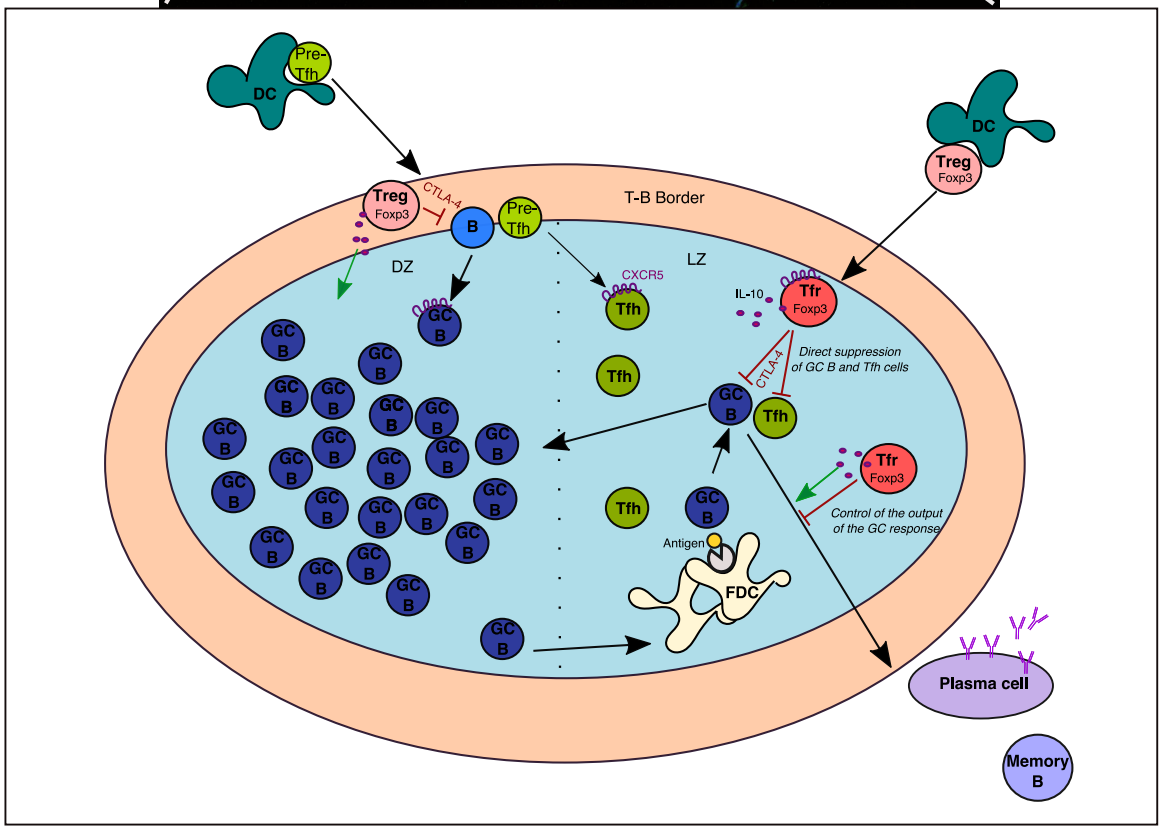

DC
Pre-Tfh
Treg
Foxp3
CTLA-4
B
T-B Border
DZ
LZ
CXCR5
Tfh
GC B
IL-10
Tfr
Foxp3
Direct suppression of GC B and Tfh cells
Control of the output of the GC response
Antigen
FDC
Plasma cell
Memory B

Figure 1.3 Overview of the GC response and Tfr-mediated control of the GC response.

The upper panel shows an inguinal LN from a mouse 14 days after 4-Hydroxy-3-nitrophenylacetyl hapten conjugated to Keyhole Limpet Hemocyanin (NP-KLH)/Alum immunisation. The T cell zone is marked by CD3 in green, the B cell follicle is shown in orange and the GC is shown in blue. The bottom panel shows a 'zoom-in' cartoon of the GC response. The Tfh cell differentiation pathway is initiated upon TCR/CD28-dependent activation of naïve T cells by DCs presenting peptide:MHCII. These pre-Tfh cells migrate to the T:B border where they engage in cognate SAP-dependent interactions with B cells. This results in further differentiation of pre-Tfh cells into mature Tfh cells that are predominantly localised within the light zone (LZ) of the GC. After interaction with cognate T cells at the T:B border, B cells will form the dark zone (DZ) of the GC, where they undergo multiple rounds of somatic hyper-mutation (SHM), followed by selection in the LZ. GC B cells subsequently exit the DZ and migrate into LZ, where they capture antigen from a network of FDCs and are then subjected to selection by Tfh cells. Those GC B cells that have a BCR with the highest affinity for the antigen will be able to present more antigen to the Tfh cells as compared to their lower affinity competitors. These GC B cells will receive survival and differentiation signals from the Tfh cells to differentiate into a plasma cells secreting high-affinity antibodies, or into memory B cells. Tfr cells are defined here as $Foxp3^+$ Treg cells present within the GC. Tfr cells derive from $Foxp3^+$ Treg cells and co-opt the Tfh differentiation pathway. Treg cells at the T:B border may be able to regulate the initiation of the GC response by inhibiting B cells through the CD86-CTLA-4 axis. Within the GC, Tfr cells are thought to act at least at two different stages of the GC response. Tfr cells may inhibit both GC B cells and Tfh cells through CTLA-4. Furthermore, it has been suggested that Tfr cells regulate the output of the GC response and limit the egress of auto-reactive GC B cells that produce auto-antibodies.

1.7 Conclusions and outstanding questions

Tfr cells are a subset of Foxp3$^+$ Treg cells that adopt features of Tfh cells to enable them to migrate into the GC while maintaining their suppressive function. These Tfr cells control the magnitude of the GC response and form within the GC, whereas extra-follicular Foxp3$^+$ Treg cells likely regulate the initiation of, and input to, the GC response. Although it is clear that Tfr cells exert a suppressive function on the GC, some controversy remains about the mechanisms and targets of their suppression. Further research is required in order to unravel the exact mechanisms by which Tfr cells suppress the GC response, as well as to disentangle the intra- and extra-follicular roles of Foxp3$^+$ Treg cells.

At the outset of this work, the major barrier to understanding Tfr cells specifically, without affecting Tfh cell or Treg cell subsets, was the lack of appropriate models to study these cells. Therefore, to be able to study these cells we needed to develop new tools. In addition, it was well established that Bcl6 is an essential driver for Tfr differentiation, but how this transcriptional repressor facilitates commitment to the Tfr cell subset is unknown.

This thesis has two main aims: (1) to generate a Tfr cell-deficient model by manipulating chemokine-dependent migration of Treg cells to the GC, and (2) to decipher the role of Bcl6 in Tfr cell differentiation.

2 Materials and Methods

2.1 Mice

The following mice were used for the experiments described in this thesis:

Mouse strain	Description	Source	**Key publications**
C57BL/6Babr	Wild-type mice	Babraham maintained colony, originally from JAX	n/a
Cxcr5$^{fl/fl}$	Mice have a targeted insertion of *loxP* sites flanking exon 2 of the *Cxcr5* gene	Roslin Institute	Bradford BM, *et al.*, 2017
Cxcr5$^{fl/fl}$*Cd4*^{cre}	Mice have a targeted deletion of *Cxcr5* in $CD4^+$ T cells	Bred in house	Unpublished

Cd4^{cre}	Mice express the cre-recombinase protein from the *Cd4* locus	Taconic Biosciences	Lee PP, *et al.*, 2001
Foxp3$^{YFP\text{-}cre}$	Mice express the cre-recombinase protein from the *Foxp3* locus	JAX	Rubtsov YP, *et al.*, 2008
Cxcr5$^{fl/fl}$*Foxp3*$^{YFP\text{-}cre}$	Mice to facilitate cre-mediated deletion of *Cxcr5* in *Foxp3*-expressing Treg cells	Bred in house	Unpublished
Foxp3$^{EGFP\text{-}cre\text{-}ERT2}$	*The EGFP-cre-ERT2* coding sequence was inserted into the 3' UTR of the *Foxp3* locus allowing for tamoxifen-induced recombination	JAX	Rubtsov YP, *et al.*, 2010
Cxcr5$^{fl/fl}$*Foxp3*$^{EGFP\text{-}cre\text{-}ERT2}$	Inducible deletion of *Cxcr5* in *Foxp3* expressing Treg cells can be achieved by tamoxifen administration	Bred in house	Unpublished
Foxp3^{GFP}	Mice have a targeted insertion of the complete Green Fluorescent Protein (eGFP) coding sequence in exon 1 of the *Foxp3* gene.	Adrian Liston, KULeuven	Fontenot JD, *et al.*, 2005
Cxcr4$^{fl/fl}$	Mice possess a targeted insertion of *loxP* sites on either side of intron 2 of the	JAX	Nie Y , *et al.*, 2004

	Cxcr4 gene		
Cxcr4$^{fl/fl}$*Foxp3*$^{EGFP\text{-}cre\text{-}ERT22}$	Inducible deletion of *Cxcr4* in *Foxp3*-expressing Treg cells can be achieved by tamoxifen admistration	Bred in house	Unpublished
Cxcr4$^{fl/fl}$*Cxcr5*$^{fl/fl}$*Foxp3* $^{EGFP\text{-}cre\text{-}ERT2}$	Inducible deletion of *Cxcr5* and *Cxcr4* in *Foxp3* expressing Treg cells can be achieved by tamoxifen administration	Bred in house	Unpublished
Cxcr4$^{fl/fl}$*Cxcr5*$^{fl/fl}$*Cd4*^{cre}	Inducible deletion of *Cxcr5* and *Cxcr4* in CD4 T cells can be achieved by tamoxifen administration	Bred in house	Unpublished
Bcl6$^{fl/fl}$*Cd4*$^{cre/+}$	Mice show cre-mediated deletion of *Bcl6* in $CD4^+$ T cells	JAX	Hollister K, *et al.*, 2013
Bcl6$^{fl/fl}$	Mice possess *loxP* sites flanking exon 7-9 in *Bcl6*	JAX	Hollister K, *et al.*, 2013
Bcl6$^{fl/fl}$*Foxp3*$^{EGFP\text{-}cre\text{-}ERT2}$	Inducible deletion of *Bcl6* in *Foxp3*-expressing Treg cells can be achieved by tamoxifen administration	Bred in house	Unpublished
Rag2$^{-/-}$	Mice lack T and B cells	Babraham-maintained colony	Hao Z, *et al.*, 2001

B6.SJL	Mice carry the *Cd45.1* allele	Babraham-maintained colony	Komuro K, *et al*., 1975

Table 1. List of mouse models used in this thesis.

With the exception of the experiments performed using 4-day old $Bcl6^{fl/fl}Cd4^{cre/+}$ mice, all mice were between three and 12 weeks old at the start of the experiment, and age- and sex-matched controls were used, unless stated otherwise. All experiments were performed according to the regulations of the UK Home Office Scientific Procedures Act (1986), under project license number P4D4AF812. Mice were housed under specific pathogen-free conditions at the Biological Services Unit, Babraham Research Campus, UK.

2.1.1 Tamoxifen administration

Inducible deletion of floxed alleles mediated by the cre-recombinase linked to a human mutated oestrogen ligand binding receptor (ERT2) was achieved by supplementing the food with tamoxifen. From the age of three weeks, mice received a soy-free, 16 % global protein rodent diet (Teklad, cat # 2916) for ten days. After ten days, mice were fed *ad libitum* for 4-6 weeks with Tecklad CRD $TAM^{400/CreER}$ Tamoxifen pellets (Teklad), containing 400mg tamoxifen citrate/kg (w/v), softened in 20% (w/v) sucrose in water solution (Sigma, cat # S0389).

2.2 Generation of bone-marrow chimeric mice

Recipient $Rag2^{-/-}$ or B6.SJL mice were sub-lethally irradiated with ten Gray (Gy) and reconstituted by intravenous (*i.v.*) injection of $2x10^6$ total bone marrow cells from donor $Bcl6^{fl/fl}Cd4^{cre}$ mice and B6.SJL mice. Bone marrow cells were isolated from the hind legs collected in PBS and excess flesh was removed from the leg bone. The femur and tibia were separated and the ends of the bones were cut off. The bone marrow was subsequently isolated by centrifugation at 400*g* for two minutes, and a single-cell suspension was prepared by resuspending the bone marrow in PBS followed by passage through a 70µm cell strainer. Next, a 50:50 bone marrow mix was prepared by pooling $Bcl6^{fl/fl}Cd4^{cre/+}$ (or $Bcl6^{fl/fl}Cd4^{+/+}$ controls) and B6.SJL bone marrow to a final concentration of $1x10^7$cells/ml in PBS. Recipient mice received a 200µl single cell suspension ($2x10^6$ cells) by *i.v.* injection. Mice received neomycin sulphate in the drinking water (0.9g/250mL) for four weeks after irradiation.

Chimeric mice were immunised with NP-KLH *s.c.* (as per 2.3.1), or infected with influenza (as per 2.3.3), 10 weeks after reconstitution.

2.3 Immunisations and infections

2.3.1 NP-KLH immunisations

NP-KLH (Conjugation ratio 29-33, Biosearch Technologies, cat # N-5060-25) was dissolved in PBS to 1 mg/ml and mixed with Imject Alum (ThermoFisher Scientific, cat # 7761) in a 1:1 ratio by vortexing to give a final working concentration of 0.5 mg/ml. Mice were immunised subcutaneously (*s.c.*) on each side of the hind flank with 100µl per flank of NP-KLH/Alum, and inguinal LN were harvested 14, 48 or 56 days after immunisation. Alternatively, mice were injected with 150µl NP-KLH intraperitoneally (*i.p.*) and the spleens and bone marrow were harvested 48 or 56 days after immunisation. Blood was collected after each experiment by cardiac puncture to determine NP-specific antibody production.

2.3.2 SRBC immunisations

Five ml of Sheep Red Blood cells (SRBC) in Alsever's were washed in 45ml of PBS, followed by centrifugation at 600*g* for ten minutes. After centrifugation, the supernatant was removed by pipet and the cell pellet was resuspended in 2ml of PBS. Mice were immunised *i.p*. with 200µl SRBC and the spleen was harvested 14 days after immunisation.

2.3.3 Influenza A infections

Mice were inoculated intranasally (*i.n.*) with 10^4 plaque-forming units of the influenza A/HK/x31 (H3N2) virus under inhalation anaesthesia using isoflurane. The lungs, mediastinal LNs and spleen were harvested 14 days post infection (dpi).

2.4 Flow cytometry

2.4.1 Antibodies

Marker	Fluorochrome	Clone	Dilution	Supplier	Cat #
B220	BV510	RA-3-6B2	1/200	Biolegend	103241
B220	BV785	RA3-6B2	1/400	Biolegend	103246
Bcl6	AF647	K112-91	1/50	Becton Dickinson	561525
Bcl6	PE	K112-91	1/50	Becton Dickinson	561522
CD138	Biotin	281-2	1/100	Biolegend	142512
CD16/ CD32	Purified	2.4G2	1/100	ThermoFisher Scientific, eBioscience	14-0161-82
CD19	Percp-Cy5.5	1D3	1/200	ThermoFisher Scientific, eBioscience	45-0193-82
CD25	APC-ef780	PC61.5	1/200	ThermoFisher Scientific, eBioscience	47-0251-82
CD25	Percp-Cy5.5	PC61.5	1/200	ThermoFisher Scientific, eBioscience	45-0251-82
CD38	eF450	90	1/200	ThermoFisher Scientific,	48-0381-80

				eBioscience	
CD4	APC	GK1.5	1/500	ThermoFisher Scientific, eBioscience	17-0041-83
CD4	BV605	RM4-5	1/500	Biolegend	100547
CD4	eF450	GK1.5	1/500	ThermoFisher Scientific, eBioscience	48-0041-82
CD4	FITC	GK1.5	1/500	ThermoFisher Scientific, eBioscience	11-0041-85
CD4	PB	RM4-5	1/500	ThermoFisher Scientific, eBioscience	48-0042-82
CD4	PE	GK1.5	1/500	ThermoFisher Scientific, eBioscience	12-0041
CD4	PE-Cy7	RM4-5	1/500	Biolegend	100528
CD4	Percp-Cy5.5	RM4-5	1/500	ThermoFisher Scientific, eBioscience	45-0042-82
CD44	AF700	IM7	1/400	Biolegend	103026
CD44	APC	IM7	1/400	ThermoFisher Scientific, eBioscience	17-0441-83

CD44	PB	IM7	1/400	Biolegend	103020
CD62L	PE-Cy7	MEL14	1/200	ThermoFisher Scientific, eBioscience	25-0621-82
CD69	PE-Cy7	H1.2F3	1/100	ThermoFisher Scientific, eBioscience	25-0691-82
CD86	BV510	GL-1	1/100	Becton Dickinson	563077
CD8a	BUV395	53-6.7	1/300	Becton Dickinson	563786
CD95	PE-Cy7	Jo2	1/200	Becton Dickinson	557653
CTLA-4	PE	UC10-4B01	1/100	ThermoFisher Scientific, eBioscience	12-1522-82
CTLA-4	PE-eF610	UC10-4B01	1/100	ThermoFisher Scientific, eBioscience	61-1522
CXCR3	BV605	CXCR3-173	1/100	Biolegend	126523
CXCR3	Percp-Cy5.5	CXCR3-173	1/100	Biolegend	126514
CXCR4	PE	L276F12	1/100	Biolegend	146506
CXCR4	Percp-eF710	2B11	1/100	ThermoFisher Scientific, eBioscience	46-9991-82

CXCR5	APC	L138D7	1/100	Biolegend	145506
CXCR5	BV421	L138D7	1/100	Biolegend	145512
Foxp3	AF488	FJK-16S	1/50	ThermoFisher Scientific, eBioscience	53-5773-82
Foxp3	eF450	FJK-16S	1/50	ThermoFisher Scientific, eBioscience	48-5773-82
GL-7	AF488	GL7	1/200	ThermoFisher Scientific, eBioscience	53-5902-82
IgD	AF647	11.26C.2a	1/200	Biolegend	405708
IgG1	BV605	A85-1	1/100	Becton Dickinson	563285
IgM	BUV395	R6-60.2	1/100	Becton Dickinson	564025
IL-17	FITC	eBIO17B7	1/100	ThermoFisher Scientific, eBioscience	11-7177-81
IL-2	PE	JES6-5H4	1/100	ThermoFisher Scientific, eBioscience	1870743
Ki67	AF700	SolA15	1/200	ThermoFisher Scientific, eBioscience	56-5698-82

Ki67	FITC	SolA15	1/400	ThermoFisher Scientific, eBioscience	11-5698-82
Ki67	PE-Cy7	SolA15	1/200	ThermoFisher Scientific, eBioscience	25-5698-82
NP	PE	n/a	1/100	Biosearch technologies	N-5070-1
Nrp-1 / CD304	Percp-eF710	3DS304M	1/100	ThermoFisher Scientific, eBioscience	46-3041
PD-1	APC-ef780	J43	1/200	ThermoFisher Scientific, eBioscience	47-9985-82
PD-1	PE	RMP1-30	1/200	Biolegend	109104
PD-1	PE-Cy7	RMP1-30	1/200	Biolegend	109110
Streptavidin	APC	n/a	1/1000	Biolegend	405207
T-bet	PE	eBio4B10	1/300	ThermoFisher Scientific, eBioscience	12-5825-80
T-bet	PE-Cy7	eBio4B10	1/300	ThermoFisher Scientific,	25-5825-82
Zombie Aqua Fixable viablity dye	Zombie Aqua	n/a	1/1000	Biolegend	423101

Zombie Green Fixable viablity dye	Zombie Green	n/a	1/1000	Biolegend	423111
CD4	BV510	GK5.1	1/400	Biolegend	100449
CD103	BV785	M290	1/100	Becton Dickinson	564322
CD24	BV605	M1/69	1/200	Biolegend	101827
Helios	APC	22F6	1/100	Biolegend	137221
GATA3	AF488	TWAN	1/100	ThermoFisher Scientific, eBioscience	53-9966-42
GITR	FITC	DTA-1	1/200	Biolegend	12306
CD69	BV786	H1 2F3	1/200	Becton Dickinson	564683
CD45.1	AF700	A20	1/200	Biolegend	110724

Table 2. List of anti-mouse antibodies used for flow cytometry.

Dilutions for each antibody were determined by prior titration.

2.4.2 Cell preparation

The spleen, LNs, lungs, thymus and bone marrow, were dissected from the mice. The bone marrow was isolated from bones by centrifugation for one min at 500*g*. The lungs were cut into fragments prior to mashing. A single cell suspension was prepared by mashing the tissues through a 40µm or 7 µm Falcon nylon cell strainer (Becton Dickinson, cat # 352063) using a syringe plunger and filtering the cell suspension. Cells were then re-suspended in ice-cold FACS buffer (PBS containing 2% (v/v) heat inactivated Foetal Bovine Serum (FBS) (Sigma, cat # F9665)) and centrifuged for five minutes at 400*g* at 4°C to pellet the cells. Cells from the spleen, bone marrow and lungs were treated with Ammonium-Chloride-Potassium (ACK)

buffer (150mM NH_4Cl (Sigma, cat # 254134), 10mM $KHCO_3$ (Sigma, cat # 60339), 0.1mM NA_2EDTA in H_20) in order to lyse the red blood cells prior to surface staining. Live cells were counted using a CASY cell counter and Analyser (Roche).

2.4.3 Staining procedure

2.4.3.1 Surface staining

Between $1x10^6$ and $5x10^6$ cells were stained with the specific antibody cocktail made according to the dilutions in Table 2 in 100µl FACS Buffer or, if using more than one antibody conjugated to a brilliant violet fluorochrome, in Brilliant Stain buffer (Becton Dickinson, cat # 563794). Cells were incubated with surface antibodies for one hour at 4°C.

2.4.3.2 Intra-cellular staining

After surface staining, 3ml ice cold FACS buffer was added and cells were pelleted by centrifugation for five minutes at *400g* at 4°C. Cells were fixed and permeabilised for intracellular staining for Foxp3, Ki67, Bcl6, Helios, GATA3 and Tbet using the eBioscience Foxp3/ Transcription Factor Fixation/Permeabilisation Staining buffer set (ThermoFisher Scientific, cat # 00-5523) according to manufacturer's instructions. In brief, cells were fixed using 100µl 1x Fixation/permeabilisation solution (ThermoFisher Scientific, cat # 00-5123), for 30 minutes at room temperature. After washing in 1x Permeabilisation Buffer (10 times stock diluted in distilled water, ThermoFisher Scientific, cat # 00-8333), the cells were incubated with the relevant antibodies diluted in 1x Permeabilisation Buffer. Intra-cellular staining for IgG1 and NP was performed using the BD Cytofix/Cytoperm Kit (Becton Dickinson, cat # 554714) according to manufacturer's instructions. In brief, cells were fixed in Cytofix/Cytoperm (Becton Dickinson, cat # 554722) for 30 minutes at 4°C. After washing the cells in 1x BD Perm/Wash (Becton Dickinson, cat # 554723), they were incubated with 100µl of the relevant antibody cocktail diluted in 1x BD Perm/Wash at the concentrations indicated in Table 2.

2.4.4 Analysis

Prior to acquiring the samples, fluorescence compensation was calculated using single stain controls of UltraComp eBeads (ThermoFisher Scientific, cat # 01-2222) labelled with the relevant flurochromes for that experiment. Stained cells were subsequently acquired using a BD LSR Fortessa, 5 lasers (488nm, 405nm, 561nm, 640nm, UV) (Becton Dickinson).

Analysis of the flow cytometry data was performed using FlowJo software (Becton Dickinson). Analysis of the flow cytometry data was performed using FlowJo software (Becton Dickinson).

2.5 In-depth phenotyping of *Bcl6$^{fl/fl}$Cd4$^{cre/+}$* mice by high-paramater flow cytometry

This experiment was performed in collaboration with Dr. Oliver Burton and Prof. Adrian Liston, at KU Leuven, Belgium. Spleens and thymi were obtained from 6-week old *Bcl6$^{fl/fl}$Cd4$^{cre/+}$* and *Bcl6$^{fl/fl}$* mice, and a single cell suspension was prepared as described in 2.4.2, and cells were stained using the following markers: TCR-β, CTLA-4, Eomes, IL-5, Tbet, Foxp3, ICOS, CD11b, CD3, Viability dye, CD4, IL-21, CD69, GM-CSF, CD19, Tnf-α, CD8a, IL-17, NK1.1, IL-4, GITR, IL-10, ST2, Amphiregulin, Nrp-1, IL-2, CD103, IL-21, CD45, IL-3, Helios, IL-22, Ki67, IL-6, Rorγt, IL-13, CD44, IL-3, CD127, IL-5, CD25, TCRγδ, KLRG-1, Tgf-β, GATA3, IL-1β, CD62L.

This experiment was performed using a novel optimised staining panel for the simultaneous analysis of 27 parameters by flow cytometry using a BD FACSymphony (Becton Dickinson). Due to the novelty of this method and the fact that it will not have been published by the time of submission of this thesis, we are unable to include details on the staining panel and procedure used in this experiment. Analysis of the flow cytometry data was performed using FlowJo software (Becton Dickinson).

2.5.1 tSNE analysis

The raw data for t-Distributed Stochastic Neighbor Embedding (tSNE) analysis was compensated flow cytometry data exported as .csv files from a 24-colour panel run on the BD symphony. All data was arc-sin transformed in R using cut-off values manually determined for each fluorophore. For each analysis outlined below, markers and parameters for tSNE and DBSCAN algorithms were selected using iterative process to until data suitable clustering of the data was achieved, and cell clusters were not overly fractured. This typically involved removing markers without discrete positive and negative populations.

2.5.1.1 Spleen and thymus: Foxp3^{+}CD4^{+} cells

To ensure equal cells from each tissue and mouse, 888 cells were analysed for each sample. tSNE used seven markers and ran for 2000 iterations with a perplexity value of 75. DBSCAN

algorithm was used to identify clusters of cells, with clusters defined using an epsilon value of 3.5 and with 260 minimum points. The proportion of cells in each cluster was determined for each individual. These percentages were used to compare between wild-type (WT) and *Bcl6*$^{fl/fl}$*Cd4*$^{cre/+}$ mice using a Mann-Whitney U test, with p values adjusted using the false discovery rate (FDR method). Significant clusters were defined as those having FDR-adjusted p values of less than 0.04.

2.5.1.2 Spleen and thymus: All cells

To ensure equal cells were analysed from each mouse 10,000 cells were randomly subsampled. tSNE used 12 markers and ran for 2500 iterations with a perplexity value of 100. DBSCAN algorithm was used to identify clusters of cells, with clusters defined using an epsilon value of 2.40 and with 600 minimum points. The proportion of cells in each cluster was determined for each individual. These percentages were used to compare between WT and *Bcl6*$^{fl/fl}$*Cd4*^{cre} mice by Mann-Whitney U test, with p values adjusted using the FDR method. Significant clusters were defined as those having FDR-adjusted p values of less than 0.04.

2.5.1.3 Spleen: Foxp3^{-}CD4^{+}

To ensure equal cells from each mouse, 5000 cells were randomly subsampled. tSNE used nine markers and ran for 2000 iterations with a perplexity value of 100. DBSCAN algorithm was used to identify clusters of cells, with clusters defined using an epsilon value of 3.15 and with 500 minimum points. The proportion of cells in each cluster was determined for each individual. These percentages were used to compare between WT and *Bcl6*$^{fl/fl}$*Cd4*$^{cre/+}$ mice by Mann-Whitney U test, with p values adjusted using the FDR method. Significant clusters were defined as those having FDR-adjusted p values of less than 0.04.

2.5.1.4 Thymus: Foxp3^{-}CD4^{+}

To ensure equal cells from each mouse, 5000 cells were randomly subsampled. tSNE used nine markers and ran for 2000 iterations with a perplexity value of 100. DBSCAN algorithm was used to identify clusters of cells, with clusters defined using an epsilon value of 3.25 and with 520 minimum points. The proportion of cells in each cluster was determined for each individual. These percentages were used to compare between WT and *Bcl6*$^{fl/fl}$*Cd4*^{cre} mice by Mann-Whitney U test, with p values adjusted using the FDR method. Significant clusters were defined as those having FDR-adjusted p values of less than 0.04

These analyses were performed by Dr. Danika Hill, The Babraham Institute.

2.6 Trans-well migration essay

Cells were prepared as in 2.4.2 and re-suspended in Migration medium: RPMI (ThermoFisher Scientific, cat # 11875093) containing 1% (w/v) Bovine Serum Albumin (BSA) (Sigma, cat #A9418), 100µg/ml Penicillin-Streptomycin (ThermoFisher Scientific, cat # 15070063) and 0.5µM β-Mercaptoethanol. CXCL12 (Peprotech, cat # 250-20B) or CXCL13 (Peprotech, cat # 250-24) were serially diluted in migration medium and added at the indicated concentration in the bottom compartment of a 6.5mm trans-well plate with 5.0µm pore membrane inserts (Sigma, cat # CLS3421). Cells ($1.5x10^6$) were added to the top compartment of the transwell plate and incubated at 37°C in 5% CO_2 for two hours. Migrated cells were collected and further processed for analysis by flow cytometry, as described in section 2.4.3.

2.7 PCR-based genotyping

Ear biopsies were submerged in SDS lysis buffer (1M Tris HCl, 0.5M EDTA, 20% SDS, 5M NaCl, Proteinase K) and digested at 55 °C for two hours. The proteinase K was subsequently deactivated by incubating at 85 °C for 30 minutes.

A PCR reaction was performed on the samples using the primers listed in Table 3 and the reagents listed in Table 4 and thermocycling conditions described in Table 5.

Primer specificity	Primer sequences 5'-3'
CXCR5 3’ LoxP Reverse	TTCCTTAGAGCCTGGAAAAGG
CXCR5 5’ LoxP Forward	AGGAGGCCATTTCCTCAGTT
‘CXCR5 5’ LoxP Reverse	GGCTTAGGGATTGCAGTCAG

Table 3. Sequences of the CXCR5 primers (Sigma) used for PCR based genotyping assay. Primers were reconstituted to 100µM.

Master mix	**Final concentration**
10X PCR gold Buffer (ThermoFisher Scientific, cat # 4311814)	1x
$MgCl_2$ (25mM) (ThermoFisher Scientific)	2mM
25mM dNTP (Invitrogen, cat #18427-013)	200 μM each
Primer mix 10mM	1.0 μM
AmpliTaq Gold DNA polymerase(5U/ul) (ThermoFisher Scientific, cat # 4311814)	1.25U
H_20	Up to 15μl
Template DNA	<1μg
Total	Up to final reaction volume

Table 4. Reagents and concentrations used for PCR reactions.

Conditions	Initial denaturation	Denaturation-Annealing-Extension			Final extension	End
No of cycles	1	1	34		1	/
Temperature	94°C	94°C	60°C	72°C	72°C	4°C
Time	3min	30sec	30sec	45sec	10min	∞

Table 5. Thermocycling conditions used in PCR reactions.

A 3% TBE-agarose gel was prepared by mixing 3g of agarose (Bioline, cat # 41025) with 100ml of 1x Tris/Borate/EDTA (TBE) buffer (prepared in-house) and the mixture was boiled until the agarose had completely dissolved. After cooling down, 0.2µg/ml ethidium bromide (Biorad, cat #1610433) was added to the agarose solution. The solution was subsequently poured into an enclosed tray containing 15-well combs and allowed to set. PCR products were mixed 1:6 with a MassRuler DNA loading Dye (Thermo Scientific, Cat # R0621) and the samples were subsequently loaded on the agarose gel together with a DNA ladder (Biorad, Cat# 1708353), and electrophoresis was performed at 120V for two hours in 1xTBE buffer. Gels were visualised using a Molecular Imager® Gel Doc™ XR System (Biorad, cat #170-8170). The expected band sizes are listed in Table 6.

PCR results	
LoxP	375 bp
WT	214 bp
Recombined (KO)	292 bp

Table 6. Expected outcome and corresponding band sizes for each PCR reaction.

2.8 Gene expression analysis by high-throughput RT-qPCR

This experiment was performed in collaboration with Amélie Bonaud and Marion Espéli, INSERM, France. For the gene expression essay, *Foxp3*^{GFP} mice were immunised with NP-KLH/Alum and inguinal LNs were harvested 14 days after immunisation. In total, eight mice were used and the LNs from two mice were pooled to get a total of four replicate samples. Prior to sorting, the cells were enriched for CD4 T cells using the Magnisort Mouse CD4 T cell Enrichment kit (ThermoFisher Scientific, Cat # 8804-6821-74). Tfr cells ($CD4^+CXCR5^+PD\text{-}1^+GFP^+$), Tfh cells ($CD4^+CXCR5^+PD\text{-}1^+GFP^-$), Treg cells ($CD4^+CXCR5^-PD\text{-}1^-CD25^+GFP^+$) and naïve T cells ($CD4^+CD62l^+GFP^-$) were sequentially sorted using a BD Fusion sorter (Becton Dickinson). 50 cells per population were sorted directly into a 96 well plate. Cells were sorted directly in well containing 5µl master mix for cDNA synthesis made up of 1.15µl Tris-EDTA (TE) buffer (prepared in-house), 1.25µl primer mix which is composed of 48 Taqman probes (Table 8) diluted at 1/100 with TE buffer (Applied Biosystems, see Table 8 for all the references of probes), 0.1µl SuperScript® III RT/Platinum® Taq Mix and 2.5µl 2X Reaction mix (ThermoFisher Scientific, cells direct™ one step qPR-PCR kit), as recommended by the Fluidigm protocol.

No of cycles	**1**	**1**	**20**		**1**
Temperature	50°C	95°C	95°C	60°C	4°C
Time	15min	2min	15sec	4min	∞

Table 7. Thermocycling conditions used for reverse transcription.

After cell sorting, the plate was centrifuged at 300*g* for one minute and cDNA was generated by reverse transcription with a specific pre-amplification step for target genes described in Table 7.The plate was subsequently centrifuged at 300*g* for one minute and 20µl TE buffer was added to each well and stored at -20°C. The plate was then sent to Amélie Bonaud, INSERM, France, who performed the RT-qPCR on a Biomark^{TM} HD system (Fluidigm).

A 48.48 Dynamic Array primed chip containing the different primers was prepared by adding 3µl of each primer as specified in Table 8 to separate wells. The primers were subsequently diluted by adding 3µl of 2x Assay Loading Buffer (Fluidigm). In parallel 2.9µl of the previously generated cDNA from the sorted cells in separate wells was prepared by adding 0.32µl of 20x GE Sample Loading Reagent (Fluidigm) and 3.25µl Universal PCR Master Mix (Applied Biosystem) to each well.

The data were analysed using the Real-Time PCR Analysis software (Fluidigm). IgJ was used as negative control. Relative gene expression values were calculated by normalising Ct values to the house keeping genes (*Actin B* and *Gapdh*) using the following formula: $2^{(-\Delta Ct)}$, where $\Delta Ct = Ct_{\text{gene of interest}} - Ct_{\text{mean of } Gapdh \text{ and } Actin\ B}$.

	Gene	Reference
Adhesion molecules	CD62L / sell	Mm00441291_m1
Chemokine receptors	CXCR4	Mm01996749_s1
	CCR5	Mm01963251_s1
	CXCR2	Mm00438258_m1
	CXCR3	Mm00438259_m1
	CXCR4	Mm01292123_m1
	CXCR5	Mm00432086_m1
	CXCR7	Mm01290382_m1
	CCR1	Mm01216147_m1
	CCR2	Mm00438270_m1
	CCR3	Mm01216172_m1

	CCR4	Mm00438271_m1
	CCR6	Mm01700298_m1
	CCR7	Mm01301785_m1
	CX3CR1	Mm00438354_m1
	CCR10	Mm01292449_m1
Receptors	BCMA	Mm00495683_m1
	TACI	Mm00840182_m1
	BAFF-R	Mm00840578_g1
	IL6-R	Mm00439653_m1
	EphB6	Mm00432456_m1
	Sema4c	Mm01229764_m1
	PlexinB2	Mm00507118_m1

	CXCL9	Mm00434946_m1
Chemokines	CXCL10	Mm00445235_m1
	CXCL11	Mm00444662_m1
	CXCL12	Mm00445553_m1
	CCL2	Mm00441242_m1
	CCL3	Mm99999057_m1
	CCL4	Mm00443111_m1
	CCL8	Mm01297183_m1
	CCL27a	Mm04206819_gH
	CCL28	Mm00445039_m1
	CCL5	Mm01302427_m1
Cytokines	Il10	Mm01288386_m1
Controls	CD3e	Mm00599684_g1

	Foxp3	Mm00475162_m1
	Prmd1	Mm00476128_m1
	Bcl6	Mm00477633_m1
	IgJ	Mm00461780_m1
	GAPDH	Mm99999915_g1
	Actin	Mm01205647_g1

Table 8. List of TaqMan probes used for Biomark essay (Applied Biosystems).

2.9 RNA-Seq analysis

RNA-Seq data from Wing J *et al.* 2017(Wing et al., 2017) (Accession n° DRA004824) and Kitagawa *et al.* 2017 (Kitagawa et al., 2017) (Accession n° DRA004738) was downloaded from www.ddbj.nig.ac.jp. RNA- Seq data sets for αβ T cells (comprising DN1, DN2a, DN2b, DN3, DN4 and DP) were downloaded from https://www.immgen.org/. The raw data was processed by the standard Babraham Bioinformatics pipeline at the Babraham Institute.

In brief, quality control of the raw reads was performed using FastQC (http://www.bioinformatics.babraham.ac.uk/projects/fastqc/), and adaptor sequences were trimmed and poor-quality bases were eliminated using Trim Galore! (https://www.bioinformatics.babraham.ac.uk/projects/trim_galore/). The reads were subsequently mapped to the GRCm38 reference genome (Ensembl) using HiSat2 (https://ccb.jhu.edu/software/hisat2/). Analysis of Bcl6 expression in RNA-seq data from Immgen and Kitagawa *et al.* 2017, was performed by Dr Christel Krueger.

The mapped sequence data from Wing J *et al.* 2017 was analysed using SeqMonk and hierarchical clustering was performed on a custom list of genes (https://www.bioinformatics.babraham.ac.uk/projects/seqmonk/).

2.10 ELISA

Mouse blood samples were collected by cardiac puncture after euthanasia and serum was separated from the blood by centrifuging the samples for 15 minutes at 800*g*.

2.10.1 NP-ELISA

Nunc Maxisorb 96-well plates (ThermoFisher Scientific, cat # 44-2404-21) were coated with 50µl per well NP7-BSA (Biosearch Technologies, cat # N-5050L) at 10µg/ml or NP20-BSA (Biosearch Technologies, cat # N-5050H) at 2.5µg/ml, and incubated overnight at 4°C. Plates were washed with PBS containing 0.05% (v/v) Tween 20 (Sigma, cat # P2287) by flooding the wells and removing the wash buffer by flicking the plate. Plates were then blocked with 200µl 2% (w/v) BSA in PBS for one hour at room temperature. Serum samples were added at a starting dilution of 1/200 and were further titrated 1:3 down the plate and incubated at room temperature for two hours. 50µl Horseradish Peroxidase (HRP) conjugated goat anti-mouse IgG1 (Abcam, cat # Ab97240), IgM (Abcam, cat # Ab9730) or IgG (Abcam, cat # Ab97023) were added at 1:8000 dilution in PBS and incubated for two hours at room temperature. Plates were developed using the 3,3',5,5'-Tetramethylbenzidine (TMB) substrate set (Biolegend, cat # 421101) and the reaction was stopped by adding 50µl 0.5M H_2SO_4 (Sigma, cat # 339741). Plates were read at 450nm using a PHERAstar FS plate reader (BMG Labtech) and analysed using Microsoft Excel.

2.11 Confocal imaging

I optimised this method during my PhD, and the method was published as a book chapter in 2017 (Vanderleyden and Linterman, 2017).

2.11.1 Preparation of frozen tissue and cryo-sectioning

Mediastinal or inguinal LNs were fixed in Periodate-lysine-paraformaldehyde (PLP) containing 1% (v/v) PFA (Sigma, cat # P6148), 0.075M L-Lysine (Sigma, cat # L5501), 0.37M Na_3PO_4 (pH 7.4) (Sigma, cat # 342483) and 0.01M $NaIO_4$ (Sigma, cat # 210048), for

four hours at 4°C. After fixation, the samples were cryoprotected in 30% (w/v) sucrose (Sigma, cat # S0389) and embedded in Optimum Cutting Temperature (OCT) (VWR, cat # 25608-930) and stored at -80 °C until further use. The frozen tissues were cut into 10µm serial sections at -20°C using a cryostat (Leica Biosystems) and stored at -80 °C until further use.

2.11.2 Immunofluorescence staining

Slides were air-dried and rehydrated with wash buffer (0.5% (v/v) Tween 20 in PBS by submerging them in a coplin jar. Non-specific binding of primary antigens was blocked with 200µl blocking buffer (PBS, 2% (w/v) BSA (Bovine Serum Albumin), 10% (v/v) normal goat serum (NGS)). Prior to primary antibody staining, samples were permeabilised with 200µl PBS containing 2% (v/v) Triton X (Sigma, cat # X100). After washing the slides with wash buffer in the coplin jar three times, the samples were incubated overnight at 4°C with 200µl of the following primary antibodies diluted in 1% (w/v) BSA in wash buffer: eFluor 450-conjugated Rat anti-mouse/rat Foxp3 (clone clone FJK16S, ThermoFisher Scientific, cat # 48-5773-82) (1:50), Alexa Fluor 488-conjugated Rat anti-mouse/rat Foxp3 (clone clone FJK16S, ThermoFisher Scientific, cat # 48-5773-82) (1:50), Hamster anti-mouse CD3ε purified (Clone 500A2, ThermoFisher Scientific, cat # 14-0033-81) (1:200), Rabbit anti-mouse Ki67 (Abcam, cat # Ab 15580) (1:100), eFluor 450-conjugated Rat anti-mouse Ki67 (Clone, SolA15, ThermoFisher Scientific, cat # 48-5678-82) (1:100), and Alexa 647-sonjugated Rat anti-mouse IgD (clone 11-26c.2a, Biolegend, cat # 405707) (1:100). Secondary antibodies, Alexa-568-conjugated goat anti-hamster IgG (LifeTechnologies, cat # A-21112) (1:500) and Alexa-488-conjugated goat anti rabbit (Abcam, cat # 150077) (1:400), were added in 200µl 2% (v/v) NGS in wash buffer and incubated for two hours at room temperature or overnight at 4°C. Samples were mounted in Hydromount aqueous mounting medium (National diagnostics, HS-106), with the coverslip gently added using forceps to avoid the generation of bubbles. Slides were dried overnight for the mounting medium to set.

2.11.3 Imaging and analysis

Images were acquired using a Zeiss 780 microscope using 20x and 40x objectives. Image analysis was performed using Volocity (PerkinElmer). At least three different cross-sections were analysed per mouse and each GC within those cross sections was imaged. The germinal centre (GC) area (μm^2) was manually defined as IgD^-Ki67^+. The number of Tfr cells within the GC (defined as $CD3^+Foxp3^+$), and the number of Tfh cells ($CD3^+Foxp3^-$), within the GC

were counted manually. The image analysis was performed blinded. The number of Tfh cells and Tfr cells were normalised to the GC area or to the number of Tfh cells. This analysis was performed by Sigrid Fra-Bido.

2.12 Bcl6 motif analysis

The sequences for the positions of super-enhancers (SE) specific for Treg cells and Tconv cells as defined by Kitagawa *et al.*(Kitagawa et al., 2017) were downloaded from the UCSC Genome Browser (NCBI37). FIMO (MEME Suite) was used to find occurrences of the Bcl6-consensus motif (TTCCTAGAA) in Treg and Tconv-specific SE. The frequency of the Bcl6 motif per kilobase (kb) was calculated. The subset of Treg SE with a motif frequency higher than 0.35 motifs per kb were imported in SeqMonk and the positions of the genes associated with these Treg-specific SE were determined. This analysis was performed by Dr. Christel Krueger, Babraham Bioinformatics, The Babraham Institute.

2.13 Statistical analysis

Statistical analysis was carried out using the Graphpad Prism v6 and v7 software. All data points were analysed and outliers were not removed unless there were technical errors. Statistical tests were chosen in advance as part of the experimental design. Sample sizes were determined in advance based on the availability of age-matched experimental mice and controls. Due to the small sample sizes ($n \leq 10$), the data was assumed to follow non-gaussian distributions, therefore p values were determined by non-parametric tests. Unpaired comparisons were performed using the Mann-Whitney U test. Multiple comparisons were analysed using the Kruskall-wallis test with Dunn's multiple comparison test. Grouped analyses were performed by a 2-way ANOVA with Sidak's multiple comparisons, and the multiplicity adjusted p value was reported for the comparisons indicated on the figures. All experiments were repeated at least three times, unless stated otherwise. Data are presented as the median with single data points. $p < 0.05$ (or $p<0.04$ for tSNE) was used as a threshold for statistical significance.

3 Validation of *Cxcr5*$^{fl/fl}$*Foxp3*^{cre} mice as a follicular regulatory T cell-deficient mouse model

3.1 Background

Follicular regulatory T (Tfr) cells are a subset of Foxp3^{+} Treg cells located within the GC where they suppress the size and output of the germinal centre response. The first description of Tfr cells in the literature was by Lim *et al.* who identified Foxp3^{+} T cells within human tonsil GCs in 2004 (Lim et al., 2004). In 2011, three independent groups demonstrated in detail that Foxp3^{+}CD4^{+} T cells are able to undergo functional differentiation into a specialised subset of Treg cells that control the magnitude and output of the GC response (Chung et al., 2011, Linterman et al., 2011, Wollenberg et al., 2011). While the field has grown exponentially in recent years, relatively little is known about the exact role of Tfr cells within the GC, and the mechanism/s through which they exert their suppressive function. Given the central role of the GC response in generating highly effective humoral immune responses and immunological memory, it is of considerable biological interest to understand how Tfr cells curtail this response (Vanderleyden et al., 2014). At the outset of this work, the major obstacle in examining Tfr cell biology was the lack of appropriate tools to study Tfr cells specifically, without affecting Tfh cells or other Treg cell subsets. A unique feature of Tfr cells is their

localisation within the GC and this discriminates them from other Treg cell subsets. Therefore, genetic strategies that prohibit Treg cells from entering the GC are a rational approach to generating mouse models that lack Tfr cells.

3.1.1 Treg homing to the GC

Tfr cells are Treg cells within the GC, but how do Treg cells gain access to the GC? Akin to Tfh cells, CXCR5 expression is essential for Treg homing to the GC (Chung et al., 2011, Wollenberg et al., 2011). Chung *et al.* adoptively transferred Treg cells from *Cxcr5*$^{-/-}$ mice into *Tcrb*$^{-/-}$ mice and then immunised them with KLH in complete freund's adjuvant (CFA). *Tcrb*$^{-/-}$ mice lack the αβ TCR due to the absence of a functional β chain, and thus lack functional αβ T cells (but retain γδ T cells). Mice receiving CXCR5-deficient Treg cells showed impaired recruitment of the Treg cells to the GC as well as an increase in the frequency of GC B cells (Chung et al., 2011). Similar results were obtained by a study of Wollenberg *et al.* in which CXCR5-deficient Treg cells were co-transferred with OT-II cells into *Tcra*$^{-/-}$ mice (in which a lack of the TCR α chain results in deficiency in the αβ TCR and therefore αβ T cells) followed by Ovalbumin (OVA) in Alum immunisation. In this study, CXCR5-deficient Treg cells could not migrate to the GC, which resulted in an increased GC size (Wollenberg et al., 2011). Consequently, these pioneering studies show that CXCR5 expression is indispensable for Treg homing to the GC.

In summary, Treg cell access to the GC, and therefore Tfr cell development, appears to be uniquely dependent on CXCR5-driven chemotaxis towards the GC. In this regard, this migratory behavior distinguishes Tfr cells from Tfh cells, and makes genetic targeting of CXCR5 in Foxp3^{+} Treg cells an appealing approach for generating a mouse that specifically lacks Tfr cells.

3.1.2 *In vivo* models to study Treg cells within the GC

In vitro Treg cell suppression assays showed that Tfr cells have a similar suppressive capacity as Treg cells (Linterman et al., 2011). However, their role *in vivo* has not been as easy to dissect. The three groups that initially described mouse Tfr cells used varying experimental strategies to determine their function *in vivo,* leading to conflicting results (Chung et al., 2011, Linterman et al., 2011, Wollenberg et al., 2011). In one study, mixed bone marrow chimaeras (bone marrow from SAP-deficient mice and Foxp3-Diphteria toxin Receptor (DTR) mice) were used to examine the effect of a specific reduction in Tfr cells on the GC response. These

experiments demonstrated that a reduction in Tfr cell number leads to increased Tfh cells and GC B cells in response to immunisation with a T-dependent antigen, suggesting that Tfr cells can suppress features of the GC response *in vivo*. The reduction in Tfr cells was accompanied by a slight decrease in high-affinity antibodies. Furthermore, there were fewer antigen-specific GC B cells, indicating that Tfr cells can partly control the GC response by limiting development of non-antigen specific B cells (Linterman et al., 2011). In contrast, Chung *et al.* used an adoptive transfer model in which *Cxcr5*$^{-/-}$ or *Bcl6*$^{-/-}$ Treg cells together with naïve CD4^{+} T cells were transferred into *Tcrb*$^{-/-}$ mice. An increase in the number of GC B cells as well as antibody titres of both high and low affinity could be observed after immunisation, although the number of Tfh cells was unaffected (Chung et al., 2011). Similar results were obtained in the study of Wollenberg *et al.,* in which transfer of *Cxcr5*$^{-/-}$ Treg cells into *Tcra*$^{-/-}$ mice resulted in an increased GC response characterised by increased antibody secretion (Wollenberg et al., 2011). A later study demonstrated that Tfr cells could suppress both activation and proliferation of responder T cells and IgG production *in vitro* (Sage et al., 2013).

While these studies agree that Tfr cells can limit the size of the GC response, whether they also control antigen-specific antibody production remains contentious. The discrepancies between these studies may arise from the use of different immunisation strategies, slightly different environmental conditions, as well as different experimental systems such as bone marrow chimaera and adoptive T cell transfer models. These experimental systems are contrived and require a high degree of manipulation, which may confound interpretation of the results. An additional possible explanation might be the fact that knocking out either CXCR5, SAP or Bcl6 in Treg cells in these experiments might not affect the Tfr population alone, but may also have an impact on other aspects of Treg biology. New tools will need to be generated to study the role(s) that Tfr cells play in the GC.

In this chapter I aimed to generate a strain of mice that lack Tfr cells by genetically removing CXCR5 expression from Foxp3^{+} regulatory T cells. To this end, I used *Foxp3*$^{YFP\text{-}cre}$ mice in which the *cre recombinase* gene is inserted in the *Foxp3* locus, and *Cxcr5*$^{fl/fl}$ mice (Rubtsov et al., 2008). To generate *Cxcr5*$^{fl/fl}$ mice, exon 2 of the *Cxcr5* gene was flanked by two *Loxp* sites. In this *Cxcr5*$^{fl/fl}$*Foxp3*^{cre} model, *Cxcr5* should be excised in all cells expressing Foxp3 and, therefore, all Treg cells. Based on previous reports demonstrating the requirement of CXCR5 for Tfr cell localisation to the GC, we hypothesised that *Cxcr5*$^{fl/fl}$*Foxp3*^{cre} mice would be devoid of Tfr cells without compromising Tfh cells or other Treg subsets (Chung et al.,

2011). Therefore, this system can be used to explore changes in the GC response in the absence of Tfr cells and will provide fundamental insights into Tfr biology.

3.2 Results

3.2.1 Deletion of CXCR5 on Treg cells in *Cxcr5$^{fl/fl}$Foxp3^{cre} mice* after SRBC immunisation

To test the use of *Cxcr5$^{fl/fl}$Foxp3*^{cre} mice as a model system for mice that lack Tfr cells within the GC, *Cxcr5$^{fl/fl}$Foxp3^{cre}* mice were immunised with sheep red blood cells (SRBC) *i.p.*, which induces a strong GC response in the spleen, and analysed the GC response 14 days after immunisation (Figure 3.1 A). This time-point was chosen as kinetic data shows that Tfr cells peak 14 days after SRBC immunisation as opposed to Tfh cells, which peak between 7 and 11 days after SRBC immunisation (Vanderleyden et al., 2014). To confirm cre activity in Foxp3$^+$ Treg cells, I determined successful excision of CXCR5 by cell surface staining. *Cxcr5$^{fl/fl}$Foxp3^{cre}* mice showed a significant reduction in frequency and absolute number of CD4$^+$Foxp3$^+$CXCR5$^+$PD-1$^+$ cells using flow cytometry (Figure 3.1 B-D). This decrease in CXCR5$^+$ Treg cells was not due to a decrease in the number of total Foxp3$^+$ Treg cells (Figure 3.1 E-G). These results show that genetic ablation of CXCR5 on Foxp3$^+$ cells was successful in *Cxcr5$^{fl/fl}$Foxp3^{cre}* mice.

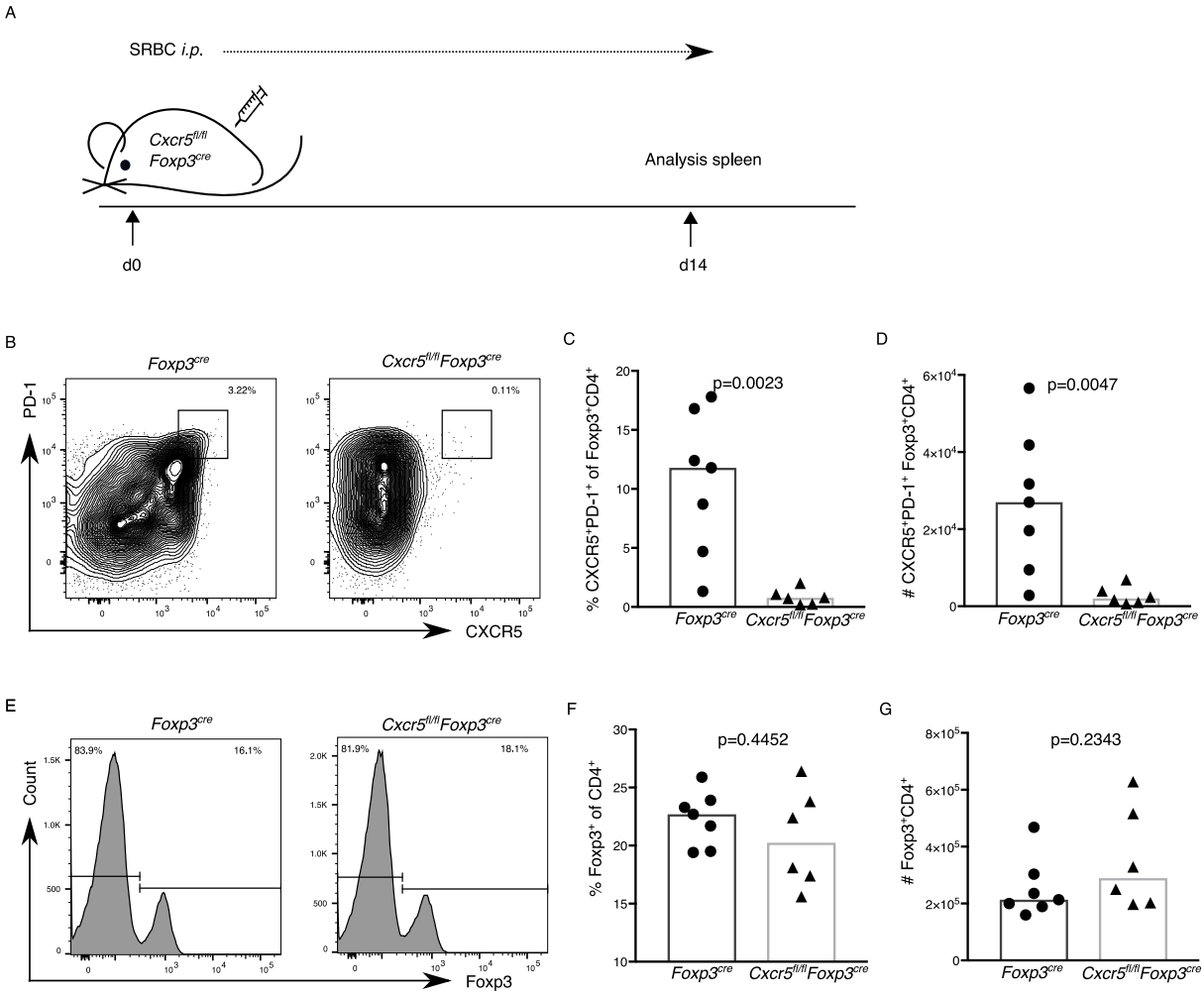


Figure 3.1 Deletion of CXCR5 on Treg cells *in Cxcr5$^{fl/fl}$Foxp3^{cre}* mice.

Analysis of Tfr cells 14 days after *i.p.* immunisation with SRBC. **A.** Diagram shows experimental set-up. Mice were immunised with SRBC *i.p.* and 14 days after immunisation the spleen was collected and the GC response was analysed. **B.** Representative flow cytometry contour plots of PD-1^{+}CXCR5^{+} cells from Foxp3^{+}CD4^{+} cells. **(C-D)** Quantification of **C.** the frequency and **D.** absolute numbers of CXCR5^{+}PD-1^{+}Foxp3^{+}CD4^{+} cells. **E.** Representative flow cytometry histograms of Foxp3^{+} Treg cells as a proportion of CD4^{+} cells. **(F-G)** Quantification of **F.** the frequency and **G**. the absolute numbers of Foxp3^{+} Treg cells. Each symbol represents one mouse, and the horizontal bars represent the median values. P values were determined using a Mann-Whitney U test. Data represent two independent experiments.

3.2.2 *Cxcr5*$^{fl/fl}$*Foxp3*^{cre} mice show normal numbers of GC B cells and Tfh cells

The initial studies identifying Tfr cells in the GC showed that the absence of Tfr cells is associated with an increased GC size and an increased number of Tfh cells (Chung et al., 2011, Linterman et al., 2011, Wollenberg et al., 2011). If deletion of CXCR5 on Treg cells is indeed sufficient to generate Tfr-deficient mice, an increase in the GC size and/or the Tfh population should be observed in our model. To test this, mice were immunised with SRBC and the frequency of GC B cell and Tfh cell populations was analysed 14 days after immunisation. *Cxcr5*$^{fl/fl}$*Foxp3*^{cre} mice had a comparable GC B cell (Figure 3.2 A-C) and Tfh cell (Figure 3.2 D-F) frequency and numbers, compared with *Foxp3*^{cre} control animals.

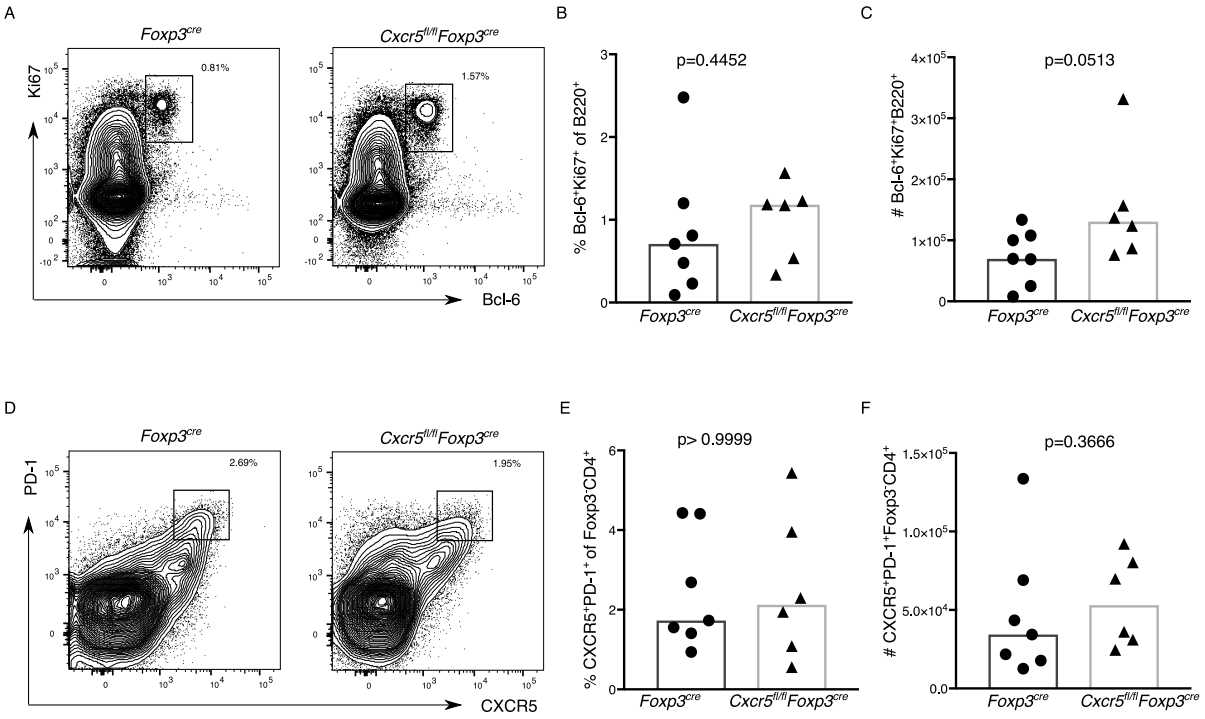


Figure 3.2 *Cxcr5$^{fl/fl}$Foxp3^{cre}* mice show normal numbers of GC B cells and Tfh cells.

Analysis of splenic GC B and Tfh cells 14 days after *i.p.* SRBC immunisation. **A.** Representative flow cytometry contour plots of GC B cells, gated as Bcl6^{+}Ki67^{+} cells from B220^{+} cells. **(B-C)** Quantification of **B**. the frequency and **C.** absolute numbers of GC B cells. **D.** Representative flow cytometry histograms of CXCR5^{+}PD-1^{+} Tfh cells from Foxp3^{-}CD4^{+} cells. **(E-F)**. Quantification of **E.** the frequency and **F**. absolute numbers of CXCR5^{+}PD-1^{+} Tfh cells. Each symbol represents one mouse, and the horizontal bars represent the median values. P values were determined using a Mann-Whitney U test. Data represent two or more independent experiments.

3.2.3 *Cxcr5*$^{fl/fl}$*Foxp3*^{cre} mice show normal plasma cell responses after re-challenge

As I did not observe any differences in the GC size or Tfh cell population in *Cxcr5*$^{fl/fl}$*Foxp3*^{cre} mice, it was of interest to investigate the long-term immune response as well as the recall immune response. Furthermore, it is possible that Tfr cells predominantly regulate the quality of the output of the GC (Linterman et al., 2011). To evaluate the possibility that Tfr cells might not only regulate the size but also play a role in fine-tuning the output of the GC, we investigated antigen-specific plasma cells and GC B cells. For this purpose, I immunised mice with NP-KLH. NP is a hapten and hence acts as an antigen that B cells are able to bind, but T cells cannot recognise. When the NP hapten is linked to the carrier molecule KLH, the NP-KLH complex elicits a T-dependent immune response and allows for the analysis of antigen-specific (NP^+) B cells.

Mice were immunised *i.p.* with NP-KLH in alum and two groups of mice were analysed at different time points post immunisation. The first group had the spleen and bone marrow collected and analysed for plasma cells 48 days after immunisation. In the second group mice received a booster immunisation of NP-KLH in Alum 48 days after primary immunisation and the spleen and bone marrow were analysed 7 days after secondary immunisation, at day 56 after the primary immunisation (Figure 3.3 A).

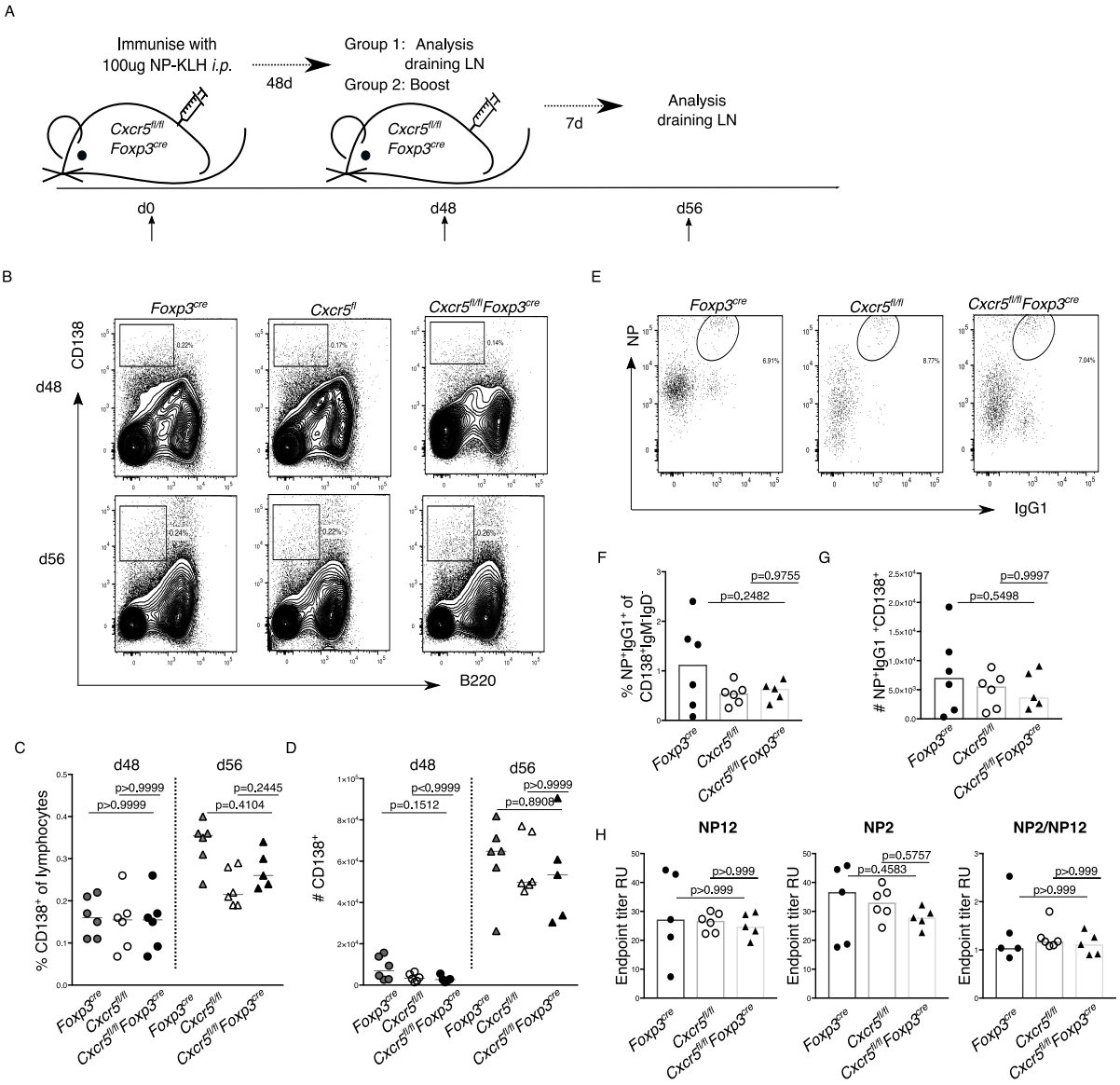

A
Immunise with
100ug NP-KLH i.p.
48d
Group 1: Analysis
draining LN
Group 2: Boost
7d
Analysis
draining LN
Cxcr5fl/fl
Foxp3cre
d0
d48
d56
B
Foxp3cre
Cxcr5fl
Cxcr5fl/flFoxp3cre
CD138
d48
d56
B220
E
NP
IgG1
C
d48
d56
% CD138+ of lymphocytes
p>0.9999
p>0.9999
p=0.4104
p=0.2445
D
# CD138+
p=0.1512
p<0.9999
p=0.8908
p>0.9999
F
% NP+IgG1+ of CD138+IgM-IgD-
p=0.2482
p=0.9755
G
# NP+IgG1 +CD138+
p=0.5498
p=0.9997
H
NP12
NP2
NP2/NP12
Endpoint titer RU
p>0.999
p>0.999
p=0.4583
p=0.5757
p>0.999
p>0.999

Figure 3.3 *Cxcr5*$^{fl/fl}$*Foxp3*^{cre} mice show normal plasma cell responses in the spleen after re-challenge.

Analysis of the plasma cell response 48 days and 56 days (7 days post boost) after *i.p.* immunisation with NP-KLH in the spleen. **A**. Diagram shows experimental set-up. Mice were immunised with NP-KLH *i.p.* and 48 days after immunisation the spleen was collected for group 1 and the plasma cell response was analysed. Group 2 received a booster immunisation with NP-KLH *i.p.* at day 48 and 7 days after receiving the boost, on day 56 after the first immunisation, the spleen was collected and the plasma cell response was analysed. **B.** Representative flow cytometry plots of $CD138^+$ plasma cells ($CD138^+B220^{int}$) at day 48 and day 56. **(C-D)**. Quantification of **C.** the frequency and **D.** absolute numbers of $CD138^+$ plasma cells. **E.** Representative flow cytometry plots of NP^+IgG1^+ plasma cells gated from $IgM^-IgD^-CD138^+$ cells at day 56. **(F-G)**. Quantification of **F.** the frequency and **G.** absolute number of NP^+IgG1^+ plasma cells. **H.** Levels of IgG1 specific for NP2 or NP20 in the sera (day 56). Each symbol represents one mouse, and the horizontal bars represent the median values. P values were determined using a two-way ANOVA or a Kruskal-Wallis test with Dunn's multiple comparisons test. Data are from one experiment.

As expected, there was an increase in both the frequency and the absolute number of plasma cells at day 56 as compared to day 48. However, *Cxcr5*$^{fl/fl}$*Foxp3*^{cre} mice did not show any differences in plasma cell frequency, or absolute number (Figure 3.3 B-D). We next monitored antigen-specific plasma cells in *Cxcr5*$^{fl/fl}$*Foxp3*^{cre} mice but did not detect any changes in the frequency or number of NP^{+}IgG1^{+} (antigen-binding and class-switched) plasma cells (Figure 3.3 E-G). Finally, I tested whether affinity maturation was affected in *Cxcr5*$^{fl/fl}$*Foxp3*^{cre} mice by ELISA at day 56. For this purpose I tested the affinity of serum IgG1 for NP2 (to which only high-affinity antibodies will bind due to the low NP/BSA Ratio) and NP12 (to which both low and high affinity antibodies will bind). A relative increase in NP12 binding compared to NP2 would be indicative of diminished affinity maturation in *Cxcr5*$^{fl/fl}$*Foxp3*^{cre} mice. There were no changes in NP2 specific IgG1, NP12 specific IgG1, or in the NP2/N12 ratio (Figure 3.3 H)

I next tested the GC (GL-7^{+}) B cell response and the memory (CD38^{+}) B cell response (Figure 3.4 A) in *Cxcr5*$^{fl/fl}$*Foxp3*^{cre} mice after re-challenge using the same immunisation protocol as in Figure 3.3. *Cxcr5*$^{fl/fl}$*Foxp3*^{cre} mice developed normal GC B cell responses and memory B cell responses after re-challenge (Figure 3.4 A-E). In addition, there were no changes in the number or frequency of antigen-specific (NP^{+}) GC B cells (Figure 3.4 F-H) or memory B cells (Figure 3.4 I-K).

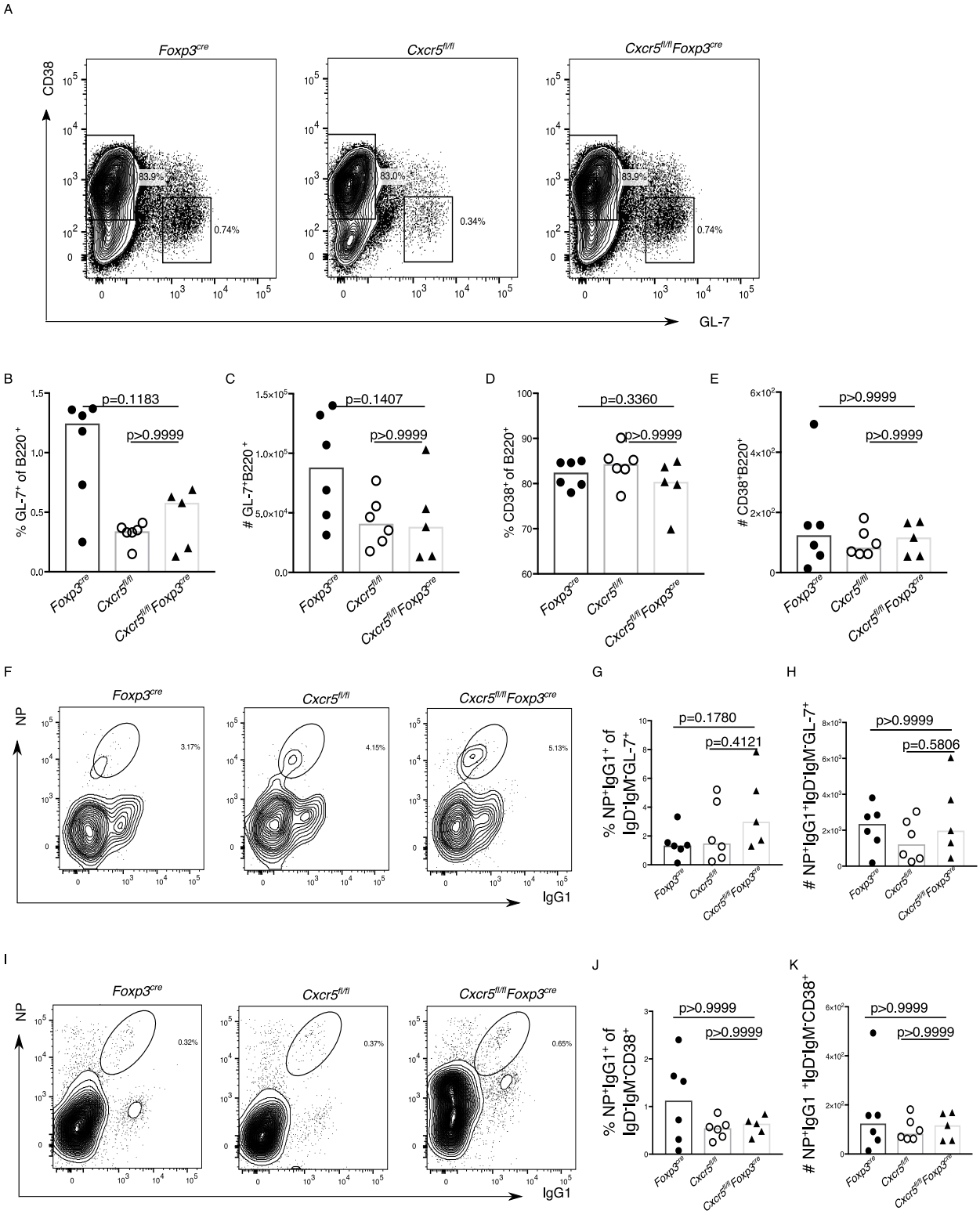

A
Foxp3cre
Cxcr5fl/fl
Cxcr5fl/flFoxp3cre
CD38
GL-7
83.9%
0.74%
83.0%
0.34%
83.9%
0.74%
B
% GL-7+ of B220+
p=0.1183
p>0.9999
C
# GL-7+B220+
p=0.1407
p>0.9999
D
% CD38+ of B220+
p=0.3360
p>0.9999
E
CD38+B220+
p>0.9999
p>0.9999
F
NP
IgG1
3.17%
4.15%
5.13%
G
% NP+IgG1+ of IgD-IgM-GL-7+
p=0.1780
p=0.4121
H
NP+IgG1+IgD-IgM-GL-7+
p>0.9999
p=0.5806
I
NP
IgG1
0.32%
0.37%
0.65%
J
% NP+IgG1+ of IgD-IgM-CD38+
p>0.9999
p>0.9999
K
NP+IgG1 +IgD-IgM-CD38+
p>0.9999
p>0.9999

Figure 3.4 *Cxcr5*$^{fl/fl}$*Foxp3*^{cre} mice show normal GC B cell and memory B cell responses in the spleen after re-challenge.

Analysis of the GC B cell response and memory B cell response 56 days (7 days post boost) after *i.p.* immunisation with NP-KLH in the spleen. **A**. Representative flow cytometry plots of $CD38^+$ memory B cells and GL-7^+ GC B cells pre-gated from $B220^+$ cells. **(B-C)** Quantification of **B.** the frequency and **C**. Absolute numbers of GL-7^+ GC B cells. **(D-E)** Quantification of **D.** the frequency and **E.** absolute number of $CD38^+$ memory B cells. **F.** Representative flow cytometry plots of NP^+IgG1^+ cells pre-gated from IgD^-IgM^-GL-7^+ $B220^+$ cells. **(G-H)** Quantification of **G.** the frequency and **H.** absolute numbers of NP^+IgG1^+ GC B cells. **I.** Representative flow cytometry plots of NP^+IgG1^+ cells pre-gated from $IgD^-IgM^-CD38^+$ $B220^+$. (**J-K)** Quantification of **J.** the frequency and **K.** absolute numbers of NP^+IgG1^+ memory B cells. Each symbol represents one mouse, and the horizontal bars represent the median values. P values were determined using a Kruskal-Wallis test with Dunn's multiple comparisons test. Data are from one experiment.

Long-lived plasma cells home to the bone marrow, so I tested if the homing of these plasma cells was affected in *Cxcr5*$^{fl/fl}$*Foxp3*^{Cre} mice (Slifka et al., 1998). The same immunisation protocol was used as in Figure 3.3 A. The proportion and absolute numbers of CD138^{+} plasma cells in the bone marrow was not changed in our model indicating that plasma cell homing to the bone marrow was not affected by the absence of CXCR5^{+}PD-1^{+} Tfr cells (Figure 3.5 A-C). Collectively, these results indicate that *Cxcr5*$^{fl/fl}$*Foxp3*^{cre} mice develop normal plasma cell, memory B cell and GC B cell recall responses after NP-KLH immunisation.

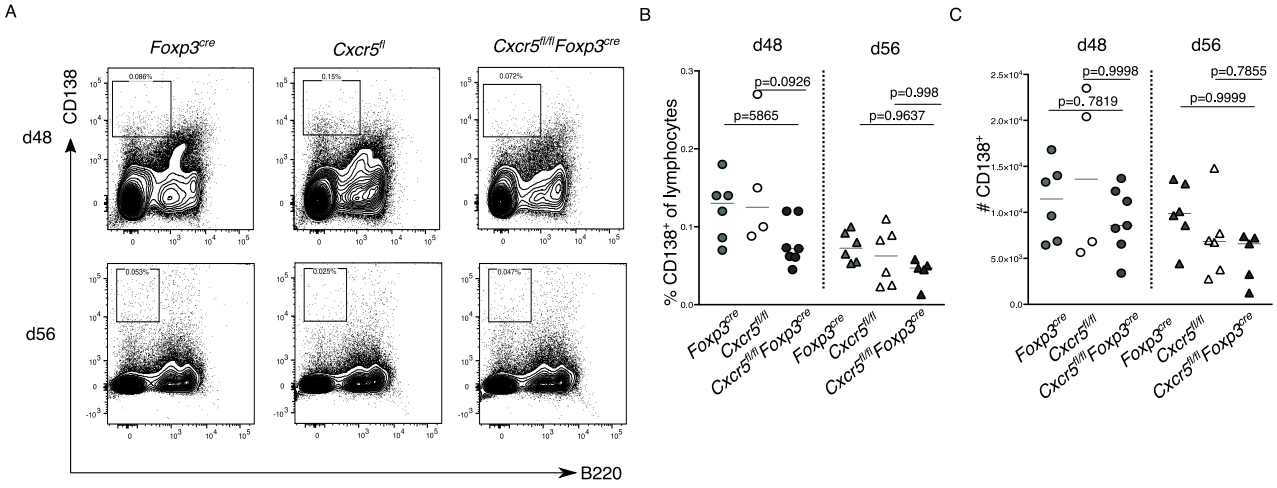


Figure 3.5 *Cxcr5*$^{fl/fl}$*Foxp3*^{cre} mice show normal plasma cell homing to the bone marrow.

Analysis of the plasma cell response 48 days and 56 days (7 days post boost) after *i.p.* immunisation with NP-KLH in the bone marrow. **A.** Representative flow cytometry plots of CD138^{+} plasma cells (CD138^{+}B220^{int}) at day 48 and day 56. **(B-C)** Quantification of **B.** the frequency and **C**. absolute numbers of CD138^{+} plasma cells. Each symbol represents one mouse, and the horizontal bars represent the median values. Statistical significance was determined using a Kruskal-Wallis test with Dunn's multiple comparisons test. Data represent one experiment.

3.2.4 *Cxcr5*$^{fl/fl}$*Foxp3*^{cre} mice show non-specific deletion of CXCR5

Since I was unable to observe phenotypic differences in *Cxcr5*$^{fl/fl}$*Foxp3*^{cre} mice using non-replicating antigens such as SRBC and NP-KLH, I decided to use a stronger immune stimulus reasoning that subtle changes in the immune system might go undetected using milder immunisation strategies. For this purpose, mice were infected with the influenza A virus, HKx31. The GC response was analysed in the mediastinal LN at day 13, the peak of the GC response in influenza infection. I first determined the magnitude of the GC response and was unable to find any differences between *Cxcr5*$^{fl/fl}$*Foxp3*^{cre} mice and controls (Figure 3.6 A-C). Surprisingly, there was a significant decrease in CXCR5^{+}PD-1^{+}Foxp3^{-} Tfh cells (Figure 3.6 D-F). This was unexpected as an increase in Tfh cells would be anticipated if Tfr cells are absent from the GC based on previous reports (Linterman et al., 2011).

To confirm this decrease in Tfh cells, Tfh cells were analysed by co-expression of PD-1 and Bcl6 instead of PD-1 and CXCR5. Bcl6 is the transcriptional regulator for Tfh cells and is necessary and sufficient to drive Tfh development (Yu et al., 2009). Therefore, Tfh cells can be identified as Bcl6^{+}PD-1^{+} CD4 T cells as a proxy for CXCR5^{+}PD-1^{+} Tfh cells. Interestingly, I did not observe a decrease in Bcl6^{+}PD-1^{+} Tfh cells (Figure 3.6G-I). These results suggested that there might be non-specific deletion of CXCR5 in our model. Indeed, I identified a substantial population CXCR5-negative B cells in *Cxcr5*$^{fl/fl}$*Foxp3*^{cre} mice, not observed in control mice (Figure 3.6 J-L). The non-specific deletion of CXCR5 on B cells and non-Foxp3^{+} T cells may be due to non-specific cre recombinase activity. *Cxcr5*$^{fl/fl}$*Foxp3*^{cre} mice have a targeted insertion of LoxP sites into inton 1 and intron 2 of the *Cxcr5* gene. Therefore, cre-mediated recombination deletes intron 1 and 2 and this deletion can be detected as a 214 base pair PCR product. If cre expression is not finely controlled by the Foxp3 locus, off-target excision of this allele can be detected in the biopsy material. Therefore, a group of control and *Cxcr5*$^{fl/fl}$*Foxp3*^{cre} mice was tested for the presence of the excised CXCR5 allele using PCR and gel electrophoresis on ear biopsy samples. All but one *Cxcr5*$^{fl/fl}$*Foxp3*^{cre} mouse expressed the *Cxcr5* excised allele (Figure 3.6 M). Therefore, it is probable that cre recombinase is active in cells other than Foxp3^{+} Treg cells. Together, these data confirm that the *Cxcr5*$^{fl/fl}$*Foxp3*^{cre} model shows deletion of *Cxcr5* outside the Treg cell compartment due to a "leaky" cre recombinase allele. This makes interpretation of the phenotype of these animals difficult, as CXCR5 is important on T and B cells for homing to

the B cell follicle, and loss of this receptor on these cells may dampen the GC response due to non-Treg effects.

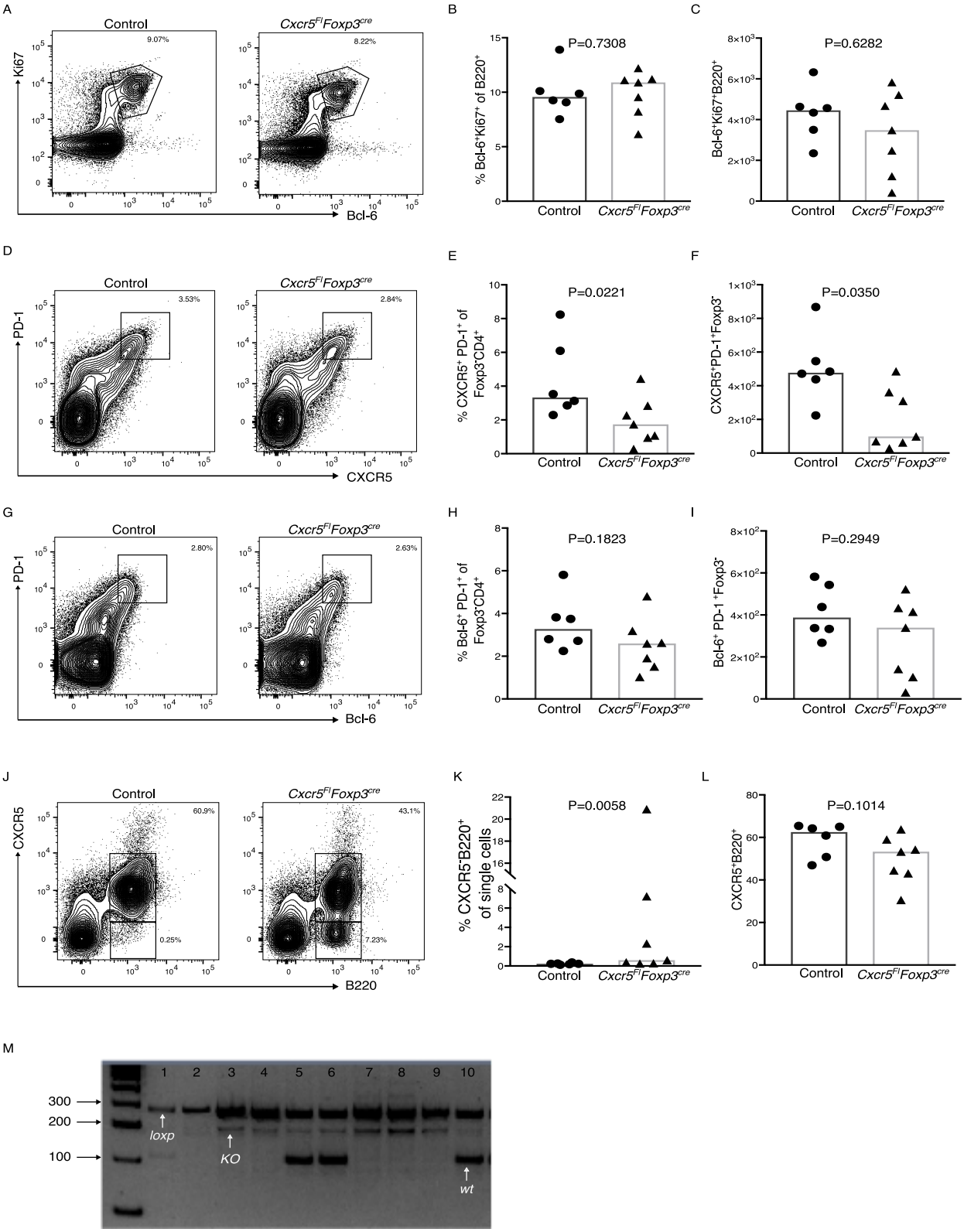


Figure 3.6 *Cxcr5*$^{fl/fl}$*Foxp3*^{cre} mice show non-specific deletion of CXCR5 in non-Treg cells.

Analysis of the GC response 13 days after influenza A (HKx31) infection in *Cxcr5*$^{fl/fl}$*Foxp3*^{cre} mice and controls (mix of *Cxcr5*$^{fl/fl}$*Foxp3*^{wt} mice and *Cxcr5*$^{+/+}$*Foxp3*^{cre} mice). **A.** Representative flow cytometry contour plots of GC B cells, gated as Bcl6^{+}Ki67^{+} cells of B220^{+} cells. **(B-C)** Quantification of **B.** the frequency and **C.** absolute numbers of Bcl6^{+}Ki67^{+} GC B cells. **D.** Representative flow cytometry contour plots of CXCR5^{+}PD-1^{+} Tfh cells from Foxp3^{-}CD4^{+} cells. **(E-F)** Quantification of **E.** the frequency and **F.** absolute numbers of Bcl6^{+}PD-1^{+} Tfh cells. **G.** Representative flow cytometry contour plots of Bcl6^{+}PD-1^{+} Tfh cells of Foxp3^{-}CD4^{+} cells. **(H-I)** Quantification of **H**. the frequency and **I.** absolute numbers of Bcl6^{+}PD-1^{+}Foxp3^{-}CD4^{+} Tfh cells. **J.** Representative flow cytometry contour plots of CXCR5^{+}B220^{+} and CXCR5^{-}B220^{+} B cells. **K.** Quantification of the frequency of CXCR5^{-}B220^{+} B cells. **L.** Quantification of CXCR5^{+}B220^{+} B cells. **M.** Image from gel electrophoresis showing results from a PCR reaction for the Wt *Cxcr5* allele (214bp), *Cxcr5* excised allele (292bp) and the *Cxcr5* floxed allele (375bp) using ear notches from *Cxcr5*$^{+/+}$*Foxp3*^{cre} mice and controls. Each symbol represents one mouse, and the horizontal bars represent the median values. P values were determined using a Mann-Whitney *U* test. Data represent two or more independent experiments.

3.2.5 Treg cells are still present in the GC of *Cxcr5$^{fl/fl}$Foxp3cre* mice, albeit in reduced numbers

To confirm that loss of CXCR5 on Foxp3^{+} Treg cells was sufficient to impair Treg cell access to the GC, and therefore inhibit Tfr cell formation, the number of Bcl6^{+}PD-1^{+} Treg cells in *Cxcr5$^{fl/fl}$Foxp3^{cre}* mice was determined (Figure 3.7 A-E). Even though CXCR5 was deleted on Foxp3^{+} Treg cells (Figure 3.7 A-B), Bcl6^{+}PD-1^{+} Tfr cells could still be identified by flow cytometry in *Cxcr5$^{fl/fl}$Foxp3^{cre}* mice. The proportion of Bcl6^{+}PD-1^{+} Tfr cells was significantly reduced although the absolute number of these cells was not changed in *Cxcr5$^{fl/fl}$Foxp3^{cre}* mice relative to *Foxp3^{cre}* controls. To confirm these results, I determined the number of Treg cells present within the GC in cryosections of the spleen using confocal imaging (Figure 3.7 F). Tfr cells could still be identified within the GC of *Cxcr5$^{fl/fl}$Foxp3^{cre}* mice. The GC size was not significantly different from controls in *Cxcr5$^{fl/fl}$Foxp3^{cre}* mice (Figure 3.7 H). The number of Tfr cells within the GC was reduced in *Cxcr5$^{fl/fl}$Foxp3^{cre}* mice, but this reduction was not significantly different from control mice (Figure 3.7 I).

Collectively, the above results suggest that deletion of CXCR5 in Treg cells is not sufficient to impair their access to the GC in *Cxcr5$^{fl/fl}$Foxp3^{cre}* mice. However, due to aberrant cre expression in this model, these results need to be interpreted with caution as the deletion of CXCR5 on non-Treg cells in *Cxcr5$^{fl/fl}$Foxp3^{cre}* mice might affect the experimental outcome.

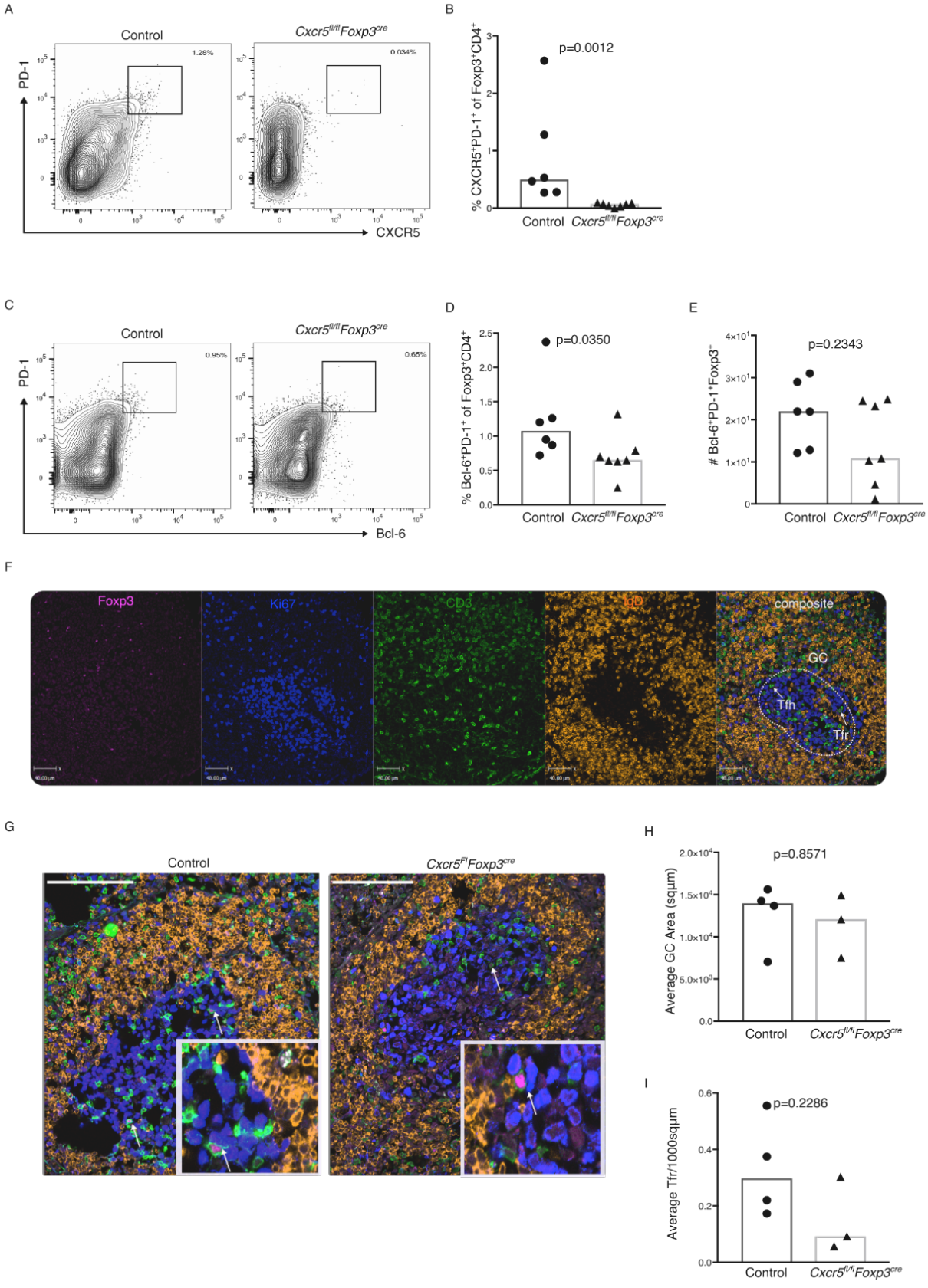

A
Control
Cxcr5fl/flFoxp3cre
1.28%
0.034%
PD-1
CXCR5
B
p=0.0012
% CXCR5+PD-1+ of Foxp3+CD4+
Control
Cxcr5fl/flFoxp3cre
C
Control
Cxcr5fl/flFoxp3cre
0.95%
0.65%
PD-1
Bcl-6
D
p=0.0350
% Bcl-6+PD-1+ of Foxp3+CD4+
Control
Cxcr5fl/flFoxp3cre
E
p=0.2343
# Bcl-6+PD-1+Foxp3+
Control
Cxcr5fl/flFoxp3cre
F
Foxp3
Ki67
CD3
IgD
composite
GC
Tfh
Tfr
G
Control
Cxcr5FlFoxp3cre
H
p=0.8571
Average GC Area (sqμm)
Control
Cxcr5fl/flFoxp3cre
I
p=0.2286
Average Tfr/1000sqμm
Control
Cxcr5fl/flFoxp3cre

Figure 3.7 Foxp3^{+} Treg cells are still present in the GC of *Cxcr5$^{fl/fl}$Foxp3^{cre}* mice.

Analysis of Tfr cells 13 days after influenza A virus (HKx31) infection in *Cxcr5$^{fl/fl}$Foxp3^{cre}* mice and controls (mix of *Cxcr5$^{fl/fl}$Foxp3^{wt}* mice and *Cxcr5$^{+/+}$Foxp3^{cre}* mice). **A.** Representative flow cytometry contour plots of Tfr cells, gated as CXCR5^{+}PD-1^{+} from Foxp3^{+}CD4^{+} T cells. **B.** Quantification of the frequency CXCR5^{+} Tfr cells. **C.** Representative flow cytometry contour plots of Tfr cells, gated as Bcl6^{+}PD-1^{+} of Foxp3^{+}CD4^{+}. **(D-E)** Quantification of **D.** the frequency and **E.** absolute number of Bcl6^{+}PD-1^{+}Foxp3^{+}CD4^{+} Tfr cells. **F.** Cryosections were stained with Foxp3 (magenta), Ki67 (Blue), CD3 (Green) and IgD (orange). Objective magnification 40x, scale bar = 40µm **G.** Representative confocal image of the GC with Tfr cells indicated by the arrows. Objective magnification 40x, scale bar 100µm. **H.** Quantification of the average GC area in µm^{2}. Each dot represents the average GC area of at least 5 different GCs for one mouse. **I.** Quantification of the average number of Tfr cells, defined as CD3^{+}Foxp3^{+}, per 1000µm^{2}. Each dot represents the average number of Tfr per 1000 µm^{2}, in at least 4 different GCs per mouse. Each symbol represents one mouse, and the horizontal bars represent the median values. P values were determined using a Mann-Whitney *U* test. Data represent two independent experiments.

3.2.6 *Cxcr5*$^{fl/fl}$*Cd4*$^{cre/+}$ mice show a normal GC response

To confirm that deletion of CXCR5 on Treg cells is insufficient to impair Treg cell access to the GC in a different model, I infected *Cxcr5*$^{fl/fl}$*Cd4*$^{cre/+}$ mice with influenza A virus and analysed the GC response 14 days after infection. In *Cxcr5*$^{fl/fl}$*Cd4*$^{cre/+}$ mice, CXCR5 will be deleted in all CD4^{+} T cells, and therefore I hypothesised that there would be reduced homing of Tfh and Tfr cells to the GC in these mice.

I first tested the excision of CXCR5 on Foxp3^{+} and Foxp3^{-} T cells using protein surface staining. As expected, CXCR5^{+} Treg and CXCR5^{+} Th cells are absent in *Cxcr5*$^{fl/fl}$*Cd4*$^{cre/+}$ mice (Figure 3.8) due the cre-mediated deletion.

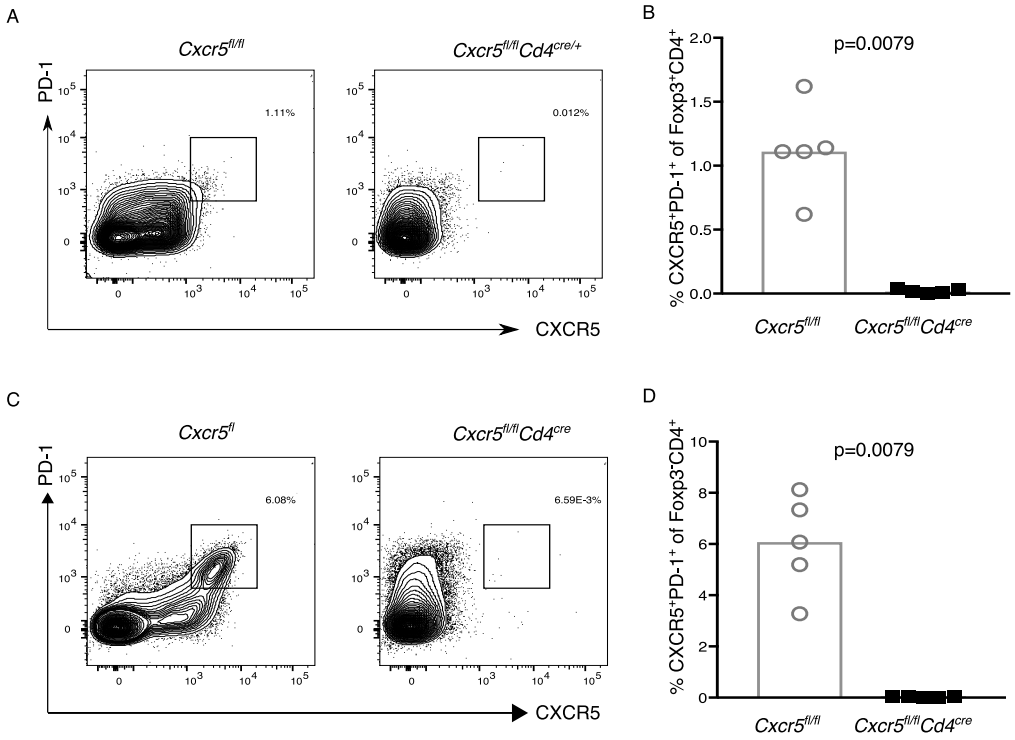


Figure 3.8 *Cxcr5$^{fl/fl}$Cd4$^{cre/+}$* mice lack CXCR5 on Foxp3^{+} and Foxp3^{-} cells.

Analysis of CXCR5^{+} T cells 14 days after influenza A virus (HKx31) infection. **A.** Representative flow cytometry plot of CXCR5^{+}PD-1^{+}Foxp3^{+}CD4^{+} cells gated from Foxp3^{+}CD4^{+} T cells. **B.** Quantification of the frequency of CXCR5^{+}PD-1^{+}Foxp3^{+}CD4^{+} cells. **C.** Representative flow cytometry plot of CXCR5^{+}PD-1^{+}cells gated from Foxp3^{-}CD4^{+} T cells. **D.** Quantification of the frequency of CXCR5^{+}PD-1^{+}Foxp3^{-}CD4^{+} cells. Each symbol represents one mouse, and the horizontal bars represent the median values. P values were determined using a Mann-Whitney *U* test. Data represent two independent experiments.

Next, I tested whether deletion of CXCR5 in $CD4^+$ T cells changes the GC size and is sufficient to impair Tfh and Tfr cell formation. *Cxcr5*$^{fl/fl}$*Cd4*$^{cre/+}$ mice show a normal GC size (Figure 3.9 A-C) and are able to form $Bcl6^+PD\text{-}1^+CD4^+$ Tfh and Tfr cells (Figure 3.9 D-I). To confirm these results, I analysed the number of Tfr and Tfh cells within the GC (per μm^2) in tissue sections by immunofluorescence staining followed by confocal imaging (Figure 3.9 J). Interestingly, GCs in *Cxcr5*$^{fl/fl}$*Cd4*$^{cre/+}$ mice did not have altered GC morphology and contained normal numbers of Tfh and Tfr cells despite the loss of CXCR5 (Figure 3.9 K-L). Collectively, these data strongly suggest that in contrast to previous reports, CXCR5 deletion is not sufficient to impair $CD4^+$ T cell access to the GC.

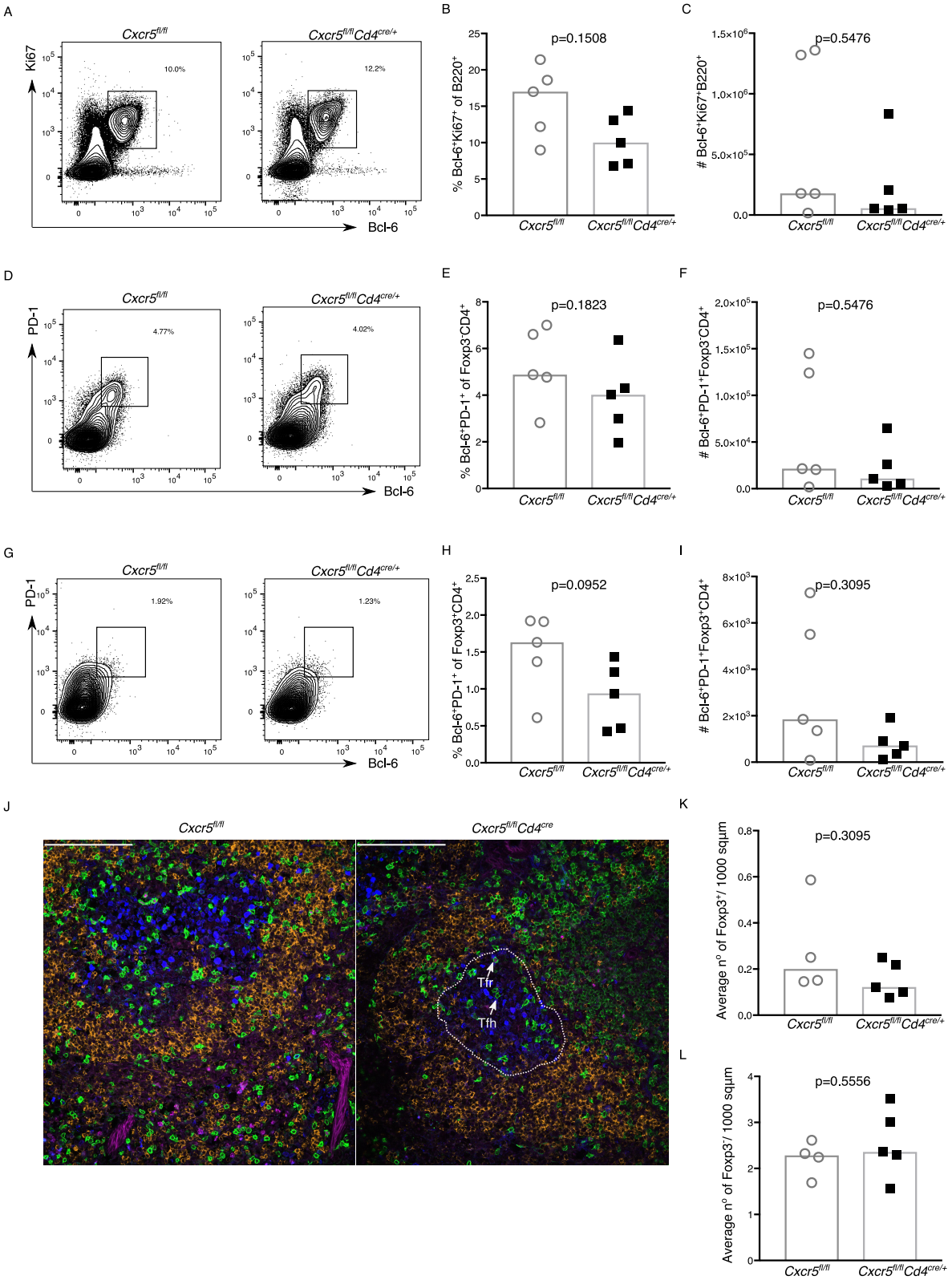

A
Cxcr5fl/fl
Cxcr5fl/flCd4cre/+
Ki67
Bcl-6
10.0%
12.2%
B
p=0.1508
% Bcl-6+Ki67+ of B220+
C
p=0.5476
# Bcl-6+Ki67+B220+
D
PD-1
4.77%
4.02%
E
p=0.1823
% Bcl-6+PD-1+ of Foxp3-CD4+
F
p=0.5476
# Bcl-6+PD-1+Foxp3-CD4+
G
1.92%
1.23%
H
p=0.0952
% Bcl-6+PD-1+ of Foxp3+CD4+
I
p=0.3095
# Bcl-6+PD-1+Foxp3+CD4+
J
Cxcr5fl/flCd4cre
Tfr
Tfh
K
p=0.3095
Average n° of Foxp3+/ 1000 sqμm
L
p=0.5556
Average n° of Foxp3+/ 1000 sqμm

Figure 3.9 *Cxcr5*$^{fl/fl}$*Cd4*$^{cre/+}$ mice show a normal GC response with regular numbers of Tfh and Tfr cells.

Analysis of the GC response 14 days after influenza A virus (HKx31) infection in *Cxcr5*$^{fl/fl}$*Cd4*$^{cre/+}$ mice and *Cxcr5*$^{fl/fl}$*Cd4*$^{+/+}$ controls. **A.** Representative flow cytometry contour plots of GC B cells, gated as Bcl6^{+}Ki67^{+} of B220^{+} B cells. **(B-C)** Quantification of **B.** the frequency and **C.** absolute numbers of GC B cells. **D.** Representative flow cytometry contour plots of Tfh cells, gated as Bcl6^{+}PD-1^{+} from Foxp3^{-}CD4^{+} T cells. **(E-F)**. Quantification of **E.** the frequency and **F.** absolute number of Bcl6^{+}PD-1^{+} Tfh cells. **G**. Representative flow cytometry contour plots of Tfr cells, gated as Bcl6^{+}PD-1^{+} from Foxp3^{+}CD4^{+} T cells. **(H-I)** Quantification of **H.** the frequency and **I.** absolute number of Bcl6^{+}PD-1^{+} Tfr cells. **J.** Representative confocal image of the GC with Tfr (arrows) and Tfh (arrowheads) cells as indicated. Objective magnification 40x, scale bar 100μm. **K.** Quantification of the average number of Tfh cells, defined as CD3^{+}Foxp3^{-}, per 1000 μm^{2}. **L.** Quantification of the average number of Tfh cells, defined as CD3^{+}Foxp3^{+}, per 1000 μm^{2}. Each dot represents the average number of Tfr per 1000 μm^{2}, in at least 4 different GCs per mouse. Each symbol represents one mouse, and the horizontal bars represent the median values. P values were determined using a Mann-Whitney *U* test. Data represent two independent experiments.

3.3 Discussion

In this chapter, I tested whether *Cxcr5*$^{fl/fl}$*Foxp3*^{cre} mice can be used as a Tfr cell-deficient mouse model. I showed that CXCR5^{+}PD-1^{+}Foxp3^{+}CD4^{+} cells are not present in *Cxcr5*$^{fl/fl}$*Foxp3*^{cre} mice after immunisation with SRBC, NP-KLH and after influenza A virus infection, confirming deletion of CXCR5 on cells with a Tfr cell-phenotype in this mouse strain. This result is expected based on our genetic strategy as we are excising CXCR5 in Foxp3^{+} Treg cells. Furthermore, I demonstrated that the loss of CXCR5 on Foxp3^{+} Treg cells is not sufficient to alter the GC size, or Tfh cell number in the spleen following immunisation with model antigens such as NP-KLH or SRBC. There was no evidence for altered long-term antigen specific plasma cell responses in *Cxcr5*$^{fl/fl}$*Foxp3*^{cre} mice. Infection with influenza A virus, which induces a respiratory infection resulting in robust immune responses in the lungs and the mediastinal LN, did not result in an altered GC size in *Cxcr5*$^{fl/fl}$*Foxp3*^{cre} mice. I did, however, find that the frequency and absolute number of CXCR5^{+} Tfh cells was reduced in *Cxcr5*$^{fl/fl}$*Foxp3*^{cre} mice. This was a surprising observation as we would expect to see an increase in Tfh cells in the absence of Tfr cells (Linterman et al., 2011). When Tfh cells were defined by co-expression of Bcl6 and PD-1, an alternative gating strategy to identify Tfh cells, I did not observe a reduction in these cells, indicative of off–target CXCR5 deletion in our *Cxcr5*$^{fl/fl}$*Foxp3*^{cre} model (Nurieva et al., 2009, Yu et al., 2009). Indeed, considerable population of CXCR5-deficient B cells was found in *Cxcr5*$^{fl/fl}$*Foxp3*^{cre} mice compared to controls. Moreover, detection of the excised allele of CXCR5 in *Cxcr5*$^{fl/fl}$*Foxp3*^{cre} mouse ear biopsy samples further indicates that CXCR5 has been deleted in multiple cell types, and is therefore uncontrolled by Foxp3 expression, rendering this model inappropriate for the study of Tfr cell biology. The off-target effects of the cre recombinase in *Foxp3*$^{cre\text{-}YFP}$ mice are of note given the widespread use of this mouse strain in Foxp3^{+} Treg cell research, as has been described previously (Franckaert et al., 2015).

While the *Cxcr5*$^{fl/fl}$*Foxp3*^{cre} model was inappropriate for the study of Tfr cell biology, these results demonstrate that Foxp3^{+} Treg cells are able to migrate to and localise within the GC in the absence of CXCR5 expression. I confirmed this observation in *Cxcr5*$^{fl/fl}$*Cd4*$^{cre/+}$ mice, where the presence of both Foxp3^{+} as well as Foxp3^{-} T cells in the GC suggests that alternative mechanisms control the ability of T cells to enter the GC. These results directly contradict previous publications, which have shown that the CXCR5-CXCL13 axis is the major migration cue for T cells entering the GC (Ansel et al., 1999, Haynes et al., 2007, Chung et al., 2011, Wollenberg et al., 2011, Kim et al., 2017). One possible explanation for

the discrepancy between our study and previously published studies is the use of different experimental systems. So far, the experimental systems to study CXCR5-expressing $CD4^+$ T cells, *i.e.* Tfr and Tfh cells, were limited to adoptive transfer models and bone marrow chimaeras, perhaps influencing the immunological environment to a greater extent than that seen in transgenic mouse models. In support of this hypothesis, the initial studies of Tfr cells used either bone marrow chimaera or adoptive transfer systems, leading to divergent results. Nevertheless, our data strongly suggest the existence of redundant T cell homing mechanisms in the GC. This raises the interesting question of how Treg cells gain access to the GC in order to undergo Tfr cell differentiation. The following chapters will further explore the role of CXCR5 on Treg cells for Tfr cell homing as well as the potential redundant mechanisms involved in Treg cell localisation within the GC.

4 *Cxcr5*$^{fl/fl}$*Foxp3*$^{cre\text{-}ERT2}$ mice show a reduction, but not a complete absence of follicular regulatory T cells

4.1 Background

Chapter 3 demonstrated that *Cxcr5*$^{fl/fl}$*Foxp3*^{cre} mice delete CXCR5 outside the Treg compartment due to a 'leaky' cre recombinase. CXCR5 is not only important for Tfr cell homing to the GC, but is also required in B cells and Tfh cells. Therefore, non-specific deletion of CXCR5 rendered interpretation of the phenotype observed in these mice difficult. To be able to study the role of CXCR5 on Tfr cells, a new system to delete CXCR5 in Treg cells was required. An alternative approach to delete CXCR5 in Treg cells is the use of *Foxp3*$^{eGFP\text{-}Cre\text{-}ERT2}$ (*Foxp3*$^{cre\text{-}ERT2}$) mice (Rubtsov et al., 2010). These mice have a cre recombinase and mutated human oestrogen receptor ligand binding domain (ERT2) inserted into the 3' untranslated region (UTR) of the *Foxp3* gene. In *Foxp3*$^{eGFP\text{-}Cre\text{-}ERT2}$ mice, the cre-ERT2 fusion protein is sequestered in the cytosol. Administration of tamoxifen results in translocation of the fusion protein to the nucleus and excision of the floxed gene(s) (Figure 4.1). Consequently, this system allows for inducible deletion of genes within Treg cells. We crossed *Foxp3*$^{cre\text{-}ERT2}$ mice to *Cxcr5*$^{fl/fl}$ mice to generate *Cxcr5*$^{fl/fl}$*Foxp3*$^{cre\text{-}ERT2}$ mice and aimed to evaluate the use of this system to study the role of CXCR5 on Tfr cells.

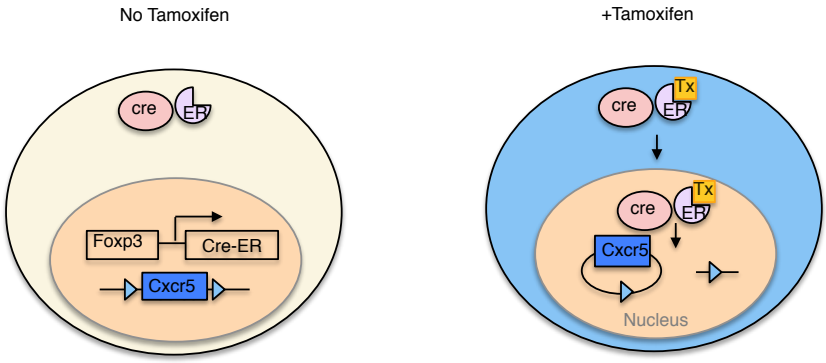


Figure 4.1 *Foxp3*$^{cre\text{-}ERT2}$ system principle.

The mutated oestrogen receptor ligand binding domain (ERT2), which is responsive to tamoxifen, is fused to the cre recombinase. The cre is inactive in the absence of tamoxifen. Addition of tamoxifen results in the translocation of the cre-ERT2 complex to the nucleus. In the nucleus, the Cre mediates the excision of the floxed allele, in this case *Cxcr5*. Adapted from Greco V, *et al*, Development 2010 (Greco and Guo, 2010).

4.2 Results

4.2.1 Specific deletion of CXCR5 in Foxp3$^+$ Treg cells in *Cxcr5*$^{fl/fl}$*Foxp3*$^{cre\text{-}ERT2}$ mice

In order to delete CXCR5 on Foxp3$^+$ Treg cells, mice were fed a 'wash-out diet', consisting of soy-free pellets for 10 days prior to a 16% tamoxifen diet. Mice received the tamoxifen-containing diet for the remainder of the study. After 30 days, I immunised mice with NP-KLH *s.c.* in the flank and analysed the GC response in the draining (*i.e.* inguinal) LNs 14 days after immunisation (Figure 4.2A). To test the use of *Cxcr5*$^{fl/fl}$*Foxp3*$^{cre\text{-}ERT2}$ mice as a model system for mice that lack Tfr cells within the GC, I evaluated whether CXCR5 expression was specifically reduced on Tfr cells. Deletion of CXCR5 on Treg cells could be observed (Figure 4.2 B-D). Using this system, I did not observe non-specific deletion of CXCR5 in Tfh cells (Figure 4.2 E-G), or B cells (Figure 4.2 H-J). Therefore, I had established a model that would allow us to study whether specific deletion of CXCR5 in Treg cells results in impaired Treg access to the GC.

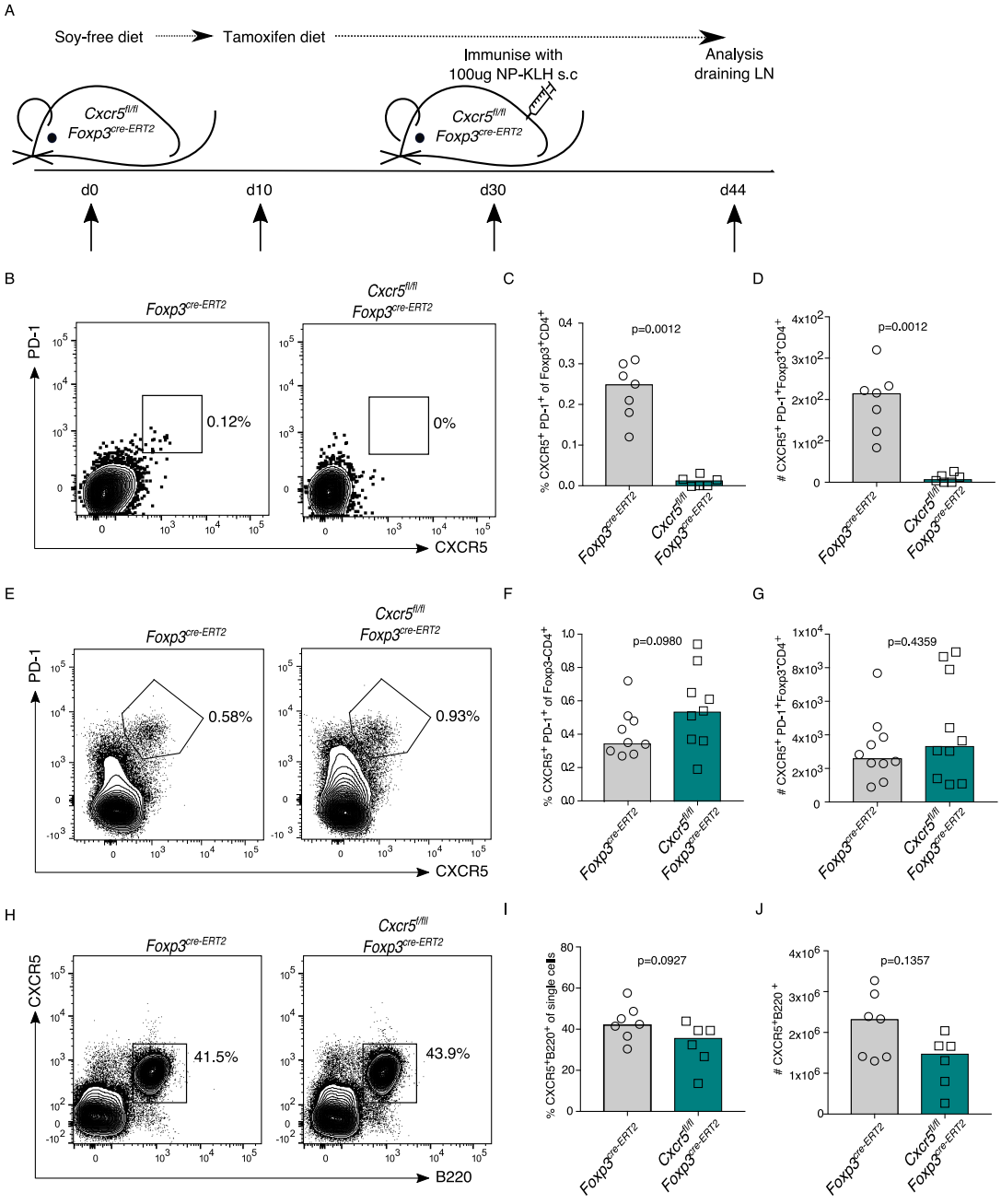

A
Soy-free diet
Tamoxifen diet
Immunise with
100ug NP-KLH s.c
Analysis
draining LN
Cxcr5fl/fl
Foxp3cre-ERT2
d0
d10
d30
d44
B
Foxp3cre-ERT2
Cxcr5fl/fl
Foxp3cre-ERT2
PD-1
CXCR5
0.12%
0%
C
p=0.0012
% CXCR5+ PD-1+ of Foxp3+CD4+
D
p=0.0012
# CXCR5+ PD-1+Foxp3+CD4+
E
0.58%
0.93%
F
p=0.0980
% CXCR5+ PD-1+ of Foxp3-CD4+
G
p=0.4359
# CXCR5+ PD-1+Foxp3-CD4+
H
CXCR5
B220
41.5%
43.9%
I
p=0.0927
% CXCR5+B220+ of single cells
J
p=0.1357
# CXCR5+B220+

Figure 4.2 *Cxcr5*$^{fl/fl}$*Foxp3*$^{cre\text{-}ERT2}$ mice show specific deletion of CXCR5 in Foxp3$^+$ Treg cells.

Analysis of CXCR5 expression on Tfr cells, Tfh cells and B cells cells 14 days after *s.c*. immunisation with NP-KLH/Alum. **A.** Diagram shows experimental set-up. Mice received a soy-free diet for 10 days. After 10 days, the mice received a diet containing tamoxifen for the remaining time of the study. After 30 days, the mice were immunised *s.c.* with NP-KLH in the flank. The inguinal LNs were harvested for analysis 14 days after immunisation. **B.** Representative flow cytometry contour plots of PD-1$^+$CXCR5$^+$ cells from Foxp3$^+$CD4$^+$ cells (Tfr cells). **(C-D)** Quantification of **C.** the frequency and **D.** absolute numbers of CXCR5$^+$ Tfr cells. **E.** Representative flow cytometry histograms of contour plots of PD-1$^+$CXCR5$^+$ Tfh cells from Foxp3$^-$CD4$^+$ cells. **(F-G)** Quantification of **F.** the frequency and **G.** absolute numbers of PD-1$^+$CXCR5$^+$ Tfh cells. **H.** Representative flow cytometry contour plots of CXCR5$^+$B220$^+$ B cells from single cells. **(I-J)** Quantification of **I.** the frequency and **J.** absolute numbers of CXCR5$^+$ B220$^+$ cells. Each symbol represents one mouse, and the horizontal bars represent the median values. P values were determined using a Mann-Whitney U test. Data represent three independent experiments.

4.2.2 *Cxcr5*$^{fl/fl}$*Foxp3*$^{cre\text{-}ERT2}$ mice show a reduced proportion, but not complete absence of Tfr cells within the GC

To determine whether loss of CXCR5 on Foxp3$^+$ Treg cells was sufficient to impair Treg cell access to the GC, and therefore inhibit Tfr cell formation, the number of Bcl6$^+$PD-1$^+$ Treg cells was analysed. Despite successful and specific deletion of CXCR5 in Treg cells, Bcl6$^+$ Tfr cells could still be identified by flow cytometry, albeit at reduced frequencies (Figure 4.3 A-C). Flow cytometry analyses cannot rule out that Treg cells with a Tfr cell phenotype form, but are not located within the GC. To quantify the number of Foxp3$^+$ cells within the follicle, I performed confocal imaging of the GC using cryosections from the inguinal LNs obtained from *Cxcr5*$^{fl/fl}$*Foxp3*$^{cre\text{-}ERT2}$ mice. Between 8 and 25 GCs per mouse were analysed. In these images, Tfr cells can be observed within the GC (Figure 4.3 D). To determine whether loss of CXCR5 altered the proportion of Tfr cells within the GC, Foxp3$^+$ cells were counted from confocal images and normalised to the either the GC area (Figure 4.3 E-F), or to the number of Tfh cells (Figure 4.3 G-H). I observed a significant reduction (approximately 3-fold reduction) in GC-localised Foxp3$^+$ cells in *Cxcr5*$^{fl/fl}$*Foxp3*$^{cre\text{-}ERT2}$ mice compared with controls, both when Tfr cell number were normalised to the GC size and the Tfh cell number. The GCs were overall larger in size in *Cxcr5*$^{fl/fl}$*Foxp3*$^{cre\text{-}ERT2}$ mice, compared with controls (Figure 4.3 I). However, the median GC area for each biological replicate was not significantly different in *Cxcr5*$^{fl/fl}$*Foxp3*$^{cre\text{-}ERT2}$ mice compared to controls (Figure 4.3 J). Collectively, these data show that the deletion of CXCR5 in Treg cells results in a decrease of Tfr cells within the GC, but not a complete absence.

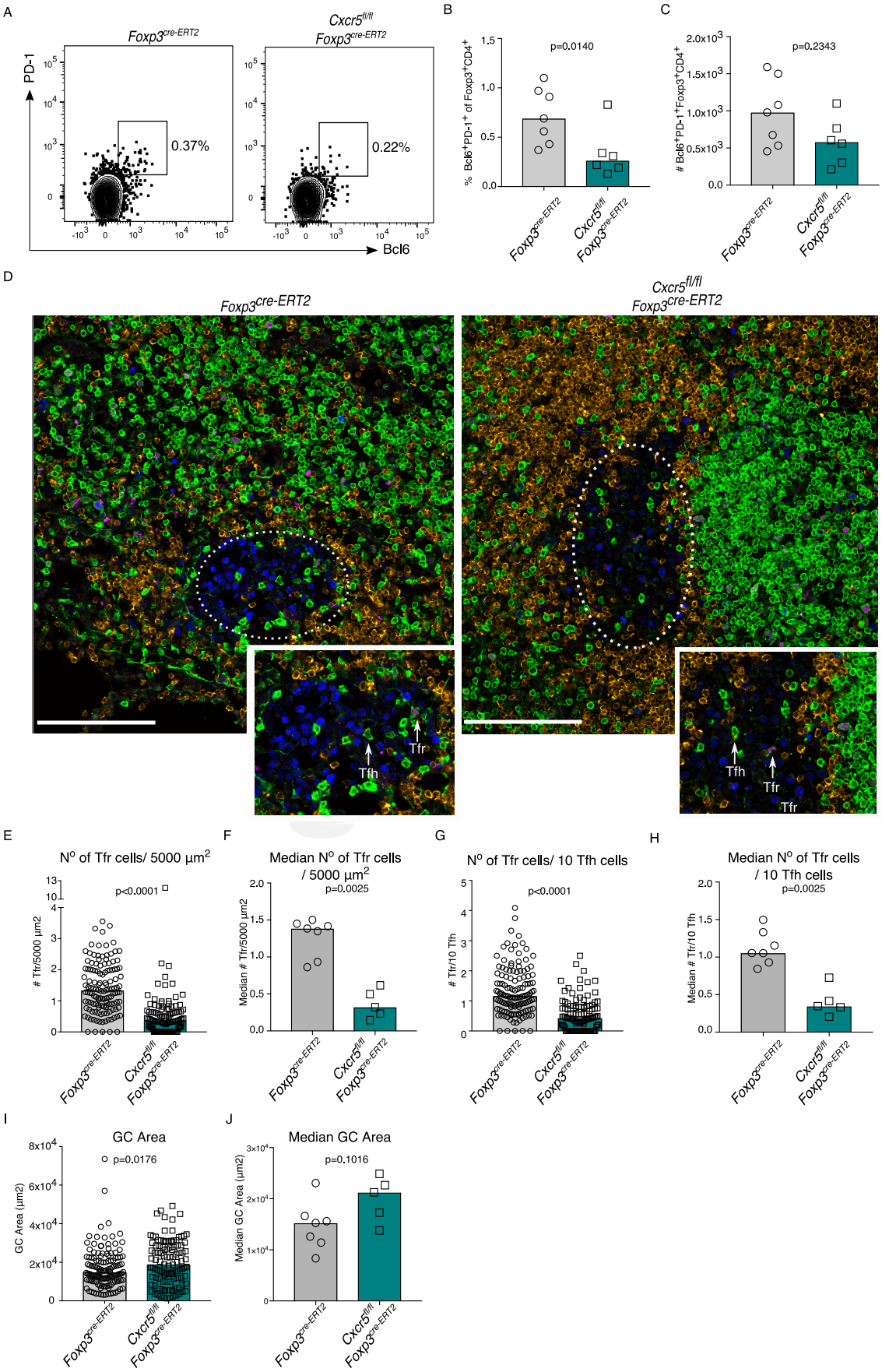

A
Foxp3cre-ERT2
Cxcr5fl/fl
Foxp3cre-ERT2
PD-1
Bcl6
0.37%
0.22%
B
p=0.0140
% Bcl6+PD-1+ of Foxp3+CD4+
C
p=0.2343
# Bcl6+PD-1+Foxp3+CD4+
D
Foxp3cre-ERT2
Cxcr5fl/fl
Foxp3cre-ERT2
Tfh
Tfr
E
Nº of Tfr cells/ 5000 µm2
p<0.0001
Tfr/5000 µm2
F
Median Nº of Tfr cells
/ 5000 µm2
p=0.0025
Median # Tfr/5000 µm2
G
Nº of Tfr cells/ 10 Tfh cells
p<0.0001
Tfr/10 Tfh
H
Median Nº of Tfr cells
/ 10 Tfh cells
p=0.0025
Median # Tfr/10 Tfh
I
GC Area
p=0.0176
GC Area (µm2)
J
Median GC Area
p=0.1016
Median GC Area (µm2)

Figure 4.3 *Cxcr5*$^{fl/fl}$*Foxp3*$^{cre\text{-}ERT2}$ mice have a reduced proportion, but not absence, of Tfr cells.

Analysis of the GC response 14 days after *s.c.* immunisation with NP-KLH. **A.** Representative flow cytometry contour plots of PD-1^{+}Bcl6^{+} cells within Foxp3^{+}CD4^{+} cells (Tfr cells). **(B-C)** Quantification of **B.** the frequency and **C.** absolute numbers of Bcl6^{+} Tfr cells. Each symbol represents one mouse, and the horizontal bars represent the median values. **D.** Cryosections were stained with Foxp3 (magenta), Ki67 (Blue), CD3 (Green) and IgD (orange). Objective magnification 40x, scale bar = 100 μm. Representative confocal image of the GC with Tfr cells and Tfh cells indicated by the arrows. **E.** Quantification of the number of Tfr cells, defined as CD3^{+}Foxp3^{+}, per 5000μm^{2}. Each symbol represents one Tfr cell, and the horizontal bars represent the median values. **F.** Quantification of the median number of Tfr cells, defined as CD3^{+}Foxp3^{+}, per 5000μm^{2}. Each symbol represents one mouse, and the horizontal bars represent the median values. **G.** Quantification of the number of Tfr cells per 10 Tfh cells, defined as Foxp3^{-}CD3^{+}. Each symbol represents one mouse, and the horizontal bars represent the median values. **H.** Quantification of the median number of Tfr cells per 10 Tfh cells, defined as Foxp3^{-}CD3^{+}. Each symbol represents the ratio of total number of Tfr per 10 Tfh in one GC, and the horizontal bars represent the median values. **I.** Quantification of the GC area in μm^{2}. Each symbol represents one GC, and the horizontal bars represent the median values. **J.** Quantification of the median GC area. Each symbol represents one mouse, and the horizontal bars represent the median values. P values were determined using a Mann-Whitney U test. Data represent two independent experiments.

4.2.3 *Cxcr5*$^{fl/fl}$*Foxp3*$^{cre\text{-}ERT2}$ mice do not show a reduction in antigen-specific B cells

Given that a tendency to slightly larger GCs was observed in *Cxcr5*$^{fl/fl}$*Foxp3*$^{cre\text{-}ERT2}$ mice, I tested whether there was an increase in the number of GC B cells. Analysis of Bcl6^{+}Ki67^{+} GC B cells did not show any changes in *Cxcr5*$^{fl/fl}$*Foxp3*$^{cre\text{-}ERT2}$ mice (Figure 4.4 A-C). To test whether the reduction of Tfr cells resulted in compromised affinity maturation, and therefore a reduced quality of the output of the GC response, the serum levels of NP-specific antibodies were determined by ELISA. For this purpose, I tested the affinity of IgM, total IgG and IgG1 for NP7 (to which only high-affinity antibodies will bind due to the low NP/BSA Ratio) and NP20 (to which both low and high affinity antibodies will bind). A relative increase in NP20 binding compared to NP7 would be indicative of diminished affinity maturation in *Cxcr5*$^{fl/fl}$*Foxp3*$^{cre\text{-}ERT2}$ mice. There were no differences in serum levels of NP7 or NP20-specific IgG, IgM or IgG1 (Figure 4.4 D-E), indicating that reduced numbers of Tfr cells in our model do not result in impaired affinity maturation, nor a general alteration in antigen-specific antibody production.

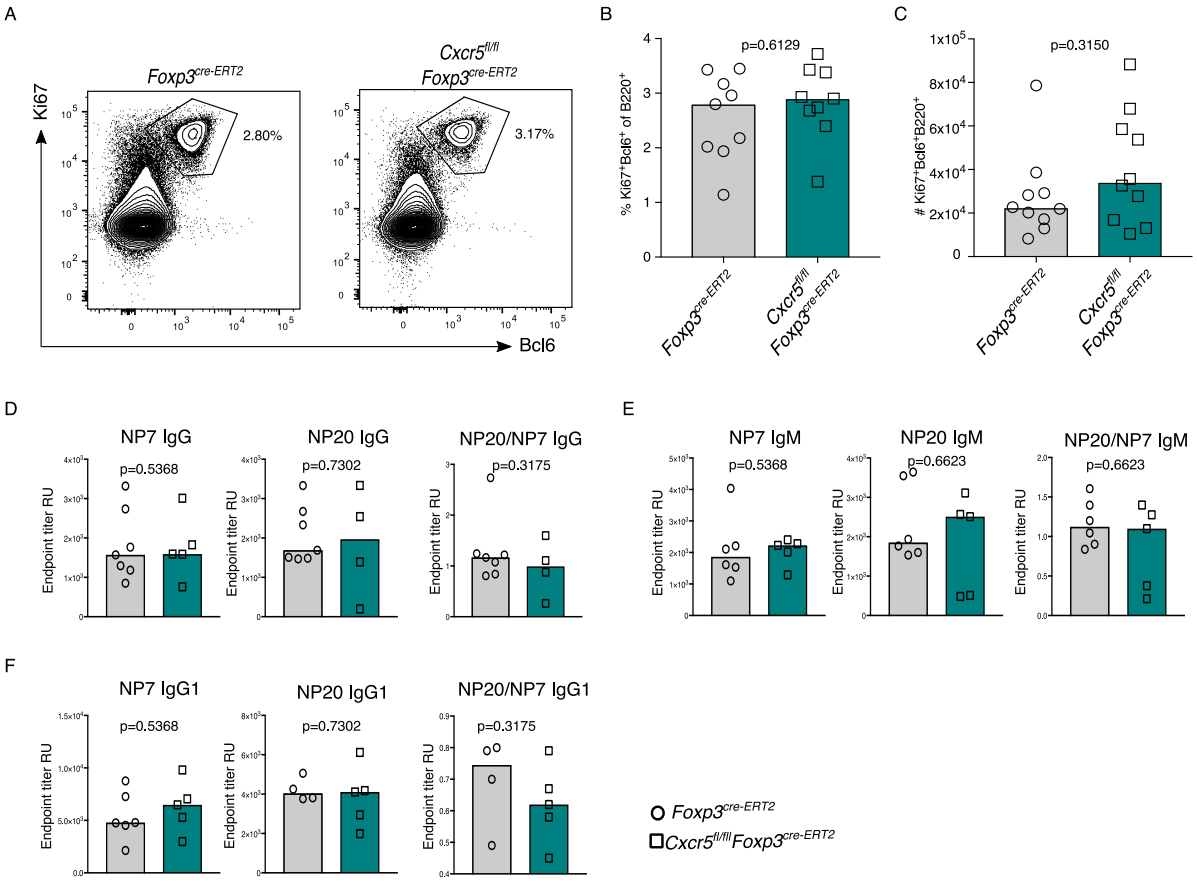


Figure 4.4 Normal GC B cell responses and immunoglobulin production in *Cxcr5$^{fl/fl}$Foxp3$^{cre-ERT2}$* mice.

Analysis of the GC response 14 days after *s.c.* immunisation with NP-KLH. **A.** Flow cytometry contour plots of GC B cells, gated as Bcl6^{+}Ki67^{+} cells of B220^{+} cells. **(B-C)** quantification of **B.** the frequency and **C.** absolute number of Bcl6^{+}Ki67^{+} B cells. **D.** Levels of IgG specific for NP7 or NP20 in the sera. **E.** Levels of IgM specific for NP7 or NP20 in the sera. **F.** Levels of IgG1 specific for NP7 or NP20 in the sera. Each symbol represents one mouse, and the horizontal bars represent the median values. P values were determined using a Mann-Whitney U test. Data represent two independent experiments.

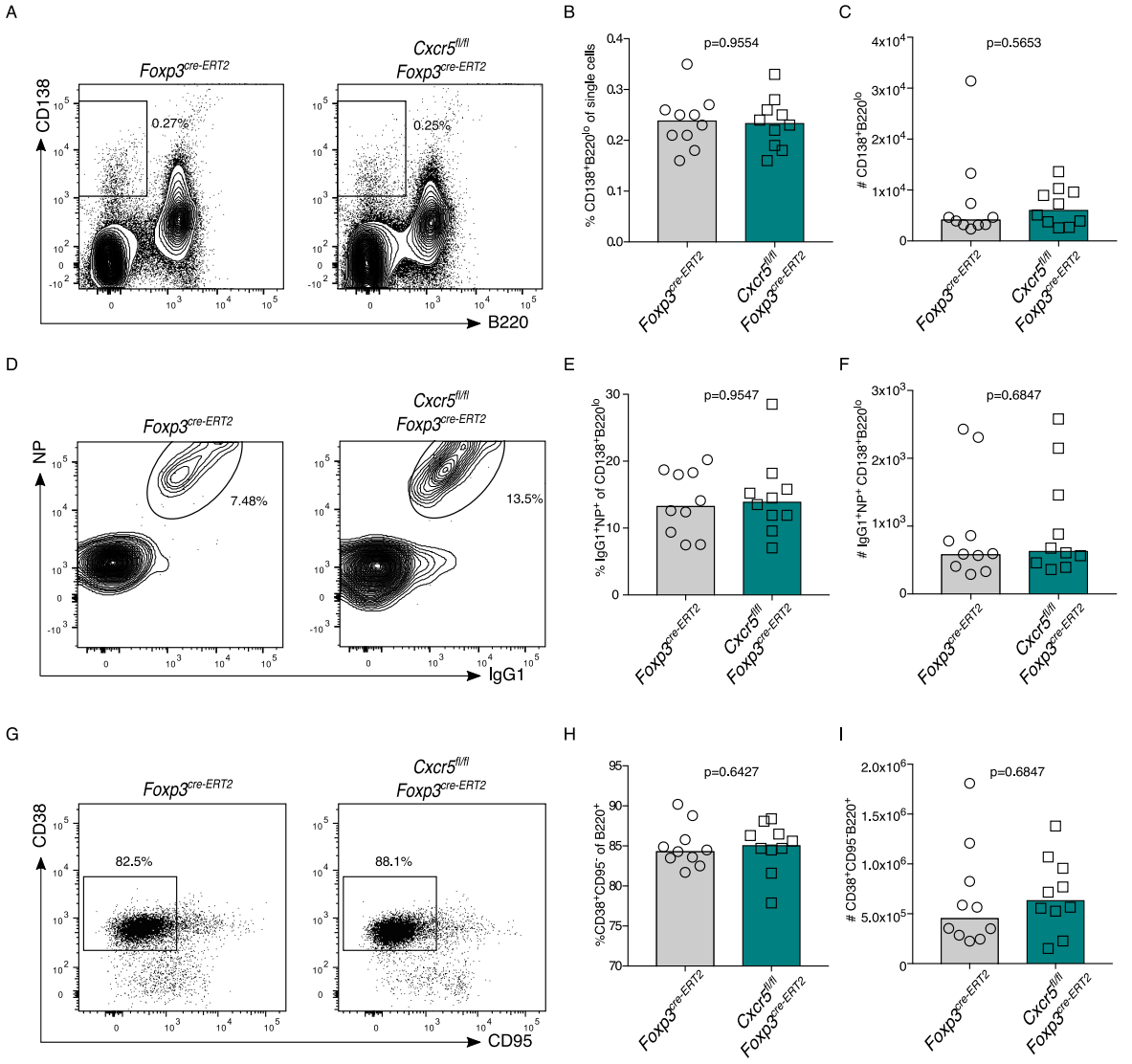


Figure 4.5 *Cxcr5*$^{fl/fl}$*Foxp3*$^{cre\text{-}ERT2}$ mice show normal plasma cell and memory B cell responses.

Analysis of the GC response 14 days after *s.c.* immunisation with NP-KLH/Alum. **A.** Flow cytometry contour plots of CD138^{+}B220^{lo} plasma cells. (**B-C)** Quantification of **B.** the frequency and **C.** absolute number of plasma cells. **D.** Flow cytometry contour plots of antigen-specific class-switched plasma cells, gated as NP^{+}IgG1^{+} cells from CD138^{+}B220^{lo} cells. **(E-F)** quantification of **E.** the frequency and **F.** absolute number of NP^{+}IgG1^{+} plasma cells. **G.** Flow cytometry contour plots of CD38^{+} B cells. **(H-I)** Quantification of **H.** the frequency and **I.** absolute number of CD38^{+} cells. Each symbol represents one mouse, and the horizontal bars represent the median values. P values were determined using a Mann-Whitney U test. Data represent two independent experiments.

Consistent with the comparable levels of anti-NP antibodies, *Cxcr5*$^{fl/fl}$*Foxp3*$^{cre\text{-}ERT2}$ mice showed normal plasma cell (CD138^{+}B220^{lo}) proportions and numbers (Figure 4.5 A-C), and I did not observe any changes in antigen-specific, class-switched (NP^{+}IgG1^{+}) plasma cells (Figure 4.5 D-F). Furthermore, *Cxcr5*$^{fl/fl}$*Foxp3*$^{cre\text{-}ERT2}$ mice showed normal CD38^{+} B cell proportions and numbers (Figure 4.5 G-I). Collectively, these data indicate that a reduction in Tfr cells does not affect affinity maturation or the output of the antigen-specific germinal centre response.

4.2.5 *Cxcr5*$^{fl/fl}$*Foxp3*$^{cre\text{-}ERT2}$ mice show normal 'long-term' immune responses

To determine whether the reduction in Tfr cells in *Cxcr5*$^{fl/fl}$*Foxp3*$^{cre\text{-}ERT2}$ mice has an impact later in the GC response, or after antigen re-challenge, I investigated the GC response 48 days after immunisation, and after secondary immunisation. Mice were immunised with NP-KLH *s.c.* and 48 days after immunisation cells obtained from the inguinal LNs were analysed. Alternatively, mice received a booster immunisation at day 48 with NP-KLH, and the LNs were analysed 7 days after the boost, 56 days after the first immunisation (Figure 4.6A).

As expected, there were fewer GC B cells on day 48, compared with day 56 (Figure 4.6 B-D). However, there were no differences in the proportion or number of GC B cells in *Cxcr5*$^{fl/fl}$*Foxp3*$^{cre\text{-}ERT2}$ mice compared with controls, at day 48 or 56 (Figure 4.6 B-D). There was no change in Tfh cell frequency or absolute number in *Cxcr5*$^{fl/fl}$*Foxp3*$^{cre\text{-}ERT2}$ mice compared to controls, at day 48 or 56 (Figure 4.6 E-G).

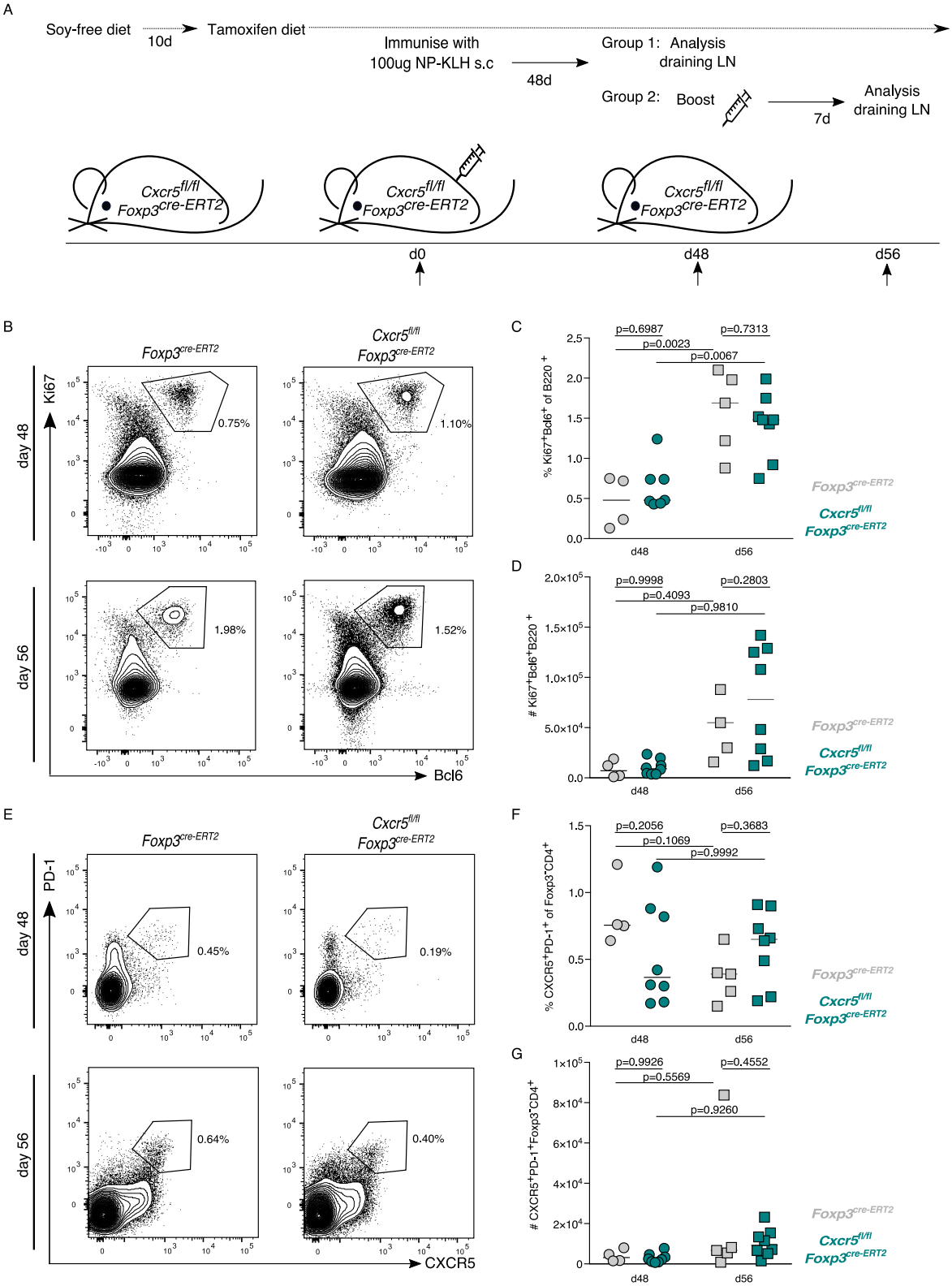

A
Soy-free diet
10d
Tamoxifen diet
Immunise with
100ug NP-KLH s.c
48d
Group 1: Analysis
draining LN
Group 2: Boost
7d
Analysis
draining LN
Cxcr5fl/fl
Foxp3cre-ERT2
d0
d48
d56
B
Foxp3cre-ERT2
Cxcr5fl/fl
Foxp3cre-ERT2
day 48
day 56
Ki67
Bcl6
0.75%
1.10%
1.98%
1.52%
C
% Ki67+Bcl6+ of B220 +
p=0.6987
p=0.0023
p=0.0067
p=0.7313
d48
d56
D
# Ki67+Bcl6+B220 +
p=0.9998
p=0.4093
p=0.9810
p=0.2803
E
PD-1
CXCR5
0.45%
0.19%
0.64%
0.40%
F
% CXCR5+PD-1+ of Foxp3-CD4+
p=0.2056
p=0.1069
p=0.9992
p=0.3683
G
# CXCR5+PD-1+Foxp3-CD4+
p=0.9926
p=0.5569
p=0.9260
p=0.4552

Figure 4.6 Normal GC response after antigen re-challenge in *Cxcr5$^{fl/fl}$Foxp3^{creERT2}* mice.

Long-term and recall immune response after *s.c.* immunisation with NP-KLH/alum. **A.** Diagram showing experimental set-up. *Cxcr5$^{fl/fl}$Foxp3$^{cre-ERT2}$* mice were fed a soy-free diet for 10 days after weaning. After 10 days, the diet was switched to a tamoxifen-containing diet for the remaining part of the study. Three weeks after starting the tamoxifen diet, the mice were immunised with 100µg NP-KLH *s.c.* (50ug/flank). 48 days after immunisation, the draining LN of one group were collected to analyse the GC response. A second group of mice received a boost with 100 µg NP-KLH *s.c.* (50 µg /flank) and the draining LN were harvested 7 days after receiving the boost to analyse the GC response. **B.** Flow cytometry contour plots of GC B cells, gated as Bcl6^{+}Ki67^{+} cells of B220^{+} cells, at day 48 and 56. **(C-D)** Quantification of **C.** the frequency and **D.** absolute number of Bcl6^{+}Ki67^{+} B cells at day 48 and 56. **E.** Flow cytometry contour plots of Tfh cells cells, gated as PD-1^{+}CXCR5^{+} cells of Foxp3^{-}CD4^{+} cells, at day 48 and 56. **(F-G)** Quantification of **F.** the frequency and **G.** absolute number of CXCR5^{+}PD-1^{+} Tfh cells at day 48 and 56. Each symbol represents one mouse, and the horizontal bars represent the median values. P values were determined using a two-way ANOVA with Sidak's multiple comparisons test. Data are from one experiment.

Next, the proportion and absolute number of plasma cells at day 48 and day 56 after primary immunisation was determined. In line with plasma cells being generated late during the GC response, the proportion of plasma cells of total B cells tended to be higher at day 48 compared with day 56 (Weisel et al., 2016). I did not observe a difference in proportion or absolute number of plasma cells in *Cxcr5*$^{fl/fl}$*Foxp3*$^{cre\text{-}ERT2}$ mice versus controls (Figure 4.7 A-C). Finally, I analysed NP-specific serum antibodies to determine whether any changes in affinity maturation could be identified by assessing the ratio of NP7 versus NP20 specific antibodies at day 56. There were no differences in either affinity maturation or the number of NP-specific IgM, IgG1 or total IgG in *Cxcr5*$^{fl/fl}$*Foxp3*^{creERT2} mice compared with controls at day 56 (Figure 4.7 D-F). Collectively, these data suggest that the reduction of Tfr cells in *Cxcr5*$^{fl/fl}$*Foxp3*^{creERT2} does not result in GCs resolving at different rates, nor a change in output of the GC response in terms plasma cells. Moreover, the reduction in Tfr cells did not seem to impact on the generation and the magnitude of the re-call GC response after booster immunisation.

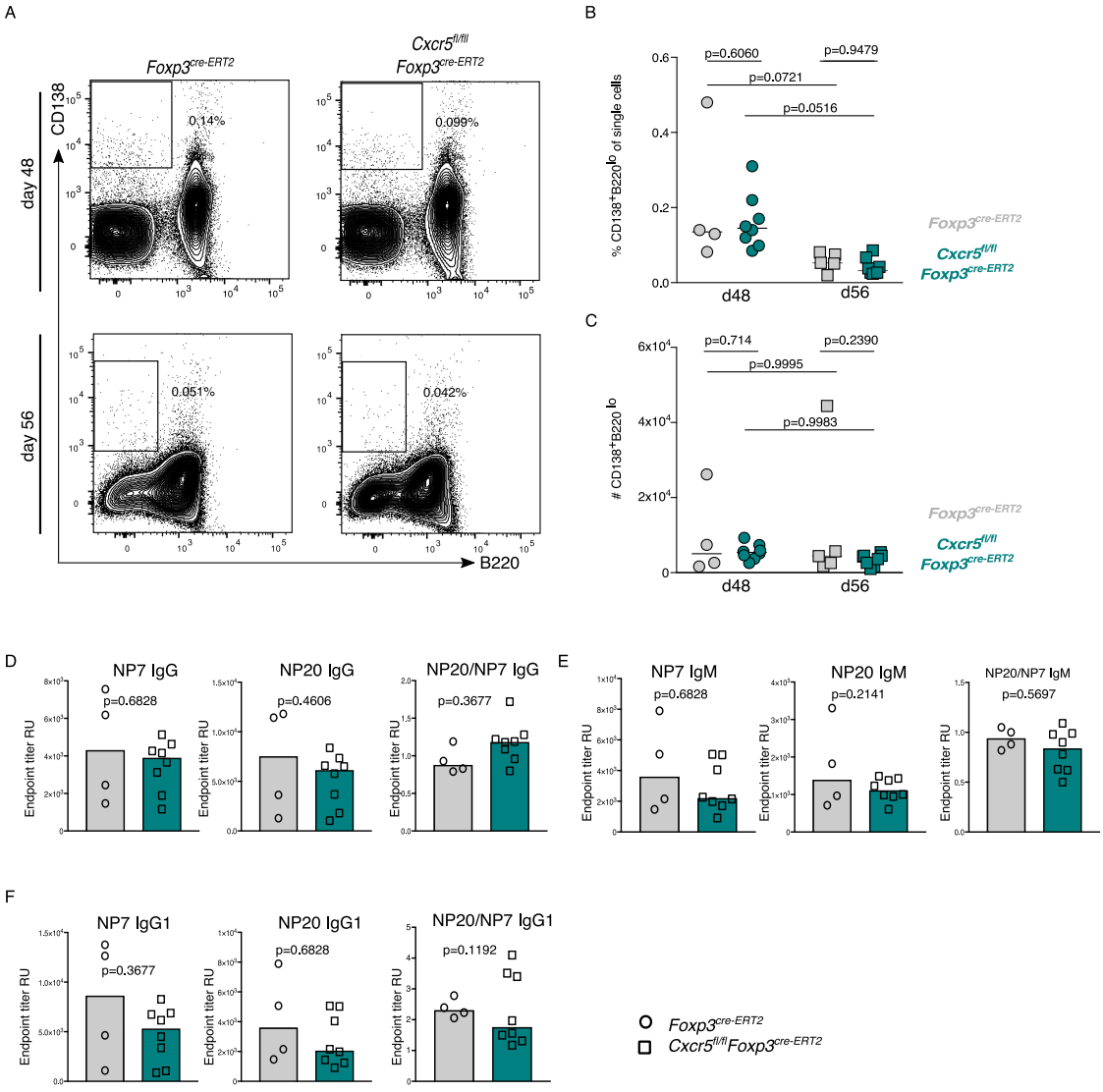


Figure 4.7 Normal plasma cell responses prior to, and after antigen re-challenge, and immunoglobulin production after re-challenge.

Long-term (day 48) and recall immune response (day 56) after *s.c.* immunisation with NP-KLH/Alum. **A.** Flow cytometry contour plots of plasma cell cells, gated as $CD138^{+}B220^{lo}$ cells at day 48 and 56. **(B-C)** Quantification of **B.** the frequency and **C.** absolute number of $CD138^{+}B220^{lo}$ plasma cells at day 48 and 56. **D.** Levels of IgG specific for NP7 or NP20 in the sera at day 56. **E.** Levels of IgM specific for NP7 or NP20 in the sera. **F.** Levels of IgG1 specific for NP7 or NP20 in the sera at day 56. Each symbol represents one mouse, and the horizontal bars represent the median values. P values were determined using a Two-Way ANOVA with Sidak's multiple comparisons test, or a Mann-Whitney U test (ELISA data). Data are from one experiment.

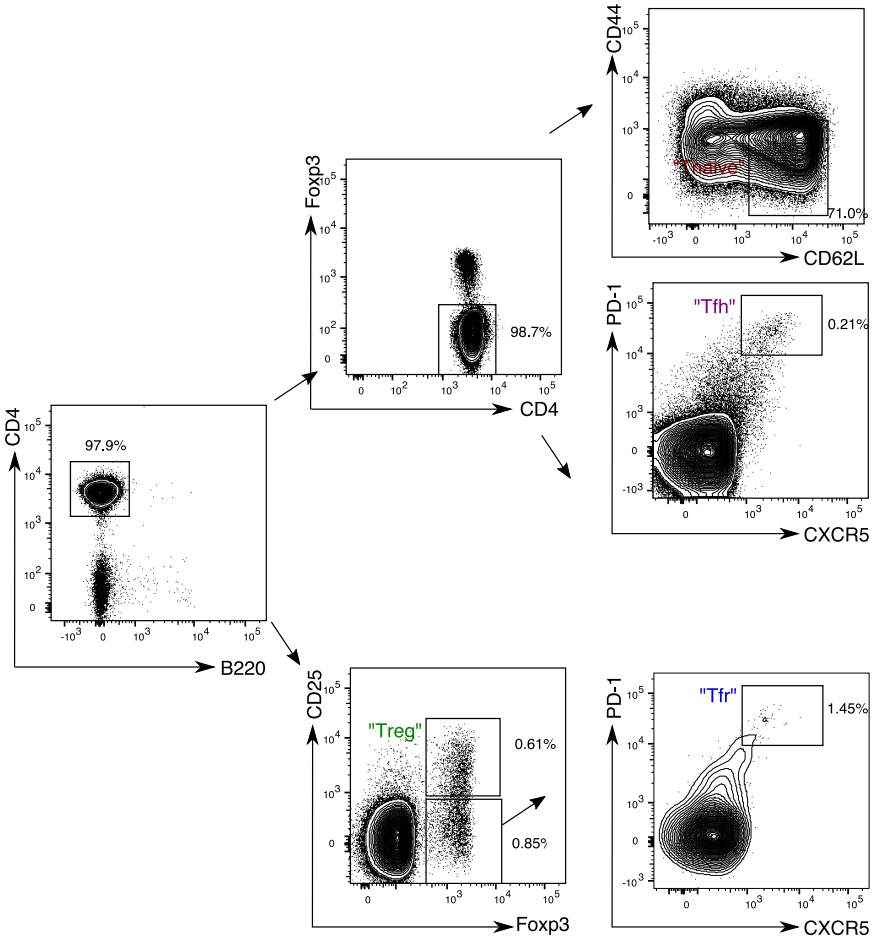
4.2.6 Gene-expression profiling of Tfr cells

Overall, the above data suggest that, while deletion of CXCR5 on Treg cells impairs Treg cell access to the GC, this was only a 50% reduction in GC-localised Tfr cells, which is not sufficient to alter the output of the GC. Thus, redundant mechanisms might be involved in Treg cell homing to the GC. This would mean that the remaining Tfr cells within the GC are fully capable of suppressing the output as well as the magnitude of the GC response, two functions previously attributed to Tfr cells (Chung et al., 2011, Linterman et al., 2011, Wollenberg et al., 2011). In order to evaluate whether redundant mechanisms are involved in Tfr homing to the GC, I investigated potential chemokine-dependent migration to and within the GC in order to identify potential redundant proteins involved in Treg homing to the GC.

In the first instance, the chemokine (receptor) expression profile as well as the expression of relevant cytokines and cytokine receptors on Tfr cells by low cell number multiplex qRT-PCR was determined. Given Tfr cells constitute between 0.5% and 2% of total Treg cells at day 14 after immunisation with NP-KLH, low cell number qRT-PCR was the most feasible approach to analyse gene expression in Tfr cells. Utilising *Foxp3*^{GFP} mice, Tfr cells (PD-1^{+}CXCR5^{+}CD25^{lo}GFP^{+}CD62L^{-}), Tfh cells (PD-1^{+}CXCR5^{+}GFP^{-}CD62L^{-}), Treg cells (PD-1^{-} CXCR5^{-} CD25^{+}GFP^{+}CD62L^{-}) and naïve T cells (PD-1^{+}CXCR5^{+}GFP^{-}CD62L^{+}) were sorted from the LNs from mice immunised with NP-KLH 14 days previously (Figure 4.8A). As an internal control, the expression of *Foxp3*, *Cd3* and *Bcl6* and *Blimp1* in all cell populations was evaluated. All cells expressed *Cd3*, whereas only Tfr cells and Treg cells expressed *Foxp3*. As expected, *Bcl6* was highly expressed in Tfr cells and Tfh cells but not in Treg cells and naïve T cells (Figure 4.8B). I evaluated the expression of 29 chemokine genes and two house-keeping genes. These 29 genes were analysed as part of a previously optimised multiplex panel. Of the 29 genes, 11 were discarded for quality control reasons, as these could not be detected (black boxes).

In Figure 4.9, the relative expression levels of genes of interest are depicted. Surprisingly, *Cxcr5* expression on Tfr cells is significantly lower compared to Tfh cells (Figure 4.9 A). Given, *Cxcr5* was used as a marker to sort Tfr cells initially this result seemed odd and might be due to a technical sensitivity issue related to the Biomark system used. There was no difference in *Cxcr4* expression in Tfr cells compared to Tfh cells, Treg and naïve T cells (Figure 4.9 B), although it is possible that we were unable to detect this transcript as most values were to equal zero. Tfr cells express higher levels of *Cxcr3* compared to naïve T cells but similar levels as compared to Treg cells and Tfh cells (Figure 4.9 C). As expected, Tfr

cells expressed significantly lower levels of *Ccr7*, a marker that T cells need to down-regulate in order to migrate to the GC (Figure 4.9 D) (Haynes et al., 2007). Tfr cells express higher levels of *Ccr4* compared to Tfh cells and naïve T cells, but similar levels to Treg cells (Figure 4.9 E). Tfr cells express higher levels of *Cxcl10* compared to Treg cells and naïve T cells. *Cxcl10* expression was also higher compared to Tfh cells, although the difference was not significant (Figure 4.9 F). As expected, *Sell* (CD62L), was highly expressed in naïve T cells and Treg cells, but not in Tfr cells and Tfh cells (Figure 4.9 G). *Gpr138* (Ebi2) is expressed at higher levels in Tfh cells compared to Tfr cells (Figure 4.9 H), and at similar levels in Tfr cells as in Treg cells and naïve T cells. Finally, *Klf2* seemed to be expressed at particularly low levels in Tfr cells and Tfh cells, compared to Treg and naïve T cells, although the difference between Tfr cells and Treg, and naïve T cells was not significant (Figure 4.9 I). *Il6ra* shows higher expression levels in Tfr cells as compared to Treg and naïve T cells (Figure 4.9 J). Tfr cells express similar levels of *Il10* compared to the bulk Treg population, but significantly higher levels compared to Tfh cells (Figure 4.9 K).


CD4
97.9%
B220
Foxp3
98.7%
CD4
CD44
"naive"
71.0%
CD62L
PD-1
"Tfh"
0.21%
CXCR5
CD25
"Treg"
0.61%
0.85%
Foxp3
PD-1
"Tfr"
1.45%
CXCR5

B

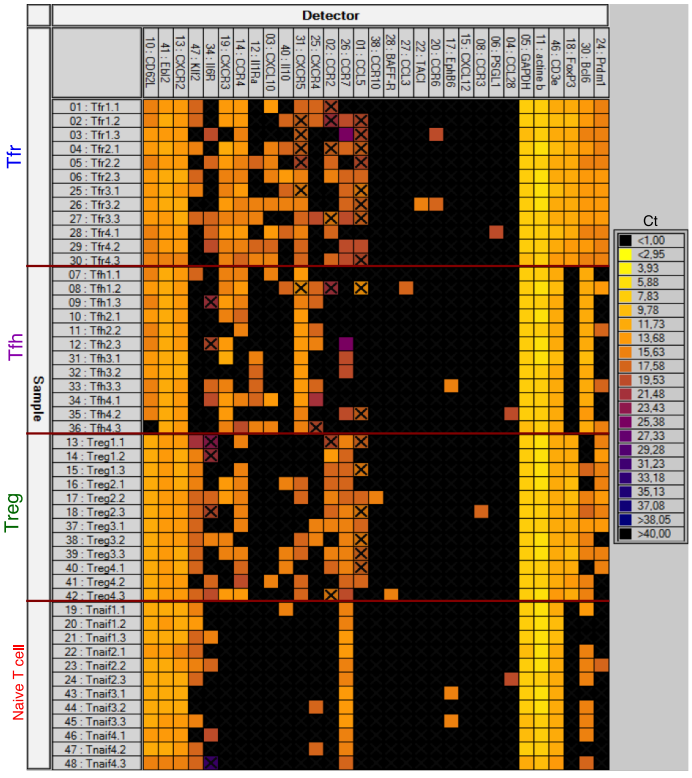

Detector
Sample
Tfr
Tfh
Treg
Naive T cell
Ct

Figure 4.8 Gene expression analysis by low-cell number multiplex qRT-PCR.

A. Gating strategy for Tfr cells ($CD4^+CXCR5^+PD\text{-}1^+$ GFP $(Foxp3)^+$), Tfh cells ($CD4^+CXCR5^+PD\text{-}1^+$ $Foxp3^-$), Treg cells ($CD4^+CXCR5^-PD\text{-}1^-CD25^+Foxp3^+$) and naïve T cells ($CD4^+$ $CD62l^+$ $Foxp3^-$) from purified $CD4^+$ T cells from *Foxp3*^{GFP} mice 14 days after immunisation with NP-KLH/Alum *s.c.*. **B.** Heatmap showing colour-coded Ct values for every reaction position on the dynamic array. The heatmap shows 4 biological and 3 technical repeats per sample for Tfr cells ($CD4^+CXCR5^+PD\text{-}1^+$ GFP $(Foxp3)^+$), Tfh cells ($CD4^+CXCR5^+PD\text{-}1^+$ $Foxp3^-$), Treg cells ($CD4^+CXCR5^-PD\text{-}1^-CD25^+Foxp3^+$) and naïve T cells ($CD4^+$ $CD62l^+$ $Foxp3^-$). The colours on the heatmap correspond to the Ct values as indicated in the legend. Boxes containing a cross, indicate no detection, or the detection of genomic DNA. The Biomark essay was run by Dr Amélie Bonaud and Dr Marion Espéli, INSERM, France.

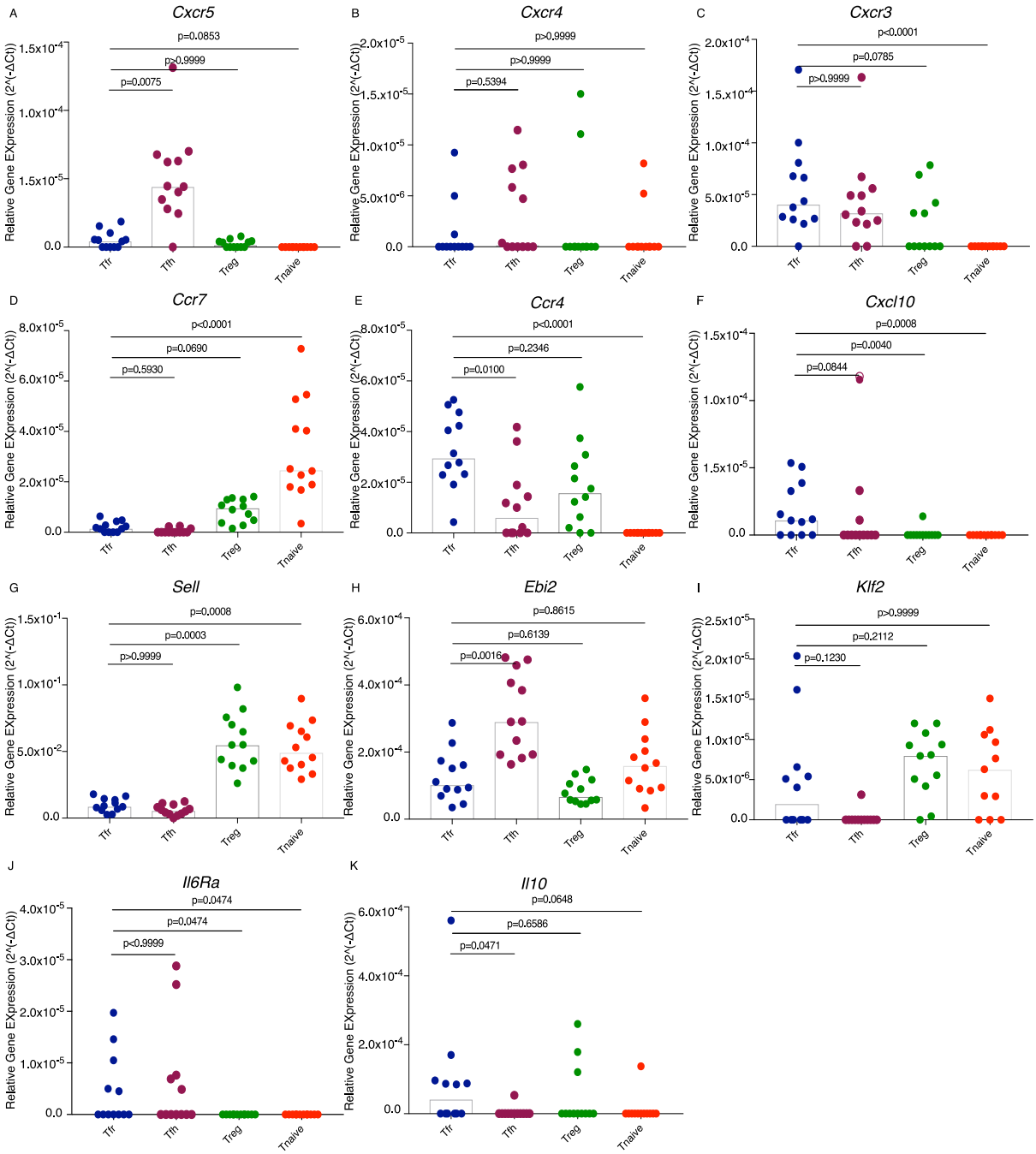


Figure 4.9 Gene expression analysis of Tfr cells compared to Tfh cells, Treg cells and naïve T cells.

A-L. Relative gene expression levels of indicated genes, normalised to *Gapdh* and *Actin B*, calculated as : 2^(-ΔCt)), where ΔCt=Ct $_{\text{gene of interest}}$-Ct $_{\text{mean of } Gapdh \text{ and } Actin\ B}$. P values were determined using a Kruskall-Wallis test with a Dunn's multiple comparison test. Data are from one experiment.

Gene expression analysis using the Biomark system described above had limitations in terms of sensitivity to detect certain transcripts (*e.g.* CXCR5 and CXCR4) as well as the availability of probes. To further explore which chemokines, and other proteins involved in GC localisation, may be involved in Tfr migration to the GC, I analysed data from Wing J, *et al.,* 2017, where Tconv, Tfh cells, $CD25^-$ Tfr cells, $CD25^+$ Tfr cells, $CD62L^{lo}$ and $CD62L^+$ Treg cells were subjected to RNA sequencing (Wing et al., 2017). CD25 was used here as a marker to distinguish GC-resident Tfr cells ($CD25^-$) versus Tfr cells outside the GC ($CD25^+$). I analysed a custom list of genes (shown in Figure 4.10 A), based on a literature review of proteins involved in GC migration and other proteins involved in Tfr and Tfh biology.

As expected, I observed a down-regulation of markers involved in localisation of T cells within the T cell zone such as *Ccr7* and *Selplg* (PSGL-1) in both Tfh cells and $CD25^-$Tfr cells (Schaerli et al., 2000, Hardtke et al., 2005, Veerman et al., 2007, Poholek et al., 2010). Consistent with their localisation outside the GC, $CD25^+$ Tfr cells expressed *Ccr7*. *Klf2*, a repressor of Tfh differentiation, was down regulated in Tfh and both $CD25^+$ and $CD25^-$ Tfr cells (Lee et al., 2015). Consistent with their activated phenotype, *Sell* (CD62L) was down regulated on Tfh cells and Tfr cells. *Prdm1*, encoding Blimp-1, is highly expressed on all Treg and $CD25^+$ Tfr cells, with slightly lower, but not absent, expression in $CD25^-$ Tfr cells, consistent with previous publications (Wing et al., 2017). $CD25^-$ Tfr cells expressed high levels of *Sh2d1a*, which encodes SLAM-associated protein (SAP), expression of which is required for both Tfh and Tfr cell formation (Qi et al., 2008, Linterman et al., 2011). Compared with $CD25^+$ Tfr cells, $CD25^-$ Tfr cells also expressed higher levels of *S1pr2*, known to act collectively with CXCR5, to retain Tfh cells in the GC (Green et al., 2011, Moriyama et al., 2014). Interestingly, $CD25^-$ Tfr cells expressed high levels of *Tnfsf13*, encoding A Proliferation-Inducing Ligand (APRIL), not observed in any other population, which is rather odd given that APRIL is a B cell helper molecule (Zhang et al., 2018).

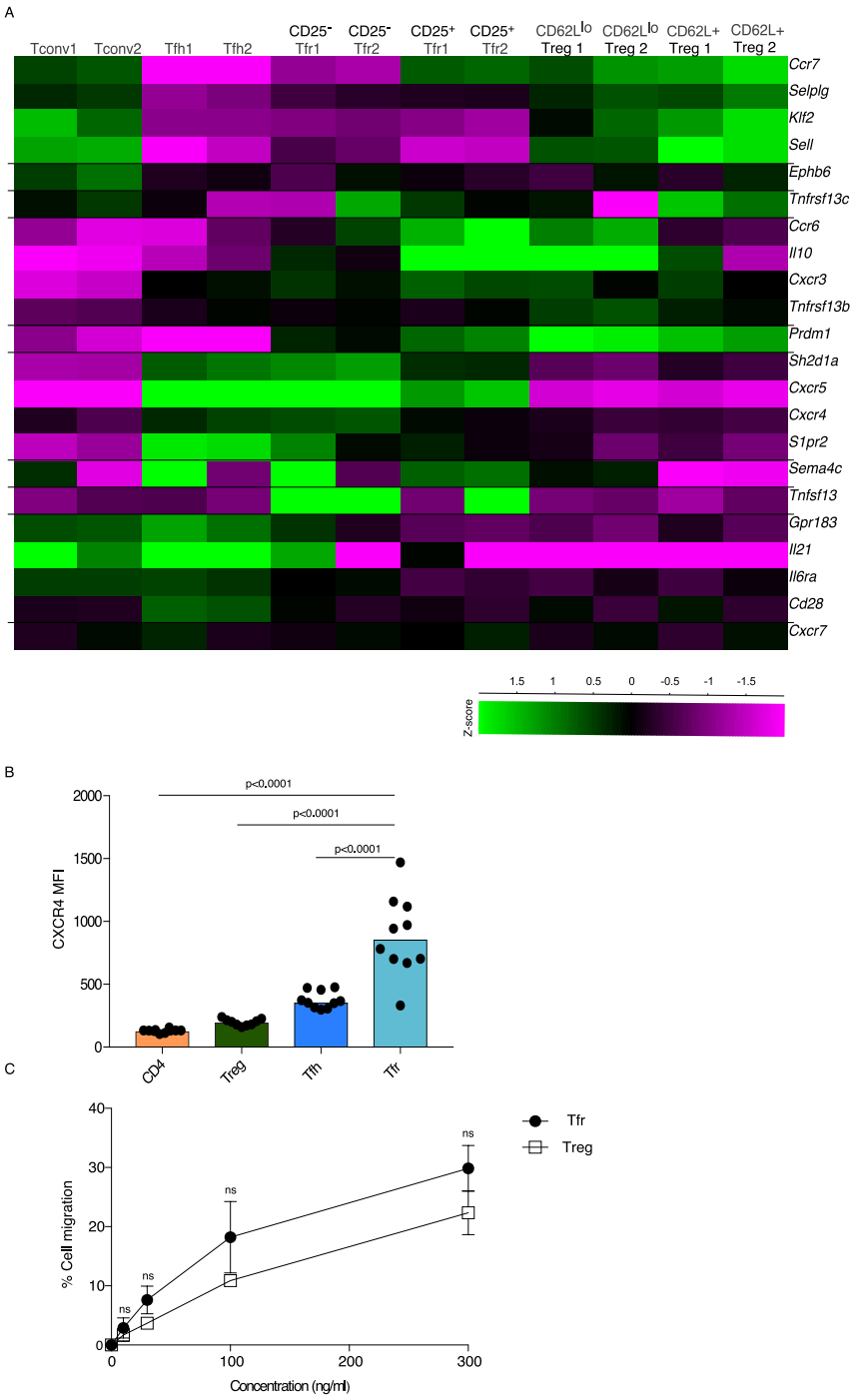


Figure 4.10 RNA–seq analysis of Tfr cells.

A. Z-scored heatmap of selected genes. RNA-seq data was obtained from Wing *et al* 2017, accession n^{o} DRA004824 and analysed using SeqMonk. **B.** CXCR4 MFI in CD4 T cells, Treg (Foxp3^{+}CD4^{+}), Tfh cells (CXCR5^{+}PD-1^{+}Foxp3^{-}CD4^{+}) and Tfr cells (CXCR5^{+}PD-1^{+}Foxp3^{+}CD4^{+}) in *Foxp3^{creERT2}* mice 14 days after immunisation with NP-KLH/Alum *s.c.*. Each symbol represents one mouse, and the horizontal bars represent the median values. P values were determined using a Kruskall-Wallis test with a Dunn's multiple comparison test **C.** Trans-well chemotaxis of either Tfr cells (CXCR5^{+}PD-1^{+}Foxp3^{+}) or Treg cells (Foxp3^{+}CD4^{+}) to the indicated concentrations of CXCL12. The mean and the standard error of the mean are shown for these data. P values were determined by a Two-way Anova with Sidak's multiple comparisons test, ns=non-signficant. Data are from one experiment.

One of the genes highly expressed in $CD25^-$, but not in $CD25^+$ Tfr cells, was CXCR4 (Figure 4.10 A). To confirm that CXCR4 was expressed in Tfr cells at the protein level, we next analysed the MFI of CXCR4 in Tfr cells, Tfh cells, Treg cells and naïve T cells. The MFI for CXCR4 was significantly higher in Tfr cells ($CXCR5^+PD\text{-}1^+$) as compared to other subsets (Figure 4.10 B). Indeed, Tfr cells tended to migrate towards CXCL12, the ligand for CXCR4, more readily compared to bulk Treg cells, although this effect was not significant (Figure 4.10 C). Collectively, these data suggest that CXCR4 may act alongside CXCR5 to mediate Treg localisation within the GC.

4.3 Discussion

Herein I developed a new strain of mice to investigate the role of CXCR5 in Treg homing to the GC. *Cxcr5*$^{fl/fl}$*Foxp3*$^{cre\text{-}ERT2}$ mice exhibited complete and specific deletion of CXCR5 in $Foxp3^+$ Treg cells, resulting in a 50% reduction in GC-localised Tfr cells, as determined by confocal microscopy. It must be noted that one caveat of this study is that I did not address whether Treg cells derived from *Cxcr5*$^{fl/fl}$*Foxp3*^{creERT2} mice were able to migrate to CXCL13 in a chemotaxis essay, something that will need to be addressed in future experiments. Despite the reduction in GC-localised Tfr cells, no change in the size or the output of the GC response was observed. The reduction in the number of Tfr cells in these mice did not affect the later stages of the GC response, nor the GC recall response. Overall, these data indicate that a 3-fold reduction in Tfr cells within the GC does not affect the GC response. These data are consistent with recent work published by Botta *et al* , and Wu *et al*, who demonstrated that *Bcl6*$^{fl/fl}$*Foxp3*^{cre} mice, that lack Tfr cells, did not show any changes in the number of GC B cells (Wu et al., 2016a, Botta et al., 2017).

In line with the findings in chapter 3, the presence of $Foxp3^+$ cells within the GC of *Cxcr5*$^{fl/fl}$*Foxp3*^{creERT2} mice suggests that alternative mechanisms exist that control the ability of Treg cells to enter the GC. To identify alternative candidates involved in Tfr migration to the GC, I analysed the gene-expression levels of proteins involved in T cell migration to the GC and compared Tfr cells, Tfh cells, Tconv and Treg cells. One attractive candidate we identified is CXCR4. I showed that CXCR4 is most highly expressed on Tfr cells compared to Tfh cells, and that Tfr cells are able to migrate towards CXCL12, the ligand for CXCR4.

CXCR4 has been shown to have multiple roles on many cells types within the GC. $CXCR4^{+}CXCR5^{-}$ T cells support extra-follicular B cell responses in the context of autoimmunity, while CXCR4 expression on B cells distinguishes the LZ ($CXCR4^{lo}$) from the DZ ($CXCR4^{hi}$) (Odegard et al., 2008). $CXCR4^{hi}$ B cells reside in the DZ where there is high expression of CXCL12, whereas $CXCR4^{lo}$ cells reside in the LZ, which has lower CXCL12 levels (Allen et al., 2004). Co-expression of CXCR5 and CXCR4 identifies T cells within the GC: CXCR4 expression levels on T cells identify their location within the germinal centre, with T cells expressing high levels of CXCR4 preferentially localising to the DZ (Elsner et al., 2012). Consistent with their localisation within the GC, $CXCR4^{+}CXCR5^{+}$ Tfh cells express the highest levels of PD-1, compared to $CXCR5^{+}CXCR4^{-}$ Tfh cells (Elsner et al., 2012). Furthermore, *Sh2d1a*$^{-/-}$ mice, which are unable to form GCs due to the impaired interaction between Tfh cells and GC B cells at the T:B border, are still able to generate $CXCR5^{+}$ $ICOS^{+}$ Tfh cells, but not $CXCR4^{+}CXCR5^{+}ICOS^{+}$ Tfh cells (Crotty et al., 2003, Qi et al., 2008, Elsner et al., 2012), indicating that CXCR4 is important for GC localisation of T cells, although this has not been formally demonstrated in studies that manipulate receptor expression.

Given this prominent role of CXCR4 in GC localisation in Tfh cells, it is of interest to study the role of CXCR4 in Treg homing to the GC. Moreover, it is possible that CXCR4 allows some Tfr cells to localise to the GC in absence of CXCR5. This prompts the hypothesis that CXCR4 can compensate for the loss of CXCR5 during Treg homing to the GC.

5 Do CXCR4 and CXCR5 act redundantly in follicular regulatory T cells?

5.1 Background

In the previous chapter I showed that deletion of CXCR5 on Treg cells resulted in a reduced number, but not complete absence, of Tfr cells within the GC, suggesting that alternative mechanisms facilitate Treg homing to the GC. I identified CXCR4 as a chemokine receptor highly expressed by Tfr cells, prompting the hypothesis that CXCR4 may promote localisation of Tfr cells within the GC.

The CXCR4:CXCL12 axis has a number of roles in the development, differentiation, proliferation and migration of T and B cells. The first biological role attributed to CXCR4 was promoting the proliferation of bone-marrow derived progenitor B cells (Nagasawa et al., 1994). It was subsequently shown that mice lacking CXCR4 display reduced B cell lymphopoiesis, as well as an absence of bone marrow myelopoiesis and defects in cerebellar development (Nagasawa et al., 1996, Ma et al., 1998, Zou et al., 1998). Targeted ablation of CXCR4 specifically in the B cell lineage revealed that CXCR4 is essential for retaining immature B cell precursors, including pro and pre-B cells, in the bone-marrow (Nie et al., 2004, Beck et al., 2014). These CXCR4-deficient B cell precursors home to splenic follicles but are unable to complete their maturation there, resulting in apoptosis of these misplaced cells and, therefore, reduced numbers of mature B cells (Nie et al., 2004). CXCR4 also has a role in mature B cells, directing B cell localisation in the Peyer's patches and peritoneal cavity

(Nie et al., 2004). In the context of the GC response, CXCR4 expression on B cells segregates the DZ from the LZ. The DZ is highly enriched in CXCL12, and centroblasts express high levels of CXCR4, required for localisation within the DZ (Allen et al., 2004). In T cells, the co-expression of CXCR5 and CXCR4 has previously been implicated in localisation within the GC (Elsner et al., 2012). Together, these data indicate that CXCR4 plays a role in homing to and segregation of the GC.

During T cell development, CXCR4 is expressed on thymocytes from the DN2 stage to the DP stage (Ara et al., 2003, Plotkin et al., 2003). During these early developmental stages, the CXCR4:CXCL12 axis directs the migration of early T cell precursors across the thymic cortex (Plotkin et al., 2003, Janas et al., 2010, Trampont et al., 2010). While CXCR4 is absolutely essential for early T cell differentiation, a study of mice with a targeted deletion of CXCR4 in CD4 T cells (*Cxcr4*$^{fl/fl}$*Cd4*$^{cre/+}$ mice), where CXCR4 is deleted at the CD4^{+}CD8^{+} DP stage, showed that CXCR4 is not essential beyond the stage of positive selection (Lucas et al., 2017). Furthermore, in contrast to previous studies that used foetal organ cultures and pharmacological inhibition of CXCR4, studies in the *Cxcr4*$^{fl/fl}$*Cd4*$^{cre/+}$ mouse model clearly showed that CXCR4 is not required for thymic egress as *Cxcr4*$^{fl/fl}$*Cd4*$^{cre/+}$ mice developed normal numbers of peripheral CD4^{+} and CD8^{+} T cells (Poznansky et al., 2002, Vianello et al., 2005, Lucas et al., 2017).

The role of CXCR4 in peripheral T cells is less well described. *Cxcr4*$^{fl/fl}$*Cd4*$^{cre/+}$ mice have normal numbers of splenic CD4 T cells as well as effector (CD44^{+}) Tconv cells, and normal numbers of splenic Treg cells (Lucas et al., 2017). These data indicate that the loss of CXCR4 does not result in impaired accumulation of mature T cells in peripheral lymphoid organs. However, more detailed phenotyping of these mice is required to better understand the role of CXCR4 in peripheral T cells.

The role of CXCR4 in Treg cells has not been directly studied before. Given that CXCR4 is involved in Tfh cell localisation, CXCR4 seems an attractive candidate for homing of Treg to the GC, acting either redundantly or perhaps synergistically with CXCR5.

In this chapter, I aimed to test the hypothesis that CXCR4 and CXCR5 act redundantly in Treg localisation to the GC. For this purpose I used two mouse models:

1) *Cxcr4*$^{fl/fl}$*Foxp3*$^{cre\text{-}ERT2}$ mice: wherein CXCR4 can be inducibly deleted on Foxp3^{+} Treg cells.

2) *Cxcr4*$^{fl/fl}$*Cxcr5*$^{fl/fl}$*Foxp3*$^{cre\text{-}ERT2}$ mice: A strain in which both CXCR4 and CXCR5 can be deleted in Foxp3-expressing cells in a temporal manner.

5.2 Results

5.2.1 Validation of the *Cxcr4*$^{fl/fl}$*Foxp3*$^{cre\text{-}ERT2}$ mouse model

In order to delete CXCR4 on Foxp3^{+} Treg cells, mice were fed a 'wash-out diet', consisting of soy-free pellets for 10 days prior to a 16% tamoxifen diet. Mice received the tamoxifen-containing diet for the remainder of the study. In contrast to the *Cxcr5*$^{fl/fl}$*Foxp3*$^{cre\text{-}ERT2}$ model described in Chapter 4, I was unable to detect deletion of CXCR4 on Treg cells after 4 weeks on the tamoxifen diet (Figure 5.1 A-C). I evaluated CXCR4 expression at five and seven weeks after starting the tamoxifen diet in mesenteric LNs of unimmunised *Cxcr4*$^{fl/fl}$*Foxp3*$^{cre\text{-}ERT2}$ mice and controls (Figure 5.1 D). Notably, at each time point only one mouse of each genotype was analysed, thus limiting the conclusions we are able to draw from this experiment. A *Cxcr5*$^{fl/fl}$*Foxp3*$^{cre\text{-}ERT2}$ mouse was included as a control to be able to exclude technical issues related to the tamoxifen diet. Five and seven weeks after starting the tamoxifen diet, *Cxcr4*$^{fl/fl}$*Foxp3*$^{cre\text{-}ERT2}$ mice still expressed considerable levels of CXCR4 on Treg cells (Figure 5.1 E-F). However, the *Cxcr5*$^{fl/fl}$*Foxp3*$^{cre\text{-}ERT2}$ mouse showed deletion of CXCR5 in Foxp3^{+} Treg cells compared with *Foxp3*$^{cre\text{-}ERT2}$ controls (Figure 5.1 E-F). Therefore, technical issues related to the tamoxifen diet can be excluded. Technical and biological variability as well as the n=1, makes it difficult to compare between week five and week seven. Nonetheless, it is clear that CXCR4 is still expressed in Treg cells from *Cxcr4*$^{fl/fl}$*Foxp3*$^{cre\text{-}ERT2}$ mice at five and seven weeks after starting the tamoxifen diet.

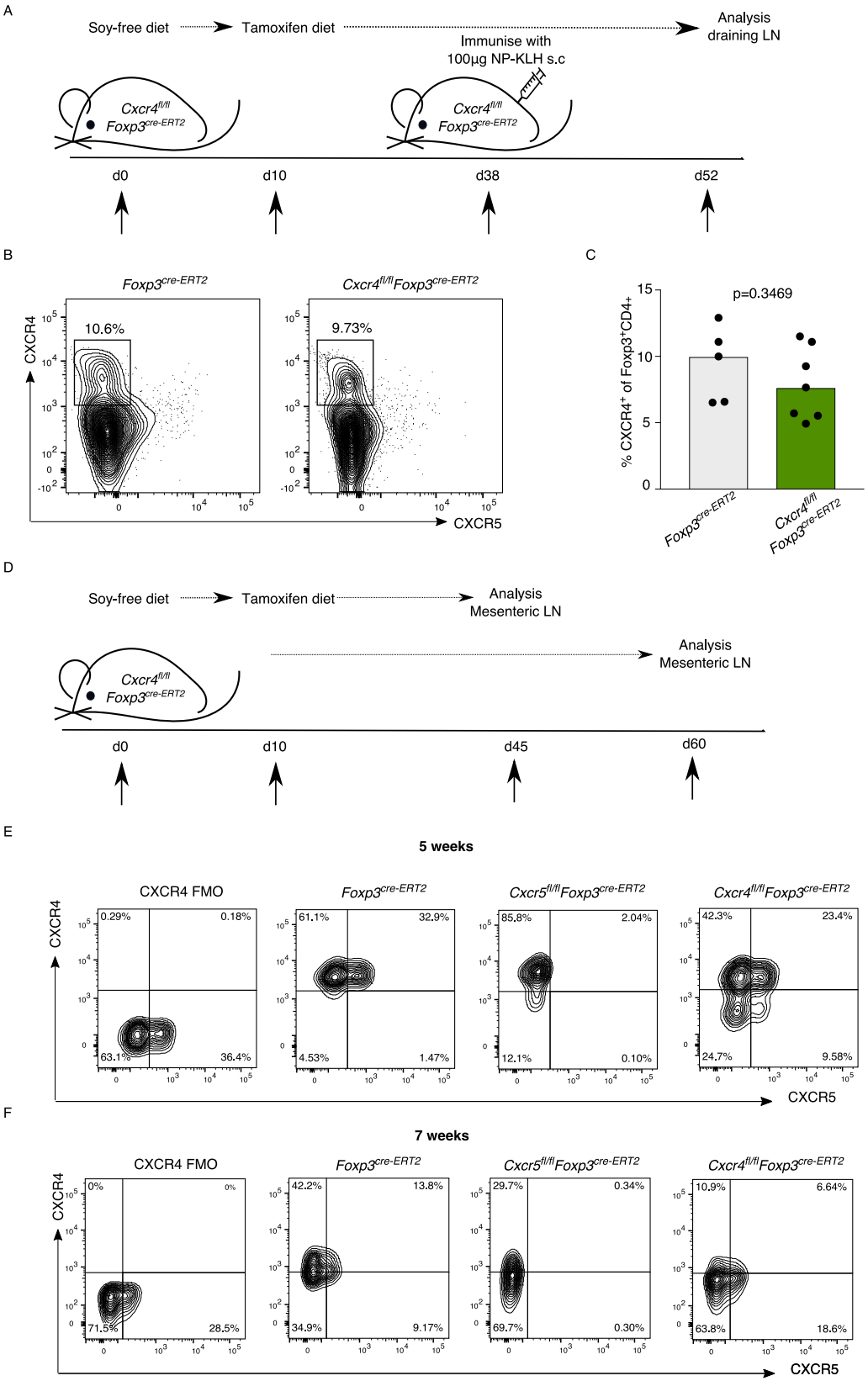

A
Soy-free diet
Tamoxifen diet
Analysis draining LN
Immunise with 100µg NP-KLH s.c
Cxcr4fl/fl Foxp3cre-ERT2
d0
d10
d38
d52
B
Foxp3cre-ERT2
Cxcr4fl/fl Foxp3cre-ERT2
10.6%
9.73%
CXCR4
CXCR5
C
p=0.3469
% CXCR4+ of Foxp3+CD4+
Foxp3cre-ERT2
Cxcr4fl/fl Foxp3cre-ERT2
D
Soy-free diet
Tamoxifen diet
Analysis Mesenteric LN
Cxcr4fl/fl Foxp3cre-ERT2
d0
d10
d45
d60
E
5 weeks
CXCR4 FMO
Foxp3cre-ERT2
Cxcr5fl/fl Foxp3cre-ERT2
Cxcr4fl/fl Foxp3cre-ERT2
0.29%
0.18%
63.1%
36.4%
61.1%
32.9%
4.53%
1.47%
85.8%
2.04%
12.1%
0.10%
42.3%
23.4%
24.7%
9.58%
CXCR4
CXCR5
F
7 weeks
CXCR4 FMO
Foxp3cre-ERT2
Cxcr5fl/fl Foxp3cre-ERT2
Cxcr4fl/fl Foxp3cre-ERT2
0%
0%
71.5%
28.5%
42.2%
13.8%
34.9%
9.17%
29.7%
0.34%
69.7%
0.30%
10.9%
6.64%
63.8%
18.6%
CXCR4
CXCR5

Figure 5.1 *Cxcr4*$^{fl/fl}$*Foxp3*$^{cre\text{-}ERT2}$ mice show delayed deletion of CXCR4 in Treg cells.

A. Diagram shows experimental set-up. Mice received a soy-free diet for 10 days. After 10 days, the mice received a diet containing tamoxifen for the remaining time of the study. After 30 days on the tamoxifen diet, the mice were immunised *s.c.* with NP-KLH/Alum in the flank. The inguinal LNs were harvested for analysis 14 days after immunisation. **B**. Representative flow cytometry contour plots of $CXCR4^{+}CXCR5^{-}$ cells from $Foxp3^{+}CD4^{+}$ cells. **C.** Quantification of the frequency of $CXCR4^{+}CXCR5^{-}$ Treg cells. **D.** Diagram shows experimental set-up. Mice received a soy-free diet for ten days. After ten days, the mice received a diet containing tamoxifen for the remaining time of the study. After five or seven weeks on the tamoxifen diet, the mesenteric LNs were harvested for analysis. **E.** Representative flow cytometry contour plots $CXCR4^{+}/CXCR5^{+}$ cells from $Foxp3^{+}CD4^{+}$ cells five weeks after starting the tamoxifen diet. **F.** Representative flow cytometry contour plots $CXCR4^{+}/CXCR5^{+}$ cells from $Foxp3^{+}CD4^{+}$ cells seven weeks after starting the tamoxifen diet. Each symbol represents one mouse, and the horizontal bars represent the median values. P values were determined using a Mann-Whitney U test. Data are from one experiment.

Immunisation with NP-KLH, nine weeks after starting the tamoxifen diet resulted in the most profound, albeit still not complete deletion of CXCR4. The draining (*i.e.* inguinal) LNs were harvested 14 days after immunisation to analyse the GC response (Figure 5.2). Even after feeding the mice the tamoxifen diet for 11 weeks, we were only able to observe a moderate, not significant, reduction in CXCR4 expression on Treg cells in *Cxcr4*$^{fl/fl}$*Foxp3*$^{cre\text{-}ERT2}$ mice, compared to controls (Figure 5.2 B-D). Surprisingly, we observed a significant increase in the proportion of CXCR5^{+} Treg cells in *Cxcr4*$^{fl/fl}$*Foxp3*$^{cre\text{-}ERT2}$ mice (Figure 5.2 B, E-F). The CXCR4^{+}CXCR5^{+} population was slightly reduced in *Cxcr4*$^{fl/fl}$*Foxp3*$^{cre\text{-}ERT2}$ mice, but this effect was not significant (Figure 5.2 B, G-H). There were no significant changes in either CXCR4 or CXCR5 expression on Tconv cells (Figure 5.3). Overall, these data indicate that CXCR4 was slightly reduced on Treg cells, but we did not achieve the desired complete ablation of CXCR4 in Treg cells, as seen for CXCR5 in Chapter 4.

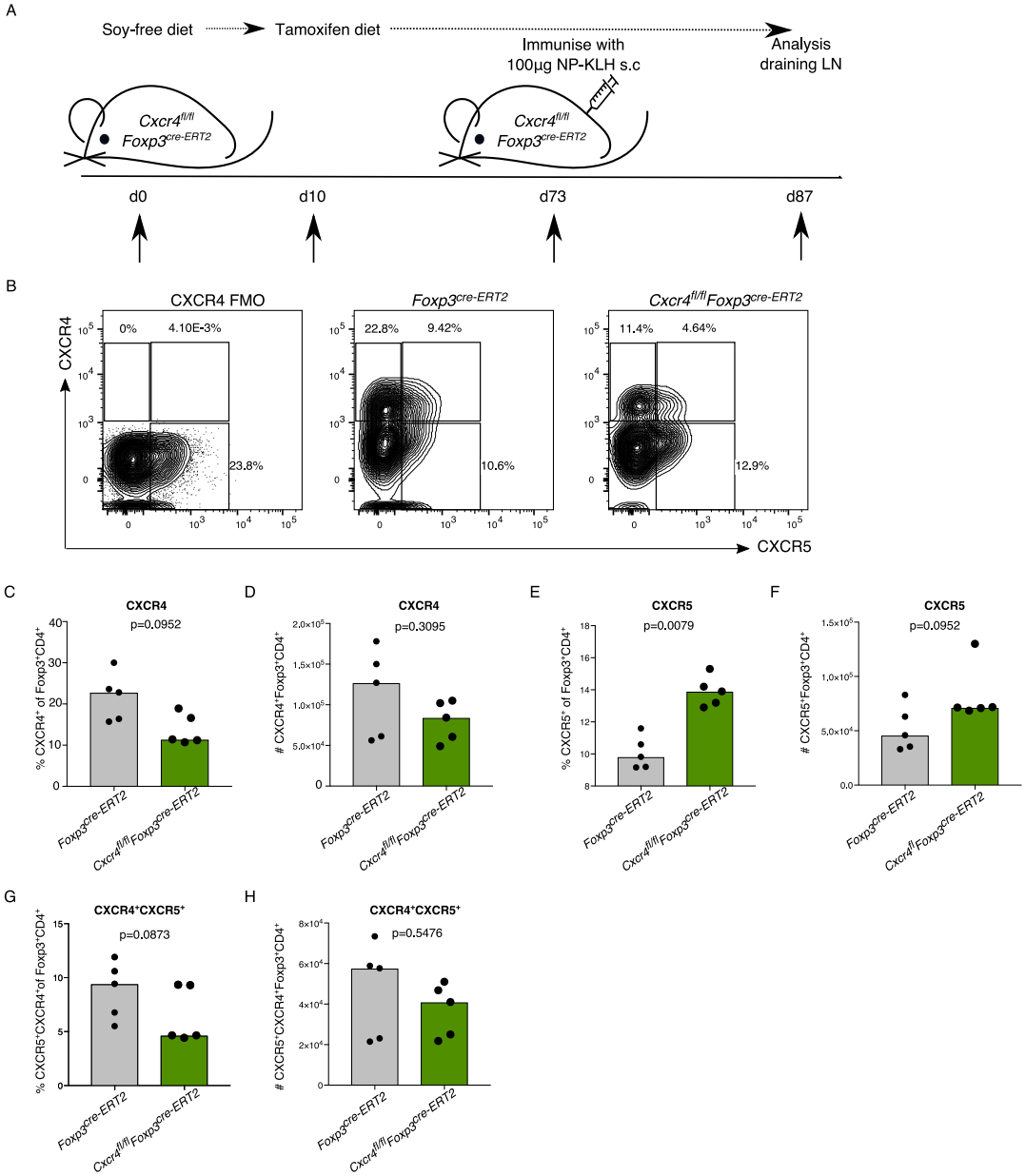


Figure 5.2 CXCR4 is reduced, but not completely deleted on Treg cells in *Cxcr4$^{fl/fl}$Foxp3$^{cre-ERT2}$* mice.

A. Diagram shows experimental set-up. Mice received a soy-free diet for 10 days. After 10 days, the mice received a diet containing tamoxifen for the remaining time of the study. After 63 days on the tamoxifen diet, the mice were immunised *s.c.* with NP-KLH/Alum in the flank. The inguinal LNs were harvested for analysis 14 days after immunisation. **B.** Representative flow cytometry contour plots of CXCR4$^+$CXCR5$^-$, CXCR5$^+$CXCR4$^-$, and CXCR4$^+$CXCR5$^+$ cells from Foxp3$^+$CD4$^+$ cells. **(C-D)** Quantification of **C.** the frequency and **D.** absolute numbers of CXCR4$^+$CXCR5$^-$ Treg cells. **(E-F)** Quantification of **E.** the frequency and **F.** Absolute numbers of CXCR4$^-$CXCR5$^+$ Treg cells. **(G-H)** Quantification of **G.** the frequency and **H.** absolute numbers of CXCR4$^+$CXCR5$^+$ Treg cells. Each symbol represents one mouse, and the horizontal bars represent the median values. P values were determined using a Mann-Whitney U test. Data represent two independent experiments.

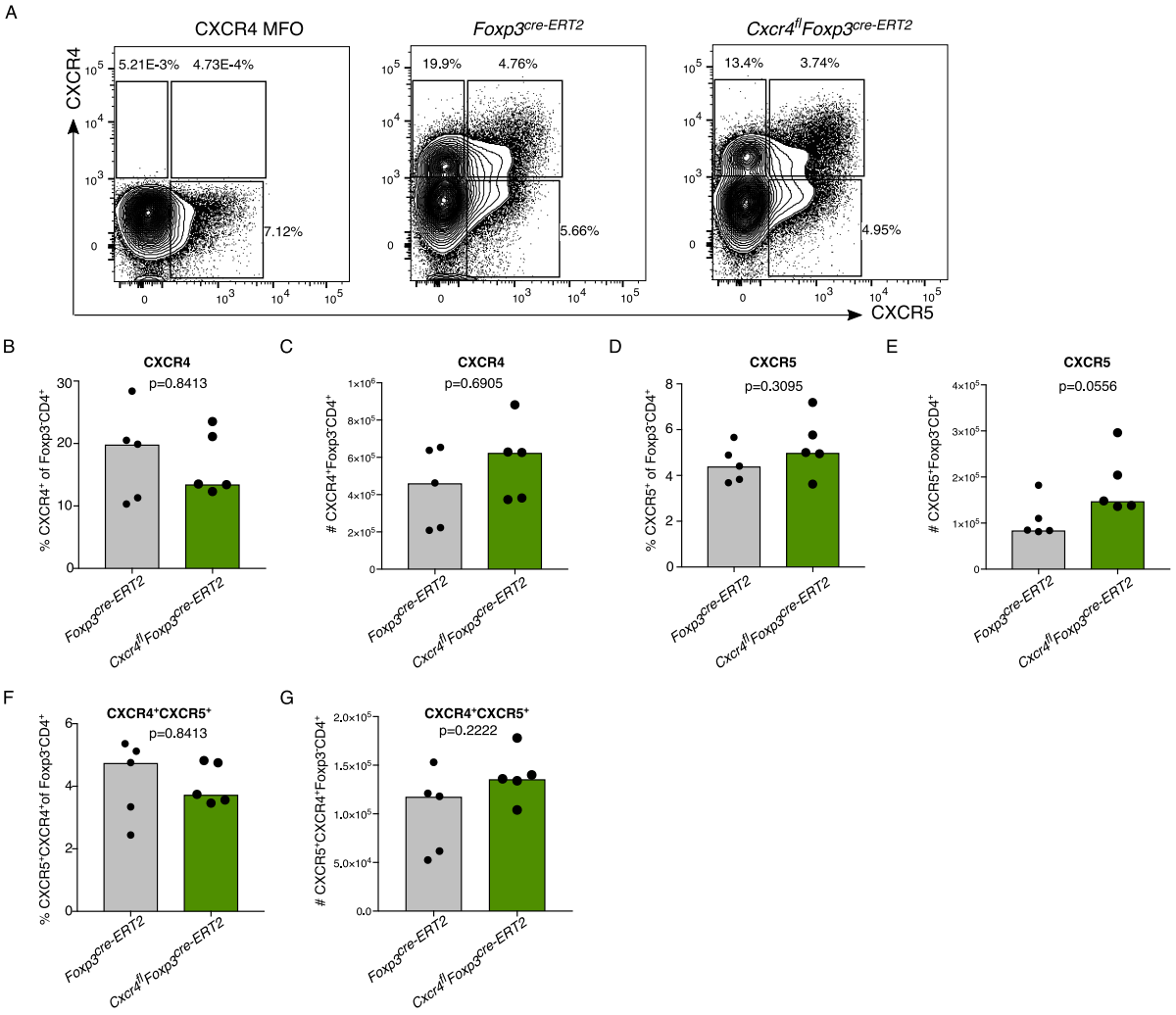


Figure 5.3 Tconv cells express normal levels of CXCR4 in *Cxcr4$^{fl/fl}$Foxp3$^{cre-ERT2}$* mice.

A. Representative flow cytometry contour plots of CXCR4^{+}CXCR5^{-}, CXCR5^{+}CXCR4^{-}, and CXCR4^{+}CXCR5^{+} cells from Foxp3^{-}CD4^{+} cells. **(B-C)** Quantification of **B.** the frequency and **C.** absolute numbers of CXCR4^{+}CXCR5^{-} Tconv cells. **(D-E)** Quantification of **D.** the frequency and **E.** absolute numbers of CXCR4^{-}CXCR5^{+} Tconv cells. **(F-G)** Quantification of **F.** the frequency and **G.** absolute numbers of CXCR4^{+}CXCR5^{+} Tconv cells. Each symbol represents one mouse, and the horizontal bars represent the median values. P values were determined using a Mann-Whitney U test. Data represent two independent experiments.

Next, the expression of CXCR4 on Tfr cells, Tfh cells and B cells was assessed. In contrast to the bulk Treg population, we observed a significant decrease in the MFI of CXCR4 in $Bcl6^{+}PD\text{-}1^{+}$ $CD25^{-}$ Tfr cells (Figure 5.4 A-B). To determine if there were off-target effects of the cre recombinase, and whether CXCR4 deletion is limited to the Treg cell compartment, I assessed CXCR4 expression on $CXCR5^{+}PD\text{-}1^{+}$ $Foxp3^{-}$ Tfh cells. The MFI of CXCR4 on Tfh cells was not different in *Cxcr4*$^{fl/fl}$*Foxp3*$^{cre\text{-}ERT2}$ mice compared to controls (Figure 5.4 C-D). Analysis of CXCR4 expression on B cells showed a trend for the MFI of CXCR4 to be increased on $B220^{+}$ B cells in *Cxcr4*$^{fl/fl}$*Foxp3*$^{cre\text{-}ERT2}$ mice, although this effect was not significant.

Together, these data show that CXCR4 expression is significantly reduced in Tfr cells and that this reduction is specific to Tfr cells, without affecting CXCR4 expression on Tfh cells or B cells. To determine whether this reduction in CXCR4 expression on Tfr cells in *Cxcr4*$^{fl/fl}$*Foxp3*$^{cre\text{-}ERT2}$ mice results in changes in the GC response, I further analysed the GC response in the *Cxcr4*$^{fl/fl}$*Foxp3*$^{cre\text{-}ERT2}$ model. The fact that I was unable to completely ablate CXCR4 in Treg cells, and therefore cannot exclude that the residual CXCR4 expression accounts for any phenotype (or lack thereof) observed, represents a major limitation in this study. Consequently, the results need to be interpreted with this caveat in mind.

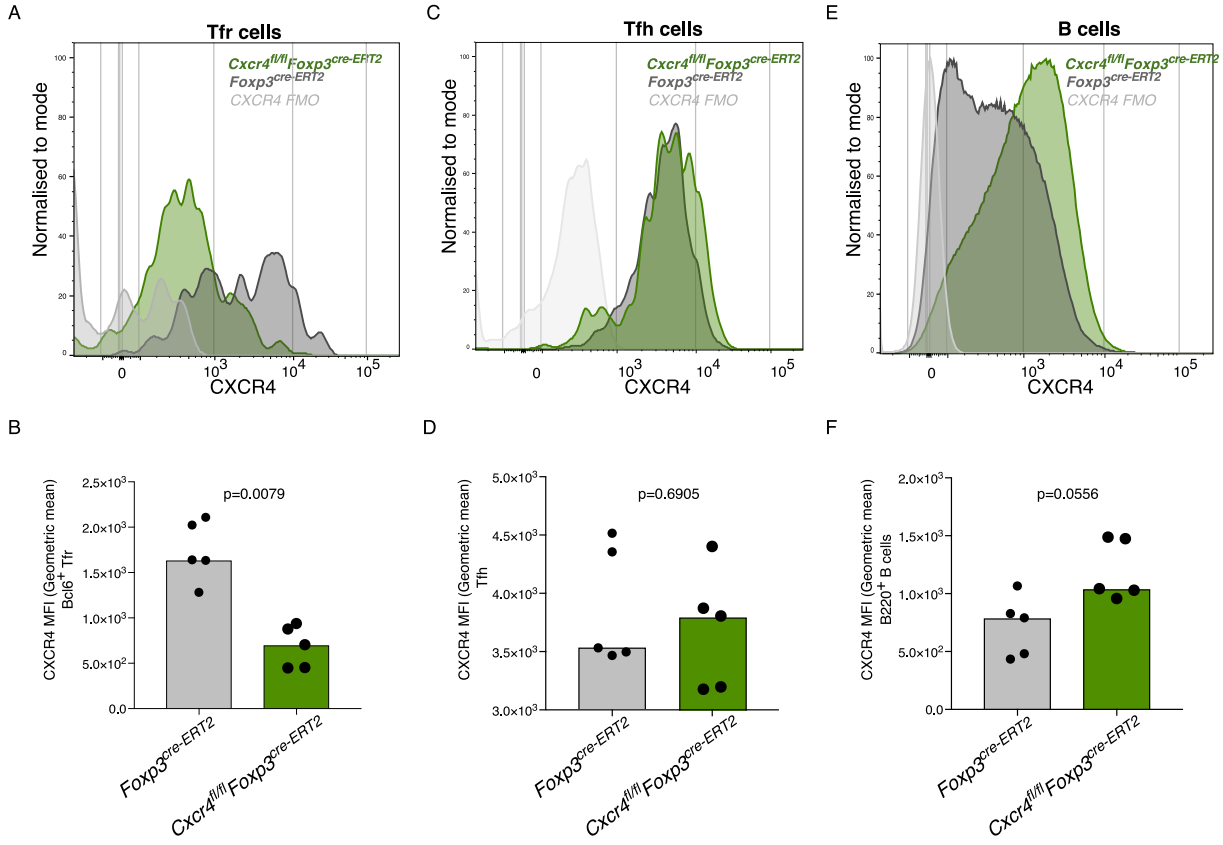


Figure 5.4 CXCR4 MFI on Tfr cells, Tfh cells and B cells.

Analysis 14 days after *s.c.* immunisation with NP-KLH. **A.** Representative overlay histogram plots of CXCR4 expression among Bcl6^{+}PD-1^{+}CD25^{-} Tfr cells in *Cxcr4$^{fl/fl}$Foxp3$^{cre\text{-}ERT2}$* mice, *Foxp3$^{cre\text{-}ERT2}$* mice, and in a CXCR4 FMO control sample. **B.** Quantification of the MFI (geometric mean) of CXCR4 in Bcl6^{+}PD-1^{+}CD25^{-} Tfr cells. **C.** Representative overlay histogram plots of CXCR4 expression among CXCR5^{+}PD-1^{+} Tfh cells in *Cxcr4$^{fl/fl}$Foxp3$^{cre\text{-}ERT2}$* mice, *Foxp3$^{cre\text{-}ERT2}$* mice, and in a CXCR4 FMO control sample. **D.** Quantification of the MFI (geometric mean) of CXCR4 in CXCR5^{+}PD-1^{+} Tfh cells. **E.** Representative overlay histogram plots of CXCR4 expression among B220^{+} B cells in *Cxcr4$^{fl/fl}$Foxp3$^{cre\text{-}ERT2}$* mice, *Foxp3$^{cre\text{-}ERT2}$* mice, and in a CXCR4 FMO control sample. **F.** Quantification of the MFI (geometric mean) of CXCR4 in B220^{+} B cells. Each symbol represents one mouse, and the horizontal bars represent the median values. P values were determined using a Mann-Whitney U test. Data represent two independent experiments.

5.2.2 *Cxcr4$^{fl/fl}$Foxp3$^{cre-ERT2}$* mice have normal GC responses

As CXCR4 expression was significantly reduced on Tfr cells, I next determined whether that reduction would result in fewer Tfr cells overall in *Cxcr4$^{fl/fl}$Foxp3$^{cre-ERT2}$* mice. Using two separate gating strategies, I identified either CXCR5^{+}PD-1^{+} Tfr cells or Bcl6^{+}PD-1^{+} Tfr cells (Figure 5.5). There were no differences in the number of CXCR5^{+}PD-1^{+} Tfr cells (Figure 5.5 A-C) or Bcl6^{+}PD-1^{+} Tfr cells (Figure 5.5 D-F), suggesting that the reduction in CXCR4 expression in Tfr cells does not result in fewer Tfr cells.

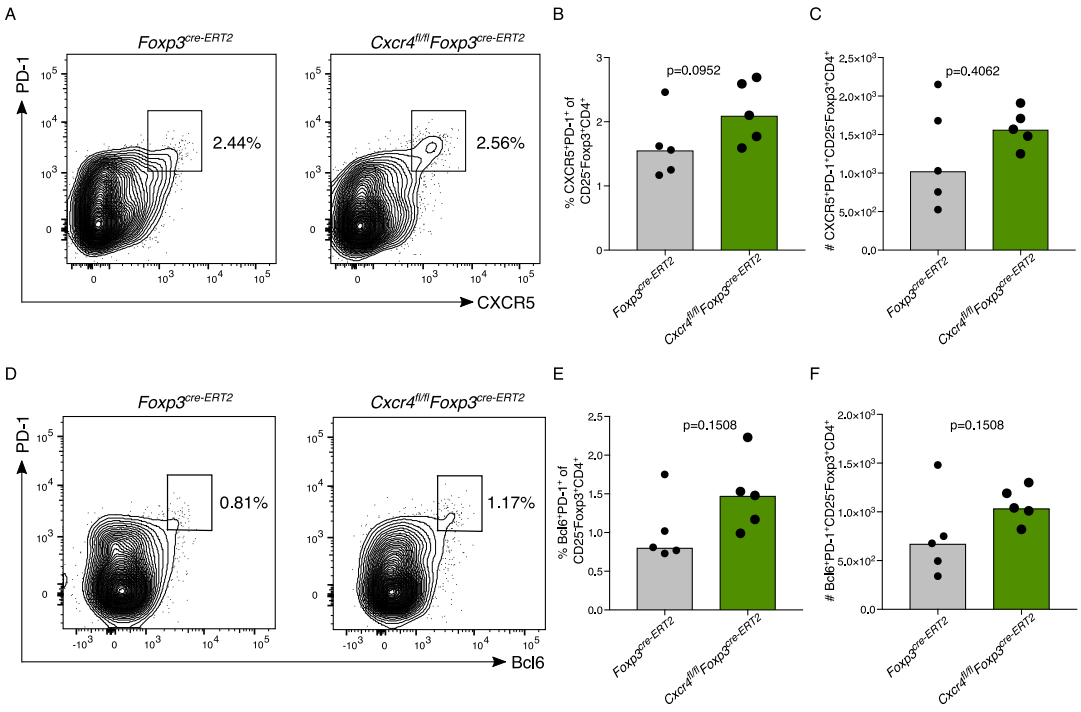


Figure 5.5 Normal numbers of Tfr cells in *Cxcr4$^{fl/fl}$Foxp3$^{cre-ERT2}$* mice.

Analysis of the GC response 14 days after *s.c.* immunisation with NP-KLH. **A.** Flow cytometry contour plots of Tfr cells, gated as PD-1^{+}CXCR5^{+} cells from CD25^{-}Foxp3^{+}CD4^{+} Treg cells. **(B-C)** Quantification of **B.** the frequency and **C.** absolute number of CXCR5^{+}PD-1^{+} Tfr cells. **D.** Flow cytometry contour plots of Tfr cells, gated as PD-1^{+}Bcl6^{+} cells from CD25^{-}Foxp3^{+}CD4^{+} Treg cells. **(E-F)** Quantification of **E.** the frequency, and **F.** absolute number of PD-1^{+}Bcl6^{+} Tfr cells. Each symbol represents one mouse, and the horizontal bars represent the median values. P values were determined using a Mann-Whitney U test. Data represent two independent experiments.

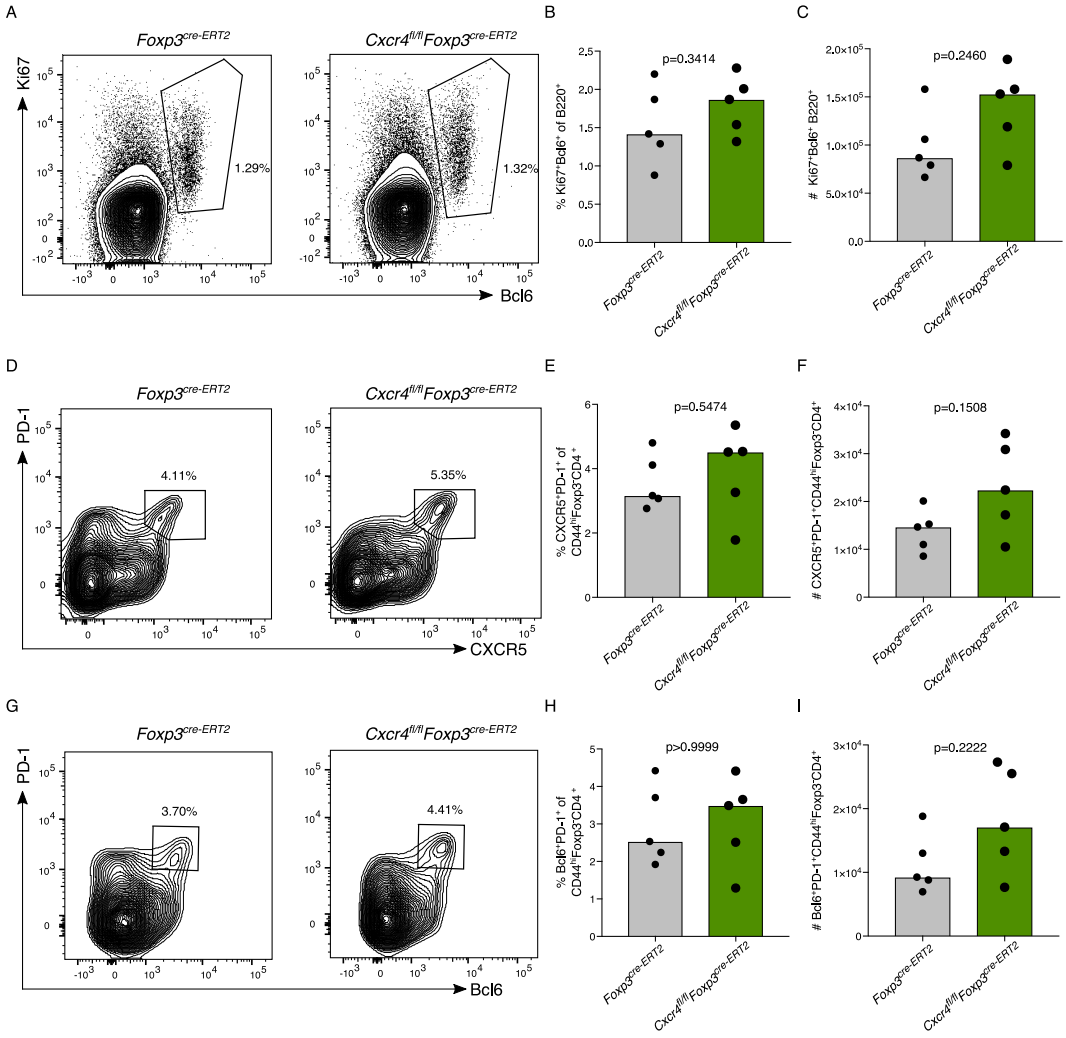


Figure 5.6 *Cxcr4*$^{fl/fl}$*Foxp3*$^{cre\text{-}ERT2}$ mice show normal numbers of GC B cells and Tfh cells.

Analysis of the GC response 14 days after *s.c.* immunisation with NP-KLH. **A.** Flow cytometry contour plots of GC B cells, gated as Bcl6^{+}Ki67^{+} cells from B220^{+} cells. **(B-C)** Quantification of **B.** the frequency and **C.** absolute number of Bcl6^{+}Ki67^{+} B cells. **D.** Flow cytometry contour plots of Tfh cells, gated as PD-1^{+}CXCR5^{+} cells from CD44^{hi} Foxp3^{-} CD4^{+} cells. **(E-F)** Quantification of **E.** the frequency and **F.** absolute number of PD-1^{+}CXCR5^{+} Tfh cells. **G.** Flow cytometry contour plots of Tfh cells, gated as PD-1^{+}Bcl6^{+} cells from CD44^{hi} Foxp3^{-} CD4^{+} cells. **(H-I)** Quantification of **H.** the frequency and **I.** absolute number of PD-1^{+}Bcl6^{+} Tfh cells. Each symbol represents one mouse, and the horizontal bars represent the median values. P values were determined using a Mann-Whitney U test. Data represent two independent experiments.

To further explore whether the reduction in CXCR4 in Tfr cells results in a functional impairment of the GC, I analysed GC B cells and Tfh cells in *Cxcr4*$^{fl/fl}$*Foxp3*$^{cre\text{-}ERT2}$ mice (Figure 5.6). *Cxcr4*$^{fl/fl}$*Foxp3*$^{cre\text{-}ERT2}$ mice showed normal proportions and absolute numbers of Ki67^{+}Bcl6^{+} GC B cells (Figure 5.6 A-C). There was no difference in the number or proportion of Tfh cells using two separate gating strategies to identify Tfh cells as CXCR5^{+}PD-1^{+} (Figure 5.6 D-F) or Bcl6^{+}PD-1^{+} (Figure 5.6 G-I). Together, these data indicate that the partial reduction of CXCR4 expression in Treg cells in *Cxcr4*$^{fl/fl}$*Foxp3*$^{cre\text{-}ERT2}$ mice does not result in altered numbers of GC B cells, Tfh cells or Tfr cells.

5.2.3 *Cxcr4*$^{fl/fl}$*Foxp3*$^{cre\text{-}ERT2}$ mice show normal plasma cell numbers and antibody production

I next tested whether the reduction in CXCR4 on Tfr cells in *Cxcr4*$^{fl/fl}$*Fopx3*$^{cre\text{-}ERT2}$ mice changes the output of the GC response. I did not observe any changes in the number of CD138^{+} plasma cells (Figure 5.7 A-B) in the draining LN. I next assessed whether *Cxcr4*$^{fl/fl}$*Foxp3*$^{cre\text{-}ERT2}$ mice showed any differences in class-switch recombination or affinity maturation by measuring serum levels of NP-specific antibodies by ELISA. We tested the affinity of serum IgG1, IgG2a and IgM for NP7 (to which only high-affinity antibodies will bind due to the low NP/BSA Ratio) and NP20 (to which both low and high affinity antibodies will bind). A relative increase in NP20 binding compared to NP7 would be indicative of diminished affinity maturation in *Cxcr4*$^{fl/fl}$*Foxp3*$^{cre\text{-}ERT2}$ mice. In addition, an increase in IgM levels compared to IgG1 or IgG2a would be indicative of reduced class-switching. *Cxcr4*$^{fl/fl}$*Foxp3*$^{cre\text{-}ERT2}$ mice showed normal levels of NP7 and NP20-specific IgG1 (Figure 5.7 C-D). Interestingly, there was an increased NP7/NP20 ratio in *Cxcr4*$^{fl/fl}$*Foxp3*$^{cre\text{-}ERT2}$ mice as compared to controls, indicating increased proportions of high-affinity antibodies in these mice (Figure 5.7 E). *Cxcr4*$^{fl/fl}$*Foxp3*$^{cre\text{-}ERT2}$ mice showed normal levels of NP7 and NP20-specific IgG2a (Figure 5.7 F-H). Finally, *Cxcr4*$^{fl/fl}$*Foxp3*$^{cre\text{-}ERT2}$ mice showed normal levels of NP7 and NP20-specific IgM (Figure 5.7 I-K). Together, these data show a mostly normal antibody response in *Cxcr4*$^{fl/fl}$*Foxp3*$^{cre\text{-}ERT2}$ mice.

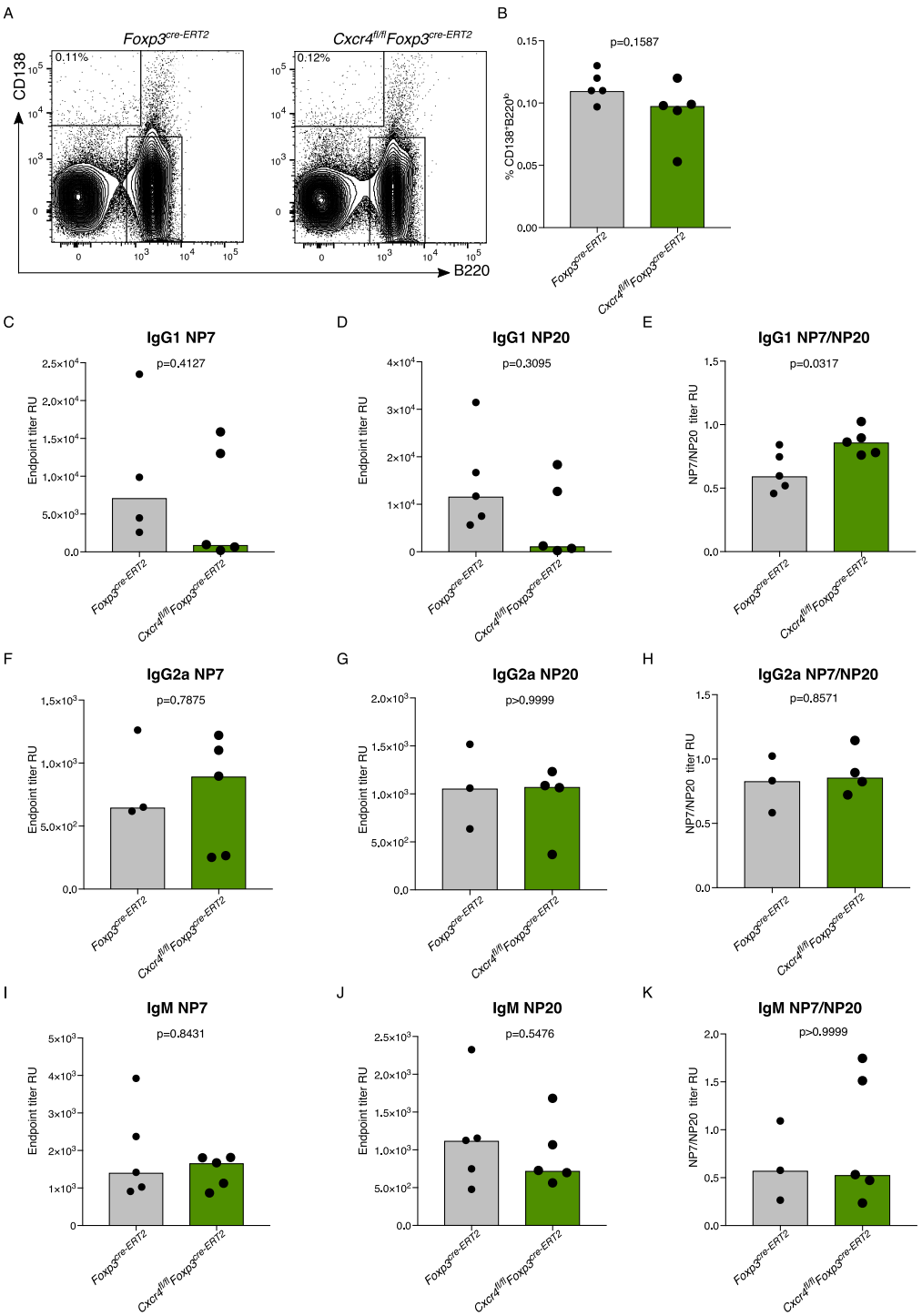

A
Foxp3cre-ERT2
Cxcr4fl/flFoxp3cre-ERT2
0.11%
0.12%
CD138
B220
B
p=0.1587
% CD138+B220lo
C
IgG1 NP7
p=0.4127
D
IgG1 NP20
p=0.3095
E
IgG1 NP7/NP20
p=0.0317
F
IgG2a NP7
p=0.7875
G
IgG2a NP20
p>0.9999
H
IgG2a NP7/NP20
p=0.8571
I
IgM NP7
p=0.8431
J
IgM NP20
p=0.5476
K
IgM NP7/NP20
p>0.9999
Endpoint titer RU
NP7/NP20 titer RU

Figure 5.7 Plasma cells and immunoglobulin production in *Cxcr4*$^{fl/fl}$*Foxp3*$^{cre\text{-}ERT2}$ mice.

Analysis day 14 after *s.c.* immunisation with NP-KLH/Alum. **A.** Flow cytometry contour plots of CD138^{+} plasma cells. **B.** Quantification of the frequency of CD138^{+} plasma cells. **(C-E)** Levels of IgG1 specific for NP7 (**C**) or NP20 (**D**) in the sera, and the ratio of NP7- to NP20-specific (**E**) IgG1. **(F-H)** Levels of IgG2a specific for NP7 (**F**) or NP20 (**G**) in the sera, and the ratio of NP7- to NP20-specific **(H**) IgG2a. **(I-K)** Levels of IgG2a specific for NP7 (**I**) or NP20 (**J**) in the sera, and the ratio of NP7- to NP20-specific (**K**) IgG2a. Each symbol represents one mouse, and the horizontal bars represent the median values. P values were determined using a Mann-Whitney U test. Flow cytometry data represent two independent experiments. ELISA data represent one experiment.

5.2.4 Validation of the *Cxcr4$^{fl/fl}$Cxcr5$^{fl/fl}$Foxp3$^{cre-ERT2}$* mouse model

As in previous mouse models, to delete CXCR4 and CXCR5 on Foxp3^{+} Treg cells, *Cxcr4$^{fl/fl}$Foxp3$^{cre-ERT2}$* mice were fed a 'wash- out diet', consisting of soy-free pellets for 10 days prior to a 16% tamoxifen diet. Mice received the tamoxifen-containing diet for the remainder of the study. The draining (*i.e.* inguinal) LNs were harvested 14 days after immunisation to analyse the GC response (Figure 5.8A). Similar to the results for *Cxcr4$^{fl/fl}$Foxp3$^{cre-ERT2}$* mice (Figure 5.2), I did not obtain deletion of CXCR4 in Treg cells (Figure 5.8 B-D). I observed a significant reduction in the proportion of CXCR5^{+} Treg cells in *Cxcr4$^{fl/fl}$Cxcr5$^{fl/fl}$Foxp3$^{cre-ERT2}$* mice (Figure 5.8 B, E-F), and the CXCR4^{+}CXCR5^{+} Treg population was significantly reduced in *Cxcr4$^{fl/fl}$Cxcr5$^{fl/fl}$Foxp3$^{cre-ERT2}$* mice (Figure 5.2 B, G-H). The fact that CXCR5 was successfully deleted, but not CXCR4, in *Cxcr4$^{fl/fl}$Cxcr5$^{fl/fl}$Foxp3cre^{-ERT2}* mice indicates that the *Cxcr4$^{fl/fl}$* allele is less sensitive to excision using this particular cre recombinase.

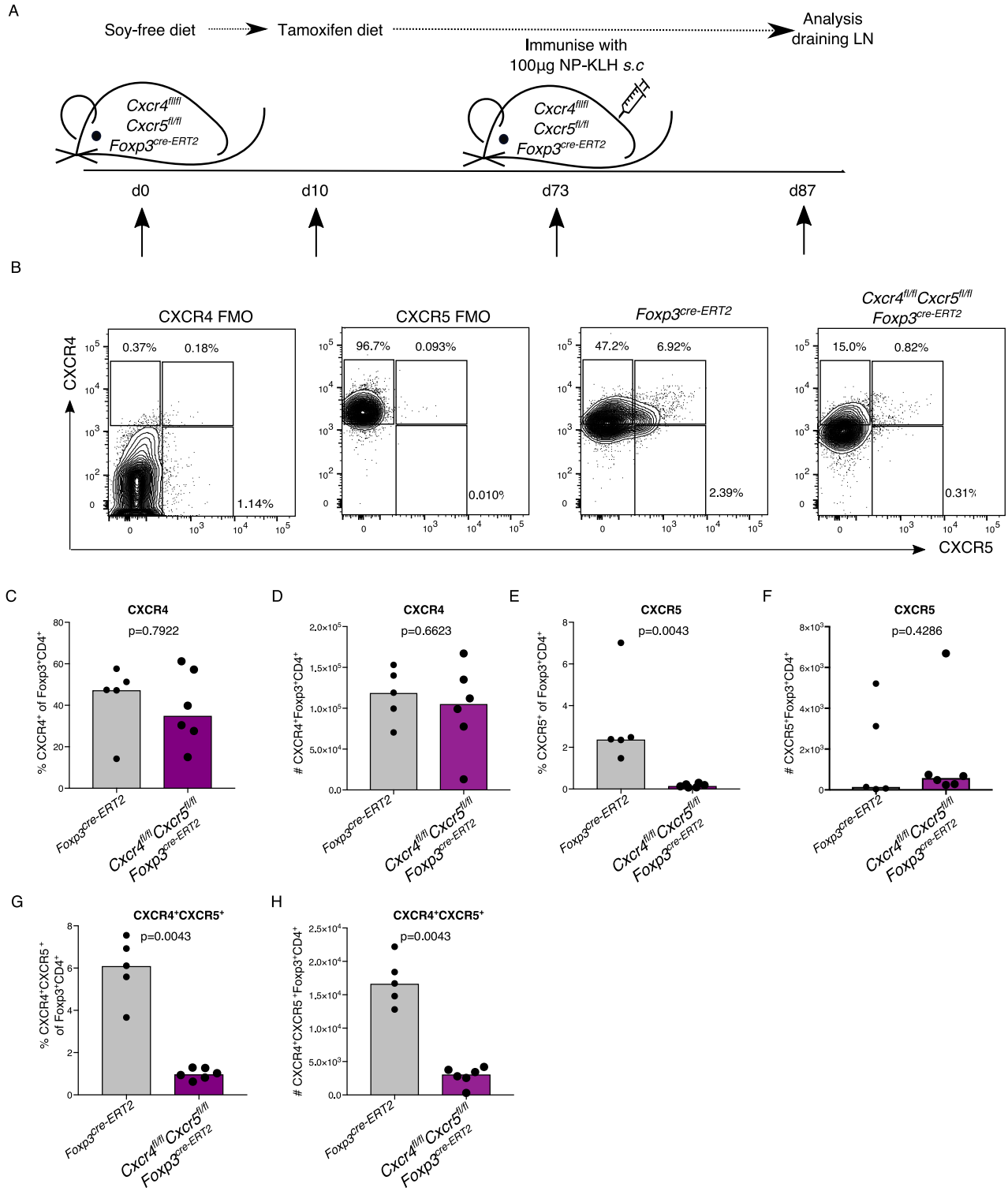

A
Soy-free diet
Tamoxifen diet
Analysis draining LN
Immunise with 100µg NP-KLH s.c
Cxcr4fl/fl Cxcr5fl/fl Foxp3cre-ERT2
d0
d10
d73
d87
B
CXCR4 FMO
CXCR5 FMO
Foxp3cre-ERT2
Cxcr4fl/fl Cxcr5fl/fl Foxp3cre-ERT2
CXCR4
CXCR5
0.37%
0.18%
1.14%
96.7%
0.093%
0.010%
47.2%
6.92%
2.39%
15.0%
0.82%
0.31%
C
CXCR4
p=0.7922
% CXCR4+ of Foxp3+CD4+
D
CXCR4
p=0.6623
# CXCR4+Foxp3+CD4+
E
CXCR5
p=0.0043
% CXCR5+ of Foxp3+CD4+
F
CXCR5
p=0.4286
# CXCR5+Foxp3+CD4+
G
CXCR4+CXCR5+
p=0.0043
% CXCR4+CXCR5+ of Foxp3+CD4+
H
CXCR4+CXCR5+
p=0.0043
# CXCR4+CXCR5+Foxp3+CD4+

Figure 5.8 Validation of the *Cxcr4$^{fl/fl}$Cxcr5$^{fl/fl}$Foxp3$^{cre-ERT2}$* mouse model.

A. Diagram shows experimental set-up. Mice received a soy-free diet for 10 days. After 10 days, the mice received a diet containing tamoxifen for the remaining time of the study. After 63 days on the tamoxifen diet, the mice were immunised *s.c.* with NP-KLH/Alum in the flank. The inguinal LNs were harvested for analysis 14 days after immunisation. **B.** Representative flow cytometry contour plots of $CXCR4^+CXCR5^-$, $CXCR5^+CXCR4^-$, and $CXCR4^+CXCR5^+$ cells from $Foxp3^+CD4^+$ cells. **(C-D)** Quantification of **C.** the frequency and **D.** absolute numbers of $CXCR4^+$ Treg cells. **(E-F)** Quantification of E. the frequency and **F.** Absolute numbers of $CXCR5^+$ Treg cells. **(G-H)** Quantification of **G.** the frequency and **H.** absolute numbers of $CXCR4^+CXCR5^+$ Treg cells. Each symbol represents one mouse, and the horizontal bars represent the median values. P values were determined using a Mann-Whitney U test. Data represent two independent experiments.

I next assessed the expression of CXCR4 on Tfr cells, Tfh cells and B cells. In contrast to the bulk Treg population, there was an overall decrease in the MFI of CXCR4 in $Bcl6^{+}PD\text{-}1^{+}CD25^{-}$ Tfr cells in *Cxcr4*$^{fl/fl}$*Cxcr5*$^{fl/fl}$*Foxp3cre*$^{-ERT2}$ mice, but this effect was not significant (Figure 5.9 A-B). To determine whether there were off-target effects of the Cre recombinase, and CXCR4 deletion is limited to the Treg cell compartment, I assessed CXCR4 expression on $CXCR5^{+}PD\text{-}1^{+}$ Tfh cells. I did not observe a difference in CXCR4 MFI in Tfh cells in *Cxcr4*$^{fl/fl}$*Cxcr5*$^{fl/fl}$*Foxp3*$^{cre\text{-}ERT2}$ mice compared to controls (Figure 5.9 C-D). Furthermore, analysis of CXCR4 expression on B cells showed that the MFI of CXCR4 was increased on $B220^{+}$ B cells, although this effect was not significant (Figure 5.9 D-F).

Together, these data indicate that *Cxcr4*$^{fl/fl}$*Cxcr5*$^{fl/fl}$*Foxp3*$^{cre\text{-}ERT2}$ mice show a deletion of CXCR5 in Treg, but only a slight, not significant, reduction in CXCR4 in Treg cells. The discrepancy in ablation efficiency between the floxed *Cxcr5* and *Cxcr4* alleles is indicative of a reduced sensitivity to deletion of the floxed region in *Cxcr4* and/or different locus accessibility of *Cxcr4*. Once again, due to the incomplete reduction of CXCR4 in *Cxcr4*$^{fl/fl}$*Cxcr5*$^{fl/fl}$*Foxp3cre*$^{-ERT2}$ mice, the results observed in this model need to be interpreted with caution and may merely serve as a clue to what the role of CXCR4 and CXCR5 might be in Treg cell homing to the GC.

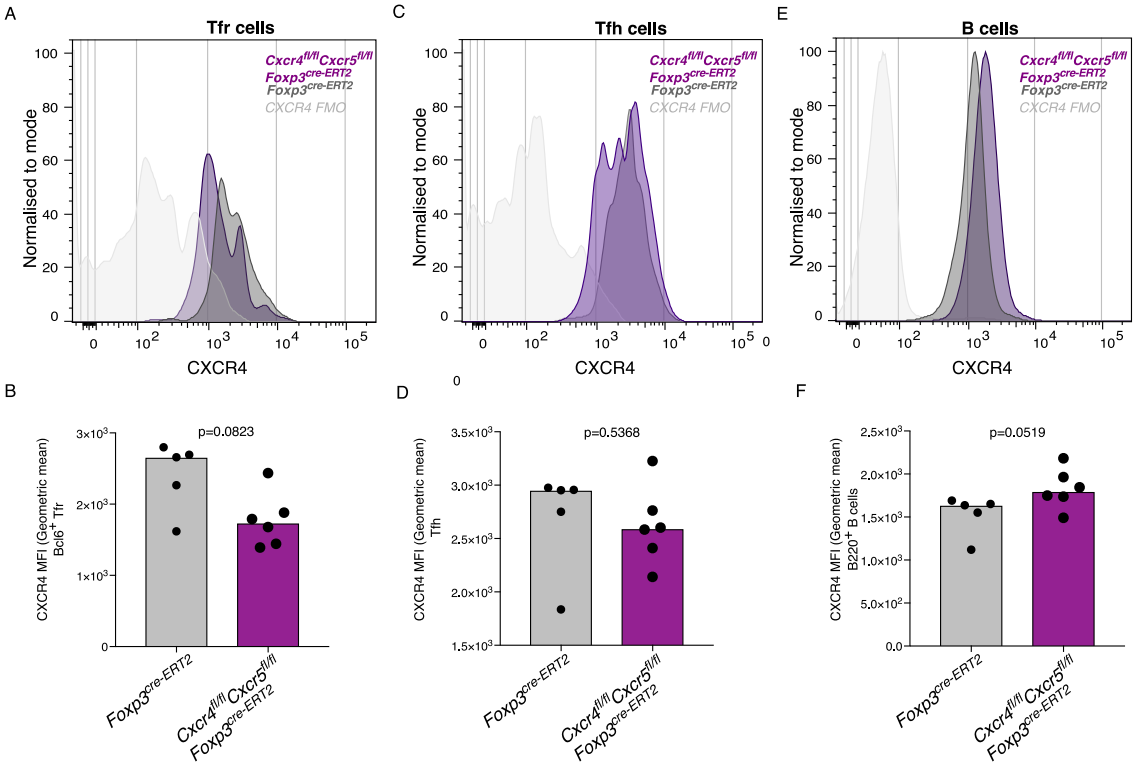


Figure 5.9 CXCR4 MFI on Tfr cells, Tfh cells and B cells.

A. Representative overlay histogram plots of CXCR4 expression among Bcl6^{+}PD-1^{+}CD25^{-} Tfr cells in *Cxcr4*$^{fl/fl}$*Cxcr5*$^{fl/fl}$*Foxp3*$^{cre\text{-}ERT2}$ mice, *Foxp3*$^{cre\text{-}ERT2}$ mice, and in a CXCR4 FMO control sample. **B.** Quantification of the MFI (geometric mean) of CXCR4 in Bcl6^{+}PD-1^{+}CD25^{-} Tfr cells. **C.** Representative overlay histogram plots of CXCR4 expression among CXCR5^{+}PD-1^{+} Tfh cells in *Cxcr4*$^{fl/fl}$*Cxcr5*$^{fl/fl}$*Foxp3*$^{cre\text{-}ERT2}$ mice, *Foxp3*$^{cre\text{-}ERT2}$ mice, and in a CXCR4 FMO control sample. **D.** Quantification of the MFI (geometric mean) of CXCR4 in CXCR5^{+}PD-1^{+} Tfh cells. **E.** Representative overlay histogram plots of CXCR4 expression among B220^{+} B cells in *Cxcr4*$^{fl/fl}$*Cxcr5*$^{fl/fl}$*Foxp3*$^{cre\text{-}ERT2}$ mice, *Foxp3*$^{cre\text{-}ERT2}$ mice, and in a CXCR4 FMO control sample. **F.** Quantification of the MFI (geometric mean) of CXCR4 in B220^{+} B cells. Each symbol represents one mouse, and the horizontal bars represent the median values. P values were determined using a Mann-Whitney U test. Data represent two independent experiments.

5.2.5 The germinal centre response in *Cxcr4$^{fl/fl}$Cxcr5$^{fl/fl}$Foxp3$^{cre-ERT2}$* mice

To explore whether *Cxcr4$^{fl/fl}$Cxcr5$^{fl/fl}$Foxp3$^{cre-ERT2}$* mice showed any functional impairment of the GC response, I analysed Tfr cells, Tfh cells and GC B cells by flow cytometry (Figure 5.10). I found a significant decrease in the proportion and absolute number of Bcl6^{+}PD-1^{+} Tfr cells in *Cxcr4$^{fl/fl}$Cxcr5$^{fl/fl}$Foxp3$^{cre-ERT2}$* mice (Figure 5.10 A-C). Despite the significant decrease in Tfr cells, I did not observe changes in the proportion or absolute number of Tfh cells (Figure 5.10 D-F), or GC B cells (Figure 5.10 G-I).

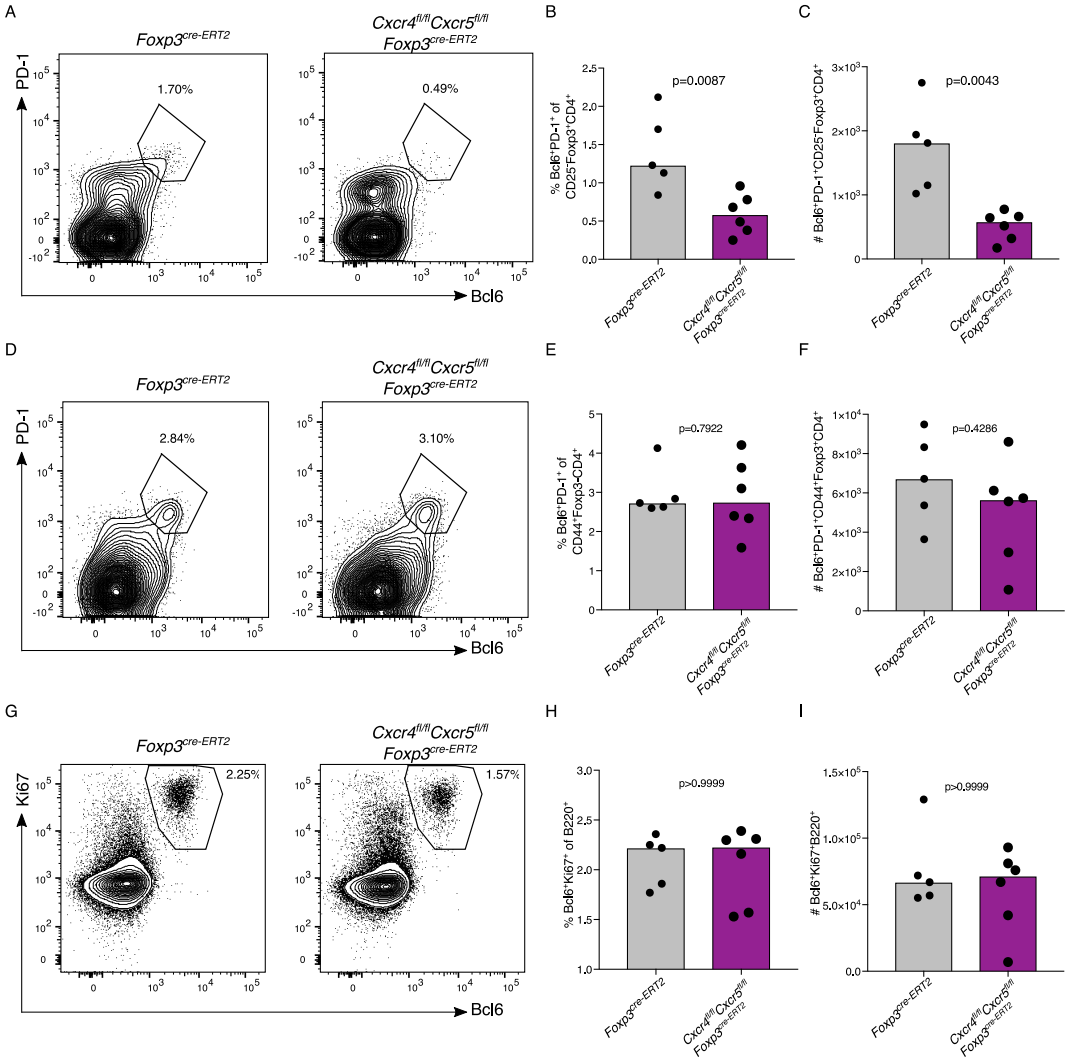


Figure 5.10 The GC response in *Cxcr4$^{fl/fl}$Cxcr5$^{fl/fl}$Foxp3$^{cre-ERT2}$* mice.

Analysis of the GC response 14 days after *s.c.* immunisation with NP-KLH/Alum. **A.** Flow cytometry contour plots of Tfr cells, gated as Bcl6^{+}PD-1^{+} cells from CD25^{-}Foxp3^{+} cells. **(B-C)** Quantification of **B.** the frequency and **C.** absolute number of Bcl6^{+}PD-1^{+} Tfr cells. **D.** Flow cytometry contour plots of Tfh cells, gated as Bcl6^{+}PD-1^{+} cells from CD44^{hi} Foxp3^{-} CD4^{+} cells. **(E-F)** Quantification of **E.** the frequency and **F.** absolute number of Bcl6^{+}PD-1^{+} Tfh cells. **G.** Flow cytometry contour plots of GC B cells, gated as Ki67^{+}Bcl6^{+} cells from CD44^{hi} Foxp3^{-} CD4^{+} cells. **(H-I)** Quantification of **H.** the frequency and **I.** absolute number of Ki67^{+}Bcl6^{+} GC B cells. Each symbol represents one mouse, and the horizontal bars represent the median values. P values were determined using a Mann-Whitney U test. Data represent two independent experiments.

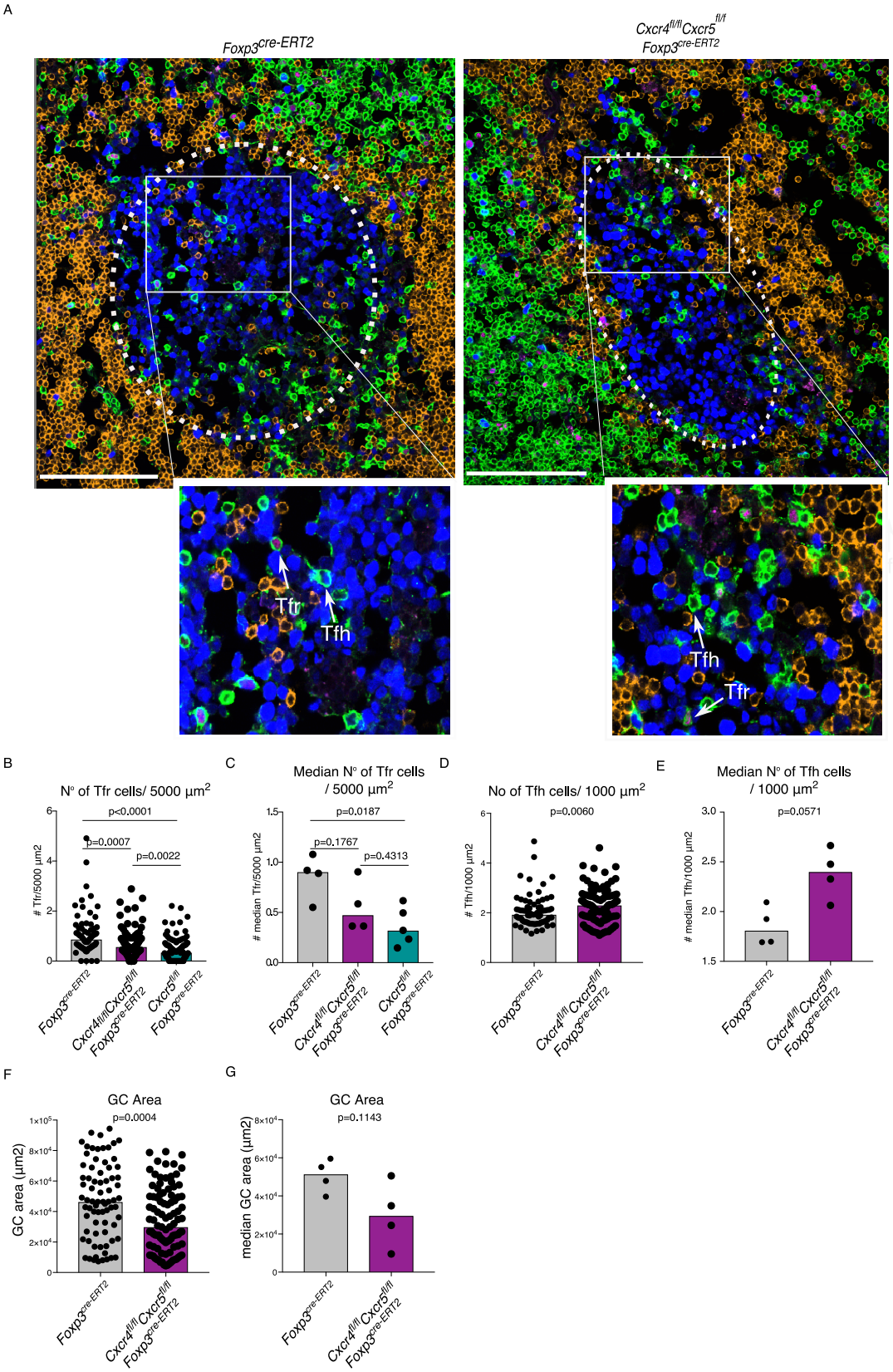

A
Foxp3cre-ERT2
Cxcr4fl/flCxcr5fl/f
Foxp3cre-ERT2
Tfr
Tfh
Tfh
Tfr
B
N° of Tfr cells/ 5000 µm2
p<0.0001
p=0.0007
p=0.0022
# Tfr/5000 µm2
C
Median N° of Tfr cells
/ 5000 µm2
p=0.0187
p=0.1767
p=0.4313
# median Tfr/5000 µm2
D
No of Tfh cells/ 1000 µm2
p=0.0060
# Tfh/1000 µm2
E
Median N° of Tfh cells
/ 1000 µm2
p=0.0571
# median Tfh/1000 µm2
Foxp3cre-ERT2
Cxcr4fl/flCxcr5fl/fl
Foxp3cre-ERT2
Cxcr5fl/fl
Foxp3cre-ERT2
F
GC Area
p=0.0004
GC area (µm2)
G
GC Area
p=0.1143
median GC area (µm2)

Figure 5.11 Confocal analysis of the GC in *Cxcr4$^{fl/fl}$Cxcr5$^{fl/fl}$Foxp3$^{cre-ERT2}$* mice 14 days after immunisation with NP-KLH/Alum.

A. Cryosections were stained with Foxp3 (magenta), Ki67 (blue), CD3 (green), and IgD (orange). Objective magnification 40x, scale bar 100μm. Representative confocal image of the GC with Tfr cells and Tfh cells indicated by the arrows. **B.** Quantification of the number of Tfr cells, defined as $CD3^+Foxp3^+$, per 5000 μm^2. Each symbol represents one GC, and the horizontal bars represent the median values. **C.** Quantification of the median number of Tfr cells, defined as $CD3^+Foxp3^+$, per 5000 μm^2. Each symbol represents one mouse and the horizontal bars represent the median values. **D.** Quantification of the number of Tfh cells, defined as $CD3^+Foxp3^-$ cells, per 1000 μm^2. Each symbol represents one GC, and the horizontal bars represent the median values. **E.** Quantification of the median number of Tfh cells, defined as $CD3^+Foxp3^-$ cells, per 1000 μm^2. Each symbol represents one mouse and the horizontal bars represent the median values. **F.** Quantification of the GC area (μm^2) (IgD^-, marked by dotted line), each symbol represents one GC. **G.** Quantification of the median GC area (μm^2). Each symbol represents one mouse, and the horizontal bars represent the median values. P values were determined using a Mann-Whitney U test or a Kruskal-Wallis test with a Dunn's multiple comparisons test where appropriate. Data represent one experiment.

To confirm the reduction in Tfr cells that was observed by flow cytometry in *Cxcr4*$^{fl/fl}$*Cxcr5*$^{fl/fl}$*Foxp3*$^{cre\text{-}ERT2}$ mice cryosections from iLNs of these mice were stained for Foxp3 (magenta), CD3 (green), Ki67 (blue), and IgD (orange) (Figure 5.11 A). Four different cryosections were analysed per mouse and within those sections all the GCs were imaged. Confocal images from *Cxcr4*$^{fl/fl}$*Cxcr5*$^{fl/fl}$*Foxp3*$^{cre\text{-}ERT2}$ revealed a significant decrease in the total number of Tfr cells, normalised to the GC area, consistent with the flow cytometry data (Figure 5.10 A-C). However, this decrease in the number of Tfr cells in *Cxcr4*$^{fl/fl}$*Cxcr5*$^{fl/fl}$*Foxp3*$^{cre\text{-}ERT2}$ mice was not as profound as the decrease in Tfr cells observed in *Cxcr5*$^{fl/fl}$*Foxp3*$^{cre\text{-}ERT2}$ mice (data from Chapter 4)(Figure 5.11 B). I next analysed the median number of Tfr cells for each biological replicate. We observed a reduction in the number of Tfr cells in *Cxcr4*$^{fl/fl}$*Cxcr5*$^{fl/fl}$*Foxp3*$^{cre\text{-}ERT2}$ mice as compared to controls, but this effect was not significant (Figure 5.11 C). *Cxcr5*$^{fl/fl}$*Foxp3*$^{cre\text{-}ERT2}$ mice had significantly fewer Tfr cells compared to controls, but the number of Tfr cells in *Cxcr5*$^{fl/fl}$*Foxp3*$^{cre\text{-}ERT2}$ mice was not significantly different from *Cxcr4*$^{fl/fl}$*Cxcr5*$^{fl/fl}$*Foxp3*$^{cre\text{-}ERT2}$ mice (Figure 5.11 C). The number of Tfh cells, normalised to GC area, was significantly increased in *Cxcr4*$^{fl/fl}$*Cxcr5*$^{fl/fl}$*Foxp3*$^{cre\text{-}ERT2}$ mice (Figure 5.11 D). Consistent with this result, analysis of the median number of Tfh cells for each biological replicate showed an increase in the number of Tfh cells, although this effect was not statistically significant (Figure 5.11 E). Analysis of the GC area showed a slight, but not significant decrease in the GC area (Figure 5.11 F-G). Together, these data indicate that there are fewer Tfr cells present within the GC of *Cxcr4*$^{fl/fl}$*Cxcr5*$^{fl/fl}$*Foxp3*$^{cre\text{-}ERT2}$ mice, and perhaps a slight increase in the number of Tfh cells, although this would need to be confirmed by repeating the experiment. Thus, these data hint at modest changes in the GC response in *Cxcr4*$^{fl/fl}$*Cxcr5*$^{fl/fl}$*Foxp3*$^{cre\text{-}ERT2}$ mice, but the effects observed are likely largely driven by the loss of CXCR5 on Treg cells.

5.2.6 *Cxcr4$^{fl/fl}$Cxcr5$^{fl/fl}$Foxp3$^{cre-ERT2}$* mice show normal plasma cell numbers and antibody production

Finally, I determined whether *Cxcr4$^{fl/fl}$Cxcr5$^{fl/fl}$Foxp3$^{cre-ERT2}$* mice showed changes in antibody responses. To this end, I determined the number of CD138^{+} plasma cells in the LNs and measured immunoglobulin levels in the serum. I did not observe any changes in the number of CD138^{+} plasma cells (Figure 5.12A-C). I next assessed whether *Cxcr4$^{fl/fl}$Cxcr5$^{fl/fl}$Foxp3$^{cre-ERT2}$* mice showed any differences in class-switch recombination or affinity maturation by measuring serum levels of NP-specific antibodies by ELISA. I tested the affinity of serum IgG1, IgG2a and IgM for NP7 and NP20. *Cxcr4$^{fl/fl}$Cxcr5$^{fl/fl}$Foxp3$^{cre-ERT2}$* mice showed normal levels of NP7 and NP20-specific IgG1 (Figure 5.12 D-F). *Cxcr4$^{fl/fl}$Cxcr5$^{fl/fl}$Foxp3$^{cre-ERT2}$* mice showed normal levels of NP7 and NP20-specific IgG2a (Figure 5.12 F-H). Finally, *Cxcr4$^{fl/fl}$Cxcr5$^{fl/fl}$Foxp3$^{cre-ERT2}$* mice showed normal levels of NP7 and NP20-specific IgM (Figure 5.12 I-K), although I was unable to perform a statistical test due to the low number of controls (n=2), due to a technical issue with the ELISA. Together, these data show a normal antibody response in *Cxcr4$^{fl/fl}$Cxcr5$^{fl/fl}$Foxp3$^{cre-ERT2}$* mice.

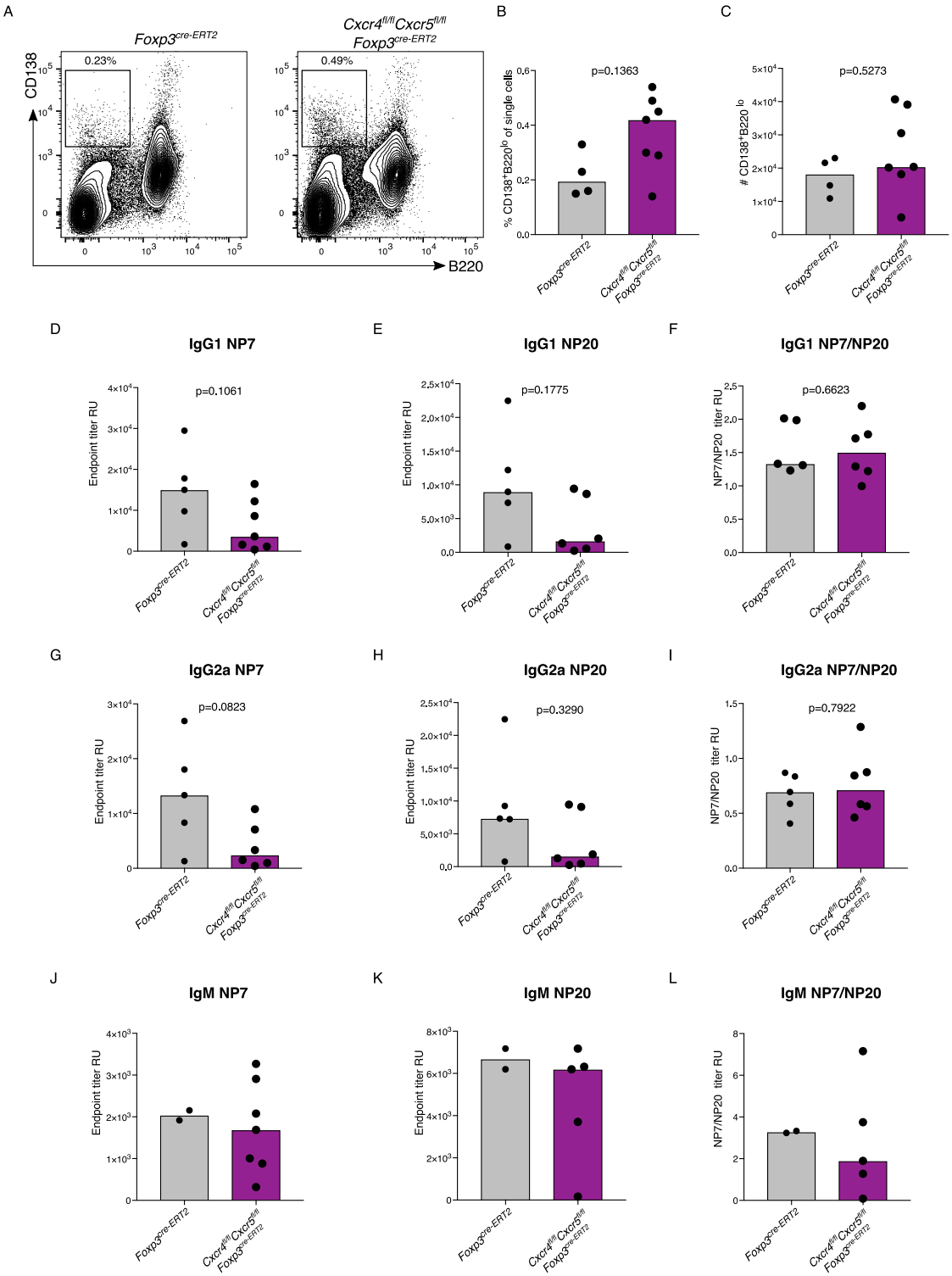

A
Foxp3cre-ERT2
Cxcr4fl/flCxcr5fl/fl Foxp3cre-ERT2
0.23%
0.49%
CD138
B220
B
p=0.1363
% CD138+B220lo of single cells
C
p=0.5273
# CD138+B220lo
D
IgG1 NP7
p=0.1061
Endpoint titer RU
E
IgG1 NP20
p=0.1775
F
IgG1 NP7/NP20
p=0.6623
NP7/NP20 titer RU
G
IgG2a NP7
p=0.0823
H
IgG2a NP20
p=0.3290
I
IgG2a NP7/NP20
p=0.7922
J
IgM NP7
K
IgM NP20
L
IgM NP7/NP20
Foxp3cre-ERT2
Cxcr4fl/flCxcr5fl/fl Foxp3cre-ERT2

Figure 5.12 Plasma cells and immunoglobulin production in *Cxcr4$^{fl/fl}$Cxcr5$^{fl/fl}$Foxp3$^{cre-ERT2}$* mice.

Analysis day 14 after *s.c.* immunisation with NP-KLH/Alum. **A.** Flow cytometry contour plots of CD138^{+} plasma cells. **(B-C)** Quantification of **C.** the frequency and **D.** absolute number of CD138^{+} plasma cells. **(D-F)** Levels of IgG1 specific for NP7 (**D**) or NP20 (**E**) in the sera, and the ratio of NP7- to NP20-specific (**F**) IgG1. **(G-I)** Levels of IgG2a specific for NP7 (**G**) or NP20 (**H**) in the sera, and the ratio of NP7- to NP20-specific (**I**) IgG2a. **(J-L)** Levels of IgG2a specific for NP7 (**J**) or NP20 (**K**) in the sera, and the ratio of NP7- to NP20-specific (**L**) IgM. Each symbol represents one mouse, and the horizontal bars represent the median values. P values were determined using a Mann-Whitney U test. Flow cytometry data represent two independent experiments. ELISA data represent one experiment.

5.3 Discussion

In this chapter, I developed *Cxcr4*$^{fl/fl}$*Foxp3*$^{cre\text{-}ERT2}$ mice to test the role of CXCR4 in Treg cell homing to the GC. In addition, to test whether CXCR4 and CXCR5 act redundantly in Treg homing to the GC, I generated *Cxcr4*$^{fl/fl}$*Cxcr5*$^{fl/fl}$*Foxp3*$^{cre\text{-}ERT2}$ mice. The experiments in this chapter relied upon the successful ablation of CXCR4, as well as CXCR5 in *Cxcr4*$^{fl/fl}$*Cxcr5*$^{fl/fl}$*Foxp3*$^{cre\text{-}ERT2}$ mice, in Treg cells. However, I was unable to completely delete CXCR4 on Treg cells in both *Cxcr4*$^{fl/fl}$*Foxp3*$^{cre\text{-}ERT2}$ mice and *Cxcr4*$^{fl/fl}$*Cxcr5*$^{fl/fl}$*Foxp3*$^{cre\text{-}ERT2}$ mice, even after feeding mice a tamoxifen diet for nine weeks, which is almost double the amount of time required for Treg-specific loss of CXCR5 in the *Cxcr5*$^{fl/fl}$*Foxp3*$^{cre\text{-}ERT2}$ mouse model, described in Chapter 4. Although there were no changes in CXCR4 levels in the bulk Treg cell population, Tfr cells in *Cxcr4*$^{fl/fl}$*Foxp3*$^{cre\text{-}ERT2}$ mice showed a significant reduction in CXCR4 expression. Furthermore, *Cxcr4*$^{fl/fl}$*Cxcr5*$^{fl/fl}$*Foxp3*$^{cre\text{-}ERT2}$ mice exhibited successful ablation of CXCR5 indicating that the failure to delete CXCR4 is not due to a technical problem with tamoxifen delivery.

The efficiency of Cre-loxP recombination decreases with increasing genetic distance between LoxP sites (Zheng et al., 2000). Thus, it is also possible that the decrease in efficiency of Cre-mediated recombination is due to the size of the floxed region. *Cxcr5* contains 4 exons, and the loxP sites in the *Cxcr5*$^{fl/fl}$ construct are flanking exon 2, encoding a ~100bp region (Ensembl)(Bradford et al., 2017). *Cxcr4,* on the other hand, contains two exons, with exon 2 consisting of ~2Kb, and encoding for 98% of the CXCR4 molecule. The loxP sites in *Cxcr4*$^{fl/fl}$*Foxp3*$^{cre\text{-}ERT2}$ mice are flanking exon 2 and thus a ~2Kb region (Ensembl). So the size of the deleted region differs considerably between these two constructs. Nevertheless, 2 Kb can still be considered a very small genomic region, so it is unlikely that the difference in ablation efficiency is due to the genetic distance between the two loxP sites. Alternatively, the difference in Cre-mediated deletion efficiency of CXCR4 compared to CXCR5 might be caused by differences in locus accessibility between genes and therefore sensitivity of ablation. One way of improving the deletion of CXCR4 in Treg cells would be increasing the dosage of tamoxifen. However, administering tamoxifen via the chow has the disadvantage that we are unable to control the precise dosage of tamoxifen the mice are ingesting. Therefore, it would be preferable to change the route of administration of tamoxifen to IP injections or oral gavages in future studies with *Cxcr4*$^{fl/fl}$*Foxp3*$^{cre\text{-}ERT2}$ mice as this will allow

us to control as well as increase the dosage of tamoxifen the mice are receiving. The fact that we were unable to delete CXCR4 completely on Treg cells is a major limitation of this study and, consequently, prevents us from drawing definite conclusions from the experiments described in this chapter.

Cxcr4$^{fl/fl}$*Foxp3*$^{cre\text{-}ERT2}$ mice showed normal numbers of Tfr cells, Tfh cells and GC B cells and did not reveal any changes in antibody responses. Interestingly, Treg cells in *Cxcr4*$^{fl/fl}$*Foxp3*$^{cre\text{-}ERT2}$ mice expressed significantly higher levels of CXCR5, but this did not result in an increase in CXCR5^{+}PD-1^{+} Tfr cells. Flow cytometry analysis of *Cxcr4*$^{fl/fl}$*Cxcr5*$^{fl/fl}$*Foxp3*$^{cre\text{-}ERT2}$ mice revealed a significant reduction in Tfr cells, but no changes in the number of Tfh cells or GC B cells. Confocal imaging of the GC confirmed the decrease in Tfr cells in the GC in *Cxcr4*$^{fl/fl}$*Cxcr5*$^{fl/fl}$*Foxp3*$^{cre\text{-}ERT2}$ mice. However, a comparison of the number of Tfr cells in *Cxcr4*$^{fl/fl}$*Cxcr5*$^{fl/fl}$*Foxp3*$^{cre\text{-}ERT2}$ versus *Cxcr5*$^{fl/fl}$*Foxp3*$^{cre\text{-}ERT2}$ mice (from Chapter 4) showed that *Cxcr4*$^{fl/fl}$*Cxcr5*$^{fl/fl}$*Foxp3*$^{cre\text{-}ERT2}$ contain more Tfr cells in the GC than *Cxcr5*$^{fl/fl}$*Foxp3*$^{cre\text{-}ERT2}$ mice. This suggests that, in contrast to our hypothesis, CXCR4 perhaps acts antagonistically with CXCR5, and that CXCR4 might limit Tfr migration to the GC. This would be consistent with the fact that there is an increase in CXCR5 expression on Treg cells in *Cxcr4*$^{fl/fl}$*Foxp3*$^{cre\text{-}ERT2}$ mice. Furthermore, there is evidence for CXCR5-CXCR4 co-immunoprecipitation *in vitro* in a prostate cancer cell line, potentially supporting cross-talk between these two chemokine receptors (El-Haibi et al., 2013). It is tempting to speculate that this CXCR5-CXCR4 interaction enhances antagonistic or other biological effects in Tfr cells.

Except for speculation, in this chapter I was unable to draw conclusions about the role of CXCR4 in Treg cells. Optimisation of the tamoxifen-inducible deletion of CXCR4 in Treg cells will need to be carried out before further analysis should be considered.

6 The role of Bcl6 in regulatory T cell development

6.1 Introduction

6.1.1 Bcl6 directs gene expression of cells within the GC, and outside of the GC

Bcl6 is a transcriptional repressor and is a member of the POZ/BTB/zinc finger family of transcription factors (Kerckaert et al., 1993, Ye et al., 1993, Miki et al., 1994). It is a key transcriptional regulator of many different immune cell types, including GC B cells, Tfh cells, Tfr cells and macrophages.

Bcl6 is essential for GC B cell formation, and supports and maintains the GC B cell phenotype by repressing genes that control cell cycle, cell death, and DNA damage responses (Ranuncolo et al., 2007, Ranuncolo et al., 2008, Cerchietti et al., 2010, Kerfoot et al., 2011). Furthermore, Bcl6 represses Blimp-1, thereby preventing terminal differentiation of GC B cells into plasma cells (Shapiro-Shelef et al., 2003).

In $CD4^+$ T cells, Bcl6 is required for both Tfh and Tfr cell differentiation (Johnston et al., 2009, Nurieva et al., 2009, Yu et al., 2009). In activated $CD4^+$ T cells, Bcl6 acts as a transcriptional repressor of numerous pathways, including T cell signalling and migration pathways (Hatzi et al., 2013). It is thought that the main role for Bcl6 is to suppress the expression of other transcriptional regulators such as *Rorγt* and *Tbx21* (Tbet), which drive Th17 and Th1 differentiation, respectively (Nurieva et al., 2009, Yu et al., 2009). Additionally, Bcl6 represses *Gata3* expression during Th17 differentiation (Yu et al., 2009).

In Treg cells, Bcl6 controls Th2 immune responses by repressing GATA3 function (Sawant et al., 2012). Bcl6 reinforces Tfh cell identity by repressing Blimp-1, which promotes non-Tfh effector differentiation (Crotty et al., 2010). Thus, Bcl6 is known to be an important transcriptional repressor in mature $CD4^+$ T cells.

6.1.2 Transcriptional mechanism of Bcl6

6.1.2.1 Bcl6 structure

Bcl6 contains an evolutionary conserved N-terminal BTB/POZ domain, a middle unstructured region (RD2), and 6 kruppel-type zinc finger domains at the C-terminus, enabling binding to the DNA consensus motif (Figure 6.1)(Kawamata et al., 1994). The BTB domain, as well as the RD2 domain have autonomous repressor activity and recruit distinct sets of co-repressor partner proteins (Ahmad et al., 2003, Fujita et al., 2004). The zinc finger domain has no inherent suppressor activity, but is able to repress transcription by competing for overlapping binding sites with STAT proteins (Huang et al., 2013).

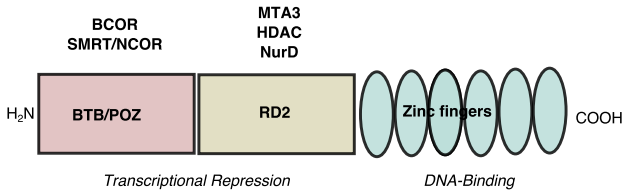


Figure 6.1 Bcl6 structure.

The biological function of Bcl6 is mediated through different domains. The BTB/POZ and the RD2 domain that can recruit distinct co-repressor indicated in the figure and are responsible for mediating transcriptional repression. The zinc finger domain consists of six zinc fingers and mediates binding to DNA.

The BTB domain is essential for sustaining GC B cell proliferation as well as Tfh cell differentiation and function (Huang et al., 2013, Nance et al., 2015). The BTB domain folds as an obligate homodimer and forms two identical and symmetrical extended grooves between the homodimers that serve as a docking site for co-repressors: Silencing Mediator of Retinoic and Thyroid receptors (SMRT), Nuclear Co-Receptor (NCOR) and Bcl6 interacting Co-Repressor (BCOR) (Huynh and Bardwell, 1998, Huynh et al., 2000). The co-repressors SMRT and NCOR bind the Bcl6 BTB groove through an identical 18-amino acid Bcl6 binding peptide sequence, whereas BCOR binds to Bcl6 using an entirely different Bcl6 binding peptide sequence (Ghetu et al., 2008). SMRT and NCOR are highly related and both

form higher order complexes with histone deacetylase (HDAC) 3 (Karagianni and Wong, 2007). BCOR is entirely different from SMRT and NCOR and forms a complex akin to the polycomb receptor complex 1 (Ghetu et al., 2008). The mechanisms by which these protein interactions translate into transcriptional repression have so far only been studies in B cells. During GC B cell proliferation, Bcl6 BTB domain-dependent repression involves two simultaneous but functionally independent mechanisms (Hatzi et al., 2013). The first mechanism involves the formation of ternary BCOR/SMRT/NCOR complexes at promoters. Despite Bcl6 binding thousands of promoters, it only represses those where it is able to form a unique complex with simultaneous recruitment of BCOR and SMRT/NCOR complexes. The formation of these complexes is associated with specific epigenetic repressive marks (Hatzi et al., 2013). Secondly, Bcl6 can switch enhancers from the active to the poised state, mediated via recruiting the SMRT-HDAC3 complex, which de-acetylates the activating chromatin H3K27 acetyl mark (H3K27ac), in a process coined "enhancer toggling" (Hatzi et al., 2013). Remarkably, the genes that are repressed by Bcl6 by the formation of promoter complexes, and those that are repressed by enhancer toggling are mostly non-overlapping. Whether the formation of ternary complexes at promoters and enhancer toggling play a role in Bcl6 BTB domain mediated repression in other cells types remains to be demonstrated. However, it has been demonstrated that Bcl6 is able to bind and repress T cell enhancer networks during Tfh cell differentiation, suggesting that there might be a very similar mechanism to enhancer toggling occurring in Tfh cells (Hatzi et al., 2015).

In B cells, Tfh cells and Tfr cells, the Bcl6 RD2 domain acts together with the co-repressor MTA3, which in turn recruits the NurD-Mi-2β complex. This MTA3-NurD-Mi-2β complex mediates repression of target genes such as *Prdm1* (encoding Blimp1) in a HDAC dependent manner, and thereby suppresses terminal differentiation of B cells, and the differentiation into alternative fates in Tfh cells (Johnston et al., 2009, Hatzi et al., 2015, Shen et al., 2018).

How Bcl6 drives cell-context dependent transcription programs is not entirely clear. It is possible that Bcl6 recruits distinct co-repressor complexes to establish epigenetic marks at target genes in a cell-context dependent manner. However, further research is required to enhance our understanding of Bcl6 mediated repression in different immune cell types.

6.1.3 The balanced expression of Tbet and Bcl6 drives Th1/Tfh differentiation

At the outset of this project, I was interested in the role of Bcl6 in Tfr cell differentiation. Bcl6 has been shown to be essential for the formation of Tfr cells, but how Bcl6 drives Tfr cell differentiation is unknown. The aim of this study was to test whether Bcl6 promotes Tfr cell differentiation by repressing the differentiation of Treg cells into other Treg cell subsets. I specifically focussed on $Tbet^+$ Treg cells because it is known that in Tconv cells, competition between Bcl6 and Tbet, the driver of Th1 differentiation, is important for determining the commitment of primed $CD4^+$ Tconv cells towards the Tfh phenotype (Oestreich and Weinmann, 2012). In Th1 cells, Tbet antagonises other T cell fates partly by physically recruiting Bcl6 to certain target genes in Th1 cells (Oestreich et al., 2011). The balance between Tbet and Bcl6 expression and their relative conformational positions therefore seems to determine whether a cell commits to a Th1 or Tfh cell differentiation pathway (Oestreich and Weinmann, 2012). The Tbet/Bcl6 ratio can be skewed by environmental factors. High IL-2 levels push the cell into $Tbet^+$ Th1 cells whereas limiting IL-2 levels and ICOS signalling skews towards the Tfh fate (Choi et al., 2011). Thus, the aim of this chapter is to elucidate whether Bcl6 enables Tfr differentiation by repressing Tbet, and, consequently, to determine whether Bcl6 and Tbet are mutually repressive transcription factors in Tfr cells.

6.2 Results

6.2.1 *Bcl6$^{fl/fl}$Cd4$^{cre/+}$* mice show a cell-intrinsic increase in Tbet expression in Treg cells in the absence of infection

To test the hypothesis that Bcl6 represses Tbet$^+$ Treg cell development, I generated mixed bone marrow chimeras using *Bcl6$^{fl/fl}$Cd4$^{cre/+}$* mice as donors. In *Bc6$^{fl/fl}$Cd4$^{cre/+}$* mice, exons 7-9 of *Bcl6,* which encode the zinc finger domains, are conditionally deleted upon cre-mediated recombination in DP T cells, so in both CD4$^+$ T cells and CD8$^+$ T cells (Hollister et al., 2013). In these mice, a truncated protein is generated in T cells but it is unable to bind to its target genes, and, therefore, Tfh cells or Tfr cells are unable to form. A 50/50 mix of bone marrow derived from *Bcl6$^{fl/fl}$Cd4$^{cre/+}$* mice (or *Bcl6$^{fl/fl}$Cd4$^{+/+}$*controls) (expressing the congenic marker CD45.2) and bone marrow derived from *B6.sjl* (CD45.1$^+$) mice was transferred into irradiated *B6.sjl* recipients. Ten weeks after the transfer, mice were infected with influenza (HKx31), and the mediastinal LNs were analysed 14 days after infection (Figure 6.2A). The influenza infection model is an excellent tool to study Tfr/Th1-like Treg differentiation as it generates both a strong Th1 immune response, as well as a robust GC response.

There was a modest increase in the percentage of Tbet$^+$CXCR3$^+$ Treg cells derived from *Bcl6$^{fl/fl}$Cd4$^{cre/+}$* bone marrow (CD45.2), compared with *Bcl6$^{fl/fl}$Cd4$^{+/+}$* bone marrow (CD45.2) (Figure 6.2B-C). However, there was no difference in the frequency of Tbet$^+$ Treg cells derived from CD45.1$^+$ bone marrow in the group that received *Bcl6$^{fl/fl}$Cd4$^{+/+}$* bone marrow compared with *Bcl6$^{fl/fl}$Cd4$^{cre/+}$* bone marrow (Figure 6.2B-C). These data suggest that Bcl6 plays a cell-intrinsic role in Treg cell differentiation, and in the absence of Bcl6 Treg cells are skewed towards the Th1-like Treg cell fate.

There was no difference in the percentage of Tbet$^+$CXCR3$^+$ Tconv cells in *Bcl6$^{fl/fl}$Cd4$^{cre/+}$* bone marrow (CD45.2), compared with *Bcl6$^{fl/fl}$Cd4$^{+/+}$* bone marrow (CD45.2), or in the percentage of Tbet$^+$CXCR3$^+$ Tconv cells derived from CD45.1$^+$ bone marrow in the group that received *Bcl6$^{fl/fl}$Cd4$^{cre/+}$* bone marrow (CD45.2) compared with *Bcl6$^{fl/fl}$Cd4$^{+/+}$* bone marrow (CD45.2). Thus, Bcl6 seems to play a cell-intrinsic role in Treg differentiation, but not in differentiation of CD4$^+$ Tconv cells.

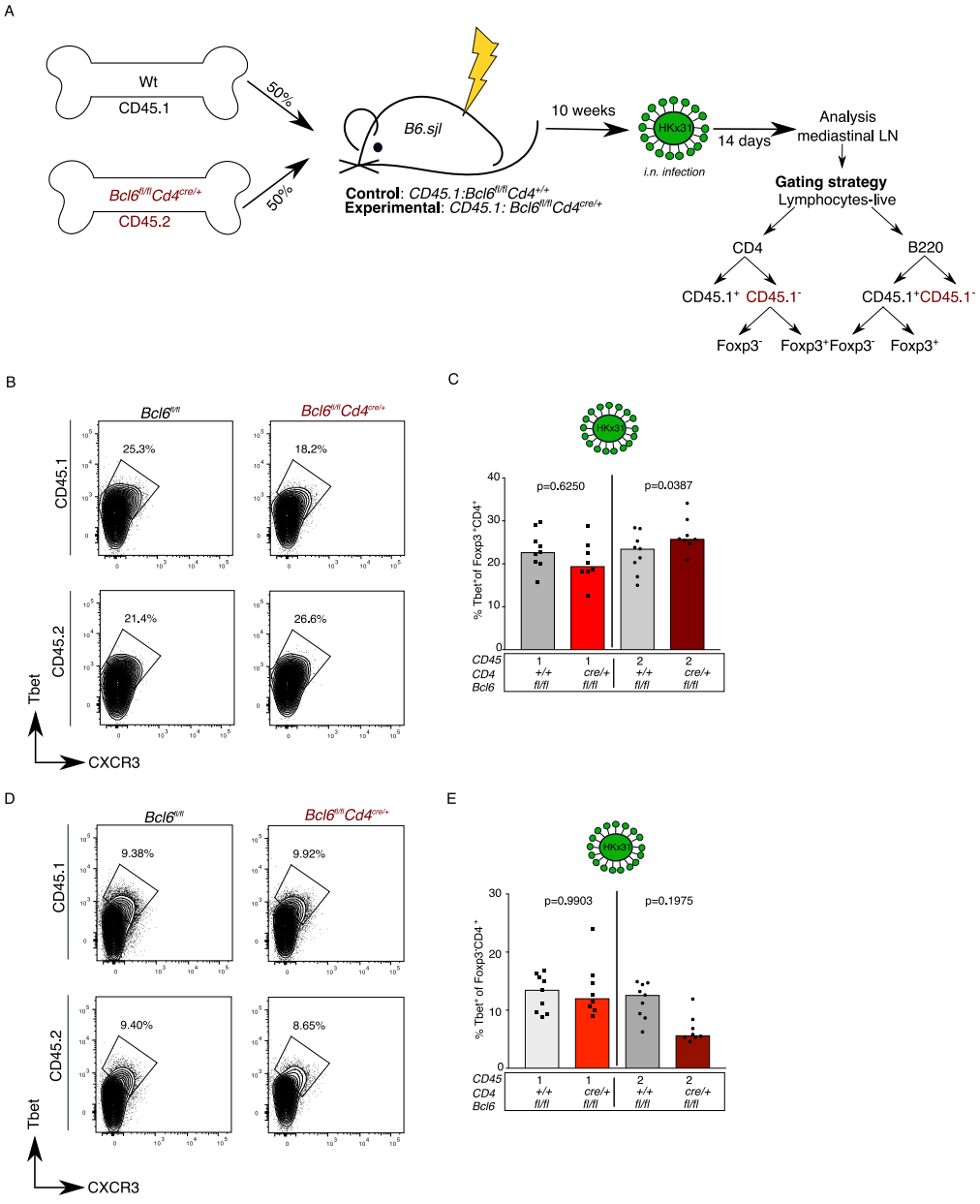

A
Wt
CD45.1
50%
Bcl6fl/flCd4cre/+
CD45.2
50%
B6.sjl
10 weeks
HKx31
i.n. infection
14 days
Analysis
mediastinal LN
Gating strategy
Lymphocytes-live
CD4
B220
CD45.1+ CD45.1-
CD45.1+CD45.1-
Foxp3- Foxp3+Foxp3- Foxp3+
Control: CD45.1:Bcl6fl/flCd4+/+
Experimental: CD45.1: Bcl6fl/flCd4cre/+
B
Bcl6fl/fl
Bcl6fl/flCd4cre/+
CD45.1
CD45.2
25.3%
18.2%
21.4%
26.6%
Tbet
CXCR3
C
HKx31
p=0.6250
p=0.0387
% Tbet+ of Foxp3+CD4+
CD45
CD4
Bcl6
1 +/+ fl/fl
1 cre/+ fl/fl
2 +/+ fl/fl
2 cre/+ fl/fl
D
Bcl6fl/fl
Bcl6fl/flCd4cre/+
CD45.1
CD45.2
9.38%
9.92%
9.40%
8.65%
Tbet
CXCR3
E
HKx31
p=0.9903
p=0.1975
% Tbet+ of Foxp3+CD4+
CD45
CD4
Bcl6
1 +/+ fl/fl
1 cre/+ fl/fl
2 +/+ fl/fl
2 cre/+ fl/fl

Figure 6.2 Cell-intrinsic increase in Tbet expression on Treg cells in *Bcl6$^{fl/fl}$Cd4$^{cre/+}$* mice after influenza infection.

A. Experimental set-up. A 50/50 mix of bone marrow derived from *Bcl6$^{fl/fl}$Cd4$^{cre/+}$* mice (CD45.2) and *B6.sjl* mice (CD45.1) was transferred into irradiated *B6.sjl* recipient mice. Ten weeks after reconstitution, the *B6.sjl* recipient mice were infected with influenza and the mediastinal LN were analysed 14 days after infection by flow cytometry. The gating strategy is depicted. **B.** Flow cytometry contour plots of Tbet$^+$CXCR3$^+$ of Foxp3$^+$CD4$^+$ cells and **C.** Quantification of the frequency of Tbet$^+$ Treg cells derived from either CD45.1$^+$ or CD45.2$^+$ bone marrow in recipients that received bone marrow from either *Bcl6$^{fl/fl}$Cd4$^{+/+}$* or *Bcl6$^{fl/fl}$Cd4$^{cre/+}$* mice. **D.** Flow cytometry contour plots of Tbet$^+$ of Foxp3$^-$CD4$^+$ T cells. **E**. Quantification of the frequency of Tbet$^+$ Tconv cells derived from either CD45.1$^+$ or CD45.2$^+$ bone marrow in recipients that received bone marrow from either *Bcl6$^{fl/fl}$Cd4$^{+/+}$* or *Bcl6$^{fl/fl}$Cd4$^{cre/+}$* mice. Each symbol represents one mouse, and the horizontal bars represent the median values. P values were determined using a one-way ANOVA with a Tukey's multiple comparisons tests. Data represent 2 independent experiments.

To confirm that the cell-intrinsic increase in Th1-like Treg cells in *Bcl6*$^{fl/fl}$*Cd4*$^{cre/+}$ mice was indeed a consequence of skewed Treg cell differentiation in response to infection or immunisation, mixed chimeras were generated that were not challenged with foreign antigen (Figure 6.3A). Interestingly, I observed an increase in the percentage of Tbet^{+} Treg cells derived from *Bcl6*$^{fl/fl}$*Cd4*$^{cre/+}$ bone marrow (CD45.2), compared with *Bcl6*$^{fl/fl}$*Cd4*$^{+/+}$ bone marrow (CD45.2) in the absence of immunisation or infection. There was no difference in the frequency of Tbet^{+} Treg cells derived from CD45.1^{+} bone marrow in the group that received *Bcl6*$^{fl/fl}$*Cd4*$^{cre/+}$ bone marrow (CD45.2) compared with *Bcl6*$^{fl/fl}$*Cd4*$^{+/+}$ bone marrow (CD45.2) (Figure 6.3 B-C). No changes were observed in the percentage of Tbet^{+} Tconv cells (Figure 6.3 D-E).

The cell-intrinsic increase in Tbet^{+} Treg cells in *Bcl6*$^{fl/fl}$*Cd4*$^{cre/+}$ mice in the absence of infection/immunisation suggested that the role of Bcl6 is not limited to driving Tfr cell differentiation, in response to an immune challenge in the periphery, but that it might also play a role in central, thymic Foxp3^{+} Treg cell differentiation.

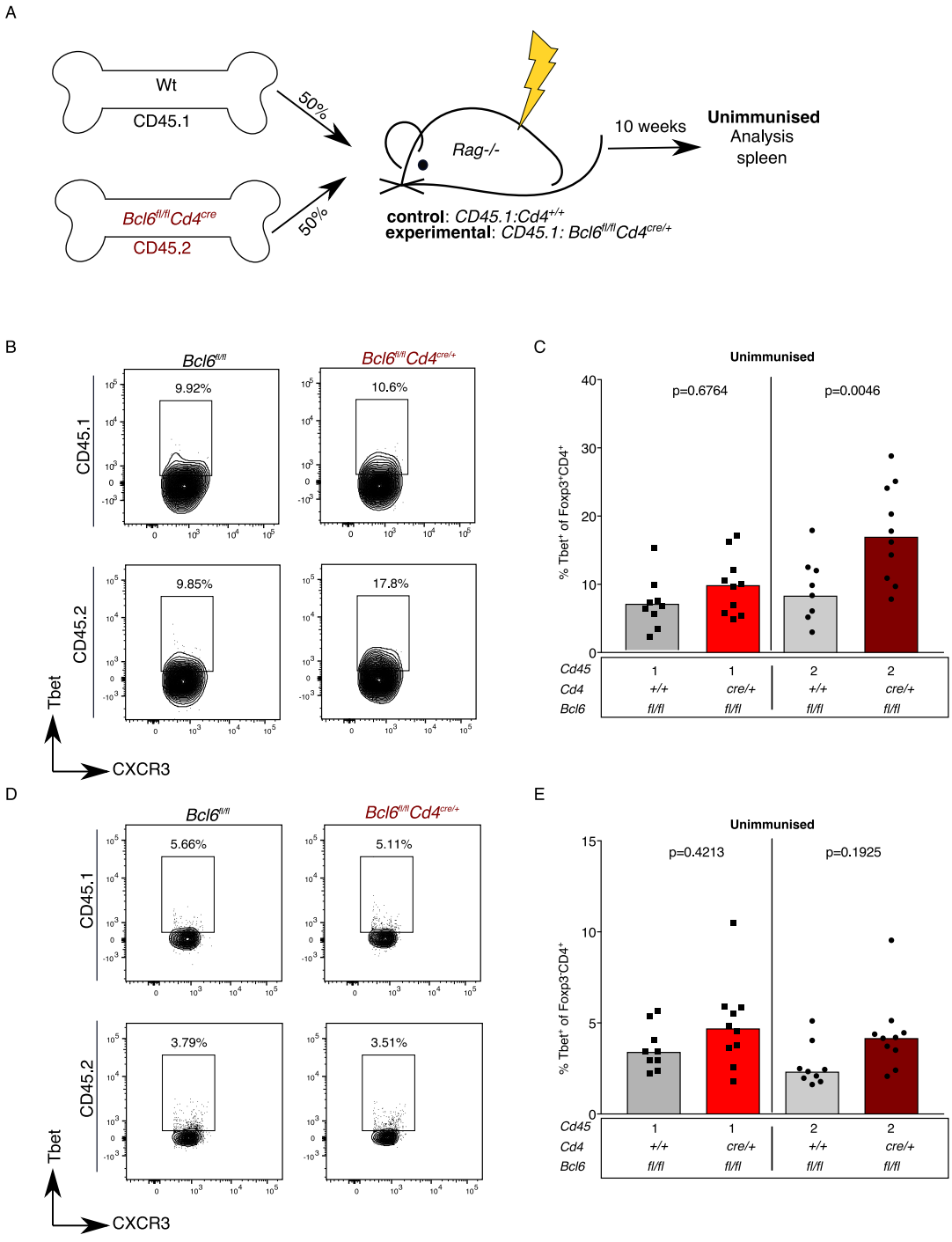

A
Wt
CD45.1
50%
Bcl6fl/flCd4cre
CD45.2
50%
Rag-/-
10 weeks
Unimmunised
Analysis
spleen
control: CD45.1:Cd4+/+
experimental: CD45.1: Bcl6fl/flCd4cre/+
B
Bcl6fl/fl
Bcl6fl/flCd4cre/+
CD45.1
CD45.2
9.92%
10.6%
9.85%
17.8%
Tbet
CXCR3
C
Unimmunised
p=0.6764
p=0.0046
% Tbet+ of Foxp3+CD4+
Cd45
Cd4
Bcl6
1 1 2 2
+/+ cre/+ +/+ cre/+
fl/fl fl/fl fl/fl fl/fl
D
Bcl6fl/fl
Bcl6fl/flCd4cre/+
CD45.1
CD45.2
5.66%
5.11%
3.79%
3.51%
Tbet
CXCR3
E
Unimmunised
p=0.4213
p=0.1925
% Tbet+ of Foxp3-CD4+
Cd45
Cd4
Bcl6
1 1 2 2
+/+ cre/+ +/+ cre/+
fl/fl fl/fl fl/fl fl/fl

Figure 6.3 Cell-intrinsic increase in Tbet expression on Treg cells in *Bcl6$^{fl/fl}$Cd4$^{cre/+}$* mice in the absence of immunisation or infection.

A. Experimental set-up. A 50/50 mix of bone marrow derived from *Bcl6$^{fl/fl}$Cd4$^{cre/+}$* mice (CD45.2) and *B6.sjl* mice (CD45.1) was transferred into irradiated *B6.sjl* recipient mice. Ten weeks after reconstitution, the *B6.sjl* recipient mice were infected with influenza and the mediastinal LN were analysed 14 days after infection by flow cytometry. **B**. Flow cytometry contour plots of Tbet^{+}CXCR3^{+} cells of Foxp3^{+}CD4^{+} Treg cells. **C.** Quantification of the frequency of Tbet^{+}CXCR3^{+} Treg cells derived from either CD45.1^{+} or CD45.2^{+} bone marrow in recipients that received bone marrow from either *Bcl6$^{fl/fl}$Cd4$^{+/+}$* or *Bcl6$^{fl/fl}$Cd4$^{cre/+}$* mice. **D.** Flow cytometry contour plots of Tbet^{+}CXCR3^{+} cells of Foxp3^{-}CD4^{+} Tconv cells. **E.** Quantification of the frequency of Tbet^{+}CXCR3^{+} Tconv cells derived from either CD45.1^{+} or CD45.2^{+} bone marrow in recipients that received bone marrow from either *Bcl6$^{fl/fl}$Cd4$^{+/+}$* or *Bcl6$^{fl/fl}$Cd4$^{cre/+}$* mice. Each symbol represents one mouse, and the horizontal bars represent the median values. P values were determined using a one-way ANOVA with a Tukey's multiple comparisons tests. Data represent 2 independent experiments.

6.2.2 Thymic Treg cells are highly activated in *Bcl6$^{fl/fl}$Cd4$^{cre/+}$* mice

Bcl6$^{fl/fl}$Cd4$^{cre/+}$ mice are expected to delete Bcl6 in all CD4^{+} and CD8^{+} T cells, not just in Treg cells, based on the genetic strategy used (*i.e.* deletion from the DP stage onwards). It is possible that Bcl6 is generally expressed at high levels in naïve Treg cells or their precursors, where it represses premature differentiation. CD4 and Foxp3 are both first expressed in T cells in the thymus, at the DP and SP stage, respectively. I first sought a better understanding of (1) when during T development and, (2) in which cell type(s) Bcl6 is expressed. For this purpose, RNA seq data from Kitagawa *et al*. and Immgen (Immgen.org) were combined, and the relative gene expression levels of *Bcl6* and *Foxp3* were determined at different stages during thymocyte development (Figure 6.4 A) (Kitagawa et al., 2017). Bcl6 is highly expressed at the DP stage and its expression rapidly declines when T cells transition to the CD4 SP stage. tTreg precursors show higher Bcl6 expression compared with CD4 SP cells. As expected, Foxp3 expression is up-regulated between the tTreg precursor stage and tTreg stage, and remains relatively high in peripheral Treg cells.

Analysis of Bcl6 protein by flow cytometry confirmed the RNA-seq data and showed that Bcl6 is expressed at the highest level in DP cells, with a decline in Bcl6 expression in both Foxp3^{-} and Foxp3^{+} CD4 SP cells (Figure 6.4 B), consistent with published data (Mathew et al., 2014). Thus, DP thymocytes express high levels of Bcl6, and Bcl6 expression readily decreases when the cell develops into a mature Treg cell or Tconv cells.

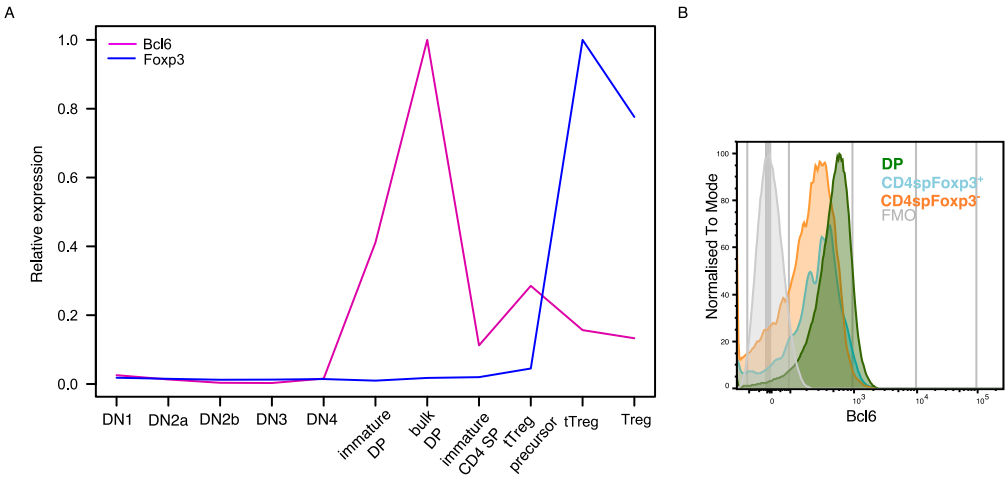


Figure 6.4 Bcl6 expression in thymocytes.

A. Relative gene expression of *Bcl6* and *Foxp3* in distinct thymocyte subsets from combined RNA seq data from Immgen and Kitagawa *et al (Kitagawa et al., 2017)*. DN1 (lin$^-$CD44^{hi}CD117^{hi}CD25$^-$), DN2a (lin$^-$CD44^{hi}CD117^{hi}CD25^{hi}), DN2b (lin$^-$CD44^{hi}CD117^{int}CD25^{hi}), DN3 (lin$^-$CD44$^-$CD25^{hi}), DN4(lin$^-$CD44$^-$CD25$^-$), immature DP (CD69^{lo},TCRβ^{lo},CD4$^+$CD8$^+$), bulk DP (CD4$^+$CD8$^+$), tTreg precursors (CD24$^+$CD25$^+$GITR$^+$CD4SP), tTreg (Foxp3$^+$CD4SP), Treg (peripheral CD25$^+$Foxp3$^+$CD4$^+$ Treg cells. This analysis was performed by Dr. Christel Krueger (Babraham Institute). **B.** Representative flow cytometry histogram of Bcl6 expression in DP thymocytes, Foxp3$^-$CD4 SP, and Foxp3$^+$ CD4 SP thymocytes.

I set out to test whether deletion of Bcl6 at the DP stage resulted in an altered development of downstream CD4 T cell subsets in unimmunised *Bcl6*$^{fl/fl}$*Cd4*$^{cre/+}$ mice compared with *Bcl6*$^{fl/fl}$ *Cd4*$^{+/+}$, *Cd4*$^{cre/+}$, and *Wt* (C57Bl/6) control mice. There was no difference in the proportion or absolute number of DP thymocytes (data not shown). The percentage of total CD4^{+} T cells and absolute number in the thymus was reduced in *Bcl6*$^{fl/fl}$*Cd4*$^{cre/+}$ mice compared with *Cd4*$^{cre/+}$ controls, but not with *Bcl6*$^{fl/fl}$ *Cd4*$^{+/+}$ controls (Figure 6.5 A-B). This effect was not observed in another study characterising *Bcl6*$^{fl/fl}$*Cd4*$^{cre/+}$ mice (Hollister et al., 2013), and may be an anomaly due to the low number of mice analysed. There was no difference in the percentage of Foxp3^{-} or Foxp3^{+} CD4^{+} T cells within the CD4 SP compartment, but the absolute number of these populations was reduced in *Bcl6*$^{fl/fl}$*Cd4*$^{cre/+}$ mice compared with *Cd4*$^{cre/+}$ and *Bcl6*$^{fl/fl}$*Cd4*$^{wt/wt}$ controls (Figure 6.5 C-E). There was a significant decrease in the percentage of CD62L^{+}CD44^{-} Treg cells in *Bcl6*$^{fl/fl}$*Cd4*$^{cre/+}$ mice compared with *Cd4*^{cre} mice, with a concomitant increase in the percentage of CD44^{+} CD62L^{-} Treg cells, although this increase was not statistically significant (Figure 6.5 F-G). Absolute numbers followed the same trend (data not shown). The failure to detect significant changes was probably due to the very small sample size of the controls (n=2, n=3), which directly affects the statistical power. Therefore, the probability of the Kruskall-Wallis test with a Dunn's multiple comparisons test picking up on a biological effect is low. Similar trends could be observed in the Tconv cell population with regards to the percentage and absolute number of CD44^{+} CD62L^{-} cells and CD44^{-} CD62L^{+} (Figure 6.5 H-I, and data not shown). However, these changes in CD44 expression and CD62L expression observed in Tconv cells were not significant. It is important to note that I did not observe differences between *Bcl6*$^{fl/fl}$ *Cd4*$^{+/+}$ and *Cd4*$^{cre/+}$ controls. In the rest of this chapter, we will be using *Bcl6*$^{fl/fl}$ *Cd4*$^{+/+}$ controls to compare with *Bcl6*$^{fl/fl}$*Cd4*$^{cre/+}$ mice, as these are littermate controls. Together, these data suggest that deletion of Bcl6 at the DP stage specifically affects Treg cell activation, with minimal effects on the Tconv cell population.

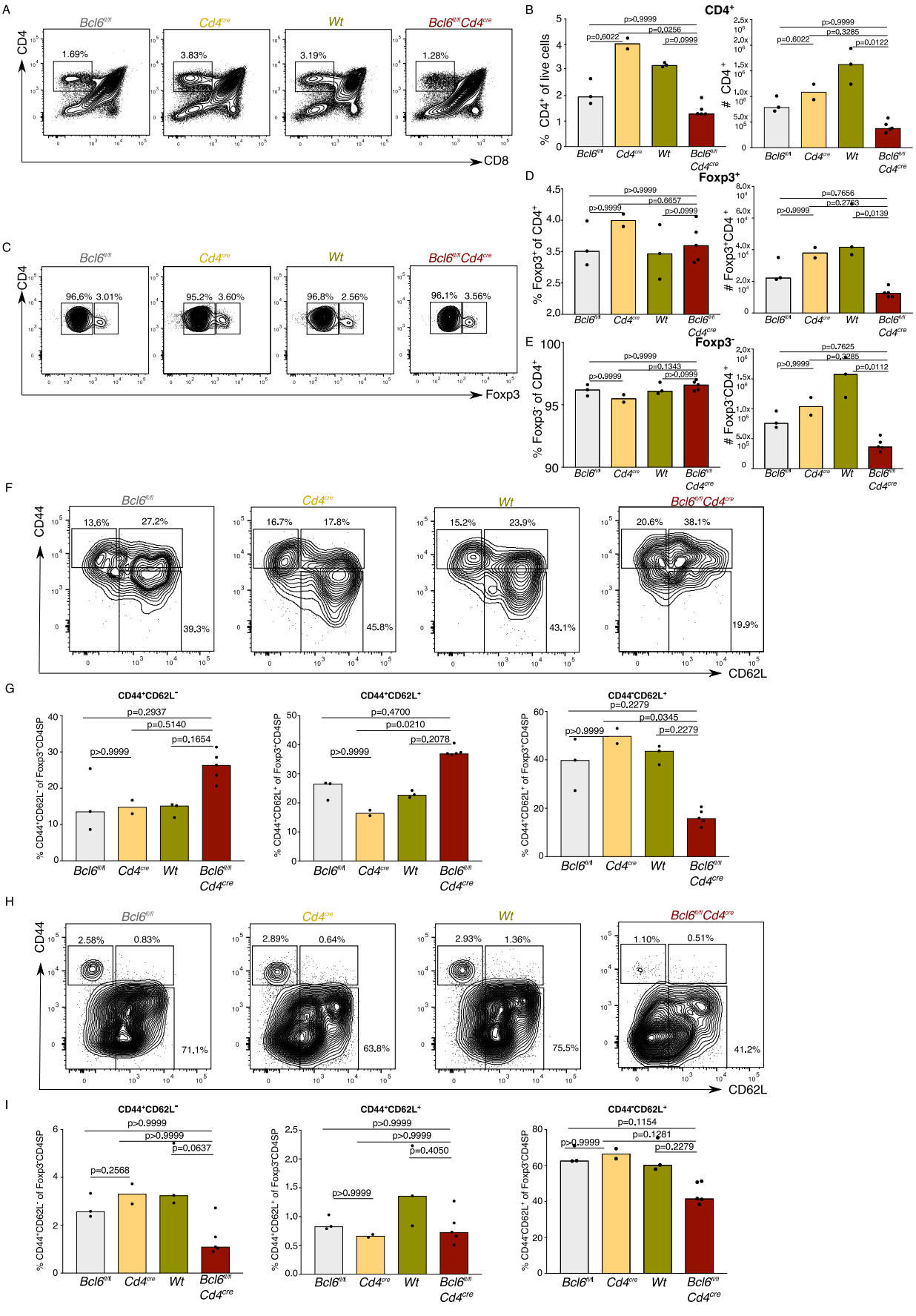

A
Bcl6fl/fl
Cd4cre
Wt
Bcl6fl/flCd4cre
CD4
CD8
1.69%
3.83%
3.19%
1.28%
B
CD4+
% CD4+ of live cells
# CD4+
p>0.9999
p=0.6022
p=0.0256
p=0.0999
p=0.3285
p=0.0122
C
Foxp3
96.6% 3.01%
95.2% 3.60%
96.8% 2.56%
96.1% 3.56%
D
Foxp3+
% Foxp3+ of CD4+
# Foxp3+CD4+
p=0.6657
p=0.7656
p=0.2763
p=0.0139
E
Foxp3-
% Foxp3- of CD4+
# Foxp3-CD4+
p=0.1343
p=0.7625
p=0.0112
F
CD44
CD62L
13.6% 27.2% 39.3%
16.7% 17.8% 45.8%
15.2% 23.9% 43.1%
20.6% 38.1% 19.9%
G
CD44+CD62L-
CD44+CD62L+
CD44-CD62L+
% CD44+CD62L- of Foxp3+CD4SP
% CD44+CD62L+ of Foxp3+CD4SP
% CD44-CD62L+ of Foxp3+CD4SP
p=0.2937
p=0.5140
p=0.1654
p=0.4700
p=0.0210
p=0.2078
p=0.2279
p=0.0345
H
2.58% 0.83% 71.1%
2.89% 0.64% 63.8%
2.93% 1.36% 75.5%
1.10% 0.51% 41.2%
I
p=0.2568
p=0.0637
p=0.4050
p=0.1154
p=0.1281
Bcl6fl/fl
Cd4cre
Wt
Bcl6fl/fl Cd4cre

Figure 6.5 Thymic T cell phenotype in *Bcl6$^{fl/fl}$Cd4$^{cre/+}$* mice.

A. Representative flow cytometry contour plots of CD4 SP thymocytes in *Bcl6$^{fl/fl}$Cd4$^{+/+}$*, *CD4$^{cre/+}$*, *Wt* and *Bcl6$^{fl/fl}$Cd4$^{cre/+}$* mice. **B.** Quantification of the frequency and absolute number of CD4^{+}CD8^{-} thymocytes. **C.** Representative flow cytometry contour plots of Foxp3^{+} and Foxp3^{-} CD4^{+} T cells in *Bcl6$^{fl/fl}$Cd4$^{+/+}$*, *CD4$^{cre/+}$*, *Wt* and *Bcl6$^{fl/fl}$Cd4$^{cre/+}$* mice. **D.** Quantification of the frequency and absolute number of Foxp3^{+}CD4^{+} thymocytes. **E.** Quantification of the frequency and absolute number of Foxp3^{-}CD4^{+} thymocytes. **F.** Representative flow cytometry contour plots of CD44^{+}CD62L^{-}, CD44^{+}CD6L^{+}, and CD44^{-}CD62L^{+} Treg cells gated from Foxp3^{+}CD4SP thymocytes in *Bcl6$^{fl/fl}$Cd4$^{+/+}$*, *CD4$^{cre/+}$*, *Wt* and *Bcl6$^{fl/fl}$Cd4$^{cre/+}$* mice. **G.** Quantification of the frequency of CD44^{+}CD62L^{-}, CD44^{+}CD6L^{+}, and CD44^{-}CD62L^{+} Treg cells. **H.** Representative flow cytometry contour plots of CD44^{+}CD62L^{-}, CD44^{+}CD6L^{+}, and CD44^{-}CD62L^{+} Treg cells gated from Foxp3^{-}CD4 SP thymocytes in *Bcl6$^{fl/fl}$Cd4$^{+/+}$*, *CD4$^{cre/+}$*, *Wt* and *Bcl6$^{fl/fl}$Cd4$^{cre/+}$* mice. **I.** Quantification of the frequency of CD44^{+}CD62L^{-}, CD44^{+}CD6L^{+}, and CD44^{-}CD62L^{+} Tconv CD4 SP cells. Each symbol represents one mouse, and the horizontal bars represent the median values. P values were determined using a Kruskall-Wallis test with a Dunn's multiple comparisons tests. Data represent 3 independent experiments.

6.2.3 Does Bcl6 control the development or functional differentiation of Treg/Tconv cells?

To determine whether deletion of Bcl6 in mature, naïve Treg cells recapitulates the *Bcl6*$^{fl/fl}$*Cd4*$^{cre/+}$ phenotype, *Bcl6*$^{fl/fl}$*Foxp3*$^{cre\text{-}ERT2}$ mice received a tamoxifen-containing diet for 30 days, after which the thymus was analysed (Figure 6.6A). There was no significant difference in the proportion of CD44^{+}, CD62L^{+}, or CD44^{+}CD62L^{+} Treg cells or Tconv cells in *Bcl6*$^{fl/fl}$*Foxp3*$^{cre\text{-}ERT2}$ mice (Figure 6.6B-E). There was no difference in the absolute number of CD44^{+}, CD62L^{+}, or CD44^{+}CD62L^{+} Treg cells or Tconv cells in *Bcl6*$^{fl/fl}$*Foxp3*$^{cre\text{-}ERT2}$ mice (data not shown). These data indicate that deletion of Bcl6 in mature, naïve Treg cells does not result in the Treg activation phenotype, based on CD44 and CD62L expression, observed in *Bcl6*$^{fl/fl}$*Cd4*$^{cre/+}$ mice. This suggests that Bcl6 acts during Treg cell development, prior to Foxp3 expression, *i.e.* at the DP or CD4 SP stage, rather than during functional Treg cell differentiation in the periphery.

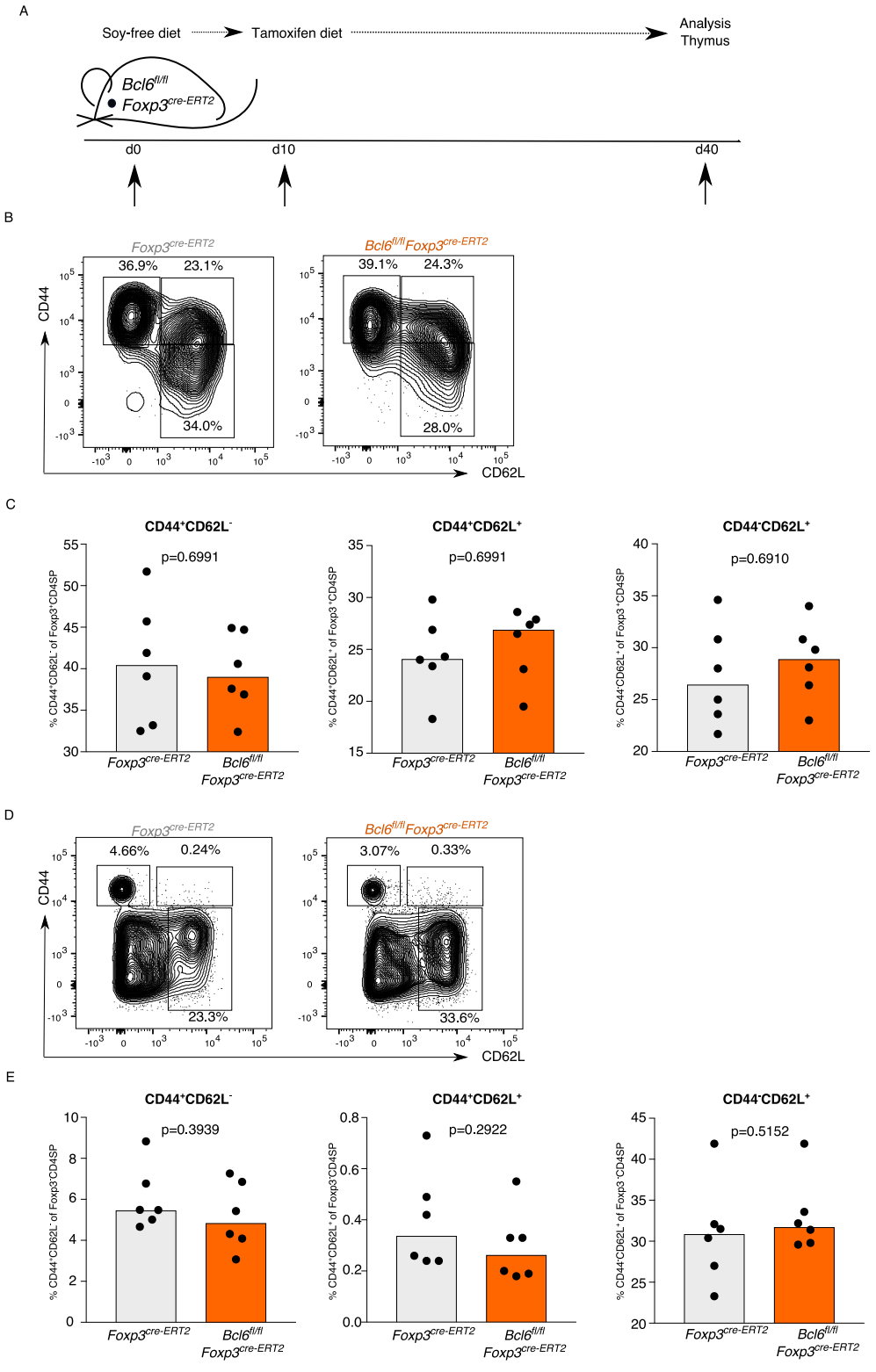

A
Soy-free diet
Tamoxifen diet
Analysis
Thymus
Bcl6fl/fl
Foxp3cre-ERT2
d0
d10
d40
B
Foxp3cre-ERT2
Bcl6fl/flFoxp3cre-ERT2
36.9%
23.1%
34.0%
39.1%
24.3%
28.0%
CD44
CD62L
C
CD44+CD62L-
CD44+CD62L+
CD44-CD62L+
p=0.6991
p=0.6991
p=0.6910
% CD44+CD62L- of Foxp3+CD4SP
% CD44+CD62L+ of Foxp3+CD4SP
% CD44-CD62L+ of Foxp3+CD4SP
Foxp3cre-ERT2
Bcl6fl/fl Foxp3cre-ERT2
D
4.66%
0.24%
23.3%
3.07%
0.33%
33.6%
E
p=0.3939
p=0.2922
p=0.5152

Figure 6.6 *Bcl6*$^{fl/fl}$*Foxp3*$^{cre\text{-}ERT2}$ mice do not show a Treg cell activation phenotype.

A. Diagram shows experimental set-up. Mice received a soy-free diet for 10 days. After 10 days, the mice received a diet containing tamoxifen for the remaining time of the study. After 30 days on the tamoxifen diet, the thymus was analysed. **B.** Representative flow cytometry contour plots of $CD44^+CD62L^-$, $CD44^+CD6L^+$, and $CD44^-CD62L^+$ Treg cells gated from $Foxp3^+CD4$ SP thymocytes. **C.** Quantification of the frequency of $CD44^+CD62L^-$, $CD44^+CD6L^+$, and $CD44^-CD62L^+$ Treg cells. **D.** Representative flow cytometry contour plots of $CD44^+CD62L^-$, $CD44^+CD6L^+$, and $CD44^-CD62L^+$ Treg cells gated from $Foxp3^-CD4$ SP thymocytes. **E.** Quantification of the frequency of $CD44^+CD62L^-$, $CD44^+CD6L^+$, and $CD44^-CD62L^+$ Tconv cells. Each symbol represents one mouse, and the horizontal bars represent the median values. P values were determined using Mann-Whitney U test. Data represent 2 independent experiments.

To confirm that the Treg cell activation phenotype observed in *Bcl6*$^{fl/fl}$*Cd4*$^{cre/+}$ mice is a result of Bcl6 acting early in thymic T cell development, the thymus and spleen obtained from 4-day old animals were analysed (Figure 6.7 A). Day 4 was chosen intentionally as mature, naïve Treg cells start to egress from the thymus from day 3 after birth, and thymectomy before day 3 results in the development of autoimmunity due to the absence of tTreg in the periphery (Asano et al., 1996). At day 4, both splenic and thymic Treg cells can be studied and at day 4 the proportion of mature Treg cells homing back to the thymus would be very low, thus ensuring we are measuring the effect on developing, rather than recirculating, CD4$^+$ T cells.

An almost two-fold increase in the proportion of CD44$^+$ Treg cells could be observed in *Bcl6*$^{fl/fl}$*Cd4*$^{cre/+}$ mice at day 4 in the thymus (Figure 6.7 B-C), concomitant with a significant reduction in the proportion and absolute number of CD62L$^+$ Treg cells (Figure 6.7 B, E). There was no difference in the proportion of CD44$^+$CD62L$^+$ Treg cells (Figure 6.7 D). Although, there were very few CD44$^+$ and CD44$^+$CD62L$^+$ Tconv cells overall, there was a significant increase in the proportion of CD44$^+$, CD44$^+$CD62L$^+$ and CD62L$^+$ Tconv cells (Figure 6.7 F-I). However, it must be noted that the Tconv population in the thymus encompasses both Foxp3$^-$CD4$^+$ T cells, as well as pre-tTreg cells (Foxp3$^-$GITR$^+$CD25$^+$), so it is possible that the increase in CD44$^+$ Tconv cells reflects premature activation of pre-tTreg cells.

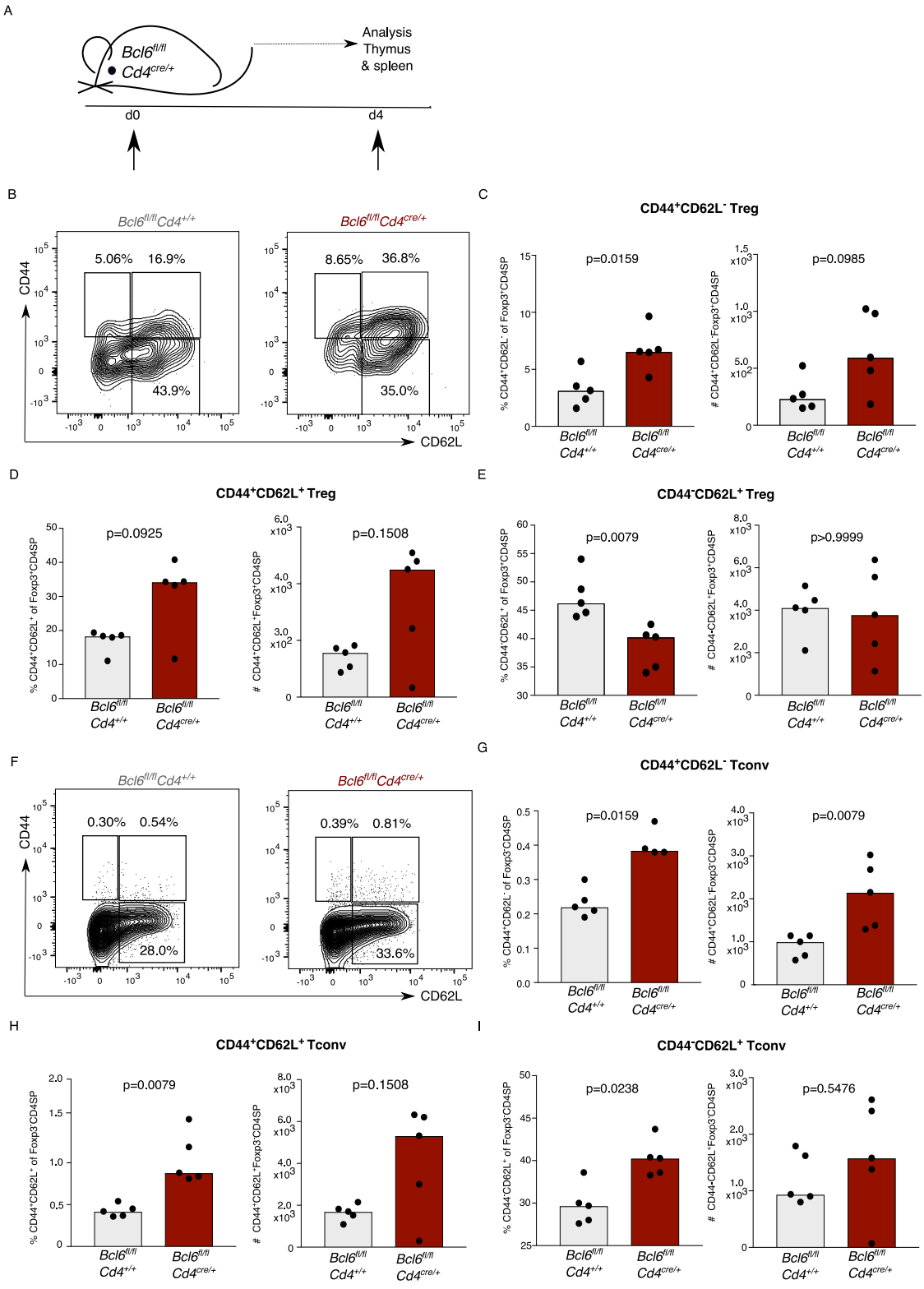

A
Bcl6fl/fl
Cd4cre/+
Analysis
Thymus
& spleen
d0
d4
B
Bcl6fl/flCd4+/+
Bcl6fl/flCd4cre/+
CD44
CD62L
5.06%
16.9%
43.9%
8.65%
36.8%
35.0%
C
CD44+CD62L- Treg
p=0.0159
p=0.0985
% CD44+CD62L- of Foxp3+CD4SP
# CD44+CD62L-Foxp3+CD4SP
D
CD44+CD62L+ Treg
p=0.0925
p=0.1508
% CD44+CD62L+ of Foxp3+CD4SP
# CD44+CD62L+Foxp3+CD4SP
E
CD44-CD62L+ Treg
p=0.0079
p>0.9999
% CD44-CD62L+ of Foxp3+CD4SP
# CD44-CD62L+Foxp3+CD4SP
F
0.30%
0.54%
28.0%
0.39%
0.81%
33.6%
G
CD44+CD62L- Tconv
p=0.0159
p=0.0079
% CD44+CD62L- of Foxp3-CD4SP
# CD44+CD62L-Foxp3-CD4SP
H
CD44+CD62L+ Tconv
p=0.0079
p=0.1508
% CD44+CD62L+ of Foxp3-CD4SP
# CD44+CD62L+Foxp3-CD4SP
I
CD44-CD62L+ Tconv
p=0.0238
p=0.5476
% CD44-CD62L+ of Foxp3-CD4SP
# CD44-CD62L+Foxp3-CD4SP

Figure 6.7 *Bcl6*$^{fl/fl}$*Cd4*$^{cre/+}$ mice show a Tconv/Treg activation phenotype early during development in the thymus.

A. Experimental set-up; the thymus and spleen of *Bcl6*$^{fl/fl}$*Cd4*$^{cre/+}$ mice and littermate controls were used in this study. **B.** Representative flow cytometry contour plots of CD44^{+}CD62L^{-}, CD44^{+}CD6L^{+}, and CD44^{-}CD62L^{+} Treg cells gated from Foxp3^{+}CD4SP thymocytes. **C.** Quantification of the frequency and absolute number of CD44^{+}CD62L^{-} Treg cells. **D.** Quantification of the frequency and absolute number of CD44^{+}CD6L^{+} Treg cells. **E.** Quantification of the frequency and absolute number of CD44^{-}CD6L^{+} Treg cells. **F.** Representative flow cytometry contour plots of CD44^{+}CD62L^{-}, CD44^{+}CD6L^{+}, and CD44^{-}CD62L^{+} Treg cells gated from Foxp3^{-}CD4SP thymocytes. **G.** Quantification of the frequency and absolute number of CD44^{+}CD62L^{-} Tconv cells. **H.** Quantification of the frequency and absolute number of CD44^{+}CD6L^{+} Tconv cells. **I.** Quantification of the frequency and absolute number of CD44^{-}CD6L^{+} Tconv cells. Each symbol represents one mouse, and the horizontal bars represent the median values. P values were determined using a Mann-Whitney U test. Data represent 2 independent experiments.

To determine whether this thymic T cell phenotype extends to the periphery, I analysed Treg and Tconv cell activation in the spleen (Figure 6.8). As early as day 4, there was a significant increase in the proportion and absolute number of $CD44^+$ Treg cells, and $CD44^+CD62L^+$ Treg cells (Figure 6.8 A-C). In addition, there was a significant decrease in the proportion of $CD62L^+$ Treg cells (Figure 6.8 D). Interestingly, there were no changes in the expression of activation markers in Tconv cells (Figure 6.8 E-H), suggesting that the increase in activated Tconv cells we observe in the thymus (Figure 6.7 F-I), is perhaps due to pre-tTreg cells being activated prematurely. Together, these data suggest that Bcl6 acts in developing Treg cells to limit premature Treg activation, and that $Bcl6^{fl/fl}Cd4^{cre/+}$ mice show an early thymic Treg activation defect that extends into the periphery.

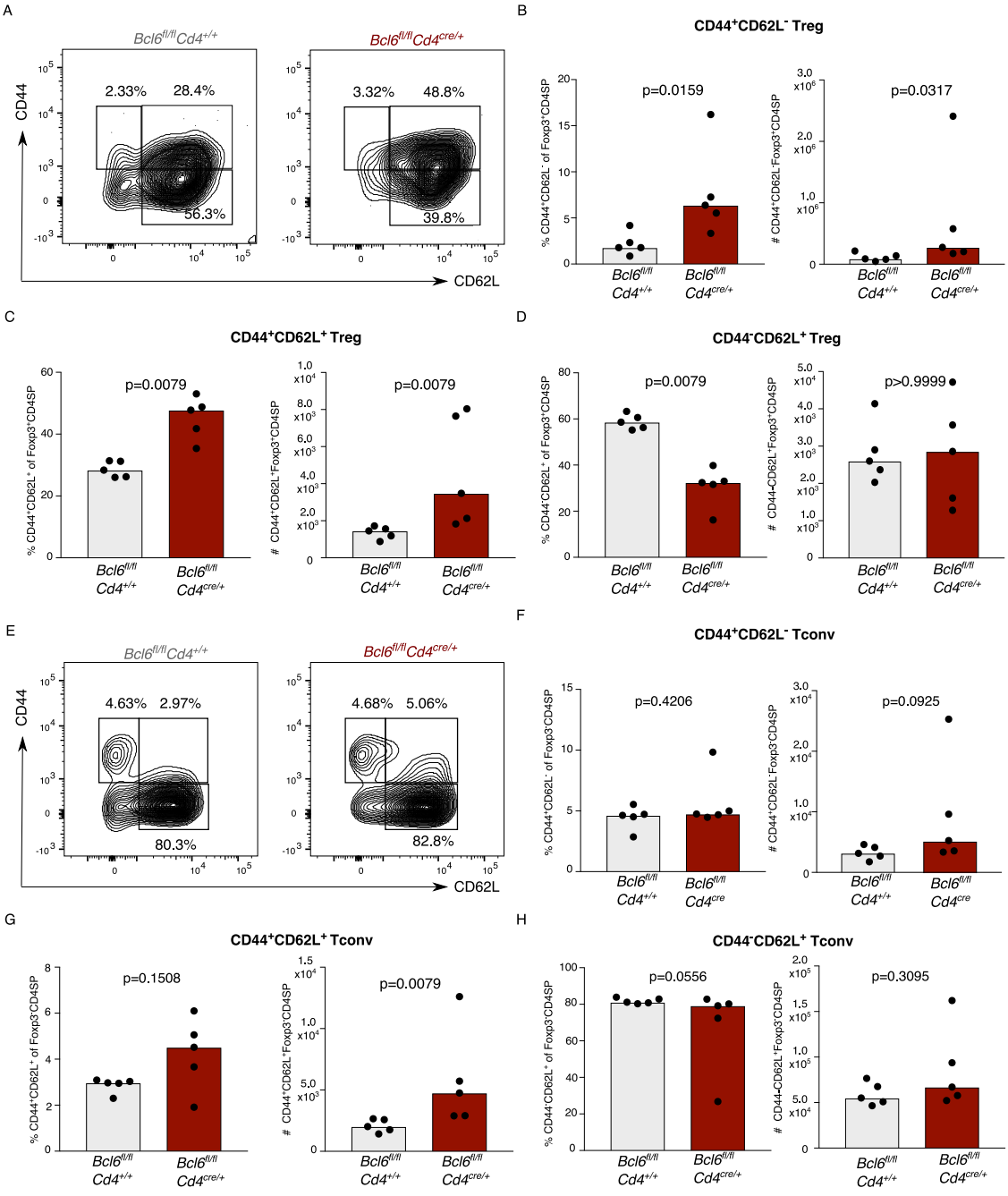

A
Bcl6fl/flCd4+/+
Bcl6fl/flCd4cre/+
CD44
CD62L
2.33%
28.4%
56.3%
3.32%
48.8%
39.8%
B
CD44+CD62L- Treg
p=0.0159
p=0.0317
% CD44+CD62L- of Foxp3+CD4SP
# CD44+CD62L-Foxp3+CD4SP
C
CD44+CD62L+ Treg
p=0.0079
p=0.0079
% CD44+CD62L+ of Foxp3+CD4SP
# CD44+CD62L+Foxp3+CD4SP
D
CD44-CD62L+ Treg
p=0.0079
p>0.9999
% CD44-CD62L+ of Foxp3+CD4SP
# CD44-CD62L+Foxp3+CD4SP
E
4.63%
2.97%
80.3%
4.68%
5.06%
82.8%
F
CD44+CD62L- Tconv
p=0.4206
p=0.0925
% CD44+CD62L- of Foxp3+CD4SP
# CD44+CD62L-Foxp3+CD4SP
Bcl6fl/fl Cd4cre
G
CD44+CD62L+ Tconv
p=0.1508
p=0.0079
% CD44+CD62L+ of Foxp3+CD4SP
# CD44+CD62L+Foxp3+CD4SP
H
CD44-CD62L+ Tconv
p=0.0556
p=0.3095
% CD44-CD62L+ of Foxp3+CD4SP
# CD44-CD62L+Foxp3+CD4SP

Figure 6.8 *Bcl6*$^{fl/fl}$*Cd4*$^{cre/+}$ mice show a Treg activation phenotype early during development in the spleen.

A. Representative flow cytometry contour plots of $CD44^+CD62L^-$, $CD44^+CD6L^+$, and $CD44^-CD62L^+$ Treg cells gated from $Foxp3^+CD4$ SP thymocytes. **B.** Quantification of the frequency and absolute number of $CD44^+CD62L^-$ Treg cells. **C.** Quantification of the frequency and absolute number of $CD44^+CD6L^+$ Treg cells. **D.** Quantification of the frequency and absolute number of $CD44^-CD6L^+$ Treg cells. **E.** Representative flow cytometry contour plots of $CD44^+CD62L^-$, $CD44^+CD6L^+$, and $CD44^-CD62L^+$ Treg cells gated from $Foxp3^-CD4$ SP thymocytes. **F.** Quantification of the frequency and absolute number of $CD44^+CD62L^-$ Tconv cells. **G.** Quantification of the frequency and absolute number of $CD44^+CD6L^+$ Tconv cells. **H.** Quantification of the frequency and absolute number of $CD44^-CD6L^+$ Tconv cells. Each symbol represents one mouse, and the horizontal bars represent the median values. P values were determined using a Mann-Whitney U test. Data represent 2 independent experiments.

6.2.4 In-depth phenotyping of *Bcl6$^{fl/fl}$Cd4$^{cre/+}$* mice by high-parameter flow cytometry

To better understand the early and broad Treg cell activation phenotype observed at day 4, in-depth phenotyping of 6-week-old *Bcl6$^{fl/fl}$Cd4$^{cre/+}$* mice was performed by high-parameter flow cytometry. In the first instance, the results obtained by flow cytometry were analysed by manual gating using Flowjo. Thymic Treg cells in *Bcl6$^{fl/fl}$Cd4$^{cre/+}$* mice showed increased expression of GATA3, ST2, Tbet, KLRG-1, CD103, ICOS, Eomes and Rorγt, and there was a reduction in the proportion of CD69^{+} Treg cells (Figure 6.9 A). *Bcl6$^{fl/fl}$Cd4$^{cre/+}$* mice show an increased proportion GATA3, Eomes and Rorγt expressing thymic T conv cells (Foxp3^{-} CD4^{+}), and a decreased proportion of Tbet and CD103 expressing Tconv cells (Figure 6.9 B). However, the expression of other markers in Tconv cells did not seem to be affected to the same extent as in Treg cells. Splenic Treg cells resembled thymic Treg cells in *Bcl6$^{fl/fl}$Cd4$^{cre/+}$* mice to a large extent, expressing significantly higher levels of GATA3, ST2, Tbet, KLRG-1 and ICOS, while the percentage of Eomes^{+} Treg cells was reduced (Figure 6.9 C). Splenic Tconv cells expressed comparable levels of the transcriptional regulators GATA3, Tbet, and Rorγt, but showed increased expression of ST2 and KLRG-1 compared to littermate controls. Furthermore, the percentage of ICOS^{+}, CD69^{+} and Eomes^{+} Tconv cells was significantly reduced in *Bcl6$^{fl/fl}$Cd4$^{cre/+}$* mice (Figure 6.9D). Both Treg cells and Tconv cells produce significantly more IL-10 in *Bcl6$^{fl/fl}$Cd4$^{cre/+}$* mice compared with controls (Figure 6.9 E). Treg cells in *Bcl6$^{fl/fl}$Cd4^{cre}* mice produce high levels of IFN-γ (Figure 6.9 G), a cytokine not typically expressed by Treg cells. Finally, Tconv cells produce significantly higher levels of IL-2, perhaps thereby sustaining the highly activated Treg cells (Figure 6.9 H). The high expression of GATA3, St2, KLRG-1, CD103 and IL-10 suggests that a subset of Treg cells might adopt a phenotype reminiscent of tissue Treg cells. Together, with the increase in Tbet and Rorγt, the transcriptional regulators associated with Th1 and Th17 differentiation these data indicate that Bcl6 may limit premature activation and differentiation of Treg cells in the thymus.

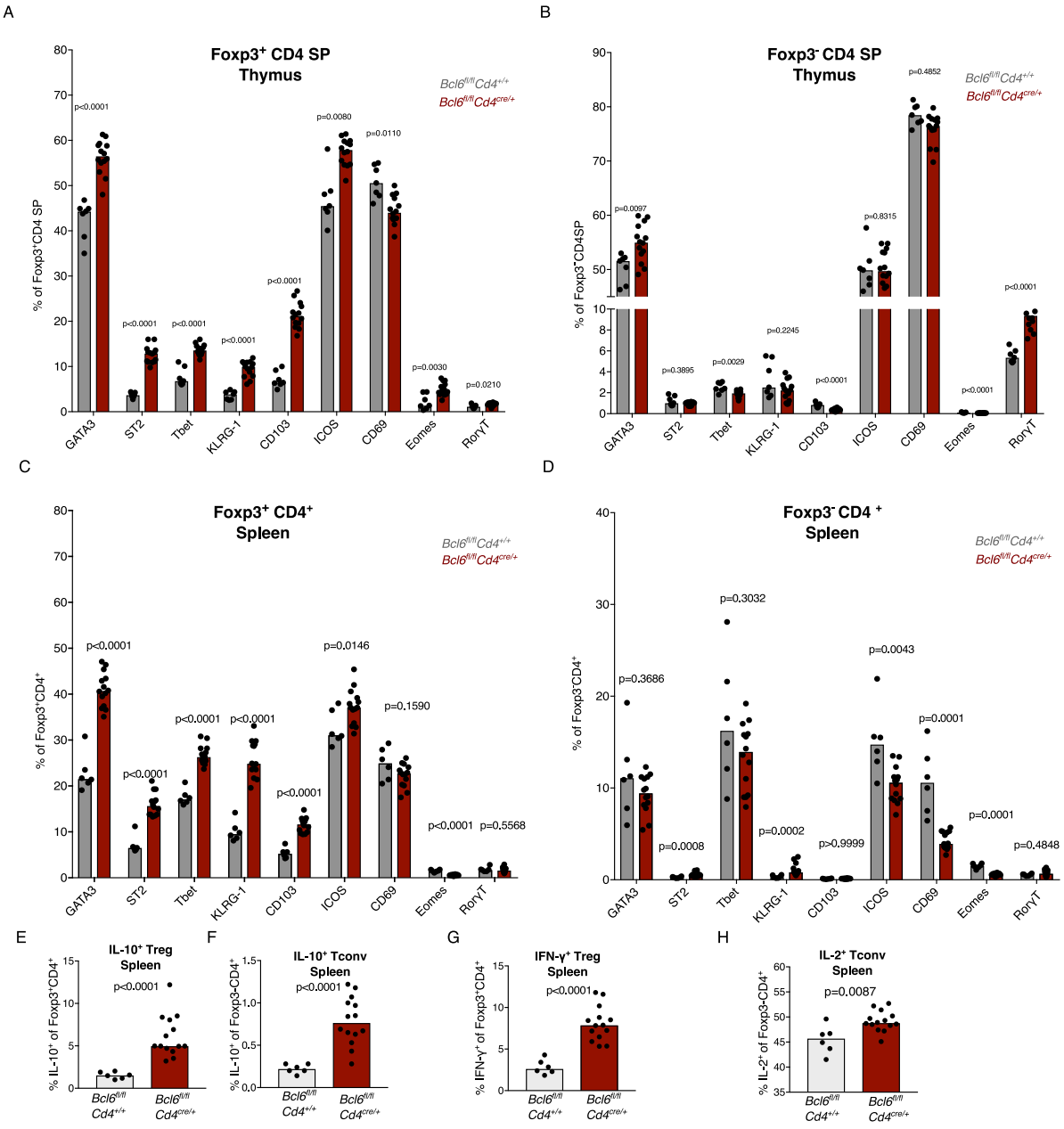


Figure 6.9 In-depth phenotyping of *Bcl6$^{fl/fl}$Cd4$^{cre/+}$* mice by high-parameter flow cytometry.

A. Quantification of the proportion of indicated markers of CD4$^+$Foxp3$^+$ Treg cells in the thymus. **B.** Quantification of the proportion of indicated markers of CD4$^+$Foxp3$^-$ Tconv cells in the thymus. **C.** Quantification of the proportion of indicated markers of CD4$^+$Foxp3$^+$ Treg cells in the spleen. **D.** Quantification of the proportion of indicated markers of CD4$^+$Foxp3$^-$ Tconv cells in the spleen. **E.** Quantification of the proportion of splenic Foxp3$^+$CD4$^+$ T cells expressing IL-10. **F.** Quantification of the proportion of splenic Foxp3$^-$CD4$^+$ T cells producing IL-10. **G.** Quantification of the proportion of splenic Foxp3$^+$CD4$^+$ T cells producing IFN-γ. **H.** Quantification of the proportion of splenic Foxp3$^-$ CD4$^+$ T cells producing IL-2. **I.** Each symbol represents one mouse, and the horizontal bars represent

the median values. P values were determined using a Mann-Whitney U test. Data are from one experiment.

Due to the relatively high number of markers used in this experiment, comparisons of single markers such as depicted in Figure 6.9 might miss out on broader, multivariate relationships, thus making data interpretation difficult. Therefore, the tSNE algorithm was applied to these flow cytometry data. tSNE reduces an n-dimensional data space into two dimensions whilst maintaining the structure of the data and calculates two new parameters from a defined list of cytometry parameters. These parameters are optimised so that data points that are closely together in the high-dimensional data remain close together in the reduced data space and 'cluster' together. The proximity of cells in the tSNE map reflects their distances in the high-dimensional space (Amir el et al., 2013). In other words, cells that are similar in their analysed protein-expression pattern will be located closely together in the tSNE map, thus enabling the visualisation of different cellular subpopulations.

The $Foxp3^+$ population represents a very small part of the total thymocyte pool (Figure 6.10 A). Consequently, to define sub-populations within the Treg cell pool, tSNE was performed on pre-gated $Foxp3^+CD4^+$ Treg cells in the thymus and the spleen (Figure 6.10 B-C, Figure 6.11). The markers used for identifying clusters of cells are CD44, CD62L, CD25, ST2, CD103, KLRG-1 and Nrp-1 (Figure 6.10 B). The markers not used for clustering but included in the analyses are depicted in Figure 6.10 C. 32 clusters could be identified within the Treg cell population of both the spleen and the thymus (Figure 6.10 D). Of the 32 clusters, 16 clusters were significantly different in the thymi of $Bcl6^{fl/fl}Cd4^{cre/+}$ mice compared with controls (Figure 6.10 E). Of those 16 clusters, six clusters showed reduced frequency in $Bcl6^{fl/fl}Cd4^{cre/+}$ mice compared with littermate controls, and ten clusters showed higher frequency in $Bcl6^{fl/fl}Cd4^{cre/+}$ mice compared with controls (Figure 6.10 E-G). Figure 6.10 H shows a heatmap displaying differential expression levels of selected markers in distinct clusters. It is clear from the heatmap that the composition of the Treg cell pool populations in $Bcl6^{fl/fl}Cd4^{cre/+}$ mice. One example of a cluster that is highly represented in $Bcl6^{fl/fl}Cd4^{cre/+}$ mice compared with controls is population 24. These cells are characterised by high levels of CD44, ST2, CD103 and KLRG-1, akin to 'tissue Treg' cells, suggesting that one function of Bcl6 may be limiting premature Treg cell differentiation.

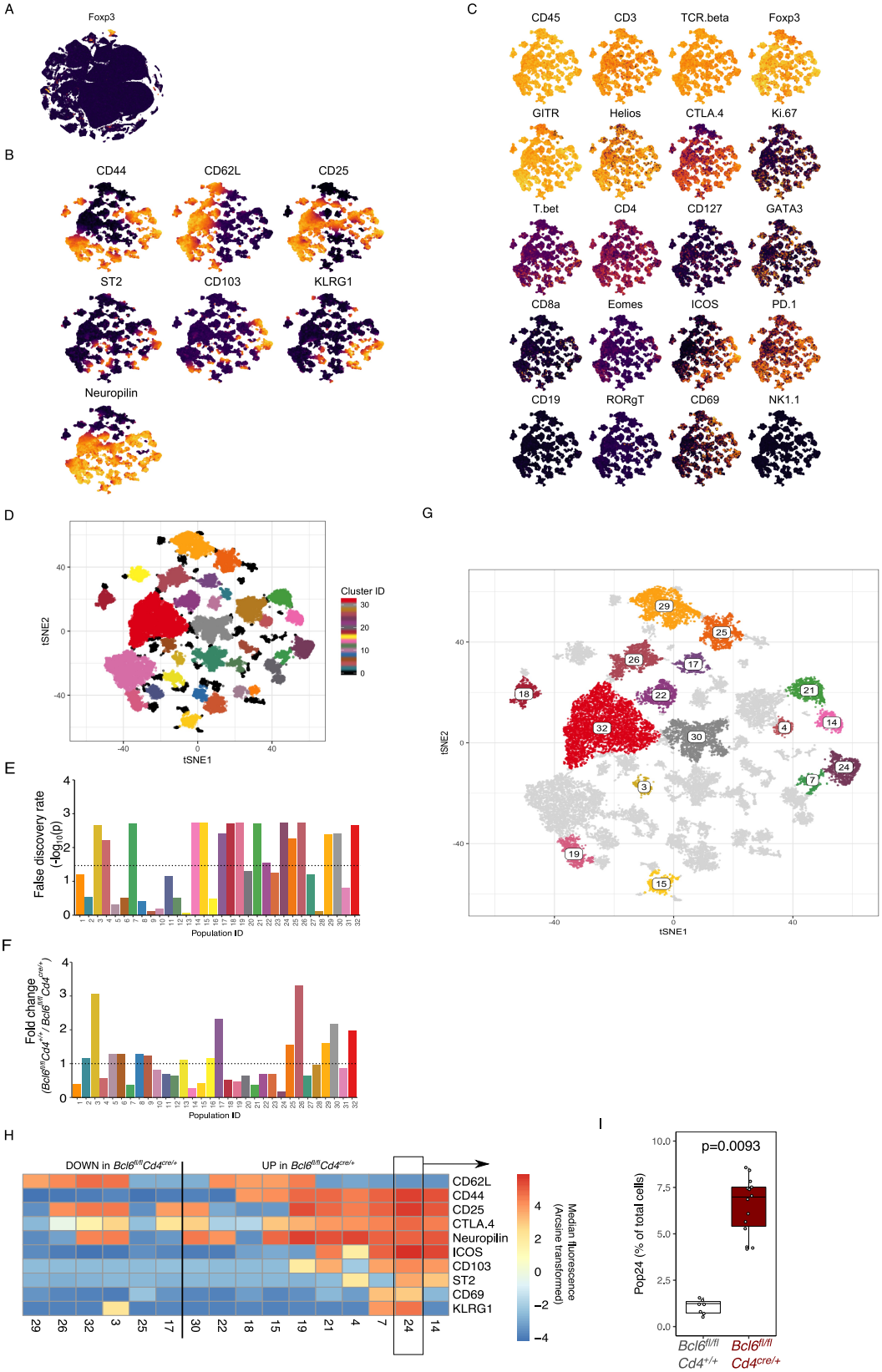

A
Foxp3
B
CD44
CD62L
CD25
ST2
CD103
KLRG1
Neuropilin
C
CD45
CD3
TCR.beta
Foxp3
GITR
Helios
CTLA.4
Ki.67
T.bet
CD4
CD127
GATA3
CD8a
Eomes
ICOS
PD.1
CD19
RORgT
CD69
NK1.1
D
Cluster ID
tSNE1
tSNE2
E
False discovery rate (-log10(p))
Population ID
F
Fold change
Population ID
G
tSNE1
tSNE2
H
DOWN in Bcl6fl/flCd4cre/+
UP in Bcl6fl/flCd4cre/+
CD62L
CD44
CD25
CTLA.4
Neuropilin
ICOS
CD103
ST2
CD69
KLRG1
Median fluorescence (Arcsine transformed)
I
p=0.0093
Pop24 (% of total cells)
Bcl6fl/fl Cd4+/+
Bcl6fl/fl Cd4cre/+

Figure 6.10 Identification of Treg cell sub-populations in the thymus by tSNE.

A. Foxp3^{+} population in the whole thymus from manually pre-gated live cells, as defined by tSNE. **B.** Markers used by the tSNE algorithm to generate clusters within a manually pre-gated Foxp3^{+}CD4^{+} cells population. 888 cells per sample were used to ensure equal cells from each tissue and mouse. tSNE used CD44, CD62L, CD25, ST2, CD103, KRLG-1 and Neuropilin-1 on the 37296 cells, and ran for 2000 iterations with a perplexity value of 75. **C.** Markers not used by the tSNE algorithm to generate clusters but included in the analysis. **D.** tSNE map of all clusters. **E.** P values for the proportion of cells in each cluster in *Bcl6*$^{fl/fl}$*Cd4*$^{+/+}$ mice compared with *Bcl6*$^{fl/fl}$*Cd4*$^{cre/+}$ mice were defined by a Mann-Whitney U test, with multiple testing correction using the false discovery rate (FDR) method. The horizontal dashed line corresponds to p=0.04, FDR=1.4. Significant clusters were defined as those having FDR-adjusted p values of less than 0.04 (above the dashed line). **F.** Fold change of the proportion of cells in each cluster in *Bcl6*$^{fl/fl}$ mice compared with *Bcl6*$^{fl/fl}$*Cd4*$^{cre/+}$ mice. **G.** Clusters defined by tSNE with p<0.04. **H.** Heatmap of markers that are differentially up or down-regulated in *Bcl6*$^{fl/fl}$*Cd4*$^{cre/+}$ mice ordered vertically per cluster. **I.** Box plot of cluster 24 in *Bcl6*$^{fl/fl}$*Cd4*$^{+/+}$ mice versus *Bcl6*$^{fl/fl}$*Cd4*$^{cre/+}$ mice with horizontal bands representing the median, and the horizontal lines delineating the box representing the upper and lower quartile, respectively. Each symbol in the box plot represents one mouse. Data are from one experiment. tSNE analysis was run by Dr Danika Hill (Babraham Institute).

Next, the same tSNE analysis was applied to Foxp3^{+}CD4^{+} Treg cells in the spleen. The first striking difference compared with the thymic analysis was that there were fewer clusters that were significantly different in *Bcl6*$^{fl/fl}$*Cd4*$^{cre/+}$ mice compared with controls in the spleen (Figure 6.11 A-C). In the spleen, of the 32 clusters, six clusters could be identified that were significantly different in *Bcl6*$^{fl/fl}$*Cd4*$^{cre/+}$ mice compared with controls, and all of those were increased in *Bcl6*$^{fl/fl}$*Cd4*$^{cre/+}$ mice (Figure 6.11 A-C). Of the six clusters, clusters 9, 13 and 20 were specifically up-regulated in the spleen, whereas cluster 3, 19 and 24 could be identified in the spleen as well as the thymus (Figure 6.10 G, Figure 6.11 A). However, cluster 3 did not follow the same pattern in both tissues as it seemed to be decreased in the thymus and increased the spleen (Figure 6.10 G, Figure 6.11 A). In contrast, cluster 24 followed exactly the same pattern in the spleen as in the thymus and was significantly up-regulated in *Bcl6*$^{fl/fl}$*Cd4*$^{cre/+}$ mice (Figure 6.11 D-E). Together, these data show that there are fewer differences in the splenic Treg cell pool compared with the thymus in *Bcl6*$^{fl/fl}$*Cd4*$^{cre/+}$ mice. Overall, these data indicate that *Bcl6*$^{fl/fl}$*Cd4*$^{cre/+}$ mice have a broad and robust Treg cell activation phenotype that arises in the thymus.

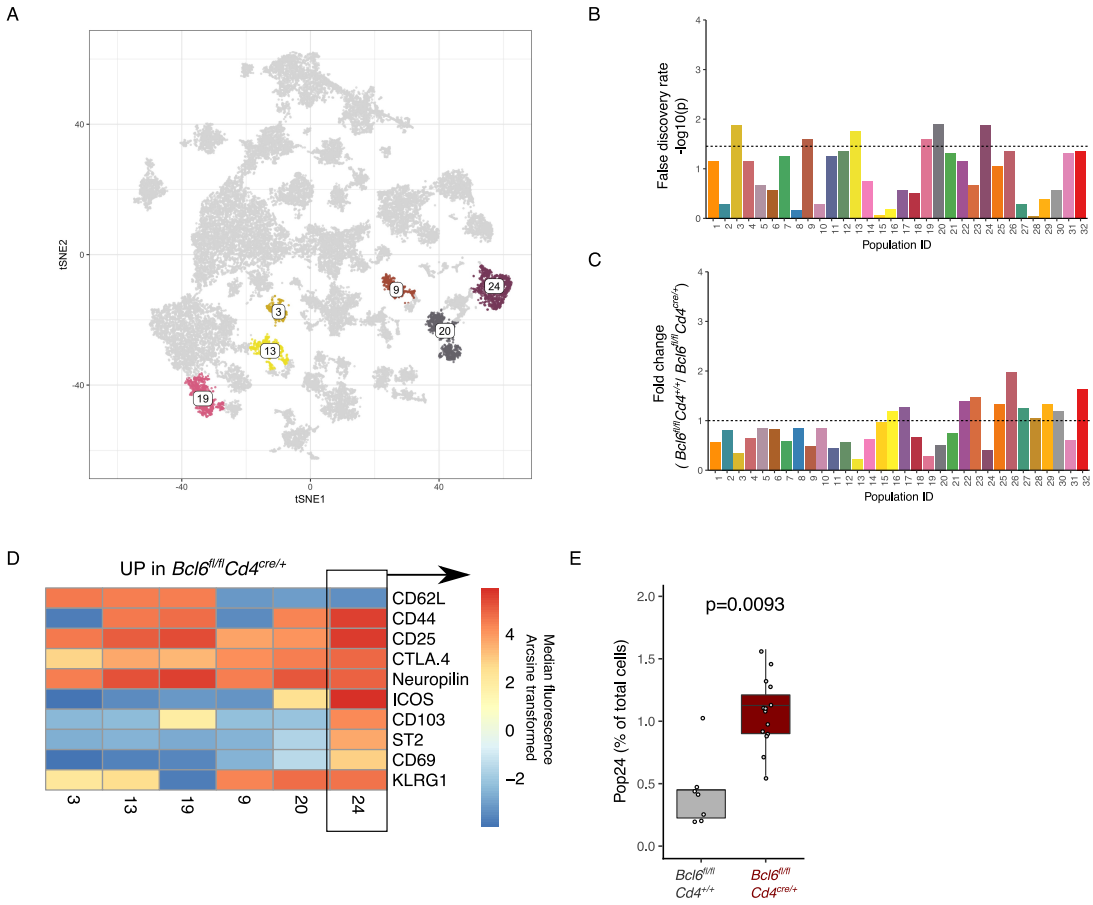


Figure 6.11 Identification of Treg cell sub-populations in the spleen by tSNE.

A. Clusters defined by tSNE with p<0.04. **B.** P values for the proportion of cells in each cluster in *Bcl6*$^{fl/fl}$*Cd4*$^{+/+}$ mice compared with *Bcl6*$^{fl/fl}$*Cd4*$^{cre/+}$ mice were defined by a Mann-Whitney U test, with multiple testing corrections using the false discovery rate (FDR) method. The horizontal dashed line corresponds to p=0.04, FDR=1.4. Significant clusters were defined as those having FDR-adjusted p values of less than 0.04 (above horizontal dashed line). **C**. Fold change of the proportion of cells in each cluster in *Bcl6*$^{fl/fl}$*Cd4*$^{+/+}$ mice compared with *Bcl6*$^{fl/fl}$*Cd4*$^{cre/+}$ mice. **D.** Heatmap of markers that are differentially up-regulated in *Bcl6*$^{fl/fl}$*Cd4*$^{cre/+}$ mice ordered vertically per cluster. **E**. Box plot of cluster 24 *in Bcl6*$^{fl/fl}$*Cd4*$^{+/+}$ mice versus *Bcl6*$^{fl/fl}$*Cd4*$^{cre/+}$ mice, with horizontal bands representing the median, and the horizontal lines delineating the box representing the upper and lower quartile, respectively. Each symbol in the box plot represents one mouse. Data are from one experiment. tSNE analysis was run by Dr Danika Hill (Babraham Institute).

tSNE analysis was subsequently applied to $CD4^{+}Foxp3^{-}$ in the thymus (Figure 6.12) and spleen (Figure 6.13). In the thymus, the markers used for clustering were CD44, CD62L, KLRG-1, CD69, Ki67, CD127, GATA3 and Rorγt (Figure 6.12 A). In the thymus, a total of 29 clusters could be identified within the Tconv cell population (Figure 6.12 C). Of these, three clusters were significantly different between $Bcl6^{fl/fl}Cd4^{cre/+}$ mice and controls. One cluster was reduced and two increased in frequency in $Bcl6^{fl/fl}Cd4^{cre/+}$ mice (Figure 6.12 D-G). In the spleen, the markers used for clustering were CD44, CD62L, KLRG-1, CD69, Ki67, CD127, GATA3 and Rorγt (Figure 6.13 A). In the spleen, a total of 25 clusters could be identified within the Tconv cell population (Figure 6.13 C). Within those clusters, ten clusters were significantly different between $Bcl6^{fl/fl}Cd4^{cre/+}$ mice and controls, with three clusters reduced in frequency and and eight clusters increased in $Bcl6^{fl/fl}Cd4^{cre/+}$ mice (Figure 6.13 D-G).

Overall, the tSNE data analysis of Treg cells and Tconv cells in the spleen and the thymus of $Bcl6^{fl/fl}Cd4^{cre/+}$ mice indicates that there are major tissue-specific and cell-type specific changes occurring in these mice, with the most prominent change in tTreg cells.

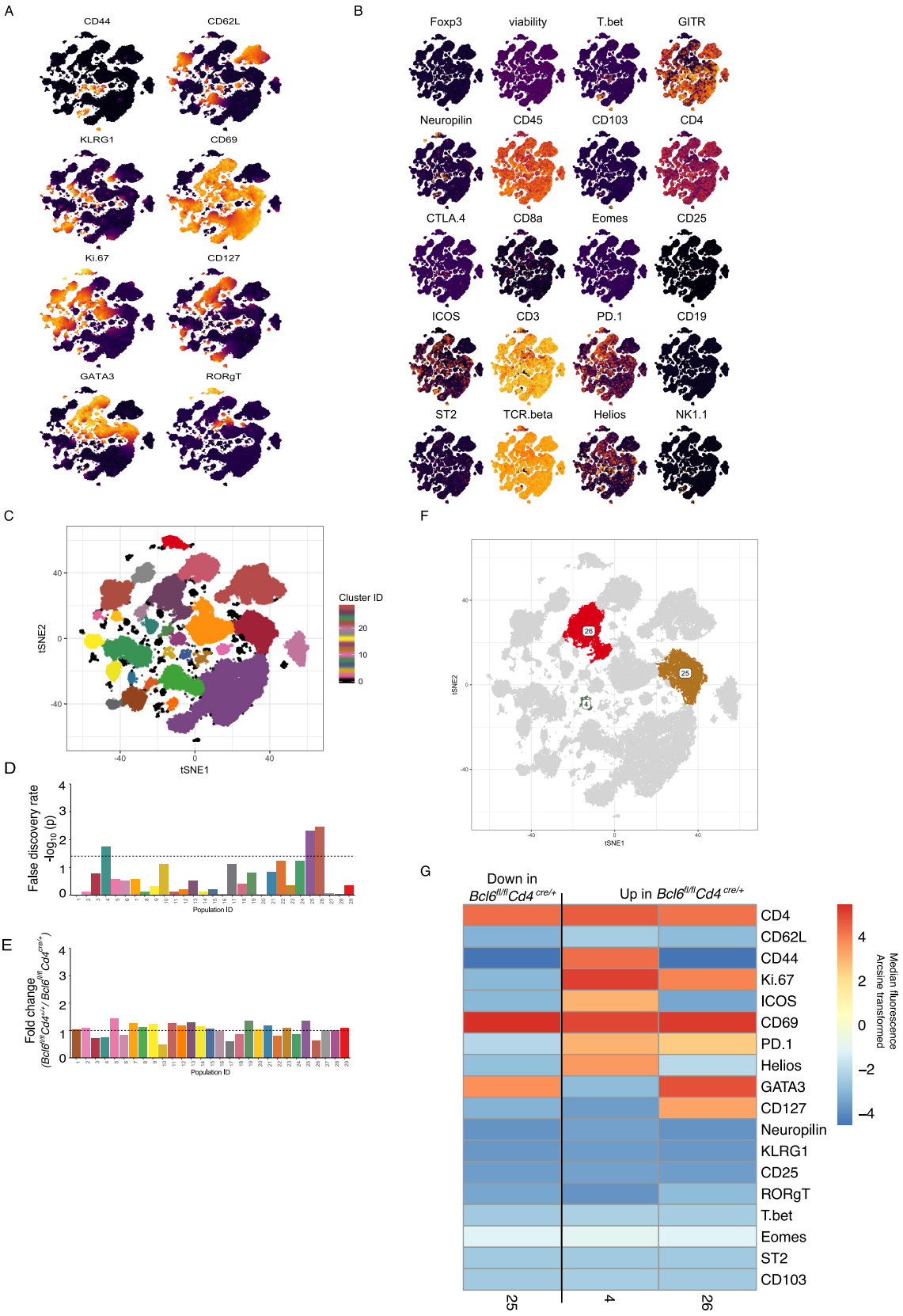

A
CD44
CD62L
KLRG1
CD69
Ki.67
CD127
GATA3
RORgT
B
Foxp3
viability
T.bet
GITR
Neuropilin
CD45
CD103
CD4
CTLA.4
CD8a
Eomes
CD25
ICOS
CD3
PD.1
CD19
ST2
TCR.beta
Helios
NK1.1
C
tSNE2
tSNE1
Cluster ID
20
10
0
D
False discovery rate
-log10 (p)
Population ID
E
Fold change
Population ID
F
tSNE2
tSNE1
26
25
4
G
Down in
Bcl6fl/flCd4cre/+
Up in Bcl6fl/flCd4cre/+
CD4
CD62L
CD44
Ki.67
ICOS
CD69
PD.1
Helios
GATA3
CD127
Neuropilin
KLRG1
CD25
RORgT
T.bet
Eomes
ST2
CD103
25
4
26
Median fluorescence
Arcsine transformed

Figure 6.12 Identification of Tconv cell sub-populations in the thymus by tSNE.

A. Markers used by the tSNE algorithm to generate clusters within a manually pre-gated Foxp3^{-}CD4^{+} cells population. 888 cells per sample were used to ensure equal cells from each tissue and mouse. tSNE used CD44, CD62L, KRLG-1, Ki-67, CD69, CD127, GATA3 and Rorγt on the 37296 cells, and ran for 2000 iterations with a perplexity value of 75. The proportion of cells in each cluster was determined for each sample. **B.** Markers not used by the tSNE algorithm to generate clusters but included in the analysis. **C.** tSNE map of all clusters. **D.** P values for the proportion of cells in each cluster in *Bcl6*$^{fl/fl}$*Cd4*$^{+/+}$ mice compared with *Bcl6*$^{fl/fl}$*Cd4*$^{cre/+}$ mice were defined by a Mann-Whitney U test, with multiple testing correction using the false discovery rate (FDR) method. The horizontal dashed line corresponds to p=0.04, FDR=1.4. Significant clusters were defined as those having FDR-adjusted p values of less than 0.04. **E.** Fold change of the proportion of cells in each cluster in *Bcl6*$^{fl/fl}$*Cd4*$^{+/+}$ mice compared with *Bcl6*$^{fl/fl}$*Cd4*$^{cre/+}$ mice. **F.** Clusters defined by tSNE with p<0.04. **G.** Heatmap of markers that are differentially up-regulated in *Bcl6*$^{fl/fl}$*Cd4*$^{cre/+}$ mice ordered vertically per cluster. Data are from one experiment. tSNE analysis was run by Dr Danika Hill (Babraham Institute).

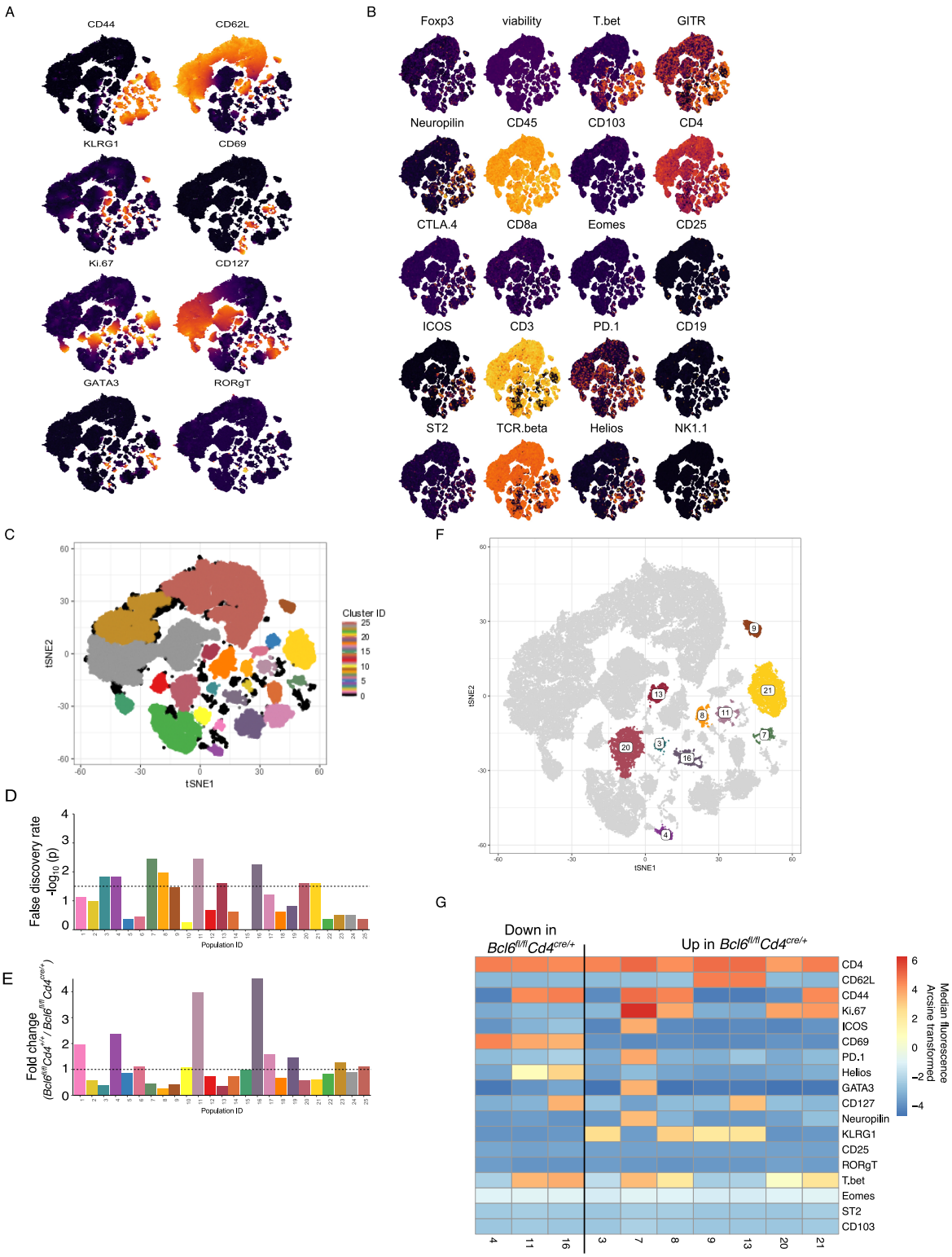

A
CD44
CD62L
KLRG1
CD69
Ki.67
CD127
GATA3
RORgT
B
Foxp3
viability
T.bet
GITR
Neuropilin
CD45
CD103
CD4
CTLA.4
CD8a
Eomes
CD25
ICOS
CD3
PD.1
CD19
ST2
TCR.beta
Helios
NK1.1
C
tSNE2
tSNE1
Cluster ID
25
20
15
10
5
0
F
tSNE2
tSNE1
9
13
21
8
11
7
20
3
16
4
D
False discovery rate
-log10 (p)
Population ID
E
Fold change
(Bcl6fl/flCd4+/+ / Bcl6fl/flCd4cre/+)
Population ID
G
Down in
Bcl6fl/flCd4cre/+
Up in Bcl6fl/flCd4cre/+
CD4
CD62L
CD44
Ki.67
ICOS
CD69
PD.1
Helios
GATA3
CD127
Neuropilin
KLRG1
CD25
RORgT
T.bet
Eomes
ST2
CD103
4
11
16
3
7
8
9
13
20
21
Median fluorescence
Arcsine transformed

Figure 6.13 Identification of Tconv cell sub-populations in the spleen by tSNE.

A. Markers used by the tSNE algorithm to generate clusters within a manually pre-gated Foxp3^{-}CD4^{+} cells population. 888 cells per sample were used to ensure equal cells from each tissue and mouse. tSNE used CD44, CD62L, KRLG-1, Ki-67, CD69, CD127, GATA3 and Rorγt on the 37296 cells, and ran for 2000 iterations with a perplexity value of 75. The proportion of cells in each cluster was determined for each sample. **B.** Markers not used by the tSNE algorithm to generate clusters but included in the analysis. **C.** tSNE map of all clusters. **D.** P values for the proportion of cells in each cluster in *Bcl6*$^{fl/fl}$*Cd4*$^{+/+}$ mice compared with *Bcl6*$^{fl/fl}$*Cd4*$^{cre/+}$ mice were defined by a Mann-Whitney U test, with multiple testing correction using the false discovery rate (FDR) method. The horizontal dashed line corresponds to p=0.04, FDR=1.4. Significant clusters were defined as those having FDR-adjusted p values of less than 0.04. **E.** Fold change of the proportion of cells in each cluster in *Bcl6*$^{fl/fl}$*Cd4*$^{+/+}$ mice compared with *Bcl6*$^{fl/fl}$*Cd4*$^{cre/+}$ mice. **F**. Clusters defined by tSNE with p<0.04. **G.** Heatmap of markers that are differentially up-regulated in *Bcl6*$^{fl/fl}$*Cd4*$^{cre/+}$ mice ordered vertically per cluster. Data are from one experiment. tSNE analysis was run by Dr Danika Hill (Babraham Institute).

6.2.5 GATA3 is highly up-regulated at the DP stage in thymus in *Bcl6$^{fl/fl}$Cd4$^{cre/+}$* mice

The early and broad Treg cell activation phenotype observed in *Bcl6$^{fl/fl}$Cd4$^{cre/+}$* mice begs the question of what is driving these changes. CD4 is first expressed at the DP stage, so Bcl6 deletion should occur at this stage in the thymus in *Bcl6$^{fl/fl}$Cd4$^{cre/+}$* mice. It was therefore of interest to examine whether there are changes in DP thymocytes in *Bcl6$^{fl/fl}$Cd4$^{cre/+}$* mice. The changes occurring at the DP stage in *Bcl6$^{fl/fl}$Cd4$^{cre/+}$* mice might provide a clue as to what mechanisms are driving the Treg cell activation phenotype. For this, the tSNE analysis algorithm was applied to CD4$^+$CD8$^+$ DP thymocytes. The markers used for clustering were Foxp3, Ki67, GITR, Nrp-1, CD103, CD4, CD62L, CD127, GATA3, CD8, CD25, CD44, PD-1, Rorγt, CD69 and TCRβ (Figure 6.14 A). A total of 35 clusters could be identified within the DP population (Figure 6.14 B). Of those 35 clusters, five clusters were significantly increased in *Bcl6$^{fl/fl}$Cd4$^{cre/+}$* compared with controls (Figure 6.14 C-F). Notably, the transcriptional regulators Rorγt and GATA3 were both up-regulated in a cluster containing CD4$^+$CD8$^+$ DP thymocytes (cluster 27). Rorγt was also up-regulated in another cluster of CD4$^+$CD8$^+$ DP cells (cluster 22), and GATA3 was also expressed in a cluster containing CD4$^+$ SP cells (cluster 13) (Figure 6.14 F). These data are in line with Bcl6 repressing transcriptional regulators that drive alternative CD4$^+$ T cell differentiation pathways including Rorγt and GATA3 in Tfh cells (Nurieva et al., 2009, Yu et al., 2009). Manual gating confirmed that GATA3 is significantly higher expressed at the DP stage in *Bcl6$^{fl/fl}$Cd4$^{cre/+}$* mice compared with *Bcl6$^{fl/fl}$Cd4$^{+/+}$* control mice (Figure 6.14 G-J). GATA3 is an essential transcriptional regulator throughout T cell development in the thymus and plays a key role in driving the CD4$^+$ T cell lineage differentiation (Hernandez-Hoyos et al., 2003, Pai et al., 2003). It is also an important regulator of Treg cell maintenance and function through binding to CNS2 in *Foxp3 (Hernandez-Hoyos et al., 2003)*. Thus, it is tempting to speculate that Bcl6 may act in thymocytes to limit GATA3 expression in a subset of DP/CD4 SP cells to curb premature Treg cell activation during development.

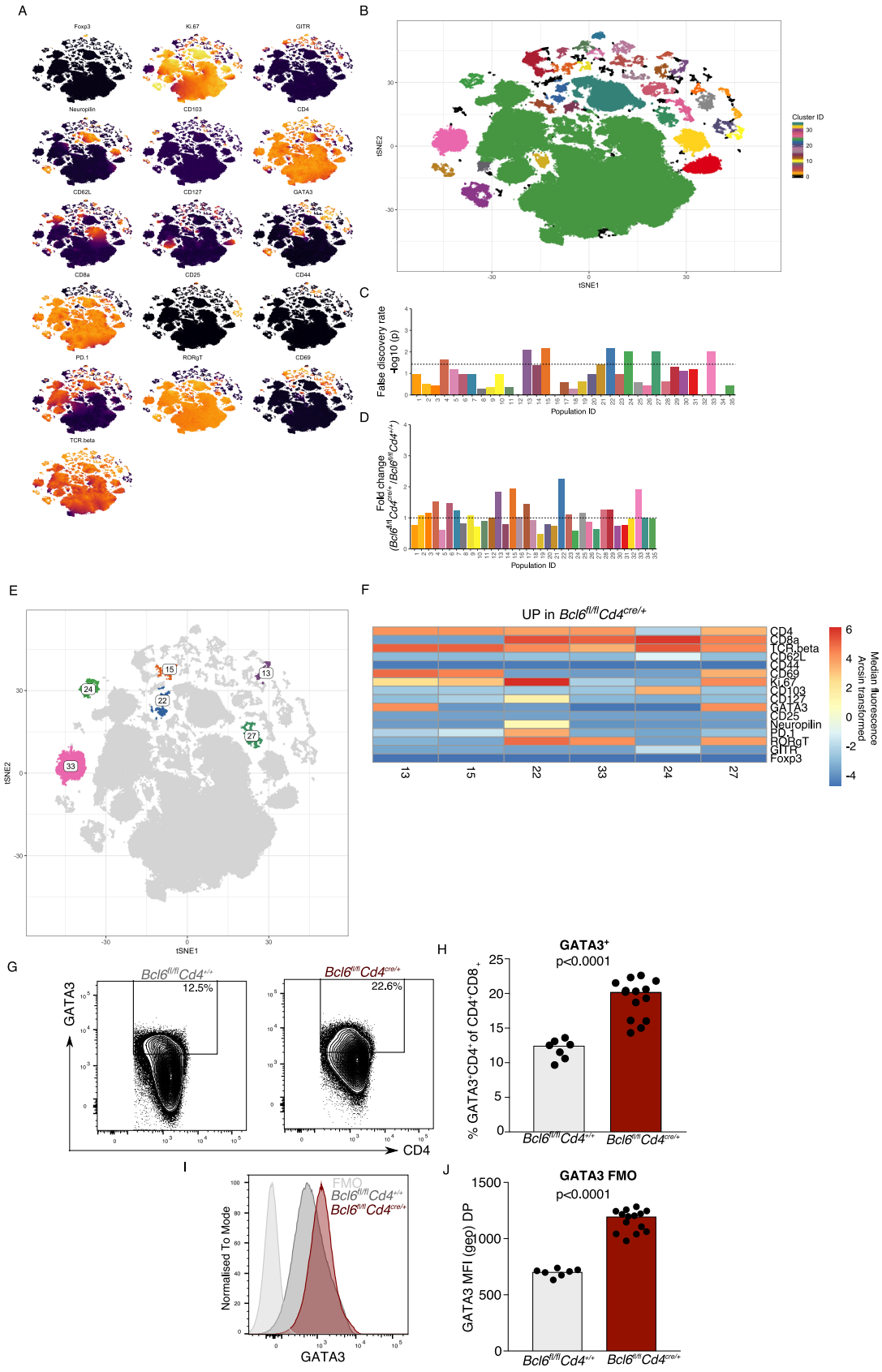

A
Foxp3
KI.67
GITR
Neuropilin
CD103
CD4
CD62L
CD127
GATA3
CD8a
CD25
CD44
PD.1
RORgT
CD69
TCR.beta
B
tSNE2
tSNE1
Cluster ID
C
False discovery rate
-log10 (p)
Population ID
D
Fold change
(Bcl6fl/fl Cd4cre/+ / Bcl6fl/fl Cd4+/+)
Population ID
E
tSNE2
tSNE1
15
13
24
22
27
33
F
UP in Bcl6fl/fl Cd4cre/+
CD4
CD8a
TCR.beta
CD62L
CD44
CD69
KI.67
CD103
CD127
GATA3
CD25
Neuropilin
PD.1
RORgT
GITR
Foxp3
13
15
22
33
24
27
Median fluorescence
Arcsin transformed
G
Bcl6fl/fl Cd4+/+
12.5%
Bcl6fl/fl Cd4cre/+
22.6%
GATA3
CD4
H
GATA3+
p<0.0001
% GATA3+CD4+ of CD4+CD8+
Bcl6fl/fl Cd4+/+
Bcl6fl/fl Cd4cre/+
I
FMO
Bcl6fl/fl Cd4+/+
Bcl6fl/fl Cd4cre/+
Normalised To Mode
GATA3
J
GATA3 FMO
p<0.0001
GATA3 MFI (gep) DP
Bcl6fl/fl Cd4+/+
Bcl6fl/fl Cd4cre/+

Figure 6.14 Identification of sub-populations of DP ($CD4^+CD8^+$) cells in the thymus by tSNE.

A. Markers used by the tSNE algorithm to generate clusters within a manually pre-gated $CD4^+CD8^+$ DP cell population. 10,000 cells were randomly subsampled to ensure equal cells from each mouse. tSNE used 12 markers on the 420,000 cells and ran for 2500 iterations with a perplexity value of 100. **B.** tSNE map of all clusters. **C.** P values for the proportion of cells in each cluster in $Bcl6^{fl/fl}Cd4^{+/+}$ mice compared with $Bcl6^{fl/fl}Cd4^{cre/+}$ mice were defined by a Mann-Whitney U test, with multiple testing corrections using the false discovery rate (FDR) method. The horizontal dashed line corresponds to p=0.04, FDR=1.4. Significant clusters were defined as those having FDR-adjusted p values of less than 0.04 (above horizontal dashed line). **D.** Fold change of the proportion of cells in each cluster in $Bcl6^{fl/fl}Cd4^{+/+}$ mice compared with $Bcl6^{fl/fl}Cd4^{cre/+}$ mice. **E.** Clusters defined by tSNE with $p<0.04$. **F.** Heatmap of markers that are differentially up-regulated in $Bcl6^{fl/fl}Cd4^{cre/+}$ mice compared with $Bcl6^{fl/fl}Cd4^{+/+}$ mice ordered vertically per cluster. **G.** Flow cytometry contour plot of $GATA3^+CD4^+$ DP thymocytes in $Bcl6^{fl/fl}Cd4^{cre/+}$ mice and $Bcl6^{fl/fl}Cd4^{+/+}$ controls. **H.** Quantification of the percentage of $GATA3^+CD4^+$ DP thymocytes. **I.** Histogram of GATA3 expression in DP cells $Bcl6^{fl/fl}Cd4^{cre/+}$ mice and $Bcl6^{fl/fl}Cd4^{+/+}$ controls. **J.** Quantification of the MFI of GATA3 in DP thymocytesEach symbol represents one mouse, and the horizontal bars represent the median values. P values were determined using a Mann-Whitney U test. Data are from 1 experiment. tSNE analysis was run by Dr Danika Hill (Babraham Institute).

6.2.6 Potential role of Bcl6 in regulating Treg cell super-enhancer genes

An alternative explanation for the Treg activation phenotype observed in *Bcl6*$^{fl/fl}$*Cd4*$^{cre/+}$ mice is that Bcl6 regulates Treg Super-enhancers (SE). SE are formed of a group of putative enhancers in close genomic proximity to each other with unusually high levels of transcriptional co-activator binding, or chromatin modification that define cell identity (Vahedi et al., 2015). Treg cell lineage specification takes place prior to Foxp3 expression during T cell development, and is driven by super-enhancers (Floess et al., 2007, Ohkura et al., 2012). Treg cell super-enhancers are initiated prior to Foxp3 expression during the early stages of thymic Treg cell development (Kitagawa et al., 2017). Thus, these Treg-SE establish a permissive epigenetic landscape for the initiation of tTreg differentiation prior to Foxp3 expression. Because deletion of Bcl6 in mature naïve Treg cells does not recapitulate the Treg activation phenotype observed in *Bcl6*$^{fl/fl}$*Cd4*$^{cre/+}$ mice (Figure 6.6), and because Bcl6 is expressed before Foxp3 in the thymus, I reasoned that Bcl6 might drive Treg cell lineage specification prior to Foxp3 expression, and that this might involve Treg-SE. In GC B cells, Bcl6 is able 'switch off' enhancers through HDAC3-dependent de-acetylation of H3K27ac (Hatzi et al., 2013). Perhaps Bcl6 acts in similar manner in pre-tTreg cells, maintaining Treg cell SE in a poised state to avoid premature Treg cell lineage specification. To investigate a Treg cell priming effect of Bcl6, I examined Bcl6 signature genes in *Bcl6*$^{fl/fl}$*Cd4*$^{cre/+}$ mice. *Bcl6*$^{fl/fl}$*Cd4*$^{cre/+}$ mice showed increased levels of 'Treg signature genes'; GITR, CTLA-4 and Helios, compared with *Bcl6*$^{fl/fl}$ controls, both in the thymus and the spleen (Figure 6.15 A-C). Next, Bcl6 motifs were analysed in Treg SE as well as Tconv SE, as defined by Kitagawa *et al*. (Kitagawa et al., 2017). The density distribution of Bcl6 motifs seemed to have a shoulder for higher Bcl6 motif frequency in the Treg SE, although this was not a significant effect compared with Tconv SE (Figure 6.15 D). The genes closely associated with those Treg SE that have a Bcl6 motif frequency of higher than 0.35 include Treg signature genes such as CTLA-4, GITR and Helios, as well as Foxp3 itself (Figure 6.15 E). These data suggest that Bcl6 might maintain Treg-SE in a poised state during Treg development, thereby preventing premature lineage specification.

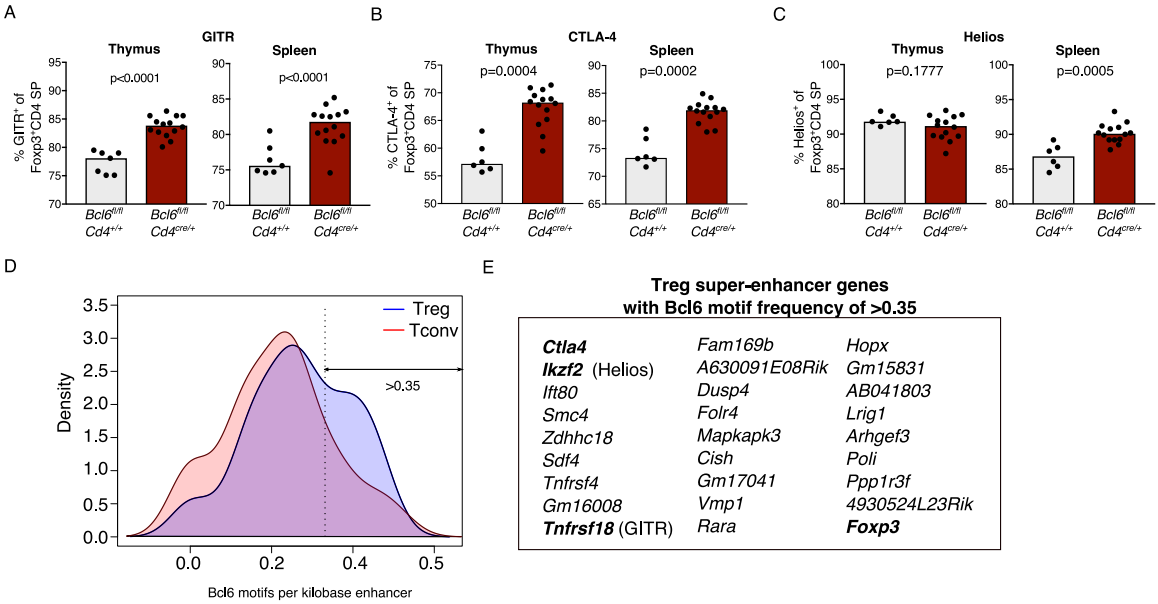


Figure 6.15 Treg super-enhancers are enriched for Bcl6 motifs.

A. Quantification of the proportion of thymic and splenic Foxp3$^+$CD4$^+$ T cells expressing GITR. **B.** Quantification of the proportion of thymic and splenic Foxp3$^+$CD4$^+$ T cells expressing CTLA-4. **C.** Quantification of the proportion of thymic and splenic Foxp3$^+$CD4$^+$ T cells expressing Helios. **D.** Density distribution of Bcl6 motifs per kilobase of enhancer in Tconv and Treg super-enhancers as defined by Kitagawa *et al.(Kitagawa et al., 2017)*. **E.** Genes closely associated with he subset of Treg super-enhancers that have a Bcl6 motif frequency higher than 0.35. Motif analysis was performed by Dr Christel Krueger (Babraham Institute).

6.3 Discussion

Initially, the aim of this chapter was to test whether the Tfr and Th1-like Treg cell differentiation pathways were linked in a mutually repressive fashion by the opposing effects of Bcl6 and Tbet. For this, I examined whether deletion of Bcl6 in $CD4^+$ T cells using *Bcl6*$^{fl/fl}$*Cd4*$^{cre/+}$ mice would result in a cell-intrinsic increase in $Tbet^+$ Treg cells. After influenza infection, there was a significant increase in $Tbet^+$ Treg cells, but not in Th1 cells. Surprisingly, in the absence of infection or immunisation, this effect was even more pronounced. These data suggested that Bcl6 could modulate non-Tfr Treg cell differentiation, a function for Bcl6 that has not been described before. Admittedly, these data require prudent interpretation as gating for Tbet was arbitrary and ideally an isotype control, or FMO control for Tbet should be used. This puzzling result led me to examine Bcl6 expression during T cell development, as *Bcl6*$^{fl/fl}$*Cd4*$^{cre/+}$ mice are expected to delete Bcl6 from the $CD4^+CD8^+$ DP stage onwards. Bcl6 is up-regulated at the DP stage both at the mRNA level and the protein level. After the DP stage, Bcl6 expression declined steadily in immature $CD4^+$ T cells. Interestingly, there was a slight increase in Bcl6 expression in pre-tTreg cells. After the pre-tTreg stage, *Bcl6* expression declined again in tTreg cells, and expression of Bcl6 remained low in mature, naïve Treg cells. These mRNA expression data need to be interpreted with caution as *Bcl6* mRNA levels do not perfectly correlate with Bcl6 protein expression. In addition, Bcl6 is highly regulated at the post-transcriptional level by acetylation, phosphorylation, and co-factor dependent degradation (Niu et al., 1998, Bereshchenko et al., 2002, Crotty et al., 2010). Furthermore, Bcl6 forms dimers and its target sequences must be accessible (Ahmad et al., 2003). Therefore, it is difficult to relate Bcl6 expression to its function. Thymic Treg cells, but not Tconv cells, from *Bcl6*$^{fl/fl}$*Cd4*$^{cre/+}$ mice were highly activated. In-depth phenotyping using high-parameter flow cytometry revealed a complex and broad Tconv and Treg cell phenotype in *Bcl6*$^{fl/fl}$*Cd4*$^{cre/+}$ mice. In order to define sub-populations within the Treg and Tconv cell pool, tSNE analysis was performed on these phenotyping data. The most striking differences were observed in the thymic Treg cell population with major changes in the composition of the Treg cell pool. To identify potential mechanisms that might drive the Treg activation phenotype, I analysed DP thymocytes in *Bcl6*$^{fl/fl}$*Cd4*$^{cre/+}$ mice. This analysis revealed that GATA3 was highly up-regulated at this stage, suggesting that Bcl6 represses GATA3 at the DP stage. Finally, A second mechanism of action of Bcl6 might involve Treg SE. Motif analysis of the Bcl6 consensus sequence in Treg-SE revealed that there was a slight enrichment in Bcl6 motifs in Treg SE compared to Tconv cells. So, Bcl6 might maintain Treg-SE in a poised state during Treg development,

thereby preventing premature lineage specification. In summary, deletion of Bcl6 in $CD4^+$ T cells leads to a thymic Treg defect that occurs very early in life and results in an activated Treg cell phenotype both in the thymus and in the periphery.

Based on the data presented herein, I hypothesise that Bcl6 acts as an important transcriptional repressor of early thymic Treg cell differentiation by establishing non-permissive epigenetic marks at Treg subset associated genes at either the DP or CD4 SP stage of T cell development. To test this hypothesis, Bcl6 protein expression at different discrete stages of development prior to Foxp3 expression needs to be determined. For this purpose, I would propose to use an ImageStream system. This would allow for visualisation of nuclear Bcl6 expression in both abundant subsets such as DP thymocytes, as well as more rare populations such as pre-tTreg cells (1-2% of CD4 SP cells). Following on from that I would suggest a broader genome-wide analysis of the mechanisms involved in Bcl6 mediated control of Treg cell development. Firstly, an assay for transposase-accessible chromatin using sequencing (ATAC-seq) will aide in determining whether the absence of Bcl6 leads to a global increased chromatin accessibility in DP cells in $Bcl6^{fl/fl}Cd4^{cre/+}$ mice. In addition, ChIP-Seq for epigenetic marks including H3K27ac and H3K4me1, and H3K4me3, histone modifications that mark promoters and enhancer regions, in DP, CD4 SP and pre-tTreg cells of $Bcl6^{fl/fl}Cd4^{cre/+}$ mice will aide in identifying cis-regulatory elements involved in Bcl6 dependent pre-tTreg cell development. Finally, to better understand the genome-wide gene target network that Bcl6 binds Bcl6 ChIP-Seq could be performed on DP thymocytes. The ATAC-seq and ChIP-seq for epigenetic marks, together with the Bcl6 ChIP-Seq data, will allow us to understand global mechanisms involved in thymic Treg development, and how Bcl6 regulates the epigenetic and transcriptional landscape of tTreg cells.

Taken together, the data presented in this chapter support a novel role for Bcl6 in regulating early Treg cell development. Further investigation of the role of Bcl6 in thymic Treg cell development, as well as the mechanisms involved in this regulation, will aide in moving this field of research forward.

7 Discussion

7.1 Generating a Tfr-deficient mouse model

Tfr cells are thought to be essential regulators of the GC response. However, the precise role that Tfr cells play in the GC was unknown at the outset of this work, and still remains elusive.

My first aim was to establish a Tfr-deficient mouse model. The generation of this mouse model would have allowed me to infer the role played by Tfr cells within the GC by describing how the response changes in their absence. For this purpose, I took advantage of the report that Tfr cells require specifically the chemokine receptor CXCR5 to access to the GC (Chung et al., 2011). Therefore, a logical and straightforward approach to achieving this aim was to establish a mouse model that specifically lacks CXCR5 on Treg cells. In Chapter 3, I demonstrated that *Cxcr5*$^{fl/fl}$*Foxp3*^{cre} mice delete CXCR5 in non-Treg cells due to a 'leaky' cre recombinase. Given CXCR5 is essential for B cell and Tfh cell localisation, I would not be able to ascribe any phenotype observed in these mice to Tfr cell function (Forster et al., 1996, Legler et al., 1998, Moser, 2015). These data are relevant with regards to the wide spread use of the *Foxp3*^{cre} mouse model in the Treg cell biology field (Rubtsov et al., 2010). In light of these, and previously published results (Franckaert et al., 2015), the specificity as well as the sensitivity of cre-mediated deletion should be reported in future studies using *Foxp3*^{cre} strains, and indeed all other cre-expressing strains.

In Chapter 4, I validated the use of an alternative model, the *Cxcr5*$^{fl/fl}$*Foxp3*$^{cre\text{-}ERT2}$ mouse model, as a putative Tfr-deficient mouse model. The use of the cre-ERT2 recombinase allowed for successful deletion of CXCR5 specifically in Treg cells. Despite the loss of CXCR5 on Treg cells, I was still able to identify Tfr cells within the GC, albeit in reduced

numbers. This is in contrast to a study published by Chung *et al* ., where transfer of CXCR5-deficient Treg cells into mice that lack T cells resulted in absence of Tfr cells within the GC after immunisation (Chung et al., 2011). I can only speculate on why the results obtained by Chung *et al*. are different from the results described in this thesis. In order for $CD4^{+}Foxp3^{-}$ T cells to enter the GC, it is not sufficient to just up-regulate CXCR5, CCR7 must be down-regulated as well to enable migration away from the T cell zone that is rich in CCR7-ligands (Haynes et al., 2007). So it is possible that the CXCR5-deficient Treg cells used by Chung *et al.* are not down-regulating CCR7, preventing them from entering the GC. Furthermore, it is plausible that these CXCR5-deficient Treg cells do not migrate to the LNs after intravenous injection compared with wild-type Treg cells. The results described herein are more physiological as the model is an intact mouse that does not require cell isolation and transfer.

I have made the observation that Tfr cells within the GC show lower expression levels of Foxp3 compared with those outside the GC as determined by quantifying the Foxp3 intensity in confocal microscopy images. Therefore, early studies characterising Tfr cells within the GC might not have been able to identify $Foxp3^{+}$ Treg cells within the GC successfully. The reduction in Foxp3 expression I observed in Tfr cells is consistent with their $CD25^{-}$ phenotype, as IL-2 signalling is required for maintenance of Foxp3 expression (Fontenot et al., 2005b). Despite lower Foxp3 expression, Tfr cells show a demethylated CNS2, indicating they are stable Treg cells (Wing et al., 2017). How Tfr cells maintain Foxp3 expression in the absence of IL-2 signalling remains to be demonstrated. One candidate could be IL-15, as it has been implicated in the induction of Foxp3 expression in pre-tTreg cells (Marshall et al., 2014). IL-15 has been shown to support Tfh differentiation *in vitro* by decreasing STAT5 activation and inducing Bcl6 expression (Cooley et al., 2015). Tfr cells still express CD122, the IL2Rβ chain that is shared between IL-15 and IL-2, so it is possible that IL-15 signalling maintains Foxp3 expression through CD122 (Botta et al., 2017), as well as support their GC phenotype. Thus, IL-15 could perhaps consolidate between the genuine Treg cell identity and the Tfh phenotype of Tfr cells.

The reduction in the number of Tfr cells observed in $Cxcr5^{fl/fl}Foxp3^{cre\text{-}ERT2}$ mice did not affect the size, or the output of the GC response. This is consistent with recently published data showing that $Bcl6^{fl/fl}Foxp3^{cre}$ mice elicit normal GC B cell responses (Wu et al., 2016a, Botta et al., 2017). Nevertheless, one of these studies also showed that Tfr cells peak from day 30-60 after influenza infection (PR8)(Botta et al., 2017). I was unable to observe a difference in the number of plasma cells at day 48 after immunisation in $Cxcr5^{fl/fl}Foxp3^{cre\text{-}ERT2}$ mice,

indicating that there might be differences depending on the antigen challenge, *i.e.* influenza A virus (PR8) infection versus NP-KLH immunisation used herein.

The observation that there was a significant reduction, but not complete lack of Tfr cells within the GC of *Cxcr5*$^{fl/fl}$*Foxp3*$^{cre\text{-}ERT2}$ mice indicates that there might be redundant mechanisms involved in Treg cell localisation to the GC. I subsequently identified CXCR4 as a marker highly expressed by Tfr cells. As CXCR4 had been implied in T cell localisation within the GC in previous studies, it was an attractive candidate for homing of Treg cells to the GC (Elsner et al., 2012). This led to the hypothesis that CXCR4 promotes localisation of Tfr cells within the GC. To validate this hypothesis, we generated *Cxcr4*$^{fl/fl}$*Foxp3*$^{cre\text{-}ERT2}$ mice, as well as *Cxcr5*$^{fl/fl}$*Cxcr4*$^{fl/fl}$*Foxp3*$^{cre\text{-}ERT2}$ mice, described in Chapter 5. I was unable to achieve complete deletion of CXCR4 in Treg cells in both mouse models, despite successful deletion of CXCR5 in *Cxcr5*$^{fl/fl}$*Cxcr4*$^{fl/fl}$*Foxp3*$^{cre\text{-}ERT2}$ mice. Thus, due to the reduced sensitivity of *Cxcr4* to ablation, I was unable to draw definite conclusions from these mouse models.

In summary, using four different mouse models, I was unable to generate a mouse model that would reliable delete all Tfr cells from the GC. Nevertheless, this study has lead to interesting insights into Tfr cell biology. First, I showed that CXCR5 expression is not an absolute requirement for Treg cell access to the GC (Chung et al., 2011). Therefore, other redundant mechanisms must be able to compensate for this loss of CXCR5. Secondly, reducing the number of Tfr cells within the GC up to 3-fold does not affect the size, or output of the GC. Furthermore, Tfr cells express high levels of CXCR4, the function of which needs to be studied in more detail in the context of the GC. Future studies should focus on identifying redundant mechanisms involved in Tfr localisation within the GC, as ell as the function of CXCR4 in Tfr cells.

7.1.1 Potential redundant mechanisms for Treg cell access to the germinal centre

Although I was unable to achieve complete deletion of CXCR4 on Treg cells in *Cxcr4*$^{fl/fl}$*Cxcr5*$^{fl/fl}$*Foxp3*^{creERT2} mice, there was a slight, although not significant decrease in CXCR4 expression in Tfr cells in these mice. Confocal imaging showed the presence of Tfr cells within the GC of *Cxcr4*$^{fl/fl}$*Cxcr5*$^{fl/fl}$*Foxp3*^{creERT2} mice. Notably, the number of Tfr cells in *Cxcr4*$^{fl/fl}$*Cxcr5*$^{fl/fl}$*Foxp3*^{creERT2} was increased compared with *Cxcr5*$^{fl/fl}$*Foxp3*^{creERT2} mice,

indicating that CXCR4 might act antagonistically with CXCR5, and hold Tfr cells in the T cell zone, a location with high expression of the ligand for CXCR4, CXCL12. These results suggest that CXCR4 may not be not responsible for migration of Treg cells to the GC in the absence of CXCR5.

This begs the question as to what the redundant mechanisms for Tfr cell migration to the GC might be. One potential candidate for this is S1PR2. S1PR2 is essential for retaining Tfh cells within the GC, and Tfh cells require both S1PR2 and CXCR5 to support a functional GC (Moriyama et al., 2014). Furthermore, S1PR2 is highly up-regulated in Tfr cells (Wing et al., 2017). Therefore, it is possible that S1PR2 is able to compensate for the loss of CXCR5 on Treg cells in *Cxcr5*$^{fl/fl}$*Foxp3*^{creERT2} mice. To determine whether CXCR5 and S1PR2 act redundantly in Tfr cell localisation, *S1pr2*$^{fl/fl}$*Cxcr5*$^{fl/fl}$*Foxp3*^{creERT2} mice could be used in future studies.

7.1.2 What is the function of Tfr cells within the GC?

Unravelling the role of Tfr cells within the GC has been difficult due to the fact that many studies yield different results. Recently, several groups have used the *Bcl6*$^{fl/fl}$*Foxp3*^{cre} system to study the role of Tfr cells within the GC (Wu et al., 2016a, Botta et al., 2017, Fu et al., 2018). First of all, in light of my findings that the cre enzyme in *Foxp3*^{cre} mice is leaky, these results should be interpreted with caution. Results obtained using the *Bcl6*$^{fl/fl}$*Foxp3*^{cre} system from a study by Botta *et al.* showed that Tfr cells are important for limiting the number of auto-reactive antibody secreting plasma cells (Botta et al., 2017). Furthermore, in the absence of Tfr cells, there is an increase in anti-nuclear antibodies after influenza infection. The authors were subsequently able to repeat the results by treating mice with recombinant IL-2, which inhibits Tfr cell formation. Thus, Tfr cells limit the generation of auto-reactive plasma cells, thereby potentially limiting autoimmunity.

It is possible that Tfr cells fine-tune the GC response rather than suppressing it. Indeed, it has been shown that Tfr cells produce IL-10, and that this IL-10 is responsible for supporting a DZ GC B cell phenotype (Laidlaw et al., 2017)(and our unpublished data). So, Tfr cells might drive a high-quality GC response by promoting further rounds of somatic hyper-mutation of GC B cells, thereby generating high affinity antibody secreting plasma cells.

This role of Tfr cells as “helpers” is in contrast to the original idea that Tfr cells act as dedicated suppressors of the GC, it now appears that they might fine-tune the GC response at

different stages instead. These results do not necessarily need to completely contradict earlier studies showing that Tfr cells limit the number of GC B cells and Tfh cells. Treg cells play a role at different locations and times during the GC response. Treg cells in the extra-follicular zone might be important for regulating the extra-follicular plasma cell responses, whereas those Treg cells (also referred to as $CD25^+$ Tfr cells) at the T:B border might inhibit cognate interactions between Tfh and GC B cells. Treg cells within the GC, the genuine Tfr cells, seem to be important in regulating the quality of the GC response, thereby preventing potential autoimmunity. Due to the fact that Tfr cells have only very recently been discovered and are therefore not completely characterised yet, it is difficult to distinguish between Tfr cells within the GC, Treg cells the T:B border and those in the extra-follicular area by flow cytometry. A better understanding of Tfr cell biology and their temporal and spatial organisation is required to understand what the effect is of conditionally deleting proteins required for Tfr cell localisation and function in Treg cells. For example, Bcl6 is expressed in waves and is up-regulated during the priming of naïve $CD4^+$ T cells. Whether this is also the case for Treg cells remains to be demonstrated, but if this is the case then deletion of Bcl6 will not only delete Treg cells within the GC, but also those at the T:B border and extra-follicular zone. Furthermore, the extent of control of the GC reaction by Tfr cells may also depend on the nature of the immune challenge. Given the TCR of Tfr cells is skewed towards self-antigens, deletion of Tfr cells in the context of a response to self antigens might have bigger consequences than in the context of immunisation with model protein antigens such as NP-KLH.

7.1.3 Final remarks

Tfr cells have only recently been discovered and because of this, there are still many essential questions that need answering. While it was initially thought that Tfr cells act to limit the size and output of the GC, it now appears that Tfr cells might have a more subtle role within the GC as well, fine-tuning the response to avoid autoimmunity. A more detailed characterisation of Tfr cells and how they differ from Treg cells at the T:B border and those in the extra-follicular zone is required to move this field of research forward. This will help in developing new tools to study Tfr cells, and perhaps in re-evaluating the seemingly contradictory results obtained by several groups in recent years.

7.2 The transcription factor Bcl6 shapes early thymic Treg development

The second aim of this thesis was to elucidate the role of Bcl6 in Tfr cell differentiation. Interestingly, the data described in Chapter 6 reveal a much broader role for Bcl6 in Treg cells than supporting Tfr cell differentiation. I have demonstrated that deletion of Bcl6 during early $CD4^+$ T cell development, prior to Foxp3 expression, in $Bcl6^{fl/fl}Cd4^{cre/+}$ mice leads to an early and broad Treg cell activation phenotype that persists in the periphery, suggesting that Bcl6 might suppress premature Treg cell activation during thymic T cell development. Although there have been many advances in understanding transcriptional regulation of thymic Treg cells in the context of Foxp3, the transcriptional requirements for thymic Treg cell differentiation prior to Foxp3 expression are not well understood. The data described in Chapter 6 led me to propose Bcl6 as a critical regulator of early thymic Treg cell differentiation by preventing premature Treg activation and differentiation.

7.2.1 Potential mechanisms for Bcl6 mediated control of thymic Treg cell development

The broad Treg cell activation phenotype observed in $Bcl6^{fl/fl}Cd4^{cre/+}$ mice indicates that Bcl6 plays a role during early Treg cell development in suppressing premature Treg cell activation, but what could drive this cellular phenotype is unclear.

I identified GATA3 as a transcription factor highly up-regulated at the DP stage of $Bcl6^{fl/fl}Cd4^{cre/+}$ mice. GATA3 is a crucial regulator of thymic T cell development, and is essential for driving the $CD4^+$ T cell fate (Hernandez-Hoyos et al., 2003). GATA3 also plays an essential role in Treg cell function through acting as an enhancer at the CNS2 locus of *Foxp3* (Wang et al., 2011). Bcl6 has previously been shown to directly bind to, and repress GATA3 in the context of Tfh cell differentiation, and is thought to maintain GATA3 enhancers in a poised state (Nurieva et al., 2009, Yu et al., 2009, Hatzi et al., 2015). In peripheral Treg cells, Bcl6 represses GATA3 and its transcriptional activity (Sawant et al., 2012). Thus, it is possible that Bcl6 controls GATA3 during early Treg cell development in the thymus to prevent premature activation of Treg cells.

Another interesting candidate for Bcl6 mediated repression is Basic leucine zipper transcription factor, ATF-like (Batf). Bcl6 binds and regulates Batf in thymocytes, and *Batf* transcripts are highly up-regulated in CD4 SP thymocytes in $Bcl6^{fl/fl}Cd4^{cre/+}$ mice (Mathew et

al., 2014). Batf is also an important regulator for the differentiation of tissue Treg cells, and mice with a targeted mutation in Foxp3 that disrupt Foxp3-DNA interaction with *Batf* results in impaired formation of tissue Treg cells (Hayatsu et al., 2017). tSNE analysis of thymic Treg cells in $Bcl6^{fl/fl}Cd4^{cre/+}$ mice identified a subset of Treg cells akin to tissue Treg cells with high expression of GATA3, St2 and KRLG-1. It is possible that Bcl6 controls Thymic Treg development through repression of *Batf*, and this could explain the tissue Treg phenotype observed in $Bcl6^{fl/fl}Cd4^{cre/+}$ mice. Notably, many more subsets of Treg cells showed altered expression levels in $Bcl6^{fl/fl}Cd4^{cre/+}$ mice, thus other mechanisms are probably involved.

Bcl6 is known to mutually repress Blimp-1 (Fu et al., 2017). Furthermore, Blimp1 drives effector Treg cell differentiation, and $Blimp1^{+}$ Treg cells express high levels of CD44, CD103, KLRG-1, while expressing low levels of CD62L, akin to the phenotype I observed in $Bcl6^{fl/fl}Cd4^{cre/+}$ mice (Cretney et al., 2011). Therefore, Bimp1 is an obvious candidate for Bcl6 mediated repression during early Treg cell differentiation.

Treg cell lineage commitment initially occurs independently of Foxp3 expression, and in response to strong and transient TCR signalling, CD4 SP cells differentiate into $CD25^{hi}$ pre-tTreg cells (Ohkura et al., 2012). Although it is clear that strong TCR signalling results in epigenetic changes that drive the Treg program, the transcriptional landscape that shapes pre-tTreg cell differentiation has not been well described. In GC B cells, Bcl6 has been shown to toggle enhancers from the activated to the poised state via de-acetylation (Hatzi et al., 2013). It is plausible that Bcl6 acts in a similar manner in pre-tTreg cells, maintaining Treg SE in a poised state to avoid premature activation. Bcl6 acting on enhancers, thus establishing a specific epigenetic landscape prior to Foxp3 expression, is in accord with the absence of a Treg activation phenotype in $Bcl6^{fl/fl}Foxp3^{cre\text{-}ERT2}$ mice. In line with the data that Bcl6 acts prior to Foxp3 expression, ChIP-seq analysis of Bcl6 in human Tfh cells showed that Bcl6 binds a network of Treg-associated genes, but not the Foxp3 locus itself (Hatzi et al., 2015). Motif analysis of the Bcl6 consensus sequence in Treg-SE revealed that there was a slight enrichment in Bcl6 motifs in Treg SE compared to Tconv cells. So, Bcl6 might maintain Treg-SE in a poised state during Treg development, thereby preventing premature lineage specification. However, the presence of the Bcl6 consensus motif does not necessarily mean Bcl6 binds at that site, and further work is required to confirm where Bcl6 binds in thymocytes. In addition, in Tfh cells, Bcl6 has been shown to bind at sites in the absence of the Bcl6 consensus motif through interaction with Activator protein 1 (AP-1) (Hatzi et al.,

2015). ChIP-seq should be performed in future experiments to determine Bcl6 binding sites during thymic Treg cell development.

7.2.2 Functional relevance

The recruitment of different co-repressors to distinct Bcl6 protein domains have been linked to different transcriptional repression mechanisms (Hatzi et al., 2013, Huang et al., 2013, Huang et al., 2014, Shen et al., 2018). Therefore, determining which domains of the Bcl6 protein are involved in Bcl6 mediated regulation of Treg cell development will provide an indication to which biochemical and biological functions Bcl6 plays during early Treg cell development. For this purpose, ideally mice with a targeted disruption of either the Bcl6 BTB domain or RD2 domain specifically in $CD4^+$ Tcells, rendering said domains unable to bind to co-repressor molecules, should be used (Huang et al., 2013, Huang et al., 2014). Alternatively, foetal thymic organ cultures (FTOC) could be used as an *in vitro* system that is easily manipulated. Using the FTOC system, the Bcl6 BTB domain could be disrupted at particular stages during development using BTB inhibitors, such as the peptide-mimetic RI-BPI compound (Cerchietti et al., 2009).

Based on the overt Treg cell activation phenotype in $Bcl6^{fl/fl}Cd4^{cre/+}$ mice one would expect an altered ability of the immune system to respond to immune challenges. However, in general, interpretation of immune pathologies observed in $Bcl6^{fl/fl}Cd4^{cre/+}$ mice is complicated due to the fact that these mice are unable to form GCs (Hollister et al., 2013). Furthermore, Tconv cells in $Bcl6^{fl/fl}Cd4^{cre/+}$ mice also showed a slightly increased activation phenotype, although not quite to the same extent as Treg cells, possibly counterbalancing the increased activation phenotype observed in Treg cells. In a mouse model of colitis, Treg cells derived from $Bcl6^{-/-}$ mice were as efficient as wild-type Treg cells in supressing gut inflammation, and $Bcl6^{-/-}$ Treg cells were better at suppressing Tconv cell proliferation in an *in vitro* suppression assay compared to wild-type Treg cells, consistent with them having a highly activated phenotype (Sawant et al., 2012). Perhaps, a better model system to evaluate the function of the highly activated Treg cells in $Bcl6^{fl/fl}Cd4^{cre/+}$, would be in the context of tumour immunology. The presence of activated Treg cells is thought to be detrimental to T cell mediated immunity to tumour-associated antigens (Zou, 2006). Thus, given the highly activated phenotype of Treg cells in $Bcl6^{fl/fl}Cd4^{cre/+}$ mice, I would hypothesise a reduced anti-tumour response in these mice.

7.2.3 Final remarks

It is clear that Bcl6 plays a broad role during early thymic Treg cell development. However, at this stage I can only speculate on the potential roles of Bcl6 in directing thymic Treg cell development. Further research will hopefully shed light on the mechanisms involved in Bcl6 mediated transcriptional regulation of thymic Treg cell development.

8 References

Abbas, A. K., Benoist, C., Bluestone, J. A., Campbell, D. J., Ghosh, S., Hori, S., Jiang, S., Kuchroo, V. K., Mathis, D., Roncarolo, M. G., Rudensky, A., Sakaguchi, S., Shevach, E. M., Vignali, D. A. & Ziegler, S. F. 2013. Regulatory T cells: recommendations to simplify the nomenclature. *Nat Immunol,* 14**,** 307-8.

Afkarian, M., Sedy, J. R., Yang, J., Jacobson, N. G., Cereb, N., Yang, S. Y., Murphy, T. L. & Murphy, K. M. 2002. T-bet is a STAT1-induced regulator of IL-12R expression in naive CD4+ T cells. *Nat Immunol,* 3**,** 549-57.

Ahmad, K. F., Melnick, A., Lax, S., Bouchard, D., Liu, J., Kiang, C. L., Mayer, S., Takahashi, S., Licht, J. D. & Prive, G. G. 2003. Mechanism of SMRT corepressor recruitment by the BCL6 BTB domain. *Mol Cell,* 12**,** 1551-64.

Allen, C. D., Ansel, K. M., Low, C., Lesley, R., Tamamura, H., Fujii, N. & Cyster, J. G. 2004. Germinal center dark and light zone organization is mediated by CXCR4 and CXCR5. *Nat Immunol,* 5**,** 943-52.

Allen, C. D. & Cyster, J. G. 2008. Follicular dendritic cell networks of primary follicles and germinal centers: phenotype and function. *Semin Immunol,* 20**,** 14-25.

Aloulou, M., Carr, E. J., Gador, M., Bignon, A., Liblau, R. S., Fazilleau, N. & Linterman, M. A. 2016. Follicular regulatory T cells can be specific for the immunizing antigen and derive from naive T cells. *Nat Commun,* 7**,** 10579.

Amir El, A. D., Davis, K. L., Tadmor, M. D., Simonds, E. F., Levine, J. H., Bendall, S. C., Shenfeld, D. K., Krishnaswamy, S., Nolan, G. P. & Pe'er, D. 2013. viSNE enables visualization of high dimensional single-cell data and reveals phenotypic heterogeneity of leukemia. *Nat Biotechnol,* 31**,** 545-52.

Anderson, M. S. & Su, M. A. 2016. AIRE expands: new roles in immune tolerance and beyond. *Nat Rev Immunol,* 16**,** 247-58.

Anderson, M. S., Venanzi, E. S., Chen, Z., Berzins, S. P., Benoist, C. & Mathis, D. 2005. The cellular mechanism of Aire control of T cell tolerance. *Immunity,* 23**,** 227-39.

Anderson, M. S., Venanzi, E. S., Klein, L., Chen, Z., Berzins, S. P., Turley, S. J., Von Boehmer, H., Bronson, R., Dierich, A., Benoist, C. & Mathis, D. 2002. Projection of an immunological self shadow within the thymus by the aire protein. *Science,* 298**,** 1395-401.

Ansel, K. M., Mcheyzer-Williams, L. J., Ngo, V. N., Mcheyzer-Williams, M. G. & Cyster, J. G. 1999. In vivo-activated CD4 T cells upregulate CXC chemokine receptor 5 and reprogram their response to lymphoid chemokines. *J Exp Med,* 190**,** 1123-34.

Apostolou, I. & Von Boehmer, H. 2004. In vivo instruction of suppressor commitment in naive T cells. *J Exp Med,* 199**,** 1401-8.

Ara, T., Itoi, M., Kawabata, K., Egawa, T., Tokoyoda, K., Sugiyama, T., Fujii, N., Amagai, T. & Nagasawa, T. 2003. A role of CXC chemokine ligand 12/stromal cell-derived factor-1/pre-B cell growth stimulating factor and its receptor CXCR4 in fetal and adult T cell development in vivo. *J Immunol,* 170**,** 4649-55.

Asano, M., Toda, M., Sakaguchi, N. & Sakaguchi, S. 1996. Autoimmune disease as a consequence of developmental abnormality of a T cell subpopulation. *J Exp Med,* 184**,** 387-96.

Ballesteros-Tato, A., Leon, B., Graf, B. A., Moquin, A., Adams, P. S., Lund, F. E. & Randall, T. D. 2012. Interleukin-2 inhibits germinal center formation by limiting T follicular helper cell differentiation. *Immunity,* 36**,** 847-56.

Ballesteros-Tato, A. & Randall, T. D. 2014. Priming of T follicular helper cells by dendritic cells. *Immunol Cell Biol,* 92**,** 22-7.

Banchereau, J. & Steinman, R. M. 1998. Dendritic cells and the control of immunity. *Nature,* 392**,** 245-52.

Barndt, R. J., Dai, M. & Zhuang, Y. 2000. Functions of E2A-HEB heterodimers in T-cell development revealed by a dominant negative mutation of HEB. *Mol Cell Biol,* 20**,** 6677-85.

Baron, U., Floess, S., Wieczorek, G., Baumann, K., Grutzkau, A., Dong, J., Thiel, A., Boeld, T. J., Hoffmann, P., Edinger, M., Turbachova, I., Hamann, A., Olek, S. & Huehn, J. 2007. DNA demethylation in the human FOXP3 locus discriminates regulatory T cells from activated FOXP3(+) conventional T cells. *Eur J Immunol,* 37**,** 2378-89.

Batista, F. D. & Harwood, N. E. 2009. The who, how and where of antigen presentation to B cells. *Nat Rev Immunol,* 9**,** 15-27.

Batten, M., Ramamoorthi, N., Kljavin, N. M., Ma, C. S., Cox, J. H., Dengler, H. S., Danilenko, D. M., Caplazi, P., Wong, M., Fulcher, D. A., Cook, M. C., King, C., Tangye, S. G., De Sauvage, F. J. & Ghilardi, N. 2010. IL-27 supports germinal center function by enhancing IL-21 production and the function of T follicular helper cells. *J Exp Med,* 207**,** 2895-906.

Beck, T. C., Gomes, A. C., Cyster, J. G. & Pereira, J. P. 2014. CXCR4 and a cell-extrinsic mechanism control immature B lymphocyte egress from bone marrow. *J Exp Med,* 211**,** 2567-81.

Benson, M. J., Pino-Lagos, K., Rosemblatt, M. & Noelle, R. J. 2007. All-trans retinoic acid mediates enhanced T reg cell growth, differentiation, and gut homing in the face of high levels of co-stimulation. *J Exp Med,* 204**,** 1765-74.

Bereshchenko, O. R., Gu, W. & Dalla-Favera, R. 2002. Acetylation inactivates the transcriptional repressor BCL6. *Nat Genet,* 32**,** 606-13.

Botta, D., Fuller, M. J., Marquez-Lago, T. T., Bachus, H., Bradley, J. E., Weinmann, A. S., Zajac, A. J., Randall, T. D., Lund, F. E., Leon, B. & Ballesteros-Tato, A. 2017. Dynamic regulation of T follicular regulatory cell responses by interleukin 2 during influenza infection. *Nat Immunol,* 18**,** 1249-1260.

Bradford, B. M., Reizis, B. & Mabbott, N. A. 2017. Oral Prion Disease Pathogenesis Is Impeded in the Specific Absence of CXCR5-Expressing Dendritic Cells. *J Virol,* 91.

Brugnera, E., Bhandoola, A., Cibotti, R., Yu, Q., Guinter, T. I., Yamashita, Y., Sharrow, S. O. & Singer, A. 2000. Coreceptor reversal in the thymus: signaled CD4+8+ thymocytes initially terminate CD8 transcription even when differentiating into CD8+ T cells. *Immunity,* 13**,** 59-71.

Bryant, V. L., Ma, C. S., Avery, D. T., Li, Y., Good, K. L., Corcoran, L. M., De Waal Malefyt, R. & Tangye, S. G. 2007. Cytokine-mediated regulation of human B cell differentiation into Ig-secreting cells: predominant role of IL-21 produced by CXCR5+ T follicular helper cells. *J Immunol,* 179**,** 8180-90.

Burchill, M. A., Yang, J., Vang, K. B., Moon, J. J., Chu, H. H., Lio, C. W., Vegoe, A. L., Hsieh, C. S., Jenkins, M. K. & Farrar, M. A. 2008. Linked T cell receptor and cytokine signaling govern the development of the regulatory T cell repertoire. *Immunity,* 28**,** 112-21.

Burchill, M. A., Yang, J., Vogtenhuber, C., Blazar, B. R. & Farrar, M. A. 2007. IL-2 receptor beta-dependent STAT5 activation is required for the development of Foxp3+ regulatory T cells. *J Immunol,* 178**,** 280-90.

Cai, G., Nie, X., Zhang, W., Wu, B., Lin, J., Wang, H., Jiang, C. & Shen, Q. 2012. A regulatory role for IL-10 receptor signaling in development and B cell help of T follicular helper cells in mice. *J Immunol,* 189**,** 1294-302.

Cannons, J. L., Qi, H., Lu, K. T., Dutta, M., Gomez-Rodriguez, J., Cheng, J., Wakeland, E. K., Germain, R. N. & Schwartzberg, P. L. 2010. Optimal germinal center responses require a multistage T cell:B cell adhesion process involving integrins, SLAM-associated protein, and CD84. *Immunity,* 32**,** 253-65.

Carrasco, Y. R. & Batista, F. D. 2007. B cells acquire particulate antigen in a macrophage-rich area at the boundary between the follicle and the subcapsular sinus of the lymph node. *Immunity,* 27**,** 160-71.

Cerchietti, L. C., Hatzi, K., Caldas-Lopes, E., Yang, S. N., Figueroa, M. E., Morin, R. D., Hirst, M., Mendez, L., Shaknovich, R., Cole, P. A., Bhalla, K., Gascoyne, R. D., Marra, M., Chiosis, G. & Melnick, A. 2010. BCL6 repression of EP300 in human diffuse large B cell lymphoma cells provides a basis for rational combinatorial therapy. *J Clin Invest,* 120**,** 4569-82.

Cerchietti, L. C., Yang, S. N., Shaknovich, R., Hatzi, K., Polo, J. M., Chadburn, A., Dowdy, S. F. & Melnick, A. 2009. A peptomimetic inhibitor of BCL6 with potent antilymphoma effects in vitro and in vivo. *Blood,* 113**,** 3397-405.

Chan, T. D., Gatto, D., Wood, K., Camidge, T., Basten, A. & Brink, R. 2009. Antigen affinity controls rapid T-dependent antibody production by driving the expansion rather than the differentiation or extrafollicular migration of early plasmablasts. *J Immunol,* 183**,** 3139-49.

Chaudhry, A., Rudra, D., Treuting, P., Samstein, R. M., Liang, Y., Kas, A. & Rudensky, A. Y. 2009. CD4+ regulatory T cells control TH17 responses in a Stat3-dependent manner. *Science,* 326**,** 986-91.

Chaudhry, A., Samstein, R. M., Treuting, P., Liang, Y., Pils, M. C., Heinrich, J. M., Jack, R. S., Wunderlich, F. T., Bruning, J. C., Muller, W. & Rudensky, A. Y. 2011. Interleukin-10 signaling in regulatory T cells is required for suppression of Th17 cell-mediated inflammation. *Immunity,* 34**,** 566-78.

Chinen, T., Kannan, A. K., Levine, A. G., Fan, X., Klein, U., Zheng, Y., Gasteiger, G., Feng, Y., Fontenot, J. D. & Rudensky, A. Y. 2016. An essential role for the IL-2 receptor in Treg cell function. *Nat Immunol,* 17**,** 1322-1333.

Choi, Y. S., Kageyama, R., Eto, D., Escobar, T. C., Johnston, R. J., Monticelli, L., Lao, C. & Crotty, S. 2011. ICOS receptor instructs T follicular helper cell versus effector cell differentiation via induction of the transcriptional repressor Bcl6. *Immunity,* 34**,** 932-46.

Chung, Y., Tanaka, S., Chu, F., Nurieva, R. I., Martinez, G. J., Rawal, S., Wang, Y. H., Lim, H., Reynolds, J. M., Zhou, X. H., Fan, H. M., Liu, Z. M., Neelapu, S. S. & Dong, C. 2011. Follicular regulatory T cells expressing Foxp3 and Bcl-6 suppress germinal center reactions. *Nat Med,* 17**,** 983-8.

Cobaleda, C., Schebesta, A., Delogu, A. & Busslinger, M. 2007. Pax5: the guardian of B cell identity and function. *Nat Immunol,* 8**,** 463-70.

Cooley, I. D., Read, K. A. & Oestreich, K. J. 2015. Trans-presentation of IL-15 modulates STAT5 activation and Bcl-6 expression in TH1 cells. *Sci Rep,* 5**,** 15722.

Coombes, J. L., Siddiqui, K. R., Arancibia-Carcamo, C. V., Hall, J., Sun, C. M., Belkaid, Y. & Powrie, F. 2007. A functionally specialized population of mucosal CD103+ DCs induces Foxp3+ regulatory T cells via a TGF-beta and retinoic acid-dependent mechanism. *J Exp Med,* 204**,** 1757-64.

Coquet, J. M., Ribot, J. C., Babala, N., Middendorp, S., Van Der Horst, G., Xiao, Y., Neves, J. F., Fonseca-Pereira, D., Jacobs, H., Pennington, D. J., Silva-Santos, B. & Borst, J. 2013. Epithelial and dendritic cells in the thymic medulla promote CD4+Foxp3+ regulatory T cell development via the CD27-CD70 pathway. *J Exp Med,* 210**,** 715-28.

Corfe, S. A. & Paige, C. J. 2012. The many roles of IL-7 in B cell development; mediator of survival, proliferation and differentiation. *Semin Immunol,* 24**,** 198-208.

Cowan, J. E., Parnell, S. M., Nakamura, K., Caamano, J. H., Lane, P. J., Jenkinson, E. J., Jenkinson, W. E. & Anderson, G. 2013. The thymic medulla is required for Foxp3+ regulatory but not conventional CD4+ thymocyte development. *J Exp Med,* 210**,** 675-81.

Cretney, E., Kallies, A. & Nutt, S. L. 2013. Differentiation and function of Foxp3(+) effector regulatory T cells. *Trends Immunol,* 34**,** 74-80.

Cretney, E., Xin, A., Shi, W., Minnich, M., Masson, F., Miasari, M., Belz, G. T., Smyth, G. K., Busslinger, M., Nutt, S. L. & Kallies, A. 2011. The transcription factors Blimp-1 and IRF4 jointly control the differentiation and function of effector regulatory T cells. *Nat Immunol,* 12**,** 304-11.

Crotty, S., Johnston, R. J. & Schoenberger, S. P. 2010. Effectors and memories: Bcl-6 and Blimp-1 in T and B lymphocyte differentiation. *Nat Immunol,* 11**,** 114-20.

Crotty, S., Kersh, E. N., Cannons, J., Schwartzberg, P. L. & Ahmed, R. 2003. SAP is required for generating long-term humoral immunity. *Nature,* 421**,** 282-7.

Deenick, E. K., Chan, A., Ma, C. S., Gatto, D., Schwartzberg, P. L., Brink, R. & Tangye, S. G. 2010. Follicular helper T cell differentiation requires continuous antigen presentation that is independent of unique B cell signaling. *Immunity,* 33**,** 241-53.

Derbinski, J., Gabler, J., Brors, B., Tierling, S., Jonnakuty, S., Hergenhahn, M., Peltonen, L., Walter, J. & Kyewski, B. 2005. Promiscuous gene expression in thymic epithelial cells is regulated at multiple levels. *J Exp Med,* 202**,** 33-45.

Devoss, J., Hou, Y., Johannes, K., Lu, W., Liou, G. I., Rinn, J., Chang, H., Caspi, R. R., Fong, L. & Anderson, M. S. 2006. Spontaneous autoimmunity prevented by thymic expression of a single self-antigen. *J Exp Med,* 203**,** 2727-35.

El-Haibi, C. P., Sharma, P., Singh, R., Gupta, P., Taub, D. D., Singh, S. & Lillard, J. W., Jr. 2013. Differential G protein subunit expression by prostate cancer cells and their interaction with CXCR5. *Mol Cancer,* 12**,** 64.

Elsner, R. A., Ernst, D. N. & Baumgarth, N. 2012. Single and coexpression of CXCR4 and CXCR5 identifies CD4 T helper cells in distinct lymph node niches during influenza virus infection. *J Virol,* 86**,** 7146-57.

Engel, I. & Murre, C. 2004. E2A proteins enforce a proliferation checkpoint in developing thymocytes. *EMBO J,* 23**,** 202-11.

Essig, K., Hu, D., Guimaraes, J. C., Alterauge, D., Edelmann, S., Raj, T., Kranich, J., Behrens, G., Heiseke, A., Floess, S., Klein, J., Maiser, A., Marschall, S., Hrabe De Angelis, M., Leonhardt, H., Calkhoven, C. F., Noessner, E., Brocker, T., Huehn, J., Krug, A. B., Zavolan, M., Baumjohann, D. & Heissmeyer, V. 2017. Roquin Suppresses the PI3K-mTOR Signaling Pathway to Inhibit T Helper Cell Differentiation and Conversion of Treg to Tfr Cells. *Immunity,* 47**,** 1067-1082 e12.

Feng, Y., Arvey, A., Chinen, T., Van Der Veeken, J., Gasteiger, G. & Rudensky, A. Y. 2014. Control of the inheritance of regulatory T cell identity by a cis element in the Foxp3 locus. *Cell,* 158**,** 749-763.

Feng, Y., Van Der Veeken, J., Shugay, M., Putintseva, E. V., Osmanbeyoglu, H. U., Dikiy, S., Hoyos, B. E., Moltedo, B., Hemmers, S., Treuting, P., Leslie, C. S., Chudakov, D. M. & Rudensky, A. Y. 2015. A mechanism for expansion of regulatory T-cell repertoire and its role in self-tolerance. *Nature,* 528**,** 132-136.

Fink, P. J. 2013. The biology of recent thymic emigrants. *Annu Rev Immunol,* 31**,** 31-50.

Floess, S., Freyer, J., Siewert, C., Baron, U., Olek, S., Polansky, J., Schlawe, K., Chang, H. D., Bopp, T., Schmitt, E., Klein-Hessling, S., Serfling, E., Hamann, A. & Huehn, J. 2007. Epigenetic control of the foxp3 locus in regulatory T cells. *PLoS Biol,* 5**,** e38.

Fonseca, V. R., Agua-Doce, A., Maceiras, A. R., Pierson, W., Ribeiro, F., Romao, V. C., Pires, A. R., Da Silva, S. L., Fonseca, J. E., Sousa, A. E., Linterman, M. A. & Graca, L. 2017. Human blood Tfr cells are indicators of ongoing humoral activity not fully licensed with suppressive function. *Sci Immunol,* 2.

Fontenot, J. D., Dooley, J. L., Farr, A. G. & Rudensky, A. Y. 2005a. Developmental regulation of Foxp3 expression during ontogeny. *J Exp Med,* 202**,** 901-6.

Fontenot, J. D., Gavin, M. A. & Rudensky, A. Y. 2003. Foxp3 programs the development and function of CD4+CD25+ regulatory T cells. *Nat Immunol,* 4**,** 330-6.

Fontenot, J. D., Rasmussen, J. P., Gavin, M. A. & Rudensky, A. Y. 2005b. A function for interleukin 2 in Foxp3-expressing regulatory T cells. *Nat Immunol,* 6**,** 1142-51.

Forster, R., Mattis, A. E., Kremmer, E., Wolf, E., Brem, G. & Lipp, M. 1996. A putative chemokine receptor, BLR1, directs B cell migration to defined lymphoid organs and specific anatomic compartments of the spleen. *Cell,* 87**,** 1037-47.

Forster, R., Schubel, A., Breitfeld, D., Kremmer, E., Renner-Muller, I., Wolf, E. & Lipp, M. 1999. CCR7 coordinates the primary immune response by establishing functional microenvironments in secondary lymphoid organs. *Cell,* 99**,** 23-33.

Franckaert, D., Dooley, J., Roos, E., Floess, S., Huehn, J., Luche, H., Fehling, H. J., Liston, A., Linterman, M. A. & Schlenner, S. M. 2015. Promiscuous Foxp3-cre activity reveals a differential requirement for CD28 in Foxp3(+) and Foxp3(-) T cells. *Immunol Cell Biol,* 93**,** 417-23.

Fu, S. H., Yeh, L. T., Chu, C. C., Yen, B. L. & Sytwu, H. K. 2017. New insights into Blimp-1 in T lymphocytes: a divergent regulator of cell destiny and effector function. *J Biomed Sci,* 24**,** 49.

Fu, W., Liu, X., Lin, X., Feng, H., Sun, L., Li, S., Chen, H., Tang, H., Lu, L., Jin, W. & Dong, C. 2018. Deficiency in T follicular regulatory cells promotes autoimmunity. *J Exp Med*.

Fujita, N., Jaye, D. L., Geigerman, C., Akyildiz, A., Mooney, M. R., Boss, J. M. & Wade, P. A. 2004. MTA3 and the Mi-2/NuRD complex regulate cell fate during B lymphocyte differentiation. *Cell,* 119**,** 75-86.

Furtado, G. C., Curotto De Lafaille, M. A., Kutchukhidze, N. & Lafaille, J. J. 2002. Interleukin 2 signaling is required for CD4(+) regulatory T cell function. *J Exp Med,* 196**,** 851-7.

Gatto, D., Paus, D., Basten, A., Mackay, C. R. & Brink, R. 2009. Guidance of B cells by the orphan G protein-coupled receptor EBI2 shapes humoral immune responses. *Immunity,* 31**,** 259-69.

Ghetu, A. F., Corcoran, C. M., Cerchietti, L., Bardwell, V. J., Melnick, A. & Prive, G. G. 2008. Structure of a BCOR corepressor peptide in complex with the BCL6 BTB domain dimer. *Mol Cell,* 29**,** 384-91.

Gitlin, A. D., Shulman, Z. & Nussenzweig, M. C. 2014. Clonal selection in the germinal centre by regulated proliferation and hypermutation. *Nature,* 509**,** 637-40.

Good-Jacobson, K. L., Szumilas, C. G., Chen, L., Sharpe, A. H., Tomayko, M. M. & Shlomchik, M. J. 2010. PD-1 regulates germinal center B cell survival and the formation and affinity of long-lived plasma cells. *Nat Immunol,* 11**,** 535-42.

Greco, V. & Guo, S. 2010. Compartmentalized organization: a common and required feature of stem cell niches? *Development,* 137**,** 1586-94.

Green, J. A., Suzuki, K., Cho, B., Willison, L. D., Palmer, D., Allen, C. D., Schmidt, T. H., Xu, Y., Proia, R. L., Coughlin, S. R. & Cyster, J. G. 2011. The sphingosine 1-phosphate receptor S1P(2) maintains the homeostasis of germinal center B cells and promotes niche confinement. *Nat Immunol,* 12**,** 672-80.

Gunn, M. D., Kyuwa, S., Tam, C., Kakiuchi, T., Matsuzawa, A., Williams, L. T. & Nakano, H. 1999. Mice lacking expression of secondary lymphoid organ chemokine have defects in lymphocyte homing and dendritic cell localization. *J Exp Med,* 189**,** 451-60.

Hadis, U., Wahl, B., Schulz, O., Hardtke-Wolenski, M., Schippers, A., Wagner, N., Muller, W., Sparwasser, T., Forster, R. & Pabst, O. 2011. Intestinal tolerance requires gut homing and expansion of FoxP3+ regulatory T cells in the lamina propria. *Immunity,* 34**,** 237-46.

Han, S., Hathcock, K., Zheng, B., Kepler, T. B., Hodes, R. & Kelsoe, G. 1995. Cellular interaction in germinal centers. Roles of CD40 ligand and B7-2 in established germinal centers. *J Immunol,* 155**,** 556-67.

Hardtke, S., Ohl, L. & Forster, R. 2005. Balanced expression of CXCR5 and CCR7 on follicular T helper cells determines their transient positioning to lymph node follicles and is essential for efficient B-cell help. *Blood,* 106**,** 1924-31.

Harrington, L. E., Hatton, R. D., Mangan, P. R., Turner, H., Murphy, T. L., Murphy, K. M. & Weaver, C. T. 2005. Interleukin 17-producing CD4+ effector T cells develop via a lineage distinct from the T helper type 1 and 2 lineages. *Nat Immunol,* 6**,** 1123-32.

Hatzi, K., Jiang, Y., Huang, C., Garrett-Bakelman, F., Gearhart, M. D., Giannopoulou, E. G., Zumbo, P., Kirouac, K., Bhaskara, S., Polo, J. M., Kormaksson, M., Mackerell, A. D., Jr., Xue, F., Mason, C. E., Hiebert, S. W., Prive, G. G., Cerchietti, L., Bardwell, V. J., Elemento, O. & Melnick, A. 2013. A hybrid mechanism of action for BCL6 in B cells defined by formation of functionally distinct complexes at enhancers and promoters. *Cell Rep,* 4**,** 578-88.

Hatzi, K., Nance, J. P., Kroenke, M. A., Bothwell, M., Haddad, E. K., Melnick, A. & Crotty, S. 2015. BCL6 orchestrates Tfh cell differentiation via multiple distinct mechanisms. *J Exp Med,* 212**,** 539-53.

Hayatsu, N., Miyao, T., Tachibana, M., Murakami, R., Kimura, A., Kato, T., Kawakami, E., Endo, T. A., Setoguchi, R., Watarai, H., Nishikawa, T., Yasuda, T., Yoshida, H. & Hori, S. 2017. Analyses of a Mutant Foxp3 Allele Reveal BATF as a Critical Transcription Factor in the Differentiation and Accumulation of Tissue Regulatory T Cells. *Immunity,* 47**,** 268-283 e9.

Haynes, N. M., Allen, C. D., Lesley, R., Ansel, K. M., Killeen, N. & Cyster, J. G. 2007. Role of CXCR5 and CCR7 in follicular Th cell positioning and appearance of a programmed cell death gene-1high germinal center-associated subpopulation. *J Immunol,* 179**,** 5099-108.

Hernandez-Hoyos, G., Anderson, M. K., Wang, C., Rothenberg, E. V. & Alberola-Ila, J. 2003. GATA-3 expression is controlled by TCR signals and regulates CD4/CD8 differentiation. *Immunity,* 19**,** 83-94.

Herzog, S., Reth, M. & Jumaa, H. 2009. Regulation of B-cell proliferation and differentiation by pre-B-cell receptor signalling. *Nat Rev Immunol,* 9**,** 195-205.

Hiramatsu, Y., Suto, A., Kashiwakuma, D., Kanari, H., Kagami, S., Ikeda, K., Hirose, K., Watanabe, N., Grusby, M. J., Iwamoto, I. & Nakajima, H. 2010. c-Maf activates the promoter and enhancer of the IL-21 gene, and TGF-beta inhibits c-Maf-induced IL-21 production in CD4+ T cells. *J Leukoc Biol,* 87**,** 703-12.

Hoffmann, J. A., Kafatos, F. C., Janeway, C. A. & Ezekowitz, R. A. 1999. Phylogenetic perspectives in innate immunity. *Science,* 284**,** 1313-8.

Hollister, K., Kusam, S., Wu, H., Clegg, N., Mondal, A., Sawant, D. V. & Dent, A. L. 2013. Insights into the role of Bcl6 in follicular Th cells using a new conditional mutant mouse model. *J Immunol,* 191**,** 3705-11.

Hori, S., Nomura, T. & Sakaguchi, S. 2003. Control of regulatory T cell development by the transcription factor Foxp3. *Science,* 299**,** 1057-61.

Hsieh, C. S., Lee, H. M. & Lio, C. W. 2012. Selection of regulatory T cells in the thymus. *Nat Rev Immunol,* 12**,** 157-67.

Hsieh, C. S., Zheng, Y., Liang, Y., Fontenot, J. D. & Rudensky, A. Y. 2006. An intersection between the self-reactive regulatory and nonregulatory T cell receptor repertoires. *Nat Immunol,* 7**,** 401-10.

Huang, C., Gonzalez, D. G., Cote, C. M., Jiang, Y., Hatzi, K., Teater, M., Dai, K., Hla, T., Haberman, A. M. & Melnick, A. 2014. The BCL6 RD2 domain governs commitment of activated B cells to form germinal centers. *Cell Rep,* 8**,** 1497-508.

Huang, C., Hatzi, K. & Melnick, A. 2013. Lineage-specific functions of Bcl-6 in immunity and inflammation are mediated by distinct biochemical mechanisms. *Nat Immunol,* 14**,** 380-8.

Huehn, J., Polansky, J. K. & Hamann, A. 2009. Epigenetic control of FOXP3 expression: the key to a stable regulatory T-cell lineage? *Nat Rev Immunol,* 9**,** 83-9.

Huynh, A., Dupage, M., Priyadharshini, B., Sage, P. T., Quiros, J., Borges, C. M., Townamchai, N., Gerriets, V. A., Rathmell, J. C., Sharpe, A. H., Bluestone, J. A. & Turka, L. A. 2015. Control of PI(3) kinase in Treg cells maintains homeostasis and lineage stability. *Nat Immunol,* 16**,** 188-96.

Huynh, K. D. & Bardwell, V. J. 1998. The BCL-6 POZ domain and other POZ domains interact with the co-repressors N-CoR and SMRT. *Oncogene,* 17**,** 2473-84.

Huynh, K. D., Fischle, W., Verdin, E. & Bardwell, V. J. 2000. BCoR, a novel corepressor involved in BCL-6 repression. *Genes Dev,* 14**,** 1810-23.

Inaba, K., Turley, S., Iyoda, T., Yamaide, F., Shimoyama, S., Reis E Sousa, C., Germain, R. N., Mellman, I. & Steinman, R. M. 2000. The formation of immunogenic major histocompatibility complex class II-peptide ligands in lysosomal compartments of dendritic cells is regulated by inflammatory stimuli. *J Exp Med,* 191**,** 927-36.

Janas, M. L., Varano, G., Gudmundsson, K., Noda, M., Nagasawa, T. & Turner, M. 2010. Thymic development beyond beta-selection requires phosphatidylinositol 3-kinase activation by CXCR4. *J Exp Med,* 207**,** 247-61.

Jandl, C., Liu, S. M., Canete, P. F., Warren, J., Hughes, W. E., Vogelzang, A., Webster, K., Craig, M. E., Uzel, G., Dent, A., Stepensky, P., Keller, B., Warnatz, K., Sprent, J. & King, C. 2017. IL-21 restricts T follicular regulatory T cell proliferation through Bcl-6 mediated inhibition of responsiveness to IL-2. *Nat Commun,* 8**,** 14647.

Janeway, C. A., Jr. 1989. Approaching the asymptote? Evolution and revolution in immunology. *Cold Spring Harb Symp Quant Biol,* 54 Pt 1**,** 1-13.

Janeway, C. A., Jr. & Medzhitov, R. 2002. Innate immune recognition. *Annu Rev Immunol,* 20**,** 197-216.

Johnston, R. J., Choi, Y. S., Diamond, J. A., Yang, J. A. & Crotty, S. 2012. STAT5 is a potent negative regulator of TFH cell differentiation. *J Exp Med,* 209**,** 243-50.

Johnston, R. J., Poholek, A. C., Ditoro, D., Yusuf, I., Eto, D., Barnett, B., Dent, A. L., Craft, J. & Crotty, S. 2009. Bcl6 and Blimp-1 are reciprocal and antagonistic regulators of T follicular helper cell differentiation. *Science,* 325**,** 1006-10.

Jordan, M. S., Boesteanu, A., Reed, A. J., Petrone, A. L., Holenbeck, A. E., Lerman, M. A., Naji, A. & Caton, A. J. 2001. Thymic selection of CD4+CD25+ regulatory T cells induced by an agonist self-peptide. *Nat Immunol,* 2**,** 301-6.

Josefowicz, S. Z., Niec, R. E., Kim, H. Y., Treuting, P., Chinen, T., Zheng, Y., Umetsu, D. T. & Rudensky, A. Y. 2012. Extrathymically generated regulatory T cells control mucosal TH2 inflammation. *Nature,* 482**,** 395-9.

Junt, T., Moseman, E. A., Iannacone, M., Massberg, S., Lang, P. A., Boes, M., Fink, K., Henrickson, S. E., Shayakhmetov, D. M., Di Paolo, N. C., Van Rooijen, N., Mempel, T. R., Whelan, S. P. & Von Andrian, U. H. 2007. Subcapsular sinus macrophages in lymph nodes clear lymph-borne viruses and present them to antiviral B cells. *Nature,* 450**,** 110-4.

Karagianni, P. & Wong, J. 2007. HDAC3: taking the SMRT-N-CoRrect road to repression. *Oncogene,* 26**,** 5439-49.

Kawamata, N., Miki, T., Ohashi, K., Suzuki, K., Fukuda, T., Hirosawa, S. & Aoki, N. 1994. Recognition DNA sequence of a novel putative transcription factor, BCL6. *Biochem Biophys Res Commun,* 204**,** 366-74.

Kawamoto, S., Tran, T. H., Maruya, M., Suzuki, K., Doi, Y., Tsutsui, Y., Kato, L. M. & Fagarasan, S. 2012. The inhibitory receptor PD-1 regulates IgA selection and bacterial composition in the gut. *Science,* 336**,** 485-9.

Kerckaert, J. P., Deweindt, C., Tilly, H., Quief, S., Lecocq, G. & Bastard, C. 1993. LAZ3, a novel zinc-finger encoding gene, is disrupted by recurring chromosome 3q27 translocations in human lymphomas. *Nat Genet,* 5**,** 66-70.

Kerfoot, S. M., Yaari, G., Patel, J. R., Johnson, K. L., Gonzalez, D. G., Kleinstein, S. H. & Haberman, A. M. 2011. Germinal center B cell and T follicular helper cell development initiates in the interfollicular zone. *Immunity,* 34**,** 947-60.

Khattri, R., Cox, T., Yasayko, S. A. & Ramsdell, F. 2003. An essential role for Scurfin in CD4+CD25+ T regulatory cells. *Nat Immunol,* 4**,** 337-42.

Kim, H. J., Verbinnen, B., Tang, X., Lu, L. & Cantor, H. 2010. Inhibition of follicular T-helper cells by CD8(+) regulatory T cells is essential for self tolerance. *Nature,* 467**,** 328-32.

Kim, Y. U., Kim, B. S., Lim, H., Wetsel, R. A. & Chung, Y. 2017. Enforced Expression of CXCR5 Drives T Follicular Regulatory-Like Features in Foxp3(+) T Cells. *Biomol Ther (Seoul),* 25**,** 130-139.

Kitagawa, Y., Ohkura, N., Kidani, Y., Vandenbon, A., Hirota, K., Kawakami, R., Yasuda, K., Motooka, D., Nakamura, S., Kondo, M., Taniuchi, I., Kohwi-Shigematsu, T. & Sakaguchi, S. 2017. Guidance of regulatory T cell development by Satb1-dependent super-enhancer establishment. *Nat Immunol,* 18**,** 173-183.

Koch, M. A., Thomas, K. R., Perdue, N. R., Smigiel, K. S., Srivastava, S. & Campbell, D. J. 2012. T-bet(+) Treg cells undergo abortive Th1 cell differentiation due to impaired expression of IL-12 receptor beta2. *Immunity,* 37**,** 501-10.

Koch, M. A., Tucker-Heard, G., Perdue, N. R., Killebrew, J. R., Urdahl, K. B. & Campbell, D. J. 2009. The transcription factor T-bet controls regulatory T cell homeostasis and function during type 1 inflammation. *Nat Immunol,* 10**,** 595-602.

Kohu, K., Sato, T., Ohno, S., Hayashi, K., Uchino, R., Abe, N., Nakazato, M., Yoshida, N., Kikuchi, T., Iwakura, Y., Inoue, Y., Watanabe, T., Habu, S. & Satake, M. 2005. Overexpression of the Runx3 transcription factor increases the proportion of mature thymocytes of the CD8 single-positive lineage. *J Immunol,* 174**,** 2627-36.

Korn, T., Mitsdoerffer, M., Croxford, A. L., Awasthi, A., Dardalhon, V. A., Galileos, G., Vollmar, P., Stritesky, G. L., Kaplan, M. H., Waisman, A., Kuchroo, V. K. & Oukka, M. 2008. IL-6 controls Th17 immunity in vivo by inhibiting the conversion of conventional T cells into Foxp3+ regulatory T cells. *Proc Natl Acad Sci U S A,* 105**,** 18460-5.

Laidlaw, B. J., Lu, Y., Amezquita, R. A., Weinstein, J. S., Vander Heiden, J. A., Gupta, N. T., Kleinstein, S. H., Kaech, S. M. & Craft, J. 2017. Interleukin-10 from CD4(+) follicular regulatory T cells promotes the germinal center response. *Sci Immunol,* 2.

Leavenworth, J. W., Verbinnen, B., Yin, J., Huang, H. & Cantor, H. 2015. A p85alpha-osteopontin axis couples the receptor ICOS to sustained Bcl-6 expression by follicular helper and regulatory T cells. *Nat Immunol,* 16**,** 96-106.

Lebien, T. W. & Tedder, T. F. 2008. B lymphocytes: how they develop and function. *Blood,* 112**,** 1570-80.

Lee, J. Y., Skon, C. N., Lee, Y. J., Oh, S., Taylor, J. J., Malhotra, D., Jenkins, M. K., Rosenfeld, M. G., Hogquist, K. A. & Jameson, S. C. 2015. The transcription factor KLF2 restrains CD4(+) T follicular helper cell differentiation. *Immunity,* 42**,** 252-64.

Legler, D. F., Loetscher, M., Roos, R. S., Clark-Lewis, I., Baggiolini, M. & Moser, B. 1998. B cell-attracting chemokine 1, a human CXC chemokine expressed in lymphoid tissues, selectively attracts B lymphocytes via BLR1/CXCR5. *J Exp Med,* 187**,** 655-60.

Leon, B., Bradley, J. E., Lund, F. E., Randall, T. D. & Ballesteros-Tato, A. 2014. FoxP3+ regulatory T cells promote influenza-specific Tfh responses by controlling IL-2 availability. *Nat Commun,* 5**,** 3495.

Levine, A. G., Arvey, A., Jin, W. & Rudensky, A. Y. 2014. Continuous requirement for the TCR in regulatory T cell function. *Nat Immunol,* 15**,** 1070-8.

Lim, H. W., Hillsamer, P., Banham, A. H. & Kim, C. H. 2005. Cutting edge: direct suppression of B cells by CD4+ CD25+ regulatory T cells. *J Immunol,* 175**,** 4180-3.

Lim, H. W., Hillsamer, P. & Kim, C. H. 2004. Regulatory T cells can migrate to follicles upon T cell activation and suppress GC-Th cells and GC-Th cell-driven B cell responses. *J Clin Invest,* 114**,** 1640-9.

Linterman, M. A., Beaton, L., Yu, D., Ramiscal, R. R., Srivastava, M., Hogan, J. J., Verma, N. K., Smyth, M. J., Rigby, R. J. & Vinuesa, C. G. 2010. IL-21 acts directly on B cells to regulate Bcl-6 expression and germinal center responses. *J Exp Med,* 207**,** 353-63.

Linterman, M. A., Denton, A. E., Divekar, D. P., Zvetkova, I., Kane, L., Ferreira, C., Veldhoen, M., Clare, S., Dougan, G., Espeli, M. & Smith, K. G. 2014. CD28 expression is required after T cell priming for helper T cell responses and protective immunity to infection. *Elife,* 3.

Linterman, M. A., Pierson, W., Lee, S. K., Kallies, A., Kawamoto, S., Rayner, T. F., Srivastava, M., Divekar, D. P., Beaton, L., Hogan, J. J., Fagarasan, S., Liston, A., Smith, K. G. & Vinuesa, C. G. 2011. Foxp3+ follicular regulatory T cells control the germinal center response. *Nat Med,* 17**,** 975-82.

Lio, C. W. & Hsieh, C. S. 2008. A two-step process for thymic regulatory T cell development. *Immunity,* 28**,** 100-11.

Liston, A. & Gray, D. H. 2014. Homeostatic control of regulatory T cell diversity. *Nat Rev Immunol,* 14**,** 154-65.

Liston, A., Lesage, S., Wilson, J., Peltonen, L. & Goodnow, C. C. 2003. Aire regulates negative selection of organ-specific T cells. *Nat Immunol,* 4**,** 350-4.

Litman, G. W., Rast, J. P. & Fugmann, S. D. 2010. The origins of vertebrate adaptive immunity. *Nat Rev Immunol,* 10**,** 543-53.

Liu, X., Chen, X., Zhong, B., Wang, A., Wang, X., Chu, F., Nurieva, R. I., Yan, X., Chen, P., Van Der Flier, L. G., Nakatsukasa, H., Neelapu, S. S., Chen, W., Clevers, H., Tian, Q., Qi, H., Wei, L. & Dong, C. 2014. Transcription factor achaete-scute homologue 2 initiates follicular T-helper-cell development. *Nature,* 507**,** 513-8.

Liu, X., Taylor, B. J., Sun, G. & Bosselut, R. 2005. Analyzing expression of perforin, Runx3, and Thpok genes during positive selection reveals activation of CD8-differentiation programs by MHC II-signaled thymocytes. *J Immunol,* 175**,** 4465-74.

Lucas, B., White, A. J., Parnell, S. M., Henley, P. M., Jenkinson, W. E. & Anderson, G. 2017. Progressive Changes in CXCR4 Expression That Define Thymocyte Positive Selection Are Dispensable For Both Innate and Conventional alphabetaT-cell Development. *Sci Rep,* 7**,** 5068.

Ma, Q., Jones, D., Borghesani, P. R., Segal, R. A., Nagasawa, T., Kishimoto, T., Bronson, R. T. & Springer, T. A. 1998. Impaired B-lymphopoiesis, myelopoiesis, and derailed cerebellar neuron migration in CXCR4- and SDF-1-deficient mice. *Proc Natl Acad Sci U S A,* 95**,** 9448-53.

Maceiras, A. R., Almeida, S. C. P., Mariotti-Ferrandiz, E., Chaara, W., Jebbawi, F., Six, A., Hori, S., Klatzmann, D., Faro, J. & Graca, L. 2017. T follicular helper and T follicular regulatory cells have different TCR specificity. *Nat Commun,* 8**,** 15067.

Mackay, C. R., Marston, W. L. & Dudler, L. 1990. Naive and memory T cells show distinct pathways of lymphocyte recirculation. *J Exp Med,* 171**,** 801-17.

Maclennan, I. C. 1994. Germinal centers. *Annu Rev Immunol,* 12**,** 117-39.

Maclennan, I. C., Toellner, K. M., Cunningham, A. F., Serre, K., Sze, D. M., Zuniga, E., Cook, M. C. & Vinuesa, C. G. 2003. Extrafollicular antibody responses. *Immunol Rev,* 194**,** 8-18.

Malek, T. R. & Castro, I. 2010. Interleukin-2 receptor signaling: at the interface between tolerance and immunity. *Immunity,* 33**,** 153-65.

Malek, T. R., Yu, A., Vincek, V., Scibelli, P. & Kong, L. 2002. CD4 regulatory T cells prevent lethal autoimmunity in IL-2Rbeta-deficient mice. Implications for the nonredundant function of IL-2. *Immunity,* 17**,** 167-78.

Maloy, K. J. & Powrie, F. 2001. Regulatory T cells in the control of immune pathology. *Nat Immunol,* 2**,** 816-22.

Mantel, P. Y., Ouaked, N., Ruckert, B., Karagiannidis, C., Welz, R., Blaser, K. & Schmidt-Weber, C. B. 2006. Molecular mechanisms underlying FOXP3 induction in human T cells. *J Immunol,* 176**,** 3593-602.

Marshall, D., Sinclair, C., Tung, S. & Seddon, B. 2014. Differential requirement for IL-2 and IL-15 during bifurcated development of thymic regulatory T cells. *J Immunol,* 193**,** 5525-33.

Mathew, R., Mao, A. P., Chiang, A. H., Bertozzi-Villa, C., Bunker, J. J., Scanlon, S. T., Mcdonald, B. D., Constantinides, M. G., Hollister, K., Singer, J. D., Dent, A. L., Dinner, A. R. & Bendelac, A. 2014. A negative feedback loop mediated by the Bcl6-cullin 3 complex limits Tfh cell differentiation. *J Exp Med,* 211**,** 1137-51.

Mayer, C. T., Gazumyan, A., Kara, E. E., Gitlin, A. D., Golijanin, J., Viant, C., Pai, J., Oliveira, T. Y., Wang, Q., Escolano, A., Medina-Ramirez, M., Sanders, R. W. & Nussenzweig, M. C. 2017. The microanatomic segregation of selection by apoptosis in the germinal center. *Science,* 358.

Medzhitov, R. & Janeway, C., Jr. 2000. Innate immunity. *N Engl J Med,* 343**,** 338-44.

Medzhitov, R. & Janeway, C. A., Jr. 2002. Decoding the patterns of self and nonself by the innate immune system. *Science,* 296**,** 298-300.

Melchers, F. 2015. Checkpoints that control B cell development. *J Clin Invest,* 125**,** 2203-10.

Miki, T., Kawamata, N., Hirosawa, S. & Aoki, N. 1994. Gene involved in the 3q27 translocation associated with B-cell lymphoma, BCL5, encodes a Kruppel-like zinc-finger protein. *Blood,* 83**,** 26-32.

Mond, J. J., Lees, A. & Snapper, C. M. 1995a. T cell-independent antigens type 2. *Annu Rev Immunol,* 13**,** 655-92.

Mond, J. J., Vos, Q., Lees, A. & Snapper, C. M. 1995b. T cell independent antigens. *Curr Opin Immunol,* 7**,** 349-54.

Moran, A. E., Holzapfel, K. L., Xing, Y., Cunningham, N. R., Maltzman, J. S., Punt, J. & Hogquist, K. A. 2011. T cell receptor signal strength in Treg and iNKT cell development demonstrated by a novel fluorescent reporter mouse. *J Exp Med,* 208**,** 1279-89.

Morinobu, A., Gadina, M., Strober, W., Visconti, R., Fornace, A., Montagna, C., Feldman, G. M., Nishikomori, R. & O'shea, J. J. 2002. STAT4 serine phosphorylation is critical for IL-12-induced IFN-gamma production but not for cell proliferation. *Proc Natl Acad Sci U S A,* 99**,** 12281-6.

Moriyama, S., Takahashi, N., Green, J. A., Hori, S., Kubo, M., Cyster, J. G. & Okada, T. 2014. Sphingosine-1-phosphate receptor 2 is critical for follicular helper T cell retention in germinal centers. *J Exp Med,* 211**,** 1297-305.

Moser, B. 2015. CXCR5, the Defining Marker for Follicular B Helper T (TFH) Cells. *Front Immunol,* 6**,** 296.

Mullen, A. C., High, F. A., Hutchins, A. S., Lee, H. W., Villarino, A. V., Livingston, D. M., Kung, A. L., Cereb, N., Yao, T. P., Yang, S. Y. & Reiner, S. L. 2001. Role of T-bet in commitment of TH1 cells before IL-12-dependent selection. *Science,* 292**,** 1907-10.

Nagasawa, T., Hirota, S., Tachibana, K., Takakura, N., Nishikawa, S., Kitamura, Y., Yoshida, N., Kikutani, H. & Kishimoto, T. 1996. Defects of B-cell lymphopoiesis and bone-marrow myelopoiesis in mice lacking the CXC chemokine PBSF/SDF-1. *Nature,* 382**,** 635-8.

Nagasawa, T., Kikutani, H. & Kishimoto, T. 1994. Molecular cloning and structure of a pre-B-cell growth-stimulating factor. *Proc Natl Acad Sci U S A,* 91**,** 2305-9.

Nance, J. P., Belanger, S., Johnston, R. J., Takemori, T. & Crotty, S. 2015. Cutting edge: T follicular helper cell differentiation is defective in the absence of Bcl6 BTB repressor domain function. *J Immunol,* 194**,** 5599-603.

Nemazee, D. 2000. Receptor selection in B and T lymphocytes. *Annu Rev Immunol,* 18**,** 19-51.

Ni, K. & O'neill, H. C. 1997. The role of dendritic cells in T cell activation. *Immunol Cell Biol,* 75**,** 223-30.

Nie, Y., Waite, J., Brewer, F., Sunshine, M. J., Littman, D. R. & Zou, Y. R. 2004. The role of CXCR4 in maintaining peripheral B cell compartments and humoral immunity. *J Exp Med,* 200**,** 1145-56.

Nishizuka, Y. & Sakakura, T. 1969. Thymus and reproduction: sex-linked dysgenesia of the gonad after neonatal thymectomy in mice. *Science,* 166**,** 753-5.

Niu, H., Ye, B. H. & Dalla-Favera, R. 1998. Antigen receptor signaling induces MAP kinase-mediated phosphorylation and degradation of the BCL-6 transcription factor. *Genes Dev,* 12**,** 1953-61.

Nurieva, R. I., Chung, Y., Martinez, G. J., Yang, X. O., Tanaka, S., Matskevitch, T. D., Wang, Y. H. & Dong, C. 2009. Bcl6 mediates the development of T follicular helper cells. *Science,* 325**,** 1001-5.

Nutt, S. L., Heavey, B., Rolink, A. G. & Busslinger, M. 1999. Commitment to the B-lymphoid lineage depends on the transcription factor Pax5. *Nature,* 401**,** 556-62.

Odegard, J. M., Marks, B. R., Diplacido, L. D., Poholek, A. C., Kono, D. H., Dong, C., Flavell, R. A. & Craft, J. 2008. ICOS-dependent extrafollicular helper T cells elicit IgG production via IL-21 in systemic autoimmunity. *J Exp Med,* 205**,** 2873-86.

Oestreich, K. J., Huang, A. C. & Weinmann, A. S. 2011. The lineage-defining factors T-bet and Bcl-6 collaborate to regulate Th1 gene expression patterns. *J Exp Med,* 208**,** 1001-13.

Oestreich, K. J. & Weinmann, A. S. 2012. Master regulators or lineage-specifying? Changing views on CD4+ T cell transcription factors. *Nat Rev Immunol,* 12**,** 799-804.

Ohkura, N., Hamaguchi, M., Morikawa, H., Sugimura, K., Tanaka, A., Ito, Y., Osaki, M., Tanaka, Y., Yamashita, R., Nakano, N., Huehn, J., Fehling, H. J., Sparwasser, T., Nakai, K. & Sakaguchi, S. 2012. T cell receptor stimulation-induced epigenetic changes and Foxp3 expression are independent and complementary events required for Treg cell development. *Immunity,* 37**,** 785-99.

Okada, T., Miller, M. J., Parker, I., Krummel, M. F., Neighbors, M., Hartley, S. B., O'garra, A., Cahalan, M. D. & Cyster, J. G. 2005. Antigen-engaged B cells undergo chemotaxis toward the T zone and form motile conjugates with helper T cells. *PLoS Biol,* 3**,** e150.

Pacholczyk, R., Ignatowicz, H., Kraj, P. & Ignatowicz, L. 2006. Origin and T cell receptor diversity of Foxp3+CD4+CD25+ T cells. *Immunity,* 25**,** 249-59.

Pai, S. Y., Truitt, M. L., Ting, C. N., Leiden, J. M., Glimcher, L. H. & Ho, I. C. 2003. Critical roles for transcription factor GATA-3 in thymocyte development. *Immunity,* 19**,** 863-75.

Paiva, R. S., Lino, A. C., Bergman, M. L., Caramalho, I., Sousa, A. E., Zelenay, S. & Demengeot, J. 2013. Recent thymic emigrants are the preferential precursors of regulatory T cells differentiated in the periphery. *Proc Natl Acad Sci U S A,* 110**,** 6494-9.

Pappu, R., Schwab, S. R., Cornelissen, I., Pereira, J. P., Regard, J. B., Xu, Y., Camerer, E., Zheng, Y. W., Huang, Y., Cyster, J. G. & Coughlin, S. R. 2007. Promotion of lymphocyte egress into blood and lymph by distinct sources of sphingosine-1-phosphate. *Science,* 316**,** 295-8.

Park, H., Li, Z., Yang, X. O., Chang, S. H., Nurieva, R., Wang, Y. H., Wang, Y., Hood, L., Zhu, Z., Tian, Q. & Dong, C. 2005. A distinct lineage of CD4 T cells regulates tissue inflammation by producing interleukin 17. *Nat Immunol,* 6**,** 1133-41.

Paul, W. E. & Zhu, J. 2010. How are T(H)2-type immune responses initiated and amplified? *Nat Rev Immunol,* 10**,** 225-35.

Pelanda, R. & Torres, R. M. 2012. Central B-cell tolerance: where selection begins. *Cold Spring Harb Perspect Biol,* 4**,** a007146.

Pereira, J. P., Kelly, L. M., Xu, Y. & Cyster, J. G. 2009. EBI2 mediates B cell segregation between the outer and centre follicle. *Nature,* 460**,** 1122-6.

Phan, T. G., Grigorova, I., Okada, T. & Cyster, J. G. 2007. Subcapsular encounter and complement-dependent transport of immune complexes by lymph node B cells. *Nat Immunol,* 8**,** 992-1000.

Phan, T. G., Paus, D., Chan, T. D., Turner, M. L., Nutt, S. L., Basten, A. & Brink, R. 2006. High affinity germinal center B cells are actively selected into the plasma cell compartment. *J Exp Med,* 203**,** 2419-24.

Plotkin, J., Prockop, S. E., Lepique, A. & Petrie, H. T. 2003. Critical role for CXCR4 signaling in progenitor localization and T cell differentiation in the postnatal thymus. *J Immunol,* 171**,** 4521-7.

Poholek, A. C., Hansen, K., Hernandez, S. G., Eto, D., Chandele, A., Weinstein, J. S., Dong, X., Odegard, J. M., Kaech, S. M., Dent, A. L., Crotty, S. & Craft, J. 2010. In vivo regulation of Bcl6 and T follicular helper cell development. *J Immunol,* 185**,** 313-26.

Powell, J. D. & Delgoffe, G. M. 2010. The mammalian target of rapamycin: linking T cell differentiation, function, and metabolism. *Immunity,* 33**,** 301-11.

Poznansky, M. C., Olszak, I. T., Evans, R. H., Wang, Z., Foxall, R. B., Olson, D. P., Weibrecht, K., Luster, A. D. & Scadden, D. T. 2002. Thymocyte emigration is mediated by active movement away from stroma-derived factors. *J Clin Invest,* 109**,** 1101-10.

Qi, H., Cannons, J. L., Klauschen, F., Schwartzberg, P. L. & Germain, R. N. 2008. SAP-controlled T-B cell interactions underlie germinal centre formation. *Nature,* 455**,** 764-9.

Qi, H., Egen, J. G., Huang, A. Y. & Germain, R. N. 2006. Extrafollicular activation of lymph node B cells by antigen-bearing dendritic cells. *Science,* 312**,** 1672-6.

Qureshi, O. S., Zheng, Y., Nakamura, K., Attridge, K., Manzotti, C., Schmidt, E. M., Baker, J., Jeffery, L. E., Kaur, S., Briggs, Z., Hou, T. Z., Futter, C. E., Anderson, G., Walker, L. S. & Sansom, D. M. 2011. Trans-endocytosis of CD80 and CD86: a molecular basis for the cell-extrinsic function of CTLA-4. *Science,* 332**,** 600-3.

Radtke, F., Wilson, A., Stark, G., Bauer, M., Van Meerwijk, J., Macdonald, H. R. & Aguet, M. 1999. Deficient T cell fate specification in mice with an induced inactivation of Notch1. *Immunity,* 10**,** 547-58.

Ranuncolo, S. M., Polo, J. M., Dierov, J., Singer, M., Kuo, T., Greally, J., Green, R., Carroll, M. & Melnick, A. 2007. Bcl-6 mediates the germinal center B cell phenotype and lymphomagenesis through transcriptional repression of the DNA-damage sensor ATR. *Nat Immunol,* 8**,** 705-14.

Ranuncolo, S. M., Polo, J. M. & Melnick, A. 2008. BCL6 represses CHEK1 and suppresses DNA damage pathways in normal and malignant B-cells. *Blood Cells Mol Dis,* 41**,** 95-9.

Ritvo, P. G., Churlaud, G., Quiniou, V., Florez, L., Brimaud, F., Fourcade, G., Mariotti-Ferrandiz, E. & Klatzmann, D. 2017. Tfr cells lack IL-2Ralpha but express decoy IL-1R2 and IL-1Ra and suppress the IL-1-dependent activation of Tfh cells. *Sci Immunol,* 2.

Rolf, J., Bell, S. E., Kovesdi, D., Janas, M. L., Soond, D. R., Webb, L. M., Santinelli, S., Saunders, T., Hebeis, B., Killeen, N., Okkenhaug, K. & Turner, M. 2010. Phosphoinositide 3-kinase activity in T cells regulates the magnitude of the germinal center reaction. *J Immunol,* 185**,** 4042-52.

Rothenberg, E. V., Zhang, J. & Li, L. 2010. Multilayered specification of the T-cell lineage fate. *Immunol Rev,* 238**,** 150-68.

Rubtsov, Y. P., Niec, R. E., Josefowicz, S., Li, L., Darce, J., Mathis, D., Benoist, C. & Rudensky, A. Y. 2010. Stability of the regulatory T cell lineage in vivo. *Science,* 329**,** 1667-71.

Rubtsov, Y. P., Rasmussen, J. P., Chi, E. Y., Fontenot, J., Castelli, L., Ye, X., Treuting, P., Siewe, L., Roers, A., Henderson, W. R., Jr., Muller, W. & Rudensky, A. Y. 2008. Regulatory T cell-derived interleukin-10 limits inflammation at environmental interfaces. *Immunity,* 28**,** 546-58.

Sage, P. T., Alvarez, D., Godec, J., Von Andrian, U. H. & Sharpe, A. H. 2014a. Circulating T follicular regulatory and helper cells have memory-like properties. *J Clin Invest,* 124**,** 5191-204.

Sage, P. T., Francisco, L. M., Carman, C. V. & Sharpe, A. H. 2013. The receptor PD-1 controls follicular regulatory T cells in the lymph nodes and blood. *Nat Immunol,* 14**,** 152-61.

Sage, P. T., Paterson, A. M., Lovitch, S. B. & Sharpe, A. H. 2014b. The coinhibitory receptor CTLA-4 controls B cell responses by modulating T follicular helper, T follicular regulatory, and T regulatory cells. *Immunity,* 41**,** 1026-39.

Sakaguchi, S., Vignali, D. A., Rudensky, A. Y., Niec, R. E. & Waldmann, H. 2013. The plasticity and stability of regulatory T cells. *Nat Rev Immunol,* 13**,** 461-7.

Sakaguchi, S., Yamaguchi, T., Nomura, T. & Ono, M. 2008. Regulatory T cells and immune tolerance. *Cell,* 133**,** 775-87.

Sansom, S. N., Shikama-Dorn, N., Zhanybekova, S., Nusspaumer, G., Macaulay, I. C., Deadman, M. E., Heger, A., Ponting, C. P. & Hollander, G. A. 2014. Population and single-cell genomics reveal the Aire dependency, relief from Polycomb silencing, and distribution of self-antigen expression in thymic epithelia. *Genome Res,* 24**,** 1918-31.

Saraiva, M. & O'garra, A. 2010. The regulation of IL-10 production by immune cells. *Nat Rev Immunol,* 10**,** 170-81.

Sawant, D. V., Sehra, S., Nguyen, E. T., Jadhav, R., Englert, K., Shinnakasu, R., Hangoc, G., Broxmeyer, H. E., Nakayama, T., Perumal, N. B., Kaplan, M. H. & Dent, A. L. 2012. Bcl6 controls the Th2 inflammatory activity of regulatory T cells by repressing Gata3 function. *J Immunol,* 189**,** 4759-69.

Schaerli, P., Willimann, K., Lang, A. B., Lipp, M., Loetscher, P. & Moser, B. 2000. CXC chemokine receptor 5 expression defines follicular homing T cells with B cell helper function. *J Exp Med,* 192**,** 1553-62.

Schatz, D. G. & Swanson, P. C. 2011. V(D)J recombination: mechanisms of initiation. *Annu Rev Genet,* 45**,** 167-202.

Schlissel, M. S. 2003. Regulating antigen-receptor gene assembly. *Nat Rev Immunol,* 3**,** 890-9.

Schnare, M., Barton, G. M., Holt, A. C., Takeda, K., Akira, S. & Medzhitov, R. 2001. Toll-like receptors control activation of adaptive immune responses. *Nat Immunol,* 2**,** 947-50.

Setoguchi, R., Tachibana, M., Naoe, Y., Muroi, S., Akiyama, K., Tezuka, C., Okuda, T. & Taniuchi, I. 2008. Repression of the transcription factor Th-POK by Runx complexes in cytotoxic T cell development. *Science,* 319**,** 822-5.

Shapiro-Shelef, M., Lin, K. I., Mcheyzer-Williams, L. J., Liao, J., Mcheyzer-Williams, M. G. & Calame, K. 2003. Blimp-1 is required for the formation of immunoglobulin secreting plasma cells and pre-plasma memory B cells. *Immunity,* 19**,** 607-20.

Shen, E., Wang, Q., Rabe, H., Liu, W., Cantor, H. & Leavenworth, J. W. 2018. Chromatin remodeling by the NuRD complex regulates development of follicular helper and regulatory T cells. *Proc Natl Acad Sci U S A,* 115**,** 6780-6785.

Shulman, Z., Gitlin, A. D., Targ, S., Jankovic, M., Pasqual, G., Nussenzweig, M. C. & Victora, G. D. 2013. T follicular helper cell dynamics in germinal centers. *Science,* 341**,** 673-7.

Singer, A. 2002. New perspectives on a developmental dilemma: the kinetic signaling model and the importance of signal duration for the CD4/CD8 lineage decision. *Curr Opin Immunol,* 14**,** 207-15.

Slifka, M. K., Antia, R., Whitmire, J. K. & Ahmed, R. 1998. Humoral immunity due to long-lived plasma cells. *Immunity,* 8**,** 363-72.

Smith, K. G., Hewitson, T. D., Nossal, G. J. & Tarlinton, D. M. 1996. The phenotype and fate of the antibody-forming cells of the splenic foci. *Eur J Immunol,* 26**,** 444-8.

Smith, K. G., Light, A., O'reilly, L. A., Ang, S. M., Strasser, A. & Tarlinton, D. 2000. bcl-2 transgene expression inhibits apoptosis in the germinal center and reveals differences in the selection of memory B cells and bone marrow antibody-forming cells. *J Exp Med,* 191**,** 475-84.

Steinman, R. M. & Idoyaga, J. 2010. Features of the dendritic cell lineage. *Immunol Rev,* 234**,** 5-17.

Steinman, R. M. & Witmer, M. D. 1978. Lymphoid dendritic cells are potent stimulators of the primary mixed leukocyte reaction in mice. *Proc Natl Acad Sci U S A,* 75**,** 5132-6.

Su, L., Creusot, R. J., Gallo, E. M., Chan, S. M., Utz, P. J., Fathman, C. G. & Ermann, J. 2004. Murine CD4+CD25+ regulatory T cells fail to undergo chromatin remodeling across the proximal promoter region of the IL-2 gene. *J Immunol,* 173**,** 4994-5001.

Suan, D., Nguyen, A., Moran, I., Bourne, K., Hermes, J. R., Arshi, M., Hampton, H. R., Tomura, M., Miwa, Y., Kelleher, A. D., Kaplan, W., Deenick, E. K., Tangye, S. G., Brink, R., Chtanova, T. & Phan, T. G. 2015. T follicular helper cells have distinct modes of migration and molecular signatures in naive and memory immune responses. *Immunity,* 42**,** 704-18.

Sun, C. M., Hall, J. A., Blank, R. B., Bouladoux, N., Oukka, M., Mora, J. R. & Belkaid, Y. 2007. Small intestine lamina propria dendritic cells promote de novo generation of Foxp3 T reg cells via retinoic acid. *J Exp Med,* 204**,** 1775-85.

Sun, G., Liu, X., Mercado, P., Jenkinson, S. R., Kypriotou, M., Feigenbaum, L., Galera, P. & Bosselut, R. 2005. The zinc finger protein cKrox directs CD4 lineage differentiation during intrathymic T cell positive selection. *Nat Immunol,* 6**,** 373-81.

Surh, C. D. & Sprent, J. 1994. T-cell apoptosis detected in situ during positive and negative selection in the thymus. *Nature,* 372**,** 100-3.

Szabo, S. J., Kim, S. T., Costa, G. L., Zhang, X., Fathman, C. G. & Glimcher, L. H. 2000. A novel transcription factor, T-bet, directs Th1 lineage commitment. *Cell,* 100**,** 655-69.

Tai, X., Cowan, M., Feigenbaum, L. & Singer, A. 2005. CD28 costimulation of developing thymocytes induces Foxp3 expression and regulatory T cell differentiation independently of interleukin 2. *Nat Immunol,* 6**,** 152-62.

Taniuchi, I., Osato, M., Egawa, T., Sunshine, M. J., Bae, S. C., Komori, T., Ito, Y. & Littman, D. R. 2002. Differential requirements for Runx proteins in CD4 repression and epigenetic silencing during T lymphocyte development. *Cell,* 111**,** 621-33.

Thornton, A. M., Korty, P. E., Tran, D. Q., Wohlfert, E. A., Murray, P. E., Belkaid, Y. & Shevach, E. M. 2010. Expression of Helios, an Ikaros transcription factor family member, differentiates thymic-derived from peripherally induced Foxp3+ T regulatory cells. *J Immunol,* 184**,** 3433-41.

Tobon, G. J., Izquierdo, J. H. & Canas, C. A. 2013. B lymphocytes: development, tolerance, and their role in autoimmunity-focus on systemic lupus erythematosus. *Autoimmune Dis,* 2013**,** 827254.

Toker, A. & Huehn, J. 2011. To be or not to be a Treg cell: lineage decisions controlled by epigenetic mechanisms. *Sci Signal,* 4**,** pe4.

Tokoyoda, K., Egawa, T., Sugiyama, T., Choi, B. I. & Nagasawa, T. 2004. Cellular niches controlling B lymphocyte behavior within bone marrow during development. *Immunity,* 20**,** 707-18.

Tonegawa, S. 1983. Somatic generation of antibody diversity. *Nature,* 302**,** 575-81.

Tonegawa, S. 1987. [Molecular biology of immunologic recognition]. *Tanpakushitsu Kakusan Koso,* 32**,** 239-50.

Trampont, P. C., Tosello-Trampont, A. C., Shen, Y., Duley, A. K., Sutherland, A. E., Bender, T. P., Littman, D. R. & Ravichandran, K. S. 2010. CXCR4 acts as a costimulator during thymic beta-selection. *Nat Immunol,* 11**,** 162-70.

Ubelhart, R. & Jumaa, H. 2015. Autoreactivity and the positive selection of B cells. *Eur J Immunol,* 45**,** 2971-7.

Vaeth, M., Muller, G., Stauss, D., Dietz, L., Klein-Hessling, S., Serfling, E., Lipp, M., Berberich, I. & Berberich-Siebelt, F. 2014. Follicular regulatory T cells control humoral autoimmunity via NFAT2-regulated CXCR5 expression. *J Exp Med,* 211**,** 545-61.

Vahedi, G., Kanno, Y., Furumoto, Y., Jiang, K., Parker, S. C., Erdos, M. R., Davis, S. R., Roychoudhuri, R., Restifo, N. P., Gadina, M., Tang, Z., Ruan, Y., Collins, F. S., Sartorelli, V. & O'shea, J. J. 2015. Super-enhancers delineate disease-associated regulatory nodes in T cells. *Nature,* 520**,** 558-62.

Vahl, J. C., Drees, C., Heger, K., Heink, S., Fischer, J. C., Nedjic, J., Ohkura, N., Morikawa, H., Poeck, H., Schallenberg, S., Riess, D., Hein, M. Y., Buch, T., Polic, B., Schonle, A., Zeiser, R., Schmitt-Graff, A., Kretschmer, K., Klein, L., Korn, T., Sakaguchi, S. & Schmidt-Supprian, M. 2014. Continuous T cell receptor signals maintain a functional regulatory T cell pool. *Immunity,* 41**,** 722-36.

Vanderleyden, I. & Linterman, M. A. 2017. Identifying Follicular Regulatory T Cells by Confocal Microscopy. *Methods Mol Biol,* 1623**,** 87-93.

Vanderleyden, I., Linterman, M. A. & Smith, K. G. 2014. Regulatory T cells and control of the germinal centre response. *Arthritis Research & Therapy,* 16.

Vang, K. B., Yang, J., Mahmud, S. A., Burchill, M. A., Vegoe, A. L. & Farrar, M. A. 2008. IL-2, -7, and -15, but not thymic stromal lymphopoeitin, redundantly govern CD4+Foxp3+ regulatory T cell development. *J Immunol,* 181**,** 3285-90.

Veerman, K. M., Williams, M. J., Uchimura, K., Singer, M. S., Merzaban, J. S., Naus, S., Carlow, D. A., Owen, P., Rivera-Nieves, J., Rosen, S. D. & Ziltener, H. J. 2007. Interaction of the selectin ligand PSGL-1 with chemokines CCL21 and CCL19 facilitates efficient homing of T cells to secondary lymphoid organs. *Nat Immunol,* 8**,** 532-9.

Vettermann, C. & Schlissel, M. S. 2010. Allelic exclusion of immunoglobulin genes: models and mechanisms. *Immunol Rev,* 237**,** 22-42.

Vianello, F., Kraft, P., Mok, Y. T., Hart, W. K., White, N. & Poznansky, M. C. 2005. A CXCR4-dependent chemorepellent signal contributes to the emigration of mature single-positive CD4 cells from the fetal thymus. *J Immunol,* 175**,** 5115-25.

Victora, G. D. & Nussenzweig, M. C. 2012. Germinal centers. *Annu Rev Immunol,* 30**,** 429-57.

Victora, G. D., Schwickert, T. A., Fooksman, D. R., Kamphorst, A. O., Meyer-Hermann, M., Dustin, M. L. & Nussenzweig, M. C. 2010. Germinal center dynamics revealed by multiphoton microscopy with a photoactivatable fluorescent reporter. *Cell,* 143**,** 592-605.

Vogelzang, A., Mcguire, H. M., Yu, D., Sprent, J., Mackay, C. R. & King, C. 2008. A fundamental role for interleukin-21 in the generation of T follicular helper cells. *Immunity,* 29**,** 127-37.

Vogler, L. B., Crist, W. M., Bockman, D. E., Pearl, E. R., Lawton, A. R. & Cooper, M. D. 1978. Pre-B-cell leukemia. A new phenotype of childhood lymphoblastic leukemia. *N Engl J Med,* 298**,** 872-8.

Vos, Q., Lees, A., Wu, Z. Q., Snapper, C. M. & Mond, J. J. 2000. B-cell activation by T-cell-independent type 2 antigens as an integral part of the humoral immune response to pathogenic microorganisms. *Immunol Rev,* 176**,** 154-70.

Walker, L. S. & Sansom, D. M. 2011. The emerging role of CTLA4 as a cell-extrinsic regulator of T cell responses. *Nat Rev Immunol,* 11**,** 852-63.

Walsh, K. P. & Mills, K. H. 2013. Dendritic cells and other innate determinants of T helper cell polarisation. *Trends Immunol,* 34**,** 521-30.

Wang, Y., Su, M. A. & Wan, Y. Y. 2011. An essential role of the transcription factor GATA-3 for the function of regulatory T cells. *Immunity,* 35**,** 337-48.

Weber, B. N., Chi, A. W., Chavez, A., Yashiro-Ohtani, Y., Yang, Q., Shestova, O. & Bhandoola, A. 2011. A critical role for TCF-1 in T-lineage specification and differentiation. *Nature,* 476**,** 63-8.

Weisel, F. J., Zuccarino-Catania, G. V., Chikina, M. & Shlomchik, M. J. 2016. A Temporal Switch in the Germinal Center Determines Differential Output of Memory B and Plasma Cells. *Immunity,* 44**,** 116-130.

Weiss, J. M., Bilate, A. M., Gobert, M., Ding, Y., Curotto De Lafaille, M. A., Parkhurst, C. N., Xiong, H., Dolpady, J., Frey, A. B., Ruocco, M. G., Yang, Y., Floess, S., Huehn, J., Oh, S., Li, M. O., Niec, R. E., Rudensky, A. Y., Dustin, M. L., Littman, D. R. & Lafaille, J. J. 2012. Neuropilin 1 is expressed on thymus-derived natural regulatory T cells, but not mucosa-generated induced Foxp3+ T reg cells. *J Exp Med,* 209**,** 1723-42, S1.

Winandy, S., Wu, L., Wang, J. H. & Georgopoulos, K. 1999. Pre-T cell receptor (TCR) and TCR-controlled checkpoints in T cell differentiation are set by Ikaros. *J Exp Med,* 190**,** 1039-48.

Wing, J. B., Ise, W., Kurosaki, T. & Sakaguchi, S. 2014. Regulatory T cells control antigen-specific expansion of Tfh cell number and humoral immune responses via the coreceptor CTLA-4. *Immunity,* 41**,** 1013-25.

Wing, J. B., Kitagawa, Y., Locci, M., Hume, H., Tay, C., Morita, T., Kidani, Y., Matsuda, K., Inoue, T., Kurosaki, T., Crotty, S., Coban, C., Ohkura, N. & Sakaguchi, S. 2017. A distinct subpopulation of CD25(-) T-follicular regulatory cells localizes in the germinal centers. *Proc Natl Acad Sci U S A,* 114**,** E6400-E6409.

Witt, C. M. & Robey, E. A. 2004. The ins and outs of CCR7 in the thymus. *J Exp Med,* 200**,** 405-9.

Wollenberg, I., Agua-Doce, A., Hernandez, A., Almeida, C., Oliveira, V. G., Faro, J. & Graca, L. 2011. Regulation of the germinal center reaction by Foxp3+ follicular regulatory T cells. *J Immunol,* 187**,** 4553-60.

Wu, H., Chen, Y., Liu, H., Xu, L. L., Teuscher, P., Wang, S., Lu, S. & Dent, A. L. 2016a. Follicular regulatory T cells repress cytokine production by follicular helper T cells and optimize IgG responses in mice. *Eur J Immunol*.

Wu, H., Chen, Y., Liu, H., Xu, L. L., Teuscher, P., Wang, S., Lu, S. & Dent, A. L. 2016b. Follicular regulatory T cells repress cytokine production by follicular helper T cells and optimize IgG responses in mice. *Eur J Immunol,* 46**,** 1152-61.

Xu, H., Li, X., Liu, D., Li, J., Zhang, X., Chen, X., Hou, S., Peng, L., Xu, C., Liu, W., Zhang, L. & Qi, H. 2013. Follicular T-helper cell recruitment governed by bystander B cells and ICOS-driven motility. *Nature,* 496**,** 523-7.

Xu, L., Huang, Q., Wang, H., Hao, Y., Bai, Q., Hu, J., Li, Y., Wang, P., Chen, X., He, R., Li, B., Yang, X., Zhao, T., Zhang, Y., Wang, Y., Ou, J., Liang, H., Wu, Y., Zhou, X. & Ye, L. 2017. The Kinase mTORC1 Promotes the Generation and Suppressive Function of Follicular Regulatory T Cells. *Immunity,* 47**,** 538-551 e5.

Yadav, M., Louvet, C., Davini, D., Gardner, J. M., Martinez-Llordella, M., Bailey-Bucktrout, S., Anthony, B. A., Sverdrup, F. M., Head, R., Kuster, D. J., Ruminski, P., Weiss, D., Von Schack, D. & Bluestone, J. A. 2012. Neuropilin-1 distinguishes natural and inducible regulatory T cells among regulatory T cell subsets in vivo. *J Exp Med,* 209**,** 1713-22, S1-19.

Yadav, M., Stephan, S. & Bluestone, J. A. 2013. Peripherally induced tregs - role in immune homeostasis and autoimmunity. *Front Immunol,* 4**,** 232.

Yang, B. H., Hagemann, S., Mamareli, P., Lauer, U., Hoffmann, U., Beckstette, M., Fohse, L., Prinz, I., Pezoldt, J., Suerbaum, S., Sparwasser, T., Hamann, A., Floess, S., Huehn, J. & Lochner, M. 2016. Foxp3(+) T cells expressing RORgammat represent a stable regulatory T-cell effector lineage with enhanced suppressive capacity during intestinal inflammation. *Mucosal Immunol,* 9**,** 444-57.

Yao, Z., Kanno, Y., Kerenyi, M., Stephens, G., Durant, L., Watford, W. T., Laurence, A., Robinson, G. W., Shevach, E. M., Moriggl, R., Hennighausen, L., Wu, C. & O'shea, J. J. 2007. Nonredundant roles for Stat5a/b in directly regulating Foxp3. *Blood,* 109**,** 4368-75.

Ye, B. H., Lista, F., Lo Coco, F., Knowles, D. M., Offit, K., Chaganti, R. S. & Dalla-Favera, R. 1993. Alterations of a zinc finger-encoding gene, BCL-6, in diffuse large-cell lymphoma. *Science,* 262**,** 747-50.

Yi, W., Gupta, S., Ricker, E., Manni, M., Jessberger, R., Chinenov, Y., Molina, H. & Pernis, A. B. 2017. The mTORC1-4E-BP-eIF4E axis controls de novo Bcl6 protein synthesis in T cells and systemic autoimmunity. *Nat Commun,* 8**,** 254.

Yu, D., Rao, S., Tsai, L. M., Lee, S. K., He, Y., Sutcliffe, E. L., Srivastava, M., Linterman, M., Zheng, L., Simpson, N., Ellyard, J. I., Parish, I. A., Ma, C. S., Li, Q. J., Parish, C. R., Mackay, C. R. & Vinuesa, C. G. 2009. The transcriptional repressor Bcl-6 directs T follicular helper cell lineage commitment. *Immunity,* 31**,** 457-68.

Yu, F., Sharma, S., Edwards, J., Feigenbaum, L. & Zhu, J. 2015. Dynamic expression of transcription factors T-bet and GATA-3 by regulatory T cells maintains immunotolerance. *Nat Immunol,* 16**,** 197-206.

Yu, Q., Erman, B., Bhandoola, A., Sharrow, S. O. & Singer, A. 2003. In vitro evidence that cytokine receptor signals are required for differentiation of double positive thymocytes into functionally mature CD8+ T cells. *J Exp Med,* 197**,** 475-87.

Yui, M. A. & Rothenberg, E. V. 2014. Developmental gene networks: a triathlon on the course to T cell identity. *Nat Rev Immunol,* 14**,** 529-45.

Yusuf, I., Kageyama, R., Monticelli, L., Johnston, R. J., Ditoro, D., Hansen, K., Barnett, B. & Crotty, S. 2010. Germinal center T follicular helper cell IL-4 production is dependent on signaling lymphocytic activation molecule receptor (CD150). *J Immunol,* 185**,** 190-202.

Zeng, H., Cohen, S., Guy, C., Shrestha, S., Neale, G., Brown, S. A., Cloer, C., Kishton, R. J., Gao, X., Youngblood, B., Do, M., Li, M. O., Locasale, J. W., Rathmell, J. C. & Chi, H. 2016. mTORC1 and mTORC2 Kinase Signaling and Glucose Metabolism Drive Follicular Helper T Cell Differentiation. *Immunity,* 45**,** 540-554.

Zhang, R., Huynh, A., Whitcher, G., Chang, J., Maltzman, J. S. & Turka, L. A. 2013a. An obligate cell-intrinsic function for CD28 in Tregs. *J Clin Invest,* 123**,** 580-93.

Zhang, Y., Meyer-Hermann, M., George, L. A., Figge, M. T., Khan, M., Goodall, M., Young, S. P., Reynolds, A., Falciani, F., Waisman, A., Notley, C. A., Ehrenstein, M. R., Kosco-Vilbois, M. & Toellner, K. M. 2013b. Germinal center B cells govern their own fate via antibody feedback. *J Exp Med,* 210**,** 457-64.

Zhang, Y., Tech, L., George, L. A., Acs, A., Durrett, R. E., Hess, H., Walker, L. S. K., Tarlinton, D. M., Fletcher, A. L., Hauser, A. E. & Toellner, K. M. 2018. Plasma cell output from germinal centers is regulated by signals from Tfh and stromal cells. *J Exp Med,* 215**,** 1227-1243.

Zheng, B., Sage, M., Sheppeard, E. A., Jurecic, V. & Bradley, A. 2000. Engineering mouse chromosomes with Cre-loxP: range, efficiency, and somatic applications. *Mol Cell Biol,* 20**,** 648-55.

Zheng, Y., Chaudhry, A., Kas, A., Deroos, P., Kim, J. M., Chu, T. T., Corcoran, L., Treuting, P., Klein, U. & Rudensky, A. Y. 2009. Regulatory T-cell suppressor program co-opts transcription factor IRF4 to control T(H)2 responses. *Nature,* 458**,** 351-6.

Zheng, Y., Josefowicz, S., Chaudhry, A., Peng, X. P., Forbush, K. & Rudensky, A. Y. 2010. Role of conserved non-coding DNA elements in the Foxp3 gene in regulatory T-cell fate. *Nature,* 463**,** 808-12.

Zotos, D., Coquet, J. M., Zhang, Y., Light, A., D'costa, K., Kallies, A., Corcoran, L. M., Godfrey, D. I., Toellner, K. M., Smyth, M. J., Nutt, S. L. & Tarlinton, D. M. 2010. IL-21 regulates germinal center B cell differentiation and proliferation through a B cell-intrinsic mechanism. *J Exp Med,* 207**,** 365-78.

Zou, W. 2006. Regulatory T cells, tumour immunity and immunotherapy. *Nat Rev Immunol,* 6**,** 295-307.

Zou, Y. R., Kottmann, A. H., Kuroda, M., Taniuchi, I. & Littman, D. R. 1998. Function of the chemokine receptor CXCR4 in haematopoiesis and in cerebellar development. *Nature,* 393**,** 595-9.